Bioengineering human bone marrow models to elucidate the triggers of the stem cell niche

Thèse N° 9543

Présentée le 12 juillet 2019

à la Faculté des sciences de la vie
Unité du Prof. Lutolf
Programme doctoral en biotechnologie et génie biologique

pour l'obtention du grade de Docteur ès Sciences

par

Queralt VALLMAJÓ MARTÍN

Acceptée sur proposition du jury

Prof. D. Ghezzi, président du jury
Prof. M. Lütolf, Dr. M. Ehrbar, directeurs de thèse
Prof. I. Martin, rapporteur
Dr S. Méndez-Ferrer, rapporteur
Prof. O. Naveiras, rapporteuse

2019

ÉCOLE POLYTECHNIQUE
FÉDÉRALE DE LAUSANNE

Al punket,

the real Empire.

A la mama, al papa i a l'Oriol,

la veritable inspiració.

Abstract

The bone marrow (BM) microenvironment, or niche, significantly affects behaviors of its resident stem cell populations. Disruptions in the BM niche contribute to a number of severe clinical pathologies. Discovery of novel therapeutic strategies for BM-related diseases necessitates development of superior preclinical models to study parameters affecting BM homeostasis. To address this, a poly(ethylene glycol) hydrogel featuring a particular crosslinking chemistry based on the enzyme transglutaminase factor XIII, dubbed TG-PEG, was utilized to engineer humanized bone marrow models. Its modular nature was exploited throughout this work to systematically evaluate contributions of biophysical, cellular, and biochemical BM niche components to stem cell biology.

Stiffness of TG-PEG hydrogels was optimized for each cell type and individual application explored. For bone formation by bone marrow stromal cells (BMSCs), an intermediate stiffness was optimal and significantly improved total bone volume over softer TG-PEG gels or natural materials. Results indicated that stability of the scaffold was more important than their chemical and biological properties. Alternatively, for hematopoietic stem and progenitor cells (HSPCs), softer gels were optimal for preserving multipotency while promoting cell proliferation.

A number of BM-specific stem and progenitor cell types with richly diverse functions were explored. Skeletal stem cells (SSCs) encapsulated in TG-PEG hydrogels demonstrated their ability to form *de novo* bone in healing critically sized calvaria defects in mice. Next, subcutaneous implantation of BMSC-laden gels revealed their significant contribution to formation of ossicles. For some BMSC donors, ossicles could be formed in absence of bone morphogenetic protein (BMP)-2 offering a novel tool to evaluate their intrinsic capacity. Later, titration of BMSC seeding densities and BMP-2 doses yielded optimal conditions for robust BM formation, regardless of donor, enabling reproducibility for follow-on studies involving BM models. In humanized mice, homing of HSPCs to BMSC-laden TG-PEG gels was observed. Finally, humanized xenograft models were employed to determine vulnerability of the BM niche to subversion by cancer cells simulating osteotropism for both leukemia and breast cancer metastasis.

Molecular factors known to trigger particular cell reactions within the niche were also investigated. Including RGD cell-adhesion ligands, as well as matrix metalloproteinase (MMP)-susceptible crosslinks to render the gels degradable, were critical for facilitating migration of recruited BM cells from murine hosts in xenograft studies. Hyaluronic acid (HA), when added to the hydrogel backbone, conferred superior engraftment to transplanted BMSCs and afforded reduced immunogenicity. Incorporation of the Notch-signaling ligands Jagged1 or DLL4 into soft TG-PEG gels during *in vitro* HSPC expansion substantially stimulated proliferation, but recovered cells could no longer ensure long-term reconstitution.

Aging, trauma, or cancer can cause disruptions of the tightly controlled balance between cells and their microenvironment in the BM niche. This body of work presents a number of bioengineered tools optimized for studying how niche components are affected by or contribute to such

pathologies. Further work with these or similar models will no doubt highlight key clinically relevant targets and inform novel therapeutic approaches.

Keywords: Bone marrow niche, osteotropic cancer model, biomimetic 3D hydrogel, bone marrow stromal cell, skeletal stem cell, hematopoietic stem cell, microenvironment, poly(ethylene glycol).

Zusammenfassung

Im Knochenmark (KM) beeinflusst das Mikromilieu, auch «Nische» genannt, das Verhalten der darin enthaltenen Stammzellpopulationen in Bezug auf deren Differenzierung und Regeneration. Störungen der KM-Nische tragen zu einer Vielfalt von schwerwiegenden klinischen Pathologien bei. Die Entwicklung von neuen Strategien für die Behandlung von KM-bedingten Krankheiten setzt den Zugang zu genauen präklinischen Modellen voraus, welche das Testen von KM-Homöostase regulierenden Faktoren mit grossem Durchsatz erlauben.

In dieser Arbeit wurde ein Poly(Ethylenglykol) Hydrogel (genannt «TG-PEG») verwendet, welches durch eine Transglutaminase vermittelte enzymatische Vernetzung von Vorläufermolekülen entsteht. Der modulare Charakter dieses TG-PEG Hydrogels wurde hier gezielt eingesetzt, um den Einfluss von biophysischen, zellulären und biochemischen Komponenten auf die Bildung von murinen und humanen KM-Nischen, sowie auf die Biologie der beteiligten Stammzellen zu evaluieren.

Dazu wurden in einer ersten Stufe murine Skelett-Stammzellen (mSSCs) in TG-PEG Hydrogele eingebettet und für die Heilung von Schädeldachdefekten verwendet. Diese Untersuchungen haben gezeigt, dass mSSCs die Knochenbildung unterstützen und sich auch ohne eine zusätzliche Gabe von knocheninduzierenden Substanzen wie zum Beispiel «bone morphogenetic protein» (BMP-2) in Konchenzellen differenzieren lassen.

Basierend auf diesem Wissen, haben wir uns in der Folge darauf konzentriert, unser System für die Bildung von humanem KM-Nischen zu optimieren. Dazu haben wir verschiedene Mengen von «human bone marrow stromal cells» (hBMSCs) und BMP-2 in TG-PEG Hydrogele eingebettet und gezeigt, dass die BMP-2-vermittelte Bildung von KM-Nischen durch hBMSCs deutlich verstärkt wird. Im Weiteren hat ein Vergleich von natürlichen Biomaterialien mit TG-PEG Hydrogelen verdeutlicht, dass für die hBMSCs vermittelte Bildung von KM-Nischen die Stabilität der getesteten Materialien wichtiger ist als deren chemischen und biologischen Eigenschaften. So konnten hBMCSs in TG-PEG Hydrogelen mit einer geeigneten Stabilität/Steifigkeit die spontane Bildung von KM-Nischen induzieren. Die dabei verwendeten Hydrogele mussten allerdings durch zelluläre Proteasen abbaubar sein und die Anhaftung der hBMSCs mittels RGD erlaubten. Durch die Bestückung der TG-PEG Hydrogele mit Hyaluronsäure (HA) konnte im Weiteren gezeigt werden, dass die Ansiedlung von transplantierten hBMSCs durch geeignete Modifikationen weiter verbessert werden kann.

Schliesslich wurden TG-PEG Hydrogele mit verschiedenen Steifigkeiten für die *in vitro*-Expansion von hämatopoetischen Stammzellen (HSCs) getestet. Unsere Untersuchungen zeigen, dass weiche Hydrogele die Expansion dieser sensiblen Stammzellen zulassen und dass diese Stammzellen ihre Langzeitpotential durch die Expansion nicht verlieren. Die Verwendung von proteolytisch abbaubaren Stellen nicht aber von RGD oder HA hatten einen wesentlichen Einfluss auf die HSC Expansion. Nur durch das Einfügen der Notch-liganden Jagged1 oder DLL4 in weiche TG-PEG-Gele konnte die *in vitro*-Expansion von eingebetteten HSCs weiter steigern. Allerdings zeigte sich, dass die daraus resultierenden HSCs keine Langzeitregeneration mehr gewährleisten.

Altern, Trauma oder Krebs können Störungen der strikt regulierten Balance zwischen Zellen und ihrem Mikro-Milieu in der KM-Nische verursachen. Erste Untersuchungen belegen, dass die etablierten KM-Nischen geeignet sind um die Infiltration von Leukämiezellen oder knochengerichteten Brustkrebs-metastasen zu studieren.

Diese Arbeit präsentiert eine Vielzahl von biotechnologischen Strategien, die optimiert wurden, um Nischenkomponenten welche von diversen Pathologien beeinflusst werden oder diese beeiflussen zu untersuchen. Künftige Forschung mit diesen oder ähnlichen Modellen wird zweifelsohne entscheidende, therapeutisch relevante Angriffspunkte hervorbringen und so neue Herangehensweisen prägen.

Schlagwörter: Knochenmarknische, Modelle für osteotrope Krebsarten, biomimetische 3D Hydrogele, Knochenmark-Stromazellen, Skelett-Stammzellen, hämatopoetische Stammzellen, Mikroumgebung, Poly(ethylenglykol)

Resum

El microentorn de la medul·la òssia (típicament BM, de l'anglicisme *bone marrow*), també anomenat *niche*, afecta significativament la pròpia població de cèl·lules mare i, particularment, la diferenciació i la regeneració d'aquestes. Possibles pertorbacions en el *BM niche* contribueixen a la propagació d'una infinitat de patologies clíniques severes. El descobriment de noves estratègies terapèutiques per malalties relacionades amb el BM necessita el desenvolupament de models preclínics precisos que permetin una major capacitat d'investigació dels paràmetres que afecten la homeòstasis del BM. Per aconseguir-ho, un hidrogel polimèric de polietilenglicol (altrament anomenat TG-PEG), basat en la polimerització enzimàtica a través de la transglutaminasa factor XIII, ha estat utilitzat per recrear models del BM. En aquest projecte, s'ha explorat la seva naturalesa per tal d'avaluar sistemàticament les contribucions dels components biofísics, cel·lulars i biomecànics del microentorn de la medul·la òssia a la biologia de les cèl·lules mare.

L'envelliment, el trauma o el càncer poden causar pertorbacions en el balanç entre les cèl·lules del BM i el seu microentorn. Aquest treball presenta diferents eines de bioenginyeria per estudiar la naturalesa i la manera en què el microentorn de la medul·la òssia es veu afectat per aquestes patologies. En el futur, investigacions amb aquests models o altres similars permetran plantejar nous objectius clínics de gran rellevància i contribuiran a proposar nous enfocaments terapèutics.

Paraules clau: Microentorn de la medul·la òssia (BM), models de càncer osteotròpic, hidrogels tri-dimensinals biomimètics, cèl·lules estromals de la medul·la òssia, cèl·lules mare esquelètiques, cèl·lules mare hematopoiètiques, microentorn, polietilenglicol.

Acknowledgments

Nobody said it would be easy. This wasn't a dream, and this was only possible for the passion, enthusiasm and work of a ton of amazing people. I could have never done this alone. I may not know many things, but of this I am certain. This thesis belongs to all and each of the people that one way or another- maybe consciously, maybe without even ever knowing it- helped me, helped us. Moltíssimes i moltíssimes gràcies! Thank you very much! Merci vielmal! Let's start with my favorite part, by far, of this thesis that of course could not be short!

Thank you to my thesis committee members for evaluating this thesis and the involved work. Thank you for your passion, your inspiration and your dedication! Thank you **Dr. Simón Méndez-Ferrer**, **Prof. Ivan Martin**, **Prof. Olaia Naveiras**, **Prof. Diego Ghezzi** and my co-thesis directors **Prof. Matthias Lütolf** and **Dr. Martin Ehrbar**. Looking forward to our discussions!

I first and most profoundly want to thank **Martin** for his insatiable commitment to this project (involving first, long days of *in vivo* experiments and later, long nights of writing), for his continuous encouragement and for believing in me throughout the whole adventure. 4.5 years is a long time, and this accumulates a lot of memories and long days together, reaching literally the summit in Snowbird. I'll keep as a treasure our long *in vivo* sessions, one mouse after the other, always clear mind, always excitement, never rush, never stress. Thank you, Martin. I know how much you have given of yourself in each of these projects, and I want to deeply thank you for all of them. It has been a pleasure to be in your team, and I can just wish that our pathways will keep on crossing.

Matthias, thank you for accepting to be my doctoral father. As the name says an inspiration, a source of knowledge, guidance, passion, and always constructive and exciting feedback that truly motivated me time after time. Thank you for all your contributions, our discussions and for always being there! I hope we can celebrate many more accomplishments together!

To the **kicking science-Ehrbar lab** of yesterday and today. The team is all, the team is the power. Thank you all, all, all! Thank you to the beginning with **Philipp** – for setting up an awesome microenvironment in and outside the lab, **Anna-Sofia** – for teaching me how the lab rolls in a awesomely sexy Finnish way, **Stéphanie** – for building up the beautiful PEG backbone, **Vincent** – for sharing with me our 8 seconds of Catalunya Freedom, **Penny** – for sharing the Mediterranean passionate blood & my *in vivo* mentor, to our delicious Greek dinners (which I'll soon compensate with Catalan ones ;), **Ulrich** – for an inexhaustible source of scientific knowledge and inspiration, a true honor to have shared together the everyday passion for our work, **Yannick** – for the best laughs and sun in the deep winter, for the last minute kicking bat figure drawings and for allowing my continuous desk invasion, a pleasure to share in and out the lab so many, many days together, thanks a l*oeö*t, **Eva –** for the Catalan revolution in the lab, this thesis was not possible without you, your incredible devotion to make it possible and your insatiable day to day support és infinit, moltíssimes gràcies!!, pel dia a dia que hem compartit i per tot el que vindrà! To all of you thank you for your immense help and infinite teaching in the lab, and foremost to all the awesome times that together we rocked outside the lab in Zürich and all over the world!! A heartfelt thank you, to you, **Esther** – the pillar of the lab, the $CD34^+$ catcher and the colors of this thesis, your effort and

devotion is a model and inspiration, thank you for all the sweat in each and all of the beautiful stainings that today shine in this thesis. Thank you, **Lisa** – for your contributions to this work, which are multiple, always with exquisite care, **Ali** – for sharing the beautiful Greek sun with tons of *free* wine, **Kathi** – for all the great westerns, and **Aida** – for the inexhaustible TG-strept stock. A very deep thank you to my students who taught me how to teach, **Alex** – un verdader plaer haver treballat, après i rigut tant amb tu i per compartir moments tan bonics dins i fora del lab, **Tabea** – for your devotion at establishing immunostainings, and **Lisa –** the master PhD. A very deep thank you to **Yvonne** and **Corina**, for their shining smile every day, for all the uncountable work always rigorously done with the heart open to just help and enjoy life, a true inspiration. And to **Sybille** for all the laughs and beers waiting for us ;), **Benji** for the warmest smile every time you are around, and **Arik** and **Stefano** for your positive energy. It's truly been the greatest pleasure to share with you every, every day for the last > 4.5 years.

Thank you, **Lütolf's lab** for all your support, especially **Sonja** for our long days at the Fortessa!, and **Andrea** for introducing me to the PDMS molding world.

And to all the **Geburtshilfe team**, thank you **Paula**, **Alex**, **Stefanie** and **Deborah** for sharing our days in the lab. And **Roland** and **Nicole** to make possible the precious cord blood.

To the G floor, the top, the magic! Thank you **Vero** for our long animal experiments, for our amazingly efficient discussions, and less efficient life-talks, and our shared late nights, especially on the last days of this thesis repairing the flow cytometer and life itself, you truly gave me a heartfelt company. Thank you **Norman** for the repeated BLI injections, a mistery that will never be revealed, with always patience and happiness. Thank you **Matthias** for every Schnitzel we have shared and for always motivating me! Also thank you, **Lara** – your FACS inside, a wealth of knowledge, **Asuka** – from cord blood isolation to Japanese best tips, **Francisco** – early mornings at the animal facility, **Renier** – the blood of the G floor, **Patrick** – a reliable weekend company, **Syndi** & **Nicole** – always helpful, **Ute** & **Stephan** & **Patrick** – for our bonding FACS experiences when it all started, **Álvaro** – for sharing the love for Girona i temps de flors. Thank you all!

To all the USZ collaborators, thank you! **Claudia**, thank you for a PCR and later on a Bioanalyzer introduction that finished in a beautiful friendship! To **Dr. Simon Bredl** and his team, thank you for those precious NSG mice. To **Flora** and **Thea** for always facilitating all the long *in vivo* experiments. To **Paolo** for having always the microCT doors open to us.

Thanks to all the core facilities for sharing your knowledge and making it all so easy! Thank you **Gosia** for teaching me FACS, and thank you, **Isabel** and **Andrés** for the SEM hydrogel adventure.

And thank you to so many labs and so many people that made this long trip happen:

Martin's lab – thank you **Ivan**, **Arnaud**, **Andrea**, **Paola**, and **Chiara** for supplying us with human cells, and passionate discussions. A lot more to come!

Fischbach's lab – thank you **Claudia**, **Aaron** and **Matt** for a great, fruitful and exciting collaboration. Thank you to all the team for hosting me at Christmas and sharing the magic in *gorges* Ithaca!

Deplancke's lab – thank you **Bart**, **Magda**, **Daniel** and **Vincent** for exciting us with the BRB-RNA seq and so much more. A pleasure to have shared beautiful days at EPFL together!

Naveiras' lab – **Olaia**, **Shanti**, **Mukul** and **Naveed** thank you for your help with NSG transplantation, and sharing your immense knowledge. Your passion in all and each of the projects is truly contagious.

Bornhauser's lab – thank you **Beat**, **Gabriele** and **Danaelle** for the leukemia cells and exciting discussions.

Zenobi-Wong's lab – thank you **Marcy**, **Nico** and **Emma** to board in the HA/PEG project together, and for your longtime friendship.

Weber's lab – thank you **Franz** for all the BMP-2, **Chafik** and **Ana** for always supporting in any and all the ways.

Thanks from the bottom of my heart to **all the collaborators** that contributed scientifically to this work reflected today in these figures, or with trials that helped us have these figures. To all the collaborators that always answer to our ideas and sometimes crazy experiments with a "Yes, of course, let's do it!". I could not finish this thesis with the biggest of the smiles if I would not have crossed my path with you, and shared our passions for science, for the unknown and for the whole adventure of learning.

To the **SSB+RM** and all the EC committee members to include me in this stimulating adventure! And to the **YS team**, especially **Emma** and **Letizia**, for sharing the excitement of learning!

Also to the amazing **EPFL** administrative team, especially **Sonja** and **Sandra**, always there to make it all the easiest, with the greatest smiles and warmth!

To all the cover **chapter artists** that enthusiastically decorated this thesis with a touch of beauty from all over the world! Thank you, **Spencerito**, **Aaron**, **Iaia**, **Pol**, **Mars**, **Anna**, **Anneta**, **Joan**, **Biel** i **Vallma**, sou uns artistes! I a tu, **Raül** per no deixar-me anar amb pantumfles al casament!

To all the amazing trips and adventures that accompanied me in this incredible step of my life, definitely **Catalunya** & **New Orleans** take the gold medal. A l'**1-O** i a la llibertat, un tresor històric que tornarem a fer. And to all the music and concerts that played intensively and happily throughout this work, **Manel**, **Txarango**, **Mumford and Sons**, **The Lumineers, The Cat Empire** and **Trombone Shorty**. I a la **Competència** per a una bona hora al dia de riure assegurat!

To the **Heritage Deli Fan Club** for adding fantasy to my PhD, and for the greatest parties together! Thank you **Kevin** for your continuous support and for our awesome friendship! And thanks, **Dan** for your support and for always exciting our lives! Thank you **Naomi** and **Nupura** for your friendship and our valuable moments together!

Züri people, **Laurent**, **Anna**, **Marcello**, **Outi**, **Julien**, **Addy**, **Luca**, **Kessi**, **Michela**, **Gemma**, **Christian**, thank you for getting me out of the lab!

Anna, la teva energia, el teu bon humor, la teva manera d'encarar la vida i pa'alante, una inspiració verdaderament difícil d'igualar. Durant aquests quatre, de fet cinc últims anys, valoro moltíssim la

teva capacitat d'entendre'm a la perfecció i de fer-ho tot possible. De tot cor, gràcies. **Joan**, nous projectes com mojitos ready-to-use esperen inventor! Som-hi!

Tites i tetes, les meves tites i tetes! Gràcies, moltíssimes gràcies per cada excusa que m'ha fet venir un cap de setmana a Catalunya, perdre la veu i ser la persona més feliç del món rodejada de tots vosaltres, sou el sol i l'energia necessària per viure. A la **Rosa** i en **Sergilin** – per tot, l'**Aina –** support incondicional, la **Diana** i en **David** – sempre a punt amb un somriure, la **Sandra** i en **Canete** – junts per Zürich, la **Núria**, en **Sergi** i la **Gal·la** – la Deutsch connection, la **Rut** i en **Linares** – les grans trobades garrotxines, en **Lluís** – cada ritme una història, l'**Alba** – moments de túlipes i surf, l'**Àlex** i la **Lara** – les converses que tant enyoro, en **Fede** – l'emprenedor de debó, en **Màrius** – tots amb la mateixa nota, en **Paton** i la **Judit** – el primer casament, la **Laura** i en **Peke** – olors delatants, en **Jaume** – el Sant Joan Boreal, la **Frans** – les grans nits a Barna, moltíssimes gràcies! Em moro de ganes d'abraçar-vos!

To my new greatest **American family**, thank you so much, sexy buddies! For the hugs with big and less big boobies, for the smiles, for the amazing parties, for being close despite the distance, for helping me pipette in the lab, for keeping Cucu company while I was spending long hours in the lab, for understanding me so well, for being with me in each and all the big moments. **Christensens** and **Millans**, I love you a lot! Thanks **Miguel** for ensuring every NOLA trip would be unforgettable! Thanks **Max** – for spicing up Zürich and Barcelona together, **Marcel** – for our traditional bonding Xmas trips together, **Maddox** – for showing *La Mirona* in Girona how to dance!, and **Spencer** – for sharing delightful summer days together floating down the river. Thanks **Mark** for your generosity and huge heart! Thank you, **Eddy** for all the amazing trips and for always being so close to us! Thank you, **Christina** for so much, for everything, for making the Ithaca adventure possible, and for triggering and inspiring, with your magnificent gift for language, nearly every word of this thesis. Sexy **Lizzy**, thank you very much for all your unconditional and continuous support! Thank you and **Dave** for all the amazing trips together all over the world! Now, ready for more surprises!

A tota la gran **família**, a tots i cadascú de vosaltres. Què hauria estat sense vosaltres? Sense les tantes celebracions tots junts, sense els nostres jocs i trampes, sense el saber que sempre, sempre us tinc al costat. Cada dia, lluny o a prop, us porto amb vosaltres i en els moments més durs d'aquesta tesis, que n'hi han hagut, sempre podia pensar en un moment nostre, en la celebració del cap de setmana següent, en una visita a Zürich, i de cop tot era més fàcil! Gràcies per ser la millor família del món, em moro de ganes de celebrar-ho amb vosaltres, perquè avui sóc aquí gràcies a vosaltres! **Tieta Maria Àngels** i **Carla**, gràcies pels missatges sempre de suport i carregats d'amor. Gràcies, **tiet** i **tieta Rosa** per sempre ser tan a prop malgrat la distància i per les grans festes i tiberis a casa vostra! I a tu **Pol**, gràcies per compartir tants dinars a casa la iaia, i jocs que ens han fet bellugar la ment, però que junts hem superat, amb més o menys trampes! Gràcies, **tieta Carme** i **José Luís** per la vostra visita a Zürich, i per compartir el nostre dia a dia, i pels tant moments a Catalunya, espontanis com la vida! Gràcies, **Anna**, per ser tu, per sempre entendre'm a la perfecció i per decorar aquests darrers 4 anys i mig de moments inoblidables, tot va començar amb la trepidant visita sorpresa a Zürich amb en **Joan**, seguit del gran casament (quin gran dia!), i una mica

després el regal més preciós: en **Biel**. El teu suport incondicional des de que érem ben petites i jugàvem a Júlies i Helenes m'ha acompanyat en tot moment. Anna, ets el meu model i si avui estic celebrant aquesta gran fita és gràcies a tu, gràcies a tot el que m'has ensenyat des de tan petita!, incloent la caiguda del cutxet! **Iaia**, muchísimas gracias por tus abrazos, por tus saltos cada vez que venía de sorpresa. Gracias iaia, por ser tú y el **avi**, si tú estás el avi está y las dos sabemos que se está riendo de mí, con su peculiar sonrisa de orgullo e ilusión. Gracias por todo, iaia, por habermelo dado todo, y sobretodo por haberme enseñado los verdaderos valores de la vida que me han hecho hoy llegar aquí. **Mireia**, gràcies per tot, especialment per fer possible les visites a Zürich sempre amb un gran somriure (tot i estar traginant caixes a les 4 am) amb una capacitat inigualable per a sorprendre. I encara més, gràcies per assegurar-te que la nostra nevera suïssa sempre tingués fuets.

La casa, la família, tots 4, l'aventura dels Vallmajó-Martín: gràcies per sempre i per tot. Per ensenyar-me el camí, per emplenar-me la motxilla fins a dalt de tot amb totes les eines més necessàries, per obrir-me la llum a cada etapa del gran viatge i per esperar-me sempre amb els braços ben oberts a qualsevol lloc i en qualsevol moment. No seria aquí sense vosaltres, de debó. El que avui celebrem us ho dec a vosaltres, absolutament tot. Sou vosaltres els qui m'heu donat els valors, l'energia i l'entusiasme necessari per afrontar la vida al màxim i sempre voler-ne més. **Mama**, poc sabies com aniria tot quan jugàvem al Quién es Quién, però el teu amor incondicional, el teu esforç immesurable no podia fallar, i has construït la família més bonica del món. Tan se val si a Girona, Barcelona o Zürich, sempre sé que em pots despertar cada matí! **Papa**, tu em vas ensenyar a pensar més enllà dels problemes de mates, a fer servir paraules refinades a la prosa, i de tu vaig aprendre a aprendre, aprendre, aprendre, ens ho podran treure tot, però mai el coneixement, l'après morirà amb nosaltres. **Oriol**, Vallmeta, l'altre OVM, el segon ;) o el primer a vegades, sempre a prop, sempre disposat a més i a tot, amb tu ho he viscut tot, totalment tot, amb tu he après la vida, des dels estius portant el nostre restaurant, a les grans festes i les trucades nocturnes (uns al lab, altres de festa), gràcies per sempre ser aquí amb mi. Us estimo moltíssim!!

I és clar, a en **Punket**, the real inspiration, the secret that I haven't lost 50 kg in the last 4.5 years, the secret for having my clothes clean (almost all of the time!) and never needing a commando experience!, the secret to the greatest words and awesomeness in this thesis, the secret to many experiments, the secret I made it to the lab every morning awake, the secret of many more that will remain secret! Titi, thank you. I know no words can describe the effort you have made for me during this incredible moment of our lives. This PhD is for both. And this journey was only possible with your unconditional love, bottomless support and infinite hard work. Thank you for always maintaining and enhancing all the stem cell potential, but mostly for the differentiating surprise of its 18M commitment on the best day (yet!) of our lives. Potential and commitment may no longer be mutually exclusive. Per tots els grans moments i aventures junts que ens esperen! T'estimo mooooltíssim!

Per als que aspiren cada dia a l'impossible,

per a una idea, per a un somni, per a una dificultat, per a quelcom.

Tot està per fer i tot és possible. Som-hi!!

List of abbreviations

Abbreviation	Definition
2D / 3D	Two / three dimensional
ALL	Acute lymphoblastic leukemia
ALP	Alkaline phosphatase
AML	Acute myeloid leukemia
Ang-1	Angiopoietin-1
ANOVA	Analysis of variance
ARS	Alizarin red S staining
ASC	Adipose-derived stromal cell
ATP	Adenosine triphosphate
B-ALL	Acute B lymphoblastic leukemia
BCSP	Bone, cartilage, stromal progenitor
BM	Bone marrow
BMP-2	Bone morphogenetic protein-2
BMSC	Bone marrow stromal cell
BSA	Bovine serum albumin
CAR cells	CXCL12-abundant reticular cells
cbHSPCs	Cord blood-derived hematopoietic progenitor stem cell
CD	Cluster of differentiation
CFU	Colony-forming unit
CFU-F	Fibroblasts colony-forming unit
CLSM	Confocal laser scanning microscopy
CMP	Common myeloid progenitor
Col	Collagen
CSF-1	Macrophage colony-stimulating factor
CT	Computed tomography
CXCL12	CXC motif chemokine 12
DAPI	4',6-diamidino-2-phenylindole
DLL4	Delta-like ligand 4
DMEM	Dulbecco's modified eagle medium
DNA	Deoxyribonucleic acid
e-BCSP	Expanded BCSP
e-SSC	Expanded SSC
EC	Endothelial cell

ECM	Extracellular matrix
EDC	1-ethyl-3-(3-dimethylaminopropyl)carbodiimide
EDTA	Ethylenediaminetetraacetic acid
EPO	Erithropoietin
FACS	Fluorescence-activated cell sorting
FBS	Fetal bovine serum
FC	Flow cytometry
FC	Fold change
Fc	Fragment crystallizable
FDR	False discovery rate
FGF-2	Fibroblast growth factor-2
FL	Fetal liver
Flt3L	FMS-like tyrosine kinase 3 ligand
FMO	Fluorescence minus one
FXIII	Blood coagulation factor XIII
G-CSF	Granulocytes colony-stimulating factor
GAG	Glycosaminoglycan
GEMM	Granulocyte, erythrocyte, macrophage and megakaryocyte
GF	Growth factor
GFP	Green fluorescent protein
Gln	Glutamine
GM	Granulocyte and macrophage
GM-CSF	Granulocyte macrophage colony stimulating factor
GMP	Granulocyte-macrophage progenitor
GO	Gene ontology
H&E	Hematoxylin and eosin
HA	Hyaluronic acid
HA/TCP	Hydroxyapatite/β-tricalcium phosphate
HBSS	Hanks' balanced salt solution
HEPES	Hydroxyethyl piperazineethanesulfonic acid
HMDS	Hexamethyldisilazane
HRP	Horseradish peroxidase
HSC	Hematopoietic stem cell
HSPC	Hematopoietic stem progenitor cell
HUVEC	Human umbilical vein endothelial cell
IF	Immunofluorescence

IgG	Immunoglobulin G
IHC	Immunohistochemistry
IL	Interleukin
IMDM	Iscove's modified Dulbecco's medium
LDL	Low density lipoprotein
LIF	Leukemia inhibitory factor
Lin	Lineage
LT-HSC	Long-term hematopoietic stem cell
Lys	Lysine
MC3T3	Murine osteoblast cell line
MDA-MB-231	M. D. Anderson metastatic breast cancer cell line
MEF	Murine embryonic fibroblast
MEMα	Minimum essential medium alpha
MLP	Multilymphoid progenitor
MMP	Matrix metalloproteinase
MP	Movat's pentachrome
MPP	Multipotent progenitor
mRNA	Messenger ribonucleic acid
MSC	Mesenchymal stem cell
MyelP	Myeloid progenitor (FACS marker)
NK	Natural killer
NMR	Nuclear magnetic resonance
NSG	NOD/SCID gamma
OP	Osteoporotic
P/S	Pennicillin/streptomycin
PBS	Phosphate-buffered saline
PDGF-BB	Platelet derived growth factor-BB
PEG	Poly(ethylene glycol)
PFA	Paraformaldehyde
RT-qPCR	Reverse transcription quantitative polymerase chain reaction
RNA	Ribonucleic acid
ROI	Region of interest
RT	Room temperature
SCF	Stem cell factor
SD	Standard deviation
SDF-1	Stromal-derived factor-1

SEM	Scanning electron microscopy
SEM	Standard error of the mean
SSC	Skeletal stem cell
ST-HSC	Short-term hematopoietic stem cell
TCEP-HCl	Tris(2-carboxyethyl)phosphine hydrochloride
TCP	Tissue culture plate
TEA	Triethanolamine
TG	Transglutaminase
TGF-β	Transforming growth factor β
TPO	Thrombopoietin
UBC	Ubiquitin C
VCAM	Vascular cell adhesion molecule-1
VEGF-A	Vascular endothelial growth factor-A
VS	Vinylsulfone

Table of contents

List of figures and tables

CHAPTER 1

CHAPTER 2

CHAPTER 3

CHAPTER 4

CHAPTER 5

CHAPTER 6

CHAPTER 7

Nothing in life is to be feared,
it is only to be understood.
Now is the time to understand more,
so that we may fear less. – Marie Curie

Artwork by Spencer Christensen
Washington, CT, USA

Scope of the thesis

Motivation

The human skeleton is often not fully appreciated for its remarkable contributions to the maintenance of homeostasis in the body. While the outer surfaces of bones provide muscle anchorage sites that enable the body's locomotion, it is in the microstructure of the bone cross-section that the true marvel of these organs lies – the bone marrow (BM). Home to hematopoietic stem cells (HSCs), that sustain the body's hematopoietic system over the course of an entire life, as well as bone marrow stromal cells (BMSCs) which drive bone formation and vascularization, the BM itself is an intricate and tightly regulated organ. This delicate intricacy speaks to the significant challenge presented to those who wish to study its architecture and function. This is especially detrimental considering shifts from homeostasis in the BM microenvironment, or niche, contribute to the propagation of a myriad of severe clinical pathologies such as hematological malignancies or bone disorders. Disruptions of this tightly controlled balance can be attributed to aging, trauma, or cancer. Studying the nature and manner in which such niche components are affected by pathologies will no doubt highlight key clinically-relevant targets and inform novel therapeutic approaches.

The discovery of impactful therapeutic and regenerative strategies for BM-related diseases necessitates the development of more accurate preclinical models that permit higher throughput screening of parameters affecting BM homeostasis. Despite tremendous advances in more complex genetically modified mouse models that recapitulate BM pathology, two prominent barriers to realizing clinical benefit remain: i) elucidating individual contributions of altered niche factors in these models is a considerable challenge owing to the dynamic complexity of the bone marrow, and ii) poor translation of murine findings to human. Models that capture the interplay between human marrow resident cells and their niche, and which permit the systematic study of niche component roles, could provide quintessential clinical benefit. For this, the development of 3D models comprising cellular niche components, such as BMSCs, HSCs and endothelial cells (ECs) and soluble niche components such as cytokines, chemokines and growth factors known to be present in the native microenvironment, have been of paramount importance enabling the study of the human BM niche *ex vivo*. Pioneering work has shown that natural hydrogels, such as collagen and fibrin, due to their high water content and viscoelastic properties, mirror important architectural qualities of the native tissue. Though these materials exhibit biocompatibility and promote many cellular functions, their inherent biological activity, batch-to-batch variability and fixed biophysical properties limit their suitability for the systematic evaluation of stem cell niche factors. Moreover, due to omission of key functional components, *ex vivo* models have repeatedly failed to fully recapitulate the BM niche, and thus, hamper their evaluation in a clinically relevant setting.

Aware of these current limitations and set to overcome them, in this thesis we propose the utility of fully defined matrices to study stem cell functions and to engineer bone marrow models *in vivo* in a xenograft model.

Specific aims

The overall aim of this project is to engineer humanized 3D bone marrow models in well-defined matrices and to systematically evaluate the role of biophysical, biochemical and cellular niche components in order to gain further insight in stem cell biology.

Biophysical properties can be assessed elegantly by engineering ECM-inspired synthetic hydrogels. Our lab pioneered the development of an enzymatically crosslinked poly(ethylene glycol) (PEG)-based hydrogel, named TG-PEG. Unlike natural hydrogels, TG-PEG allows easy tuning of its biological and mechanical properties in an independent fashion. Specific **biochemical effects** of the BM niche can be subsequently assessed. It has been previously shown that delivery of osteogenic factors such as bone morphogenetic protein-2 (BMP-2) can induce a host BM niche when subcutaneously implanted in nude mice. Taken one step further, and with the aim to develop a humanized model, **cellular participation** in the development and maintenance of the BM niches can be evaluated. Multipotent nonhematopoietic stem cells within the bone marrow stroma, referred as bone marrow stromal cells (BMSCs), were first described in the work of Friedenstein in the 1960s. Their key role in orchestrating the BM niche was rapidly validated, and their regenerative potential promptly explored. Recent discoveries have provided even further classification of a strict stem population within the BMSCs which gave rise to the definition of skeletal stem cells (SSCs).

To achieve the outlined research goal, this thesis addresses the following specific sub-aims:

1. **To interrogate the *in vivo* potential of skeletal stem cells using fully defined microenvironments.** Up to now, scaffolds of natural materials have been used to transplant SSCs *in vivo*. However, inherent biological properties and batch-to-batch variabilities affect and obscure endogenous stem cell functions. In order to interrogate the intrinsic bone marrow-inducing and osteogenic functions of stem cells, we propose to engineer mechanical and biological properties of synthetic PEG-based hydrogels.

2. **To engineer humanized functional bone marrow niches to study osteotropic cancers *in vivo*.** Leukemia and other blood-related cancers alter the bone marrow microenvironment resulting in long and often incurable malignancies. In addition, the bone marrow is the preferential site of breast, prostate and lung cancer metastasis. The goal of this work is to develop *in vivo* models for the study of potentially unknown interactions between cancer cells and the human bone stroma.

3. **To improve transplantation and engraftment efficiency of stem cells by tailoring biomaterial properties.** To unfold their full regeneration potential, stem cells must be shielded from potential adverse reactions upon host implantation. The goal is to engineer novel biomaterials that optimally support the engraftment of hBMSCs upon transplantation and yet allow cells to remodel the carrier matrices into BM organoids. With this, we aim at understanding what are the minimal needs of the cells during transplantation to translate this knowledge to the clinics.

4. **To study factors that control the *in vitro* expansion of hematopoietic stem cells in engineered hydrogels**. HSCs rapidly differentiate *in vitro* and lose their capacity to reconstitute the hematopoietic system, hampering their *ex vivo* expansion for further clinical use. Our goal is to study niche parameters that control the expansion and differentiation of HSCs by employing rationally designed synthetic hydrogels.

Thesis outline

This thesis contains seven chapters where we demonstrate that fully defined synthetic matrices can serve as BM niche analogues. In **Chapter 1**, the history and discoveries of the BM microenvironment are discussed. Only after understanding i) the myriad of cells resident in the niche and their multiple interactions, ii) the difficulties associated with stem cell characterization, and iii) the limited access to these human niches, will we be able to design smart biomaterials to accurately recapitulate this niche and serve as a tool for basic research and clinical translation.

Adult SSCs are a recently discovered resident cell type of the BM niche that exhibit promising regenerative potential. However, the definition and characterization of *bona fide* SSCs is not trivial. Motivated by the recent discoveries, in **Chapter 2** we decided to isolate strictly defined murine SSCs and evaluate their potential to regenerate critical size bone injuries in a calvarial defect model when transplanted in minimalistic scaffolds.

Next, eager to progress these findings towards clinical translation, we decided to employ human BMSCs. One limiting factor precluding the exclusive use of SSCs for treating bone defects in humans are the high cell numbers needed. The selection of SSCs among a population of hBMSCs would simply yield too few cells for such therapies. But, do hBMSCs comprise sufficient stem cells? To answer such a question is not a frivolous task, so **Chapter 3** endeavors this duty. Early results crystallized that functional stemness assays can only be performed *in vivo*. Therefore, by defining controlled matrices and systematically uncoupling biochemical and biophysical cues, we sought to establish an *in vivo* model to assess hBMSC stem cell potential.

Motivated to recapitulate the human bone marrow niche to study human malignancies, in **Chapter 4** we engineered 3D biomimetic hydrogels combined with hBMSCs and BMP-2 to develop functional bone organoids. After optimizing biophysical and biochemical conditions, we employed

these bone marrow organoids to study the dissemination of leukemic cells and metastatic breast cancer cells into these humanized niches.

Chapter 5 explores the combination of two hydrogel materials, one synthetic and one natural, that utilize a shared crosslinking mechanism. The unique chemistries involved allow seamless integration of a natural ECM component in the scaffold without compromising control over its biochemical properties afforded by the synthetic component. We showed that we can tune the properties of the hybrid scaffold to optimize proliferation versus differentiation of hematopoietic stem and progenitor cells (HSPCs). In addition, remarkably, the hybrid approach improved hBMSC transplantation efficiency *in vivo*, which is a major limitation of current clinical trials involving this particular cell type.

Intrigued by the equilibrium of proliferation and differentiation of hHSPCs, we sought to model this balance by making use of our rationally design 3D hydrogel system in the work depicted in **Chapter 6**. This enabled a systematic approach to evaluate the effect of microenvironment stiffness and presentation of cell-matrix ligands on HSCs during *in vitro* expansion. The optimized parameters were eventually validated *in vivo*.

We have learned a lot on the way and we believe that these findings provide a solid foundation on which to build in future research. Yet, there remain a plethora of open facets to explore. Where is the field heading? What are the remaining limitations that currently hamstring the potential of the presented approaches? Can we engineer more tools to speed up the discovery and optimization process? How close are we to clinical translation? These and other queries are discussed and debated in **Chapter 7**.

Que les coses que esperes
no siguin com esperes
quan les visquis. – Txarango

Artwork by Aaron Kaufman
Brooklyn, NY, USA

CHAPTER 1

The bone marrow niche

Hematopoietic stem cells (HSCs) reside within the bone marrow (BM) in a tightly controlled local microenvironment, referred to regularly as the HSC or BM niche[1]. There are distinct types of hematopoietic stem and progenitor cells suggested to reside in coexisting specialized niches created by multiple cell types that contribute to its maintenance. The key function of this niche is to regulate stem cell activity in order to adapt to the tissue demands ranging from homeostasis to differentiation. This still enigmatic niche orchestrated by cells and biochemical and biophysical cues regulates the quiescence, proliferation and differentiation of HSCs. In this dynamic environment, HSCs can continuously communicate in multiple ways including specific binding to components of the extracellular matrix, cell-cell interactions as well as soluble growth factors and other signaling cues. Identifying and harnessing these crucial regulators will be key to designing stem cell therapeutics and *ex vivo* strategies to expand and maintain HSCs.

Cellular components of the bone marrow niche

In 1978 Ray Schofield formulated the first hypothesis of a stem cell niche regulating HSC function when noting that the spleen was not capable of supporting HSCs in the same manner as the bone marrow[2]. Many studies have built upon this hypothesis since then, and many cell types have been associated with this niche. Cell types include mesenchymal stem cells (MSCs) which contribute to bone homeostasis, together with osteoprogenitors, osteoblasts, osteocytes and chondrocytes. However, other stromal cell populations including neuronal cells, glial cells, and adipocytes are known to participate as well. It is also known that the bone marrow is highly vascularized, so endothelial cells and their role in the niche have also been investigated[3] (Figure 1).

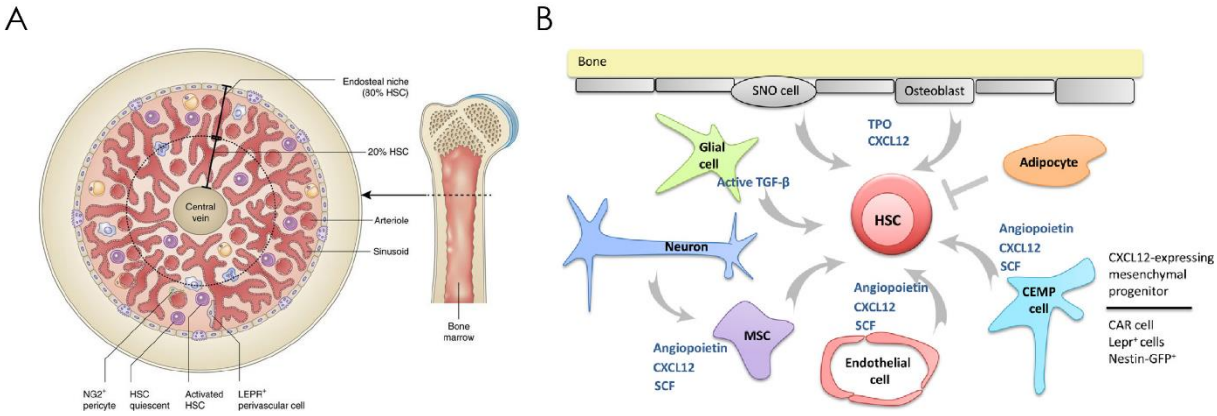

Figure 1. The bone marrow stem cell niche

(**a**) Cross-section area of the bone marrow showing that 80% of the HSCs are located close to the endosteal niche, while the rest 20% are in the perivascular area close to sinusoids. This image was adapted and reproduced with permission from Mendelson et al.[4]. (**b**) Complex and dynamic environment containing key cell types which regulate HSC maintenance through distinct and common molecular regulators. Several stromal cells have been implicated in hematopoietic stem cell (HSC) maintenance in the bone marrow via different factors. For instance, endothelial cells, mesenchymal stem cells (MSCs), and chemokine CXC ligand (CXCL)12-expressing mesenchymal progenitors (CEMP cells) produce several factors including CXCL12, angiopoietin, and SCF. CEMP cells include several stromal populations such as CXCL12-abundant reticular (CAR) cells, leptin receptor$^+$ stromal (Lepr$^+$) cells, and Nestin-GFP$^+$ cells. From the endosteal region there is also HSC regulation by osteoblasts and spindle-shaped N-cadherin$^+$ osteoblast (SNO cells) which produce thrombopoietin (TPO) as well as CXCL12. Next, sympathetic neurons indirectly regulate HSCs via MSC regulation, and glial cells produce active transforming growth factor (TGF)-β, as well HSC regulator. Last, adipocytes negatively regulate HSC dynamics. This image was adapted and reproduced from Anthony et al.[3] with permission from Elsevier.

Hematopoietic stem cells

Hematopoietic stem cells (HSCs) are the only cells capable of self-renewal and of giving rise to all blood cell lineages throughout life (Figure 2 a). HSCs can be found in the BM, cord blood and peripheral blood. HSCs are a rare population estimated to represent only a 0.01% of all nucleated cells in the bone marrow. The characterization of HSCs *in vivo* via the identification of a single distinctive cell marker has yet to be established. Thus, combinations of different markers have been proposed to isolate HSCs and characterize the hematopoietic population, for both murine and human species.

Murine HSCs were found to be Sca1^{+} and c-Kit^{+}, and negative for a selection of markers of mature hematopoietic cell lineages known as lineage cocktail (typically B220, CD4, CD8, Gr-1, Mac-1 and TER119)[5,6]. This leaves the c-Kit^{+} Lin^{-} Sca-1^{+} population, known as KLS. However, this population is not stringent enough and can also contain progenitor cells. Therefore, new markers have been proposed such as CD150^{+} CD48^{-} CD41^{-} (SLAM family markers)[7], CD34^{-} CD135^{-}[8,9], CD38^{+}[10] or Hoechst 33342 side population (SP)[11] among others.

In contrast, human HSCs were first identified within the CD34^{+} population[12]. Later on, it was shown that primitive hematopoietic cells that tend to lose their self-renewal capacity and become more committed to differentiate, concomitantly increase their expression of the CD38 antigen[13]. Another marker of interest for HSC definition is CD90 (known also as Thy-1). It was recently shown that only CD34^{+} CD38^{-} CD90^{+} Lin^{-} cells could reconstitute the immune system long term, while CD34^{+} CD38^{-} CD90^{-} Lin^{-} cells had the ability to produce all blood lineages but only for a limited time[14]. Thus, CD90 expression determined the presence of two distinct HSC populations: short-term (ST-HSC) and long term (LT-HSC). Other markers have been associated with HSCs such as CD133^{+} CD7^{-}[15], CD45RA^{-} CD71^{-}[16] and CD49f^{+}[17]. Recent studies integrating flow cytometric and transcriptomic data at single-cell resolution have challenged the classical hierarchical tree-like model of the HSC differentiation towards lineage commitment and proposed a continuous process instead[18,19] (Figure 2 b). However, there has yet not been an ultimate agreement on which are the defining markers, pointing to the fact that the term defined today as HSC might contain a fairly heterogeneous population of cells.

Despite numerous advances in HSC characterization and the discovery of new markers, the ultimate essential criteria to dub a cell as an HSC is its capability to repopulate the entire hematopoietic system as long as a lifetime. And, even more stringent for this characterization is the single cell's ability to reconstitute further hematopoietic systems in serial transplantations.

The exact physical location of the HSCs within the niche is still under debate (Figure 1 a). New imaging techniques and the discovery of new HSC markers are enhancing the disclosure of insights from this black box. In 1975 it was pointed out that HSCs were in close contact with the endosteum, the cellular lining separating bone from bone marrow[20]. More recently it has been corroborated that HSCs localize close to the endosteal lining of bone marrow cavities in trabecular regions, while the more differentiated hematopoietic progenitors are mainly found in the central bone marrow cavity, close to the central vascularization[21,22]. In contrast, other studies have shown that HSCs are mainly found in perivascular regions near bone marrow sinusoids, which are small blood vessels formed by fenestrated endothelium to allow for rapid exchange between the blood stream and the surrounding tissue[7,23]. The discrepancy between these findings might be due to different selection criteria for the HSC subsets and indicates the potential presence of unique niches for specific HSC populations.

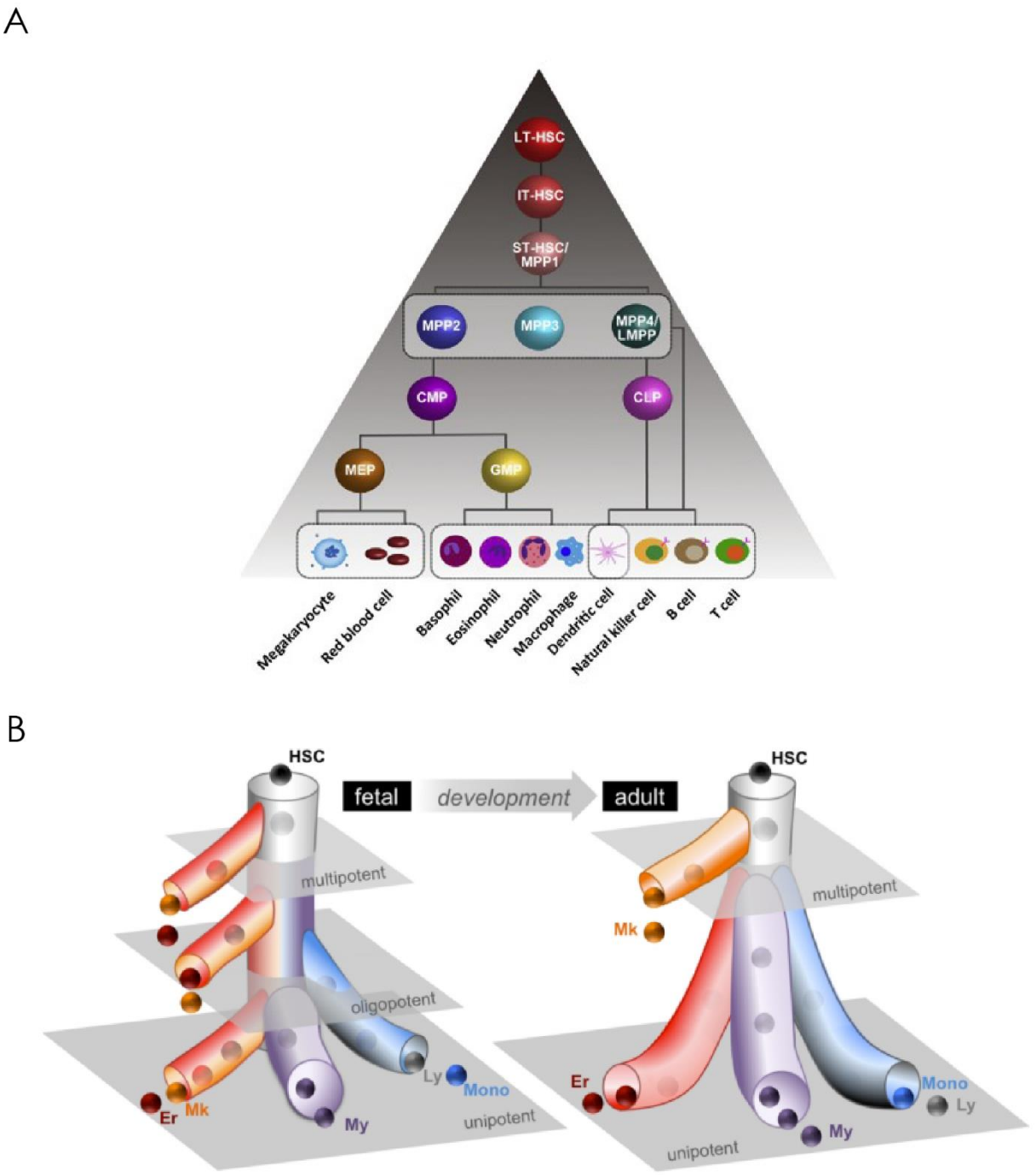

Figure 2. The hematopoietic hierarchy: discrete vs. continuous differentiation

(**a**) Schematic showing the classical hematopoietic hierarchy from stem cells to terminally differentiated cells, passing through the progenitor cells. Long-term (LT-HSCs), intermediate-term (IT-HSCs) and short-term HSCs (ST-HSCs) are all multipotent cells but differ in their self-renewing abilities. HSCs differentiate into MPPs, multipotent progenitors with limited self-renewal but transient multilineage reconstitution. MMPs consist of different subpopulations that can give rise to CMPs, common myeloid progenitors, or CLPs, common lymphoid progenitors, respectively. In turn, CMPs can produce mature hematopoietic cells via MEP (megakaryocyte/ erythroid progenitor) and GMP (granulocyte/macrophage progenitor) stages. While, CLPs yield mature lymphocytes. This image was adapted and reproduced from Zhang et al.[24] with permission from Elsevier. (**b**) Representation of the continuum-based model for BM hematopoiesis, redefining the classical hierarchical view. This models proposes that upon adulthood there are two-tier hierarchy and a continuous landscape of human steady-state hematopoiesis, rather than discrete organized populations. This image was adapted and reproduced from Notta et al.[19] with permission from The American Association for the Advancement of Science.

Non-hematopoietic cells

Osteoblasts

The endosteal surface of bone and cells of osteoblastic lineage were shown to participate in regulating the HSC population (Figure 1). These findings localized HSCs in close proximity to the endosteum. Several studies displayed that an increase in osteolineage cells lead to an increase in HSCs[21,25]. However, whether this was a result of direct cell-cell interaction or indirect effect through the secretion of soluble factors yet remains controversial. Further research pointed that less differentiated osteolineage cells could support the HSC population better than more committed osteolineage cells[26]. Thus, the apparent discrepant data of how these cells interact with the niche might be simply attributed to the heterogeneity of osteolineage cells.

Endothelial cells

Since HSCs were also located in the perivascular region, vascular and stromal cells residing in this area have been considered as potential candidate niche cells. More specifically, the adhesion molecule E-selectin, only expressed by BM endothelial cells, was suggested to promote HSC proliferation[27]. Next, endothelial cells have been proposed to contribute to HSC maintenance through production of the stem cell factor (SCF or Kit ligand)[28] and also to LT-HSC expansion by angiocrine expression of Notch ligands[29].

Bone marrow stromal cells (BMSCs) /MSCs

In mice, the perivascular region contains multiple MSC-like niche candidate cells. Mendez-Ferrer et al. identified that nestin$^+$ MSCs reside in close conjunction with HSCs and adrenergic nerve fibers, and that the selected MSCs expressed HSC maintenance genes[30]. Interestingly, these genes were downregulated during induced HSC mobilization, indicating a dynamic partnership between nestin$^+$ MSCs and HSCs. Even more, these nestin$^+$ MSCs were shown to directly respond to signals from the sympathetic nervous system (SNS). Via this network, the SNS transduces circadian information to the bone marrow microenvironment stipulating that the SNS, both directly and through stromal cells, regulates HSC behavior[31]. Other potentially involved stromal cells are the Leptin receptor (Lepr)-expressing perivascular cells, whose production of SCF seems essential for HSC maintenance in the bone marrow[28].

Another stromal cell type of interest is the CXCL12-abundant reticular cell (CAR). CAR cells are fibroblastic reticular cells that are defined by high expression of the CXC chemokine ligand 12 (CXCL12), also known as stromal-derived factor-1 (SDF-1). CAR cells are the major source of SCF and CXCL12 in the bone marrow. A recent study confirmed the importance of CAR cells demonstrating that lack of these cells induced a reduction in HSCs and HSC long term repopulating

activity, concomitant with increased HSC quiescence[32]. It was further corroborated that HSCs make direct physical contact with the CAR cells found near the sinusoids and the endosteum[33].

For **human** counterparts, STRO-1 was found to be expressed in BMSCs capable of supporting hematopoiesis[34]. Later, Sacchetti and co-workers elegantly showed for the first time the presence of skeletal progenitors in the bone marrow, a subset of BMSCs, marked by CD146 or MCAM surface expression[35]. $CD146^+$ cells, when seeded in an osteo-conductive scaffold, could ectopically form a hematopoietic microenvironment (i.e. human bone organ) in mice. Moreover, they showed that the functional characterization of these cells was only possible *in vivo*, since these cells in tissue culture plates (TCP or 2D) rapidly lose their phenotype. Remarkably, these discoveries led to controversies in the definition of the MSC-term necessitating additions to the minimal criteria of plastic-adherence and tri-lineage differentiation capacity (osteogenic, adipogenic and chondrogenic) *in vitro*[36-38]. Initially, the therapeutic potential of MSCs rapidly gained popularity and hype, though most would say too fast[39]. Over these last years, thorough experimental scrutiny has led to the undoubtful conclusion that the term "MSCs" as commonly reported in the literature is unmerited, and that it often erroneously refers to heterogeneous mixtures of cell populations containing stem and differentiated cells[40]. Insufficient markers to strictly characterize them, along with the absence of functional stemness assays, have often led to confounding results and lack of success in clinical trials[41]. In the latest years, in order to overcome these ambiguities, there has been the urge to replace the "MSC" term and restrict the stem cell-term to cells that are truly proven to be so *in vivo*. Concomitantly, recent discoveries have shed light on a *bona fide* strict stem population within the BMSCs which illuminated the definition of skeletal stem cells (SSCs) described first in mice by Alpha V[42] or Gremlin[43] expression. And more recently also human SSCs, that give rise to progenitors of bone, cartilage and stroma but not fat, have been identified[44]. The landscape of MSCs and SSCs is still not fully defined, and their differences and overlaps in cell functions remain to be elucidated.

Other cell types

A slew of other cell types have been implicated as regulators of the HSC niche including adipo-osteogenetic progenitors, macrophages, and even Schwann cells. In one study, impaired adipogenic and osteogenic differentiation potential of marrow cells was correlated with a significant reduction of the HSC population, hinting that adipo-osteogenic progenitors are required for the HSC niche maintenance[32]. While presence of the aforementioned progenitor cells has been shown to be positive, mature adipocytes may serve as negative regulators of the niche[45]. Next, macrophages and osteoclasts function has also been shown to be fundamental. In this regard, it was demonstrated that osteoclasts impairment would induce HSC differentiation *in vivo*[46]. Finally, nonmyelinating Schwann cells (glial cells) have also been postulated as components in the bone marrow niche showing that, apart from being in contact with HSCs, they may also maintain HSCs by regulating the activation of latent TGF-β[47].

In summary, it is abundantly clear that a well-orchestrated bone marrow niche relies on numerous cell types which may all contribute essential fucntions to some extent in the niche. Nevertheless, the cells present are not the sole critical players in the niche. As already pointed out, molecular regulators also play a prominent role in directing the niche behavior. Most probably, understanding the concert of molecular crosstalk between the niche cells is the key to decoding the bone marrow puzzle.

Molecular regulators of HSC fate

A vast number of molecular factors has been implicated in HSC niche regulation. To begin with, the chemokine **CXCL12**, also known as stromal-derived factor-1 (SDF-1), plays a main role in maintaining HSC function having been linked to HSC retention in the bone marrow, quiescence and repopulating activity[48]. Several cell types have been reported to express this cytokine in both vascular and endosteal niches[33]. Further studies have elucidated that only the production of CXCL12 by a subset of specific cells in the perivascular region, has an effect in HSC maintenance[49]. This subset of cells include mesenchymal progenitors, as well as endothelial cells. Interestingly, inhibition of CXCL12 expression in osteoblasts or lymphoid progenitors had no effect on HSCs[50]. However, CXCL12 deletion from CAR stromal cells triggered mobilization of hematopoietic progenitor cells (HPCs). Even the regulation of HSCs by the SNS has been linked to the CXCL12 cytokine[31]. These findings also corroborate the hypothesis previously discussed that HSCs occupy a perivascular niche, while early lymphoid progenitors occupy an endosteal niche.

Equally as important as CXCL12 is the stem cell factor (**SCF**), also known as c-Kit ligand. SCF is a cytokine that binds to the c-Kit receptor. It exists as a soluble form and as a transmembrane-bound form, and its activity has been confirmed in both cases. It was demonstrated that SCF was primarily expressed by perivascular cells present throughout the bone marrow[30]. However inhibition of SCF expression solely by endothelial cells or leptin receptor-expressing cells, using a *Tie2-cre* or *Lepr-cre* system (resp.), has been associated with HSC loss[28]. Surprisingly, there is no effect when osteoblasts or HSCs themselves have repressed SCF expression. Again, a synergy between cells and molecular signaling is clearly paramount for proper niche functionality.

The vascular growth factor angiopoietin-1 (**Ang-1**) contributes to quiescence of HSCs in the niche. Ang-1 specifically binds to its receptor tyrosine-protein kinase Tie2 (Tie2), present in endothelial cells and HSCs. Interestingly, HSCs expressing the Tie2 receptor are quiescent, anti-apoptotic, and retain their self-renewal ability. Specifically, the interaction of Tie2 with its ligand Ang-1 induced HSCs to become quiescent and triggered HSC adhesion to bone, which in turn conferred protection to HSCs from myelosuppressive stresses[51]. Another angiogenic factor is the fibroblast growth factor-2 (**FGF-2**), which is normally stored in the bone marrow extracellular matrix and released by secreted enzymes. FGF-2 acts synergistically with SCF to expand LT-HSC capacity,

both directly by upregulating SCF expression of HSCs and indirectly by expanding stromal cells that in turn produce the growth factor[52].

Another niche candidate growth factor is transforming growth factor-beta (**TGF-β**). Schwann cells normally activate this cytokine after it is produced by other cells in the BM. It follows that in the absence of Schwann cells, a reduction of activated TGF-β was correlated with a rapid loss of HSCs[47]. Furthermore, TGF-β is thought to maintain HSC quiescence[53]. As well, bone morphogenetic proteins (**BMP**), apart from having been involved in the induction of hematopoietic tissue during early embryonic development, have also been shown to regulate the niche size[21].

Finally, **pleiotrophin**, a heparin-binding growth factor secreted by BM sinusoidal endothelial cells, maintains and regenerates HSCs[54]. Moreover, deletion of **thrombopoietin**, a glycoprotein hormone produced in the liver and bone marrow among other tissues, strongly induced reduction of HSCs[55]. Another regulator is **adiponectin**, which is produced by both adipocytes and osteolineage cells and increases HSC proliferation while allowing them to retain their potential[56]. **Osteopontin**, an acidic glycoprotein synthesized by osteoblasts, is an important BM extracellular matrix component. Osteopontin was shown to direct the physical location of HSCs to the endosteal region and to downregulate the proliferation of HSCs by binding to them via β1 integrin[57].

Intrinsic signaling pathways such as Notch and Wnt have also been studied for their participation in HSC maintenance, though conflicting results have been reported. On **Notch signaling**, few studies have shown that Notch1 and Notch2 receptors promoted expansion of LT-HSCs while preserving their self-renewal ability[58]. However, other studies stated that this signaling pathway is dispensable for LT-HSC maintenance[59]. Similarly, on the **Wnt signaling**, contradicting studies have been reported. Deleting a canonical Wnt ligand led to lower HSC numbers and decreased self-renewal[60]. However, deletion of β-catenin and γ-catenin, other proteins of the canonical Wnt pathway, had no effect on HSC self-renewal[61]. These findings indicate that the complexity of these signaling pathways, and the existence of compensatory pathways, make it difficult to assess their role regarding HSCs.

As a final class of niche regulators, **inorganic elements** have also been implicated. On one side, calcium released by osteoclasts during bone resorption creates a concentration gradient that originates at the endosteal surface. HSCs express the G-protein coupled calcium-sensing receptor (CaR) which may play a role in directing HSCs to the endosteal region based on the favorable calcium gradient[62]. On the other side **hypoxia** and hypoxia-inducible factor-1 (HIF-1) seem to play a still controversial role in sustaining HSC quiescence[63].

In summary, a complex milieu of components is responsible for maintaining the HSC niche, including interactions between various cell types present in the niche, soluble mediators, the

extracellular matrix itself, intrinsic signaling pathways as well as microenvironmental signals such as local oxygen tension.

Pathology within the stem cell niche

Aware of the complexity of the BM, it is not a surprise that changes in the bone or in the hematopoietic system due to aging, obesity, stress or cancer[64,65], significantly alter the interdependent equilibrium between different cell types and molecular factors. This results in severe clinical conditions that are highly complex to cure, which include among them hematopoietic and non-hematopoietic cancers[66].

Hematological malignancies

Hematopoietic cancers primarily affect the immune system and are categorized by the cell types involved, myeloid or lymphoid cells, and the location of the neoplasm, blood or lymph nodes. The three main types of hematological cancers are leukemia, lymphoma, and myeloma[67]. These malignancies are further influenced by the tumor microenvironment, which is highly diverse and plays an important role in their progression (Figure 3). Due to the wide variety of hematopoietic cancers, the interactions between the tumor-BM microenvironment are numerous. For instance, it was shown that pre-B acute lymphoblastic leukemia (ALL) cell growth disrupted normal HSPCs by sequestration[68]. Another study reported that acute myeloid leukemia (AML) reduced bone volume by inhibiting osteoblastic cells in the bone marrow[69]. And in similar lines, that myeloproliferative neoplasia (MPN) remodels the endosteal niche to impair normal hematopoiesis and contribute to BM fibrosis[70]. Conversely, in this bidirectional crosstalk, BM niche components can also modulate the function of cancer cells (Figure 3 b). For example, disruptions of mouse osteoprogenitors have been linked to acute myelogenous leukemia and overall leukemia predisposition[71], while mutating β-catenin in mouse osteoblasts led the development of AML[72]. Other reports showed that alterations in the BM molecular factors are enough to alter leukemic cell behavior[73]. Thus, even though it is under debate which cell type is responsible for the origination of such cancers, there are no doubts that the BM niche plays a paramount role in these observed events likely depending on the malignancy. Ultimately, recent reports suggest that it is likely that, as the BM niche serves to protect HSCs over an entire lifetime, the same niche protects malignant cells and potentially plays a major role in relapse following chemotherapy[74,75].

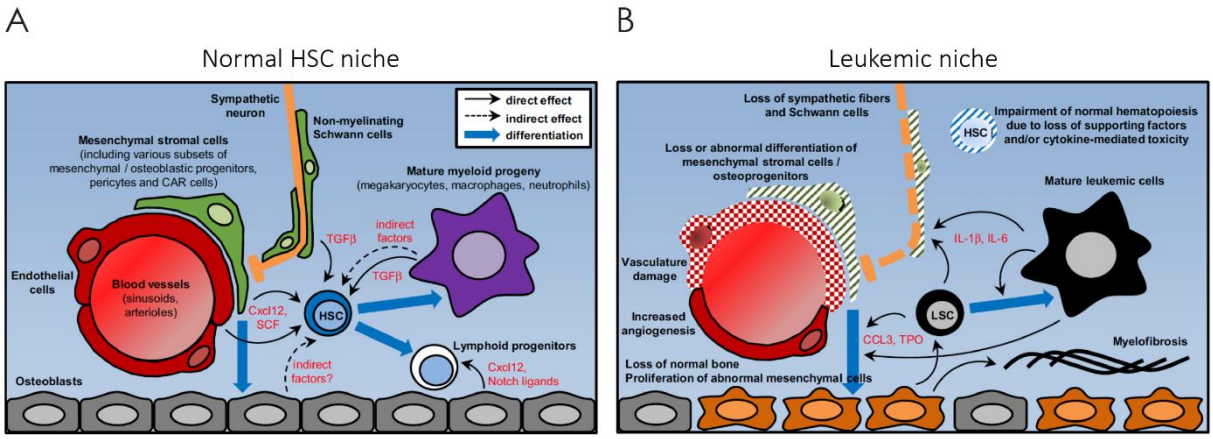

Figure 3. Healthy and leukemic states of the BM niche

(**a**) Schematic of the normal HSC niche and (**b**) some of modifications in the context of malignancy. Several cell populations and molecules have been found altered in leukemia, showing bidirectional crosstalk and alterations between malignant and supporting niche resident cells. HSC: hematopoietic stem cell; LSC: leukemia stem/initiating cell. This image was adapted from Sánchez-Aguilera et al.[76] and is open source from Springer.

Osteotropic metastasis in the BM

In addition to the tissue specific cancers discussed above, the BM is also the preferential homing site for metastatic breast, prostate, and lung cancer. At the late stage of metastatic disease, these remain largely incurable with only palliative treatment options[77]. In the last years, key findings have begun to unmask a complex interplay of cells and factors involved in preparing the pre-metastatic site[78]. Inflammation and immune cells, due to their systemic presence, were among the first to be studied as regulators of tumor progression[79]. For instance, it was shown that overexpression of macrophage colony-stimulating factor (CSF-1) did not affect primary tumor growth but significantly accelerated metastasis and correlated with higher infiltration of macrophages in the tumor site[80]. More recently, Kaplan et al. elegantly showed that even HSPCs themselves, expressing the vascular endothelial growth factor receptor 1 (VEGFR1), were attracted to tumor-specific pre-metastatic sites prior to the arrival of tumor cells[81]. Remarkably, blocking VEGFR1 prevented the formation of the pre-metastatic niche and disrupted completely tumor metastasis.

Cellular actors are not alone in preparation of the pre-metastatic niche. Extracellular vesicles (EVs), membrane-bound molecular cargo secreted by cells as a form of long range intercellular communication, are postulated to play a pivotal role in preparing the metastatic niche[82]. Hoshino et al. demonstrated that expression of particular integrins in tumor-derived EVs lead to preferential uptake in targeted tissues and organotropic changes in the pre-metastatic niche[83]. Moreover, recently, it was shown that specific chemotherapy treatments induced secretion of tumor-derived EVs with enhanced pro-metastatic capacity[84].

Due to its complexity and limited access, it has been challenging to study the BM niche and elucidate individual contributions to potentially enable more powerful targeted therapies. Advanced

imaging techniques have only recently provided critical insight on spatial distribution of cells in the BM[23,85]. Furthermore, these findings primarily originated from mouse models limiting the translation and reliability in predicting behavior in humans[86]. With this goal, efforts have been taken to try to mimic the BM niche and employ human counterparts in either *ex vivo* or *in vivo* models.

Modeling the HSC niche *ex vivo*

In light of the in-depth description of the complex interaction of players comprising the HSC niche, it should be no surprise that the culture of these cells outside of the body is anything but trivial. Hematopoietic stem cells rapidly differentiate *in vitro* and lose their intrinsic self-division potential as they proliferate, indicating that the niche not only supports them but contributes to directing their fate. Several *in vitro* approaches have been investigated with the goal of translating identified niche participants into *ex vivo* culture conditions for HSCs. However, none has yet achieved clinically relevant effects. Requisite criteria for *in vitro* culture of HSCs include the ability to expand the HSC population to cell numbers sufficient for therapeutic treatments, while simultaneously retaining their "stemness" (i.e. their therapeutic potential).

Approaches involving 2D monolayer cultures

Most attempts have to expand HSCs *in vitro* involved using cytokines such as SCF, fetal liver (FL) tyrosine kinase 2 and 3 ligands, interleukins (eg. IL-3, IL-6, IL-11, IL-12), leukemia inhibitory factor (LIF), granulocytes colony-stimulating factor (G-CSF), and thrombopoietin (TPO) among others. Interestingly, to positively effect HSC proliferation kinetics, the interaction of a minimum of two cytokines has proven necessary[87]. However, prolonged culture of human HSCs *ex vivo* solely with supplemented cytokines has failed to yield a protocol that meets the criteria of expansion and stemness maintenance. This has prompted further studies to combine cytokines and co-cultures of HSCs with candidate niche cells in order to better mimic the *in vivo* supporting microenvironment. These supporting cells, also known as feeder layers, form a cobblestone of cells on the top of which HSCs can be cultured. This monolayer of cells not only secretes soluble factors but also enables cell-cell contact with HSCs. Several studies have shown, with a number of different cell types, that the direct contact between cells has an impact on the expansion and the maintenance of multipotent capability of HSCs. The first report of a co-culture system of HSCs together with other BM cells was provided in 1977 by Dexter and colleagues[88]. Since then, many different niche cells have been considered such as osteoblasts, adipocytes, fibroblasts, endothelial cells and MSCs to be used as supportive cells. For instance, MSCs co-cultured with HSCs showed that the specific interaction between both cells would detract HSC from differentiation, whereas HSCs in the same culture that did not establish direct contact with the MSC layer would differentiate faster[89]. In parallel, since in the niche a single cellular component seems insufficient to maintain the HSC pool, cultures of several candidate niche cells with HSCs *in vitro* have also been investigated.

Despite minor advances, the 2D cultures described above have proven only limited success for reproducing the architecture of the HSC niche *ex vivo*. This, together with advances in biomaterials and tissue engineering, has recently lead to an outpouring of effort for the 3D reconstruction of the stem cell niche unit using 3D cultures[90,91].

Approaches involving 3D culture models

Several investigations have shown that HSCs cultured *in vitro* in a 3D environment containing other cell types and growth factors can retain HSC potential and, in some cases, even expand the population. A report compared the expansion of HSCs added to a 2D monolayer with MSCs or to a 3D porous poly(ethylene glycol) diacrylate hydrogel, functionalized with the RGD peptide, where MSCs had been pre-seeded. Though HSC proliferation was similar among the cultures, co-culture in 3D preserved better the stem cell potential of the HSCs[92]. Next, a thorough study used four different 3D biomaterial scaffolds (PCL, PLGA, fibrin and collagen) to evaluate the expansion of HSCs in the presence of cytokine supplementation and umbilical cord UC-MSCs. All tested scaffolds except PLGA supported HSC cell expansion. More importantly, fibrin outperformed the others by exhibiting higher HSC proliferation, better maintenance of primitive immunophenotype, and higher success rates of engraftment[93]. Another study using collagen scaffolds showed the advantage of BM-derived MSCs compared to UC-MSCs for the maintenance of HSCs[94]. And recently, the development of co-cultures with BMSCs and osteoblastic cells laden in hydroxyapatite scaffolds in bioreactors showed the maintenance of HSPCs, and the potential utility of such models to mimic pathological settings[95].

3D microenvironments to recreate the bone marrow *in vivo*

Another interesting approach to assess whether these engineering constructs can sustain HSCs is to not only add isolated HSCs *in vitro* and assess their phenotype during culture, but to implant the construct *in vivo* and evaluate its ability to recruit a host HSC population in the established model. It is logical to assume that specific conditions required for recruitment and maintenance of HSCs *in vivo* will also have application for their culture *in vitro*. A recent study showed elegantly that a collagen scaffold loaded with BMP-2 and demineralized bone powder could enhance the recruitment of host HSCs in the constructs when implanted subcutaneously in mice[96]. Eight weeks later, when the constructs were harvested, functional host HSCs were found. In addition, the murine HSCs in the constructs could be maintained *in vitro* up to 8 weeks without losing their multipotent capacity. In similar ways, others have transplanted 3D biomimetic materials as carriers for human niche candidate cells that provide a provisional extracellular matrix and harbor osteogenic signals to support encapsulated cells. Due to promising results using such xenograft models to recapitulate human traits in a partially native *in vivo* setting, they emerged as promising tools for also modeling malignant behaviors.

3D tumor models *in vivo*

The successful engraftment of human tumor cells in murine bone and bone marrow remains a major challenge for studying osteotropic metastases in mouse models rendering BM xenografts attractive alternatives. A number of reports feature combinations of i) human cells (e.g. hBMSCs) with ii) molecular factors that stimulate osteogenic differentiation of these cells (e.g. BMP-2, TGF-β3 or hydroxyapatite particles), and iii) a suitable 3D scaffold, that enable the formation of ossicles upon subcutaneous implantation in mice (Figure 4)[35,97-100]. These ossicles are rapidly vascularized by the host and become ossified within 4 to 8 weeks post-transplantation as indicated by micro-computed tomography (microCT). Histological evaluations indicate the formation of a bone marrow niche comprising contribution from hBMSCs and host cells. Use of these xenograft models to study the dissemination of tumor cells into the pre-formed ossicles has been shown in various ways including via systemic (intracardiac[100,101] or intravenous[102]) or intraossicle injections[98], or via orthotopic injection of a tumor xenograft[102,103]. These humanized bone marrows have enabled the study of stem cell intrinsic functions[35,42,44] and the recapitulation of healthy and malignant microenvironments, including leukemia[97,98,104] and osteotropic metastasis[100-102,105]. Table 1 summarizes the different bioengineered matrices and conditions currently available to mimic these BM niches, and the wide variety of biological questions that these tools have addressed.

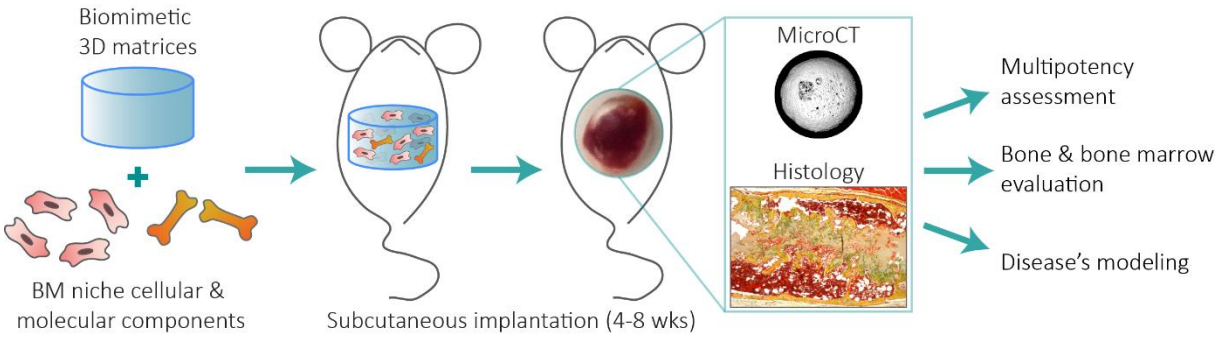

Figure 4. Heterotopic ossicle formation

Cellular and molecular components of the bone marrow niche can be combined in a 3D biomaterial for subcutaneous implantation *in vivo*. Over the time of 4 to 8 weeks, these scaffolds may undergo bone and bone marrow formation, resulting in a vascularized tissue as seen by gross morphology, with calcified regions as seen by microCT, and enclosing a rich marrow as seen by histologies. Movat's pentachrome staining of an ossicle based on an implant of hBMSCs in synthetic hydrogels with BMP-2 shows a bone shell enclosing a marrow-rich area. These BM organoids can be used to assess stem cell multipontency, as well as to compare the healthy and malignant hematopoietic system, among others.

Hydrogels as scaffolds for creation of tissue models

On the materials side, hydrogels are highly attractive 3D scaffold materials for simulating the native characteristics of the tissues since they enable high water contents and facile transport of oxygen, nutrients and waste. Moreover, many hydrogels can be crosslinked under mild and cell friendly conditions[117]. Hydrogels can be composed of natural or synthetic materials. Natural hydrogels are typically formed by ECM-derived macromolecules such as collagen, fibrin, laminin, hyaluronic acid

and fibronectin. Many of them have already been used for assessing the 3D niche reconstruction[35,42,44,96,98,107] (Table 1). Even though natural materials are biocompatible and offer a native microenvironment that promotes cell infiltration and cell growth, they are inherently bioactive. That means that it is difficult to control exactly which signals are promoted or which signals may be hindered by the material. Furthermore, tuning their material properties can be difficult and, because they are derived from natural sources, they possess an inherent batch-to-batch variability and risk of contamination. On the other hand, synthetic-based hydrogels formed of non-natural molecules are inert and non-instructive. Some examples are poly(ethylene glycol) (PEG), poly(vinyl alcohol) (PVA), poly(acrylic acid) (PAA), and nanofibrillar gels[118]. These synthetic scaffolds offer a minimalist approach to develop models in a fully controlled and reproducible manner, enabling the study of biological and cellular processes on a blank slate.

Enzymatically crosslinked PEG hydrogels (TG-PEG)

In our lab, we have developed an enzymatically crosslinked PEG-based hydrogel termed TG-PEG[119]. TG-PEG is crosslinked by the transglutaminase factor XIII (FXIII) mimicking the end of the blood coagulation cascade. In TG-PEG, 8-arm PEG-vinylsulfone molecules are functionalized with two peptides via a Michael-type addition reaction. These peptides, containing lysine or glutamine residues, act as substrates for FXIIIa crosslinking (Figure 5). PEG-based hydrogels are inert and highly reproducible. Their mild crosslinking conditions maintain the viability of encapsulated cells and allow for ECM deposition. Simultaneously during hydrogel crosslinking, growth factors, adhesion peptides, and other biological entities can be incorporated in a highly controlled manner[120]. Lastly, these hydrogels allow for facile tailoring of properties such as stiffness, degradability, and cell adhesion[121,122].

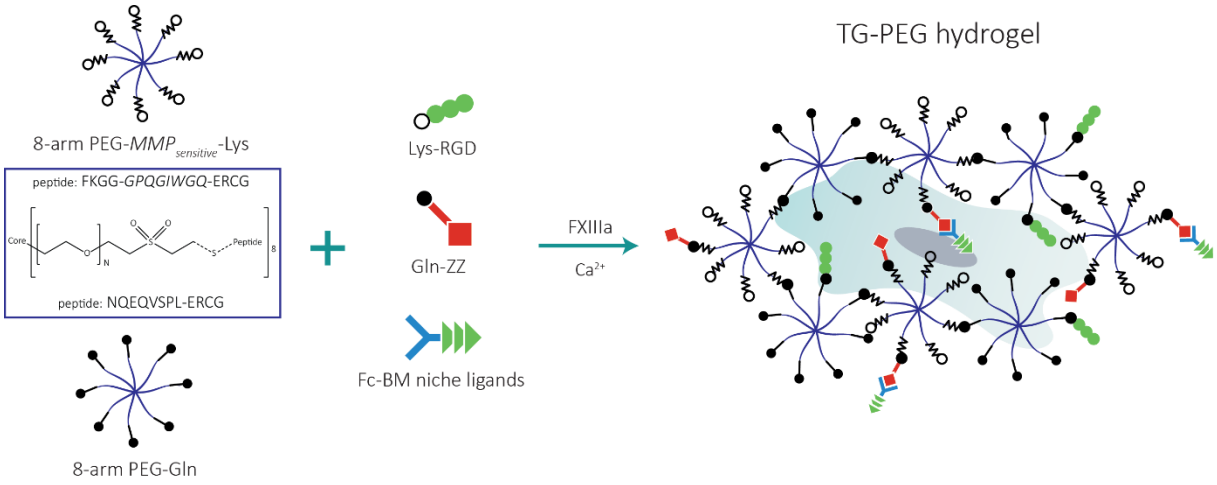

Figure 5. 3D biomimetic TG-PEG hydrogel

TG-PEG hydrogels are formed by transglutaminase FXIII crosslinking of two 8-arm PEG conjugates either containing $MMP_{sensitive}$-Lys donor (enabling cell-mediated degradation) or PEG-Gln acceptor substrates in the presence of calcium. Additionally, the cell-adhesion RGD peptide and other ligands of interest can be incorporated to the PEG backbone. These synthetic ECM-inspired matrices allow cell encapsulation at physiological conditions.

Table 1. Summary of materials and applications reported for use with *in vivo* BM-niche models

Biomaterial	Stromal cells	Supplementations	Application
Type I collagen gel	No cells	BMP-2 + BMP-4 + demineralized bone powder	Bone marrow on a chip, *in vivo* formation and *in vitro* maintenance[96]
Type I collagen mesh	Predifferentiated hBMSCs SSCs ($70{\cdot}10^6$ cells per ml)	hBMSCs pre-culture *in vitro* consisting of 3 wks in chondrogenic medium + 2 wks in hypertrophic medium	Bone organ induced by hBMSCs[99], human HSC quiescence assessment[106]
Gelfoam gelatin sponge	hBMSCs ($1{\cdot}10^5$ cells per scaffold)	hBMSCs pre-cultured for 3-5 d + hHSPCs + BMP-2 + fibrin coating	Healthy and malignant (AML) engraftment[97]
Matrigel	Murine and human SSCs (10 10^6 cells per ml)	-	Skeletal stem cell intrinsic function evaluation[42,44]
	hBMSCs ($7.5{\cdot}10^6$ cells per ml)	hECFCs (7.5 10^6 cells per ml)	Healthy and malignant (AML) engraftment[107]
ECMatrix	hBMSCs ($6.6{\cdot}10^6$ cells per ml)	pHPL + daily systemic injections of PTH after scaffold implantation	Healthy and malignant (AML) engraftment[98]
Polyacrylamide hydrogel	hBMSCs ($5{\cdot}10^5$ cells per scaffold)	Type I collagen coating	Bone metastatic processes (breast and prostate cancer)[102], human hematopoiesis[108]
Electrospun PCL scaffolds coated with CaP	hBMSCs or hOBs (2-3 10^5 cells per scaffold)	hBMSCs/hOBs pre-cultured *in vitro* for 4-10 wks in osteogenic medium + BMP-7 + fibrin glue	Bone metastatic processes (breast[105] and prostate[101,109] cancer) [110], human hematopoiesis[111]
Silk scaffolds	No cells	BMP-2	Bone metastatic processes (breast and prostate cancer)[100]
	hBMSCs ($1.5{\cdot}10^6$ cells per scaffold)	BMP-2	Bone metastatic processes (breast cancer)[103]
HA/TCP particles	$CD146^+$ osteoprogenitor cells ($2{\cdot}10^6$ cells per scaffold)	Fibrin gel	Skeletal stem cell intrinsic function evaluation[35]
Porous bioceramic HA/TCP scaffold	mBM-MSCs, mOB, hUC-MSC ($2.5{\cdot}10^6$ cells per scaffold)	Fibrin gel	Murine BM-MSC[112] versus OB[113], or human UC-MSC[114] intrinsic function
Biphasic calcium phosphate particles	hBMSCs ($2{\cdot}10^5$ cells per scaffold)	hBMSCs pre-cultured *in vitro* for 7 days in osteogenic medium	Healthy and malignant (AML)engraftment[104], patient-derived multiple myeloma[115], AML and ALL engraftment[116]

HA/TPC: hydroxyapatite tricalcium phosphate; pHPL: pool of human platelet lysate; PTH: parathyroid hormone; CaP: calcium phosphate, PCL: polycaprolactone; d: days; wks: weeks; OB: osteoblast; UC: umbilical cord; ECFC: endothelial colony-forming cells; AML: acute myeloid leukemia; ALL: acute lymphocytic leukemia

References

1 Morrison, S. J. & Scadden, D. T. The bone marrow niche for haematopoietic stem cells. *Nature* **505**, 327-334 (2014).

2 Schofield, R. The relationship between the spleen colony-forming cell and the haemopoietic stem cell. *Blood cells* **4**, 7-25 (1977).

3 Anthony, B. A. & Link, D. C. Regulation of hematopoietic stem cells by bone marrow stromal cells. *Trends in immunology* **35**, 32-37 (2014).

4 Mendelson, A. & Frenette, P. S. Hematopoietic stem cell niche maintenance during homeostasis and regeneration. *Nature medicine* **20**, 833-846 (2014).

5 Spangrude, G. J., Heimfeld, S. & Weissman, I. L. Purification and characterization of mouse hematopoietic stem cells. *Science* **241**, 58-62 (1988).

6 Ikuta, K. & Weissman, I. L. Evidence that hematopoietic stem cells express mouse c-kit but do not depend on steel factor for their generation. *Proceedings of the National Academy of Sciences* **89**, 1502-1506 (1992).

7 Kiel, M. J. *et al.* SLAM family receptors distinguish hematopoietic stem and progenitor cells and reveal endothelial niches for stem cells. *cell* **121**, 1109-1121 (2005).

8 Osawa, M., Hanada, K.-i., Hamada, H. & Nakauchi, H. Long-term lymphohematopoietic reconstitution by a single CD34-low/negative hematopoietic stem cell. *Science* **273**, 242-245 (1996).

9 Adolfsson, J. *et al.* Upregulation of Flt3 expression within the bone marrow Lin− Sca1+ c-kit+ stem cell compartment is accompanied by loss of self-renewal capacity. *Immunity* **15**, 659-669 (2001).

10 Randall, T., Lund, F., Howard, M. & Weissman, I. Expression of murine CD38 defines a population of long-term. *Blood* **87**, 4057-4067 (1996).

11 Goodell, M. A., Brose, K., Paradis, G., Conner, A. S. & Mulligan, R. C. Isolation and functional properties of murine hematopoietic stem cells that are replicating in vivo. *The Journal of experimental medicine* **183**, 1797-1806 (1996).

12 Civin, C. I. *et al.* Antigenic analysis of hematopoiesis. III. A hematopoietic progenitor cell surface antigen defined by a monoclonal antibody raised against KG-1a cells. *The Journal of Immunology* **133**, 157-165 (1984).

13 Terstappen, L., Huang, S., Safford, M., Lansdorp, P. M. & Loken, M. R. Sequential generations of hematopoietic colonies derived from single nonlineage-committed CD34+ CD38-progenitor cells. *Blood* **77**, 1218-1227 (1991).

14 Baum, C. M., Weissman, I. L., Tsukamoto, A. S., Buckle, A.-M. & Peault, B. Isolation of a candidate human hematopoietic stem-cell population. *Proceedings of the National Academy of Sciences* **89**, 2804-2808 (1992).

15 Gallacher, L. *et al.* Isolation and characterization of human CD34− Lin− and CD34+ Lin− hematopoietic stem cells using cell surface markers AC133 and CD7. *Blood* **95**, 2813-2820 (2000).

16 Lansdorp, P. M. & Dragowska, W. Long-term erythropoiesis from constant numbers of CD34+ cells in serum-free cultures initiated with highly purified progenitor cells from human bone marrow. *The Journal of experimental medicine* **175**, 1501-1509 (1992).

17 Notta, F. *et al.* Isolation of single human hematopoietic stem cells capable of long-term multilineage engraftment. *Science* **333**, 218-221 (2011).

18 Velten, L. *et al.* Human haematopoietic stem cell lineage commitment is a continuous process. *Nature cell biology* **19**, 271 (2017).

19 Notta, F. *et al.* Distinct routes of lineage development reshape the human blood hierarchy across ontogeny. *Science* **351**, aab2116 (2016).

20 Lord, B. I., Testa, N. G. & Hendry, J. H. The relative spatial distributions of CFUs and CFUc in the normal mouse femur. *Blood* **46**, 65-72 (1975).

21 Zhang, J. *et al.* Identification of the haematopoietic stem cell niche and control of the niche size. *Nature* **425**, 836-841 (2003).

22 Celso, C. L. *et al.* Live-animal tracking of individual haematopoietic stem/progenitor cells in their niche. *Nature* **457**, 92-96 (2009).

23 Acar, M. *et al.* Deep imaging of bone marrow shows non-dividing stem cells are mainly perisinusoidal. *Nature* **526**, 126-130 (2015).

24 Zhang, Y., Gao, S., Xia, J. & Liu, F. Hematopoietic hierarchy–an updated roadmap. *Trends in cell biology* **28**, 976-986 (2018).

25 Calvi, L. *et al.* Osteoblastic cells regulate the haematopoietic stem cell niche. *Nature* **425**, 841-846 (2003).

26 Nakamura, Y. *et al.* Isolation and characterization of endosteal niche cell populations that regulate hematopoietic stem cells. *Blood* **116**, 1422-1432 (2010).

27 Winkler, I. G. *et al.* Vascular niche E-selectin regulates hematopoietic stem cell dormancy, self renewal and chemoresistance. *Nature medicine* **18**, 1651-1657 (2012).

28 Ding, L., Saunders, T. L., Enikolopov, G. & Morrison, S. J. Endothelial and perivascular cells maintain haematopoietic stem cells. *Nature* **481**, 457-462 (2012).

29 Butler, J. M. *et al.* Endothelial cells are essential for the self-renewal and repopulation of Notch-dependent hematopoietic stem cells. *Cell stem cell* **6**, 251-264 (2010).

30 Méndez-Ferrer, S. *et al.* Mesenchymal and haematopoietic stem cells form a unique bone marrow niche. *Nature* **466**, 829-834 (2010).

31 Méndez-Ferrer, S., Lucas, D., Battista, M. & Frenette, P. S. Haematopoietic stem cell release is regulated by circadian oscillations. *Nature* **452**, 442 (2008).

32 Omatsu, Y. *et al.* The essential functions of adipo-osteogenic progenitors as the hematopoietic stem and progenitor cell niche. *Immunity* **33**, 387-399 (2010).

33 Sugiyama, T., Kohara, H., Noda, M. & Nagasawa, T. Maintenance of the hematopoietic stem cell pool by CXCL12-CXCR4 chemokine signaling in bone marrow stromal cell niches. *Immunity* **25**, 977-988 (2006).

34 Simmons, P. J. & Torok-Storb, B. Identification of stromal cell precursors in human bone marrow by a novel monoclonal antibody, STRO-1. *Blood* **78**, 55-62 (1991).

35 Sacchetti, B. *et al.* Self-renewing osteoprogenitors in bone marrow sinusoids can organize a hematopoietic microenvironment. *Cell* **131**, 324-336 (2007).

36 Pittenger, M. F. *et al.* Multilineage potential of adult human mesenchymal stem cells. *Science* **284**, 143-147 (1999).

37 Dominici, M. *et al.* Minimal criteria for defining multipotent mesenchymal stromal cells. The International Society for Cellular Therapy position statement. *Cytotherapy* **8**, 315-317 (2006).

38 Caplan, A. I. Mesenchymal stem cells. *Journal of orthopaedic research* **9**, 641-650 (1991).

39 Bianco, P. *et al.* The meaning, the sense and the significance: translating the science of mesenchymal stem cells into medicine. *Nature medicine* **19**, 35 (2013).

40 Kucia, M. *et al.* Bone marrow as a home of heterogenous populations of nonhematopoietic stem cells. *Leukemia* **19**, 1118 (2005).

41 Bianco, P., Robey, P. G. & Simmons, P. J. Mesenchymal stem cells: revisiting history, concepts, and assays. *Cell stem cell* **2**, 313-319 (2008).

42 Chan, C. K. *et al.* Identification and specification of the mouse skeletal stem cell. *Cell* **160**, 285-298 (2015).

43 Worthley, D. L. *et al.* Gremlin 1 identifies a skeletal stem cell with bone, cartilage, and reticular stromal potential. *Cell* **160**, 269-284 (2015).

44 Chan, C. K. *et al.* Identification of the human skeletal stem cell. *Cell* **175**, 43-56. e21 (2018).

45 Naveiras, O. *et al.* Bone-marrow adipocytes as negative regulators of the haematopoietic microenvironment. *Nature* **460**, 259-263 (2009).

46 Lymperi, S., Ersek, A., Ferraro, F., Dazzi, F. & Horwood, N. J. Inhibition of osteoclast function reduces hematopoietic stem cell numbers in vivo. *Blood* **117**, 1540-1549 (2011).

47 Yamazaki, S. *et al.* Nonmyelinating Schwann cells maintain hematopoietic stem cell hibernation in the bone marrow niche. *Cell* **147**, 1146-1158 (2011).

48 Tzeng, Y.-S. *et al.* Loss of Cxcl12/Sdf-1 in adult mice decreases the quiescent state of hematopoietic stem/progenitor cells and alters the pattern of hematopoietic regeneration after myelosuppression. *Blood* **117**, 429-439 (2011).

49 Ding, L. & Morrison, S. J. Haematopoietic stem cells and early lymphoid progenitors occupy distinct bone marrow niches. *Nature* **495**, 231-235 (2013).

50 Greenbaum, A. *et al.* CXCL12 in early mesenchymal progenitors is required for haematopoietic stem-cell maintenance. *Nature* **495**, 227-230 (2013).

51 Arai, F. *et al.* Tie2/angiopoietin-1 signaling regulates hematopoietic stem cell quiescence in the bone marrow niche. *Cell* **118**, 149-161 (2004).

52 Itkin, T. *et al.* FGF-2 expands murine hematopoietic stem and progenitor cells via proliferation of stromal cells, c-Kit activation, and CXCL12 down-regulation. *Blood* **120**, 1843-1855 (2012).

53 Batard, P. *et al.* TGF-(beta) 1 maintains hematopoietic immaturity by a reversible negative control of cell cycle and induces CD34 antigen up-modulation. *Journal of Cell Science* **113**, 383-390 (2000).

54 Himburg, H. A. *et al.* Pleiotrophin regulates the retention and self-renewal of hematopoietic stem cells in the bone marrow vascular niche. *Cell reports* **2**, 964-975 (2012).

55 Qian, H. *et al.* Critical role of thrombopoietin in maintaining adult quiescent hematopoietic stem cells. *Cell stem cell* **1**, 671-684 (2007).

56 DiMascio, L. *et al.* Identification of adiponectin as a novel hemopoietic stem cell growth factor. *The Journal of Immunology* **178**, 3511-3520 (2007).

57 Nilsson, S. K. *et al.* Osteopontin, a key component of the hematopoietic stem cell niche and regulator of primitive hematopoietic progenitor cells. *Blood* **106**, 1232-1239 (2005).

58 Kobayashi, H. *et al.* Angiocrine factors from Akt-activated endothelial cells balance self-renewal and differentiation of haematopoietic stem cells. *Nature cell biology* **12**, 1046-1056 (2010).

59 Maillard, I. *et al.* Canonical notch signaling is dispensable for the maintenance of adult hematopoietic stem cells. *Cell stem cell* **2**, 356-366 (2008).

60 Luis, T. C. *et al.* Wnt3a deficiency irreversibly impairs hematopoietic stem cell self-renewal and leads to defects in progenitor cell differentiation. *Blood* **113**, 546-554 (2009).

61 Koch, U. *et al.* Simultaneous loss of β-and γ-catenin does not perturb hematopoiesis or lymphopoiesis. *Blood* **111**, 160-164 (2008).

62 Adams, G. B. *et al.* Stem cell engraftment at the endosteal niche is specified by the calcium-sensing receptor. *Nature* **439**, 599-603 (2006).

63 Takubo, K. *et al.* Regulation of the HIF-1α level is essential for hematopoietic stem cells. *Cell stem cell* **7**, 391-402 (2010).

64 Heidt, T. *et al.* Chronic variable stress activates hematopoietic stem cells. *Nature medicine* **20**, 754 (2014).

65 Ambrosi, T. H. *et al.* Adipocyte accumulation in the bone marrow during obesity and aging impairs stem cell-based hematopoietic and bone regeneration. *Cell stem cell* **20**, 771-784. e776 (2017).

66 Bain, B. J., Clark, D. M. & Wilkins, B. S. *Bone marrow pathology*. (Wiley-Blackwell, 2019).

67 Vardiman, J. W. *et al.* The 2008 revision of the World Health Organization (WHO) classification of myeloid neoplasms and acute leukemia: rationale and important changes. *Blood* **114**, 937-951 (2009).

68 Colmone, A. *et al.* Leukemic cells create bone marrow niches that disrupt the behavior of normal hematopoietic progenitor cells. *Science* **322**, 1861-1865 (2008).

69 Frisch, B. J. *et al.* Functional inhibition of osteoblastic cells in an in vivo mouse model of myeloid leukemia. *Blood* **119**, 540-550 (2012).

70 Schepers, K. *et al.* Myeloproliferative neoplasia remodels the endosteal bone marrow niche into a self-reinforcing leukemic niche. *Cell stem cell* **13**, 285-299 (2013).

71 Raaijmakers, M. H. *et al.* Bone progenitor dysfunction induces myelodysplasia and secondary leukaemia. *Nature* **464**, 852 (2010).

72 Kode, A. *et al.* Leukaemogenesis induced by an activating β-catenin mutation in osteoblasts. *Nature* **506**, 240 (2014).

73 Hartwell, K. A. *et al.* Niche-based screening identifies small-molecule inhibitors of leukemia stem cells. *Nature chemical biology* **9**, 840 (2013).

74 Krause, D. S. *et al.* Differential regulation of myeloid leukemias by the bone marrow microenvironment. *Nature medicine* **19**, 1513 (2013).

75 Jin, L., Hope, K. J., Zhai, Q., Smadja-Joffe, F. & Dick, J. E. Targeting of CD44 eradicates human acute myeloid leukemic stem cells. *Nature medicine* **12**, 1167 (2006).

76 Sánchez-Aguilera, A. & Méndez-Ferrer, S. The hematopoietic stem-cell niche in health and leukemia. *Cellular and Molecular Life Sciences* **74**, 579-590 (2017).

77 Buijs, J. T. & van der Pluijm, G. Osteotropic cancers: from primary tumor to bone. *Cancer letters* **273**, 177-193 (2009).

78 Roodman, G. D. Mechanisms of bone metastasis. *New England journal of medicine* **350**, 1655-1664 (2004).

79 Coussens, L. M. & Werb, Z. Inflammation and cancer. *Nature* **420**, 860 (2002).

80 Lin, E. Y., Nguyen, A. V., Russell, R. G. & Pollard, J. W. Colony-stimulating factor 1 promotes progression of mammary tumors to malignancy. *Journal of Experimental Medicine* **193**, 727-740 (2001).

81 Kaplan, R. N. *et al.* VEGFR1-positive haematopoietic bone marrow progenitors initiate the pre-metastatic niche. *Nature* **438**, 820 (2005).

82 Andaloussi, S. E., Mäger, I., Breakefield, X. O. & Wood, M. J. Extracellular vesicles: biology and emerging therapeutic opportunities. *Nature reviews Drug discovery* **12**, 347 (2013).

83 Hoshino, A. *et al.* Tumour exosome integrins determine organotropic metastasis. *Nature* **527**, 329 (2015).

84 Keklikoglou, I. *et al.* Chemotherapy elicits pro-metastatic extracellular vesicles in breast cancer models. *Nature cell biology* **21**, 190 (2019).

85 Coutu, D. L., Kokkaliaris, K. D., Kunz, L. & Schroeder, T. Three-dimensional map of nonhematopoietic bone and bone-marrow cells and molecules. *Nature biotechnology* **35**, 1202 (2017).

86 Rangarajan, A. & Weinberg, R. A. Comparative biology of mouse versus human cells: modelling human cancer in mice. *Nature Reviews Cancer* **3**, 952 (2003).

87 Heike, T. & Nakahata, T. Ex vivo expansion of hematopoietic stem cells by cytokines. *Biochimica et Biophysica Acta (BBA)-Molecular Cell Research* **1592**, 313-321 (2002).

88 Dexter, T. M., Allen, T. D. & Lajtha, L. Conditions controlling the proliferation of haemopoietic stem cells in vitro. *Journal of cellular physiology* **91**, 335-344 (1977).

89 Alakel, N. *et al.* Direct contact with mesenchymal stromal cells affects migratory behavior and gene expression profile of CD133+ hematopoietic stem cells during ex vivo expansion. *Experimental hematology* **37**, 504-513 (2009).

90 Di Maggio, N. *et al.* Toward modeling the bone marrow niche using scaffold-based 3D culture systems. *Biomaterials* **32**, 321-329 (2011).

91 Vunjak-Novakovic, G. & Scadden, D. T. Biomimetic platforms for human stem cell research. *Cell stem cell* **8**, 252-261 (2011).

92 Raic, A., Rödling, L., Kalbacher, H. & Lee-Thedieck, C. Biomimetic macroporous PEG hydrogels as 3D scaffolds for the multiplication of human hematopoietic stem and progenitor cells. *Biomaterials* **35**, 929-940 (2014).

93 Ferreira, M. S. V. *et al.* Cord blood-hematopoietic stem cell expansion in 3D fibrin scaffolds with stromal support. *Biomaterials* **33**, 6987-6997 (2012).

94 Leisten, I. *et al.* 3D co-culture of hematopoietic stem and progenitor cells and mesenchymal stem cells in collagen scaffolds as a model of the hematopoietic niche. *Biomaterials* **33**, 1736-1747 (2012).

95 Bourgine, P. E. *et al.* In vitro biomimetic engineering of a human hematopoietic niche with functional properties. *Proceedings of the National Academy of Sciences* **115**, E5688-E5695 (2018).

96 Torisawa, Y.-s. *et al.* Bone marrow–on–a–chip replicates hematopoietic niche physiology in vitro. *Nature methods* **11**, 663-669 (2014).

97 Abarrategi, A. *et al.* Versatile humanized niche model enables study of normal and malignant human hematopoiesis. *The Journal of clinical investigation* **127**, 543-548 (2017).

98 Reinisch, A. *et al.* A humanized bone marrow ossicle xenotransplantation model enables improved engraftment of healthy and leukemic human hematopoietic cells. *Nature medicine* **22**, 812 (2016).

99 Scotti, C. *et al.* Engineering of a functional bone organ through endochondral ossification. *Proceedings of the National Academy of Sciences* **110**, 3997-4002 (2013).

100 Seib, F. P., Berry, J. E., Shiozawa, Y., Taichman, R. S. & Kaplan, D. L. Tissue engineering a surrogate niche for metastatic cancer cells. *Biomaterials* **51**, 313-319 (2015).

101 Holzapfel, B. M. *et al.* Species-specific homing mechanisms of human prostate cancer metastasis in tissue engineered bone. *Biomaterials* **35**, 4108-4115 (2014).

102 Bersani, F. *et al.* Bioengineered implantable scaffolds as a tool to study stromal-derived factors in metastatic cancer models. *Cancer research* **74**, 7229-7238 (2014).

103 Moreau, J. E. *et al.* Tissue-engineered bone serves as a target for metastasis of human breast cancer in a mouse model. *Cancer Research* **67**, 10304-10308 (2007).

104 Antonelli, A. *et al.* Establishing human leukemia xenograft mouse models by implanting human bone marrow–like scaffold-based niches. *Blood* **128**, 2949-2959 (2016).

105 Thibaudeau, L. *et al.* A tissue-engineered humanized xenograft model of human breast cancer metastasis to bone. *Disease models & mechanisms* **7**, 299-309 (2014).

106 Fritsch, K. *et al.* Engineered humanized bone organs maintain human hematopoiesis in vivo. *Experimental hematology* **61**, 45-51. e45 (2018).

107 Chen, Y. *et al.* Human extramedullary bone marrow in mice: a novel in vivo model of genetically controlled hematopoietic microenvironment. *Blood* **119**, 4971-4980 (2012).

108 Lee, J. *et al.* Implantable microenvironments to attract hematopoietic stem/cancer cells. *Proceedings of the National Academy of Sciences* **109**, 19638-19643 (2012).

109 Hesami, P. *et al.* A humanized tissue-engineered in vivo model to dissect interactions between human prostate cancer cells and human bone. *Clinical & experimental metastasis* **31**, 435-446 (2014).

110 Martine, L. C. *et al.* Engineering a humanized bone organ model in mice to study bone metastases. *Nature protocols* **12**, 639 (2017).

111 Holzapfel, B. M. *et al.* Tissue engineered humanized bone supports human hematopoiesis in vivo. *Biomaterials* **61**, 103-114 (2015).

112 Tasso, R. *et al.* In vivo implanted bone marrow-derived mesenchymal stem cells trigger a cascade of cellular events leading to the formation of an ectopic bone regenerative niche. *Stem cells and development* **22**, 3178-3191 (2013).

113 Tortelli, F., Tasso, R., Loiacono, F. & Cancedda, R. The development of tissue-engineered bone of different origin through endochondral and intramembranous ossification following the implantation of mesenchymal stem cells and osteoblasts in a murine model. *Biomaterials* **31**, 242-249 (2010).

114 Todeschi, M. R. *et al.* Transplanted umbilical cord mesenchymal stem cells modify the in vivo microenvironment enhancing angiogenesis and leading to bone regeneration. *Stem cells and development* **24**, 1570-1581 (2015).

115 Groen, R. W. *et al.* Reconstructing the human hematopoietic niche in immunodeficient mice: opportunities for studying primary multiple myeloma. *Blood* **120**, e9-e16 (2012).

116 Sontakke, P. *et al.* Modeling BCR-ABL and MLL-AF9 leukemia in a human bone marrow-like scaffold-based xenograft model. *Leukemia* **30**, 2064 (2016).
117 Tibbitt, M. W. & Anseth, K. S. Hydrogels as extracellular matrix mimics for 3D cell culture. *Biotechnology and bioengineering* **103**, 655-663 (2009).
118 Lutolf, M. & Hubbell, J. Synthetic biomaterials as instructive extracellular microenvironments for morphogenesis in tissue engineering. *Nature biotechnology* **23**, 47-55 (2005).
119 Ehrbar, M. *et al.* Enzymatic formation of modular cell-instructive fibrin analogs for tissue engineering. *Biomaterials* **28**, 3856-3866 (2007).
120 Metzger, S. *et al.* Modular Poly (ethylene glycol) Matrices for the Controlled 3D-Localized Osteogenic Differentiation of Mesenchymal Stem Cells. *Advanced healthcare materials* **4**, 550-558 (2015).
121 Ehrbar, M. *et al.* Biomolecular hydrogels formed and degraded via site-specific enzymatic reactions. *Biomacromolecules* **8**, 3000-3007 (2007).
122 Ehrbar, M. *et al.* Elucidating the role of matrix stiffness in 3D cell migration and remodeling. *Biophysical journal* **100**, 284-293 (2011).

Cause if we don't leave this town

We might never make it out

I was not born to drown

Baby come on. – The Lumineers

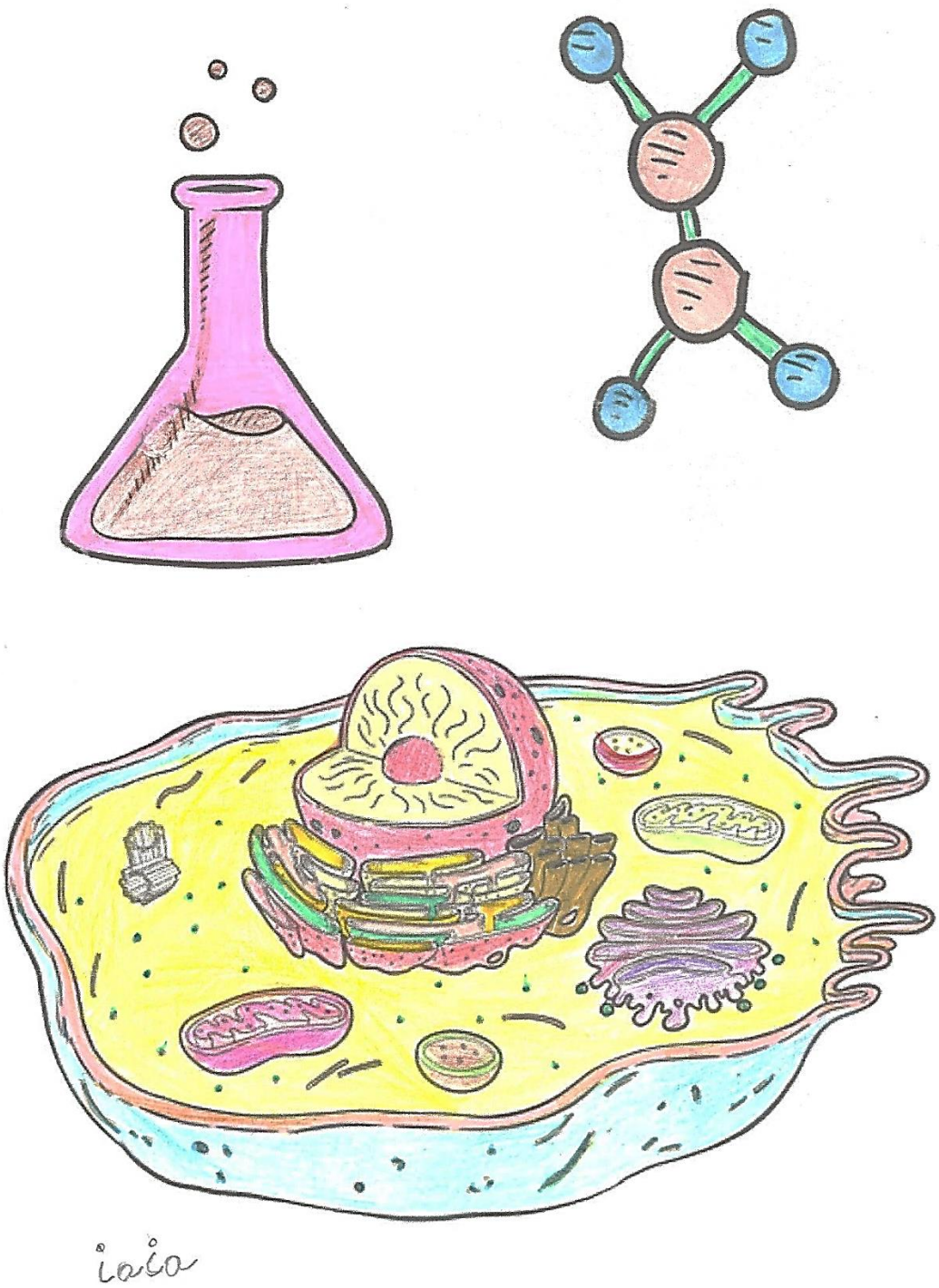

Artwork by María Dorado Prado

Girona, Catalunya

CHAPTER 2

Expanded skeletal stem and progenitor cells promote and participate in induced bone regeneration at subcritical BMP-2 dose

P Papageorgiou* [1], Q Vallmajo-Martin* [1,2], M Kisielow[3], A Sancho-Puchades[1], E Kleiner[1], M Ehrbar[1]

The content of this chapter is an adapted version of the manuscript: P Papageorgiou*, Q Vallmajo-Martin* et al. Expanded skeletal stem and progenitor cells promote and participate in induced bone regeneration at subcritical BMP-2 dose. *Biomaterials*, 2019.

[1] Laboratory for Cell and Tissue Engineering, Department of Obstetrics, UniversitätsSpital Zürich, Switzerland;
[2] Laboratory of Stem Cell Bioengineering, Institute of Bioengineering, École Polytechnique Fédérale de Lausanne, Switzerland;
[3] Flow Cytometry Core Facility, ETH Zürich, Switzerland.

* These authors contributed equally.

Statement of contributions

PP, QVM & ME designed all the experiments.

PP & QVM performed and analyzed all the experiments.

MK collaborated in flow cytometry sorting experiments, including experimental setup and analysis.

ASP collaborated in rheological measurements and material evaluations.

EK collaborated with histological evaluations.

PP, QVM & ME wrote the manuscript, and all the authors gave feedback.

Abstract

The regeneration of large bone defects remains an unsolved clinical problem, which could benefit from recent findings on the biology of skeletal stem and progenitor cells. The elucidation of conditions to specifically control their dynamic and function will likely enable the development of novel treatment strategies. In this study, we aimed at dissecting the role of osteogenic cues and skeletal stem (SSC) and bone cartilage stromal progenitor cell (BCSP) recruitment during biomimetic hydrogel-assisted bone regeneration. To do so, we employed a biomimetic synthetic hydrogel based on poly(ethylene glycol) (PEG), highly controllable and enzymatically crosslinkable. We show that hydrogel-released bone morphogenetic protein-2 (BMP-2) dose-dependently promoted the enrichment of both SSCs and BCSPs within bone defects. Furthermore, we demonstrate that prospectively isolated neonatal bone-derived, as well as expanded SSCs and BCSPs, differentiate into osteogenic cells and enhance the healing of bone defects by low BMP-2 releasing biomaterials. These results indicate that growth factor releasing materials should be designed to first augment the number of SSCs and BCSPs, followed by their osteogenic differentiation to potentiate the healing of bone defects. Additionally, we demonstrate that expanded SSCs and BCSPs are easily accessible cell sources that allow the study of novel bone healing regimen under controlled *in vitro* and *in vivo* conditions.

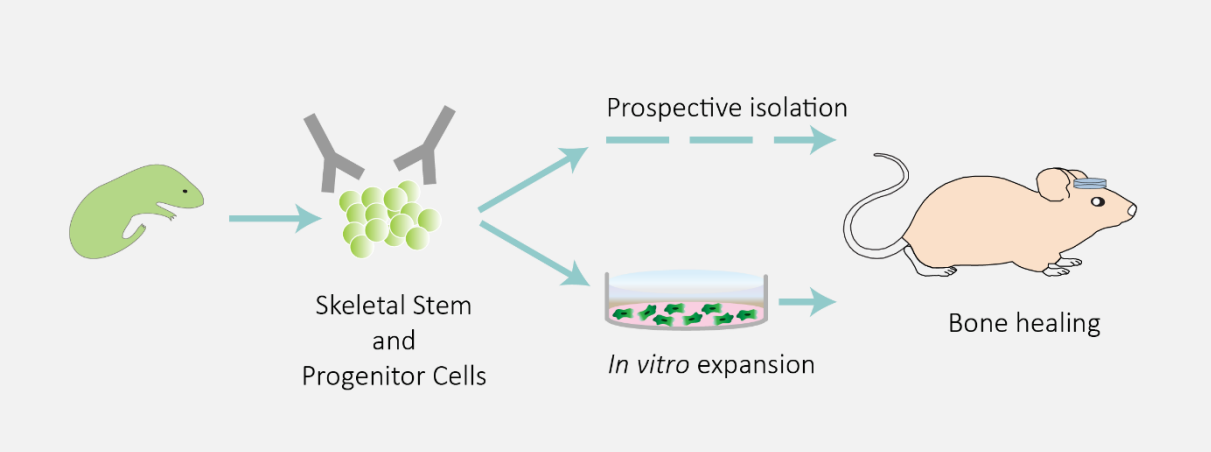

Keywords: Skeletal stem cell, bone cartilage stromal progenitor, synthetic hydrogel, low dose, BMP-2, bone formation.

Introduction

While bone morphogenetic protein-2 (BMP-2) has been demonstrated to significantly enhance bone regeneration in human patients, concerns related to the supraphysiologic doses of BMP-2 in current formulations (1.5 mg cm^{-3}) have limited its clinical use[1,2]. Reported complications include early inflammatory reaction, osteolysis, ectopic bone formation, seroma formation and an increased risk of malignancy[3]. On the other hand, the previously described inherent capacity of bone to regenerate itself has been a strong stimulus for the development of alternative treatments[4-7].

Although mesenchymal stromal cells (MSCs) hold promise for enhancing bone regeneration, their clinical implementation remains challenging[8,9]. This is most likely due to the lack of strict criteria for their specific selection and because the cells' regenerative capability cannot readily be controlled once transplanted[10]. Currently evaluated strategies to promote bone healing consist of delivering osteoinductive growth factors as well as stem or progenitor cells through osteoconductive natural or engineered biomimetic biomaterials[11,12]. While natural biomaterials such as collagen or fibrin hydrogels are excellent cell substrates, their inherent biological properties limit control over *in vivo* stability and provision of matrix-catenated or soluble signaling cues[13,14]. To overcome these limitations multiple semisynthetic and fully synthetic biomaterials have been developed[15,16]. By the use of chemically, physically and biologically defined building blocks, biomaterials with almost independently controllable stiffness, degradability, cell-adhesive functions and growth factor affinities are now becoming available[17-20]. The great advantage of these materials is that they are tailorable towards the transplantation of cells with regenerative capacity as well as the delivery of governing signals for the induction and morphogenesis of functional tissues[17,21,22].

The healing of bone defects is a complex process involving multiple cellular and molecular mechanisms[5]. For instance, neutrophils and macrophages are among the cells that control the early healing environment by releasing growth factors and secreting cytokines, which in turn can actively promote the induction and mobilization of osteogenic cells[5,23,24]. Although in recent years we have gained important insights into phenotypic properties and anatomical localization of human and murine bone forming progenitor and stem cells, the functional relation of differently characterized cell populations remains elusive[10,25-27]. Furthermore, their participation in bone healing, as well as signals responsible for their induction and mobilization, need further characterization[28,29]. Chan et al. provided evidence in mice that BMP-2 ectopic delivery can induce the *de novo* formation of skeletal stem cells (SSCs) ($CD45^-$ $TER119^-$ $Tie2^-$ $AlphaV^+$ Thy^- $6C3^-$ $CD105^-$ $CD200^+$) in extra-skeletal regions, such as subcutaneous sites and the renal capsule. They further suggested that SSCs give rise to hierarchically organized, increasingly fate-restricted progenitors with distinct cell surface marker profiles and skeletal fates[30]. One of these populations are the bone cartilage stromal progenitors (BCSPs) ($CD45^-$ $TER119^-$ $Tie2^-$ $AlphaV^+$ Thy^- $6C3^-$ $CD105^+$) which could only differentiate to bone, cartilage and bone marrow stroma. Recently, SSC populations with the capacity to self-renew and differentiate into bone, cartilage and stroma were also isolated from different human tissues[31].

To enable the translation of the newly acquired knowledge on the skeletal stem and progenitor cells it will be important to characterize and dissect factors leading to their induction, recruitment, expansion, and differentiation as well as to integrate them into novel biomaterials. Therefore, the aim of this study was to understand whether low concentrations of biomaterial-delivered BMP-2 would be able to increase the number of SSCs and BCSPs and if these cells would be able to differentiate into bone-forming cells in a defect model. Since *in vitro* culture is known to significantly change the properties of stem cells[32], we decided to compare the osteogenic potential of prospectively isolated with short-term culture expanded SSCs and BCSPs. Furthermore, we used a murine calvarial defect model as it allows relatively easy surgical procedure, good standardization and easy evaluations as compared to long bone models. While calvarial defect models do not give information on the effect of mechanical loading on bone healing, they have been extremely valuable to assess biomaterials and tissue engineered constructs[33].

Previously, our laboratory developed a modularly designed poly(ethylene glycol) (PEG)-based biomimetic hydrogel that is polymerized by the transglutaminase factor XIII[34-38]. This fully defined hydrogel, named TG-PEG, is formed from two eight-arm PEG precursor molecules functionalized with either a glutamine-acceptor or a lysine-donor substrate sequence. To enable the reciprocal interaction of cells with the TG-PEG hydrogel, a matrix metalloproteinase (MMP)-1-cleavable sequence was inserted into the lysine-donor substrate sequence and the cell-adhesion peptide RGD (50 μM) was tethered to glutamine-acceptor sequences of the hydrogel. These TG-PEG hydrogels were employed to treat critical-sized murine calvarial defects, where they were readily replaced by bone tissue when high dose (> 1 μg) of BMP-2 was incorporated[39,40]. Consequently, we reasoned that this rationally designed, blank slate biomaterial would be ideal to study the contribution of osteogenic signals as well as stem and progenitor cells to bone healing.

Our data indicate that postnatal day 3 murine bone-derived and short-term cultured SSCs and BCSPs can undergo osteogenic differentiation *in vitro*. When these subpopulations were transplanted, we show that they spontaneously differentiate towards osteogenic lineages and, in presence of low-dose (0.2 μg) BMP-2, participate in the regeneration of bone. Our results suggest that short-term expanded SSCs and BCSPs maintain their osteogenic properties and regenerate bone when applied to a healing fracture site in murine calvarial bone. Thus, we propose the use of expanded SSCs and BCSPs in combination with minimal osteoinductive signals to study cellular and molecular processes of bone healing and to elucidate novel healing stimulating signals.

Results

TG-PEG hydrogels optimized as stem cell carriers

To elucidate the role of BMP-2, SSCs and BCSPs during bone healing under highly reproducible conditions, we employed our previously developed TG-PEG hydrogels that due to their modular design are tailorable with respect to biological and mechanical properties (Figure 1 a). To show the tunability of the mechanical properties of our TG-PEG hydrogel, we determined the stiffness of

swollen hydrogels at different initial polymer concentrations, resulting in hydrogels from 130 Pa to 2.5 kPa (Figure 1 b). Furthermore, to corroborate the high batch-to-batch reproducibility of this hydrogel system we performed *in situ* rheometry measurements of 1.7% TG-PEG from different hydrogel polymer syntheses (Figure 1 c). No differences were observed among TG-PEG batches regarding stiffness. Next, to establish stable biomaterials which are optimal for cell migration and can be applied for both cell culture and *in vivo* transplantations we encapsulated human bone marrow-derived stromal cells (hBMSCs) ($1.5 \cdot 10^6$ cells per ml) in TG-PEG hydrogels that were formed with different levels of stiffness by varying the crosslinking density and contained or not immobilized RGD (Figure 1 d, e). Brightfield microscopy images after 3 days of culture showed that hBMSCs did not efficiently spread in hydrogels with a stiffness of 720 Pa or higher, neither in absence of the cell-adhesion RGD peptide. Therefore, to ensure good migration conditions and at the same time prevent too fast *in vivo* degradation, hydrogels containing RGD and having a stiffness of 380 Pa were selected for the following experiments.

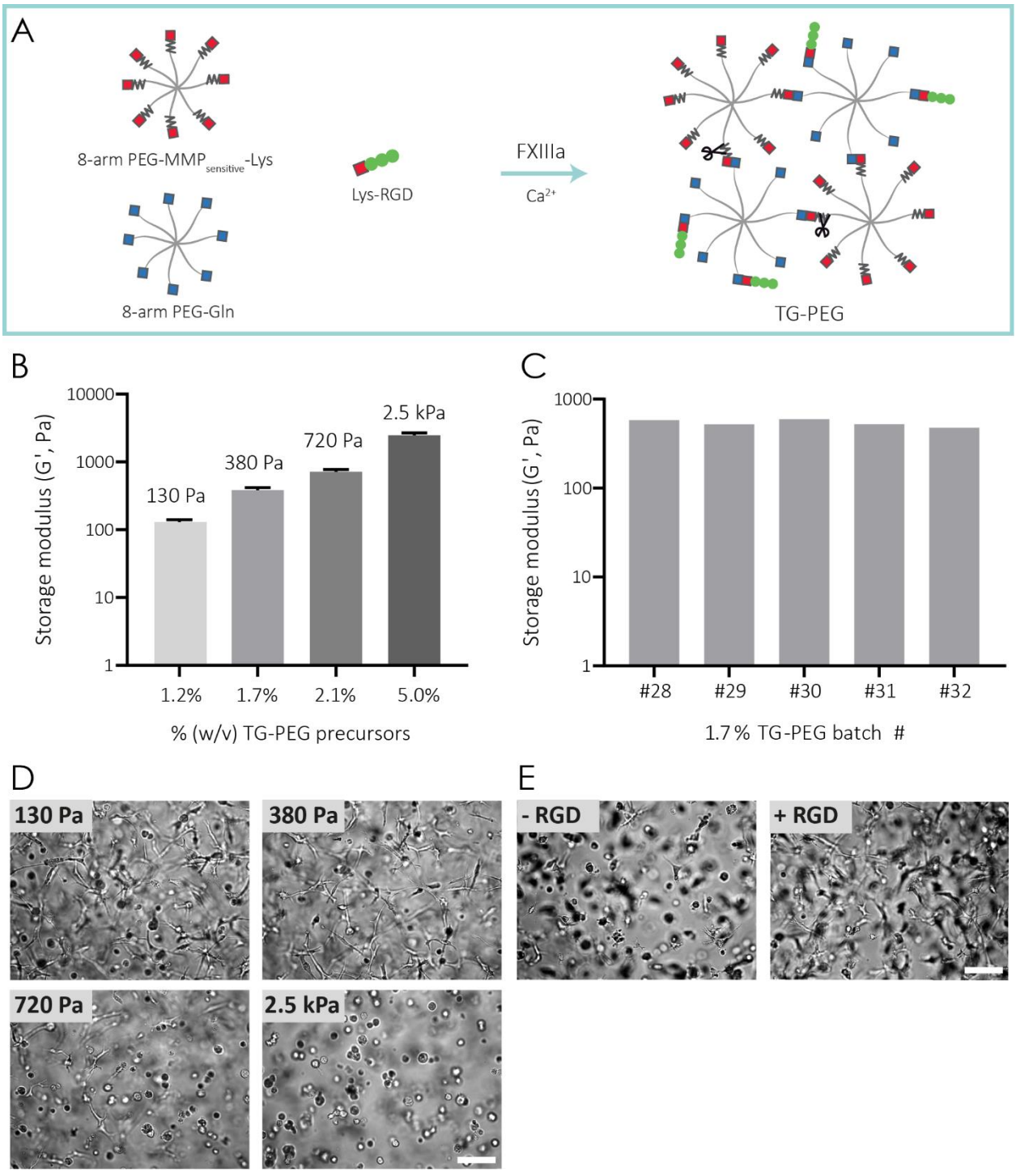

Figure 1. Rationally designed enzymatically crosslinked hydrogels as stem cell carriers

(**a**) Scheme of the biomimetic 3D hydrogel enzymatically crosslinked. 8-arm PEG-Gln and 8-arm PEG-MMP$_{sensitive}$-Lys precursors together with RGD-Lys peptide were crosslinked by the addition of the transglutaminase FXIIIa in the presence of Ca^{2+}, resulting in TG-PEG hydrogels. (**b**) Storage modulus of swollen TG-PEG hydrogels at different crosslinking densities (1.2%, 1.7%, 2.1% and 5%), and (**c**) insight into batch-to-batch reproducibility regarding stiffness for 1.7% hydrogels. Data are depicted as mean ± SD, n = 3, n = 1 for each single batch of 1.7% TG-PEG. (**d**) Representative brightfield images from hBMSCs cultured for 3 days in TG-PEG hydrogels of increasing polymer percentages, and thus, increasing stiffness (scale bar: 100 µm). (**e**) An intermediate stiffness of 380 Pa was selected and then the effect of the presence of the RGD adhesion peptide was assessed (scale bar: 100 µm).

BMP-2-mediated accumulation of SSCs and BCSPs at sites of bone healing

To determine the effect of BMP-2 on the accumulation of stem cells during bone healing, we generated 4 mm diameter critical-sized defects in calvarial bones of C57BL/6 mice and treated them with our optimized biomimetic hydrogels (380 Pa stiffness, MMP-degradable with RGD adhesion sites) which contained no, low dose (0.2 μg) or high dose (0.8 μg) of BMP-2 (Figure 2 a). Previously, we have reported that murine bone matrix deposition is initiated 1 week after treatment with high doses of BMP-2 (2 μg) in releasing biomimetic hydrogels[40]. Elsewhere the expansion of SSCs and BSCPs was shown to be most extensive during spontaneous bone healing at the phase of soft callus formation[41,42]. Therefore, to determine the participation of SSCs and BCSPs in these early stages of healing, hydrogel implants were retrieved 8 days post-treatment. Implant-trapped cells were enzymatically released and characterized by flow cytometry based on the absence of hematopoietic and endothelial markers (CD45, TER119, Tie2), the presence of the osteoblastic marker (AlphaV), as well as the differential expression of Thy, 6C3, CD105 and CD200[30]. In control implants, lineage-negative cells ($CD45^-$ $TER119^-$ $Tie2^-$ Thy^- $6C3^-$) comprised 0.93 ± 0.33% of all nucleated cells, while SSCs ($CD45^-$ $TER119^-$ $Tie2^-$ $AlphaV^+$ Thy^- $6C3^-$ $CD105^-$ $CD200^+$) and BCSPs ($CD45^-$ $TER119^-$ $Tie2^-$ $AlphaV^+$ Thy^- $6C3^-$ $CD105^+$) were almost absent, comprising 0.013 ± 0.005% and 0.017 ± 0.017%, respectively (Figure 2 b, c). Upon treatment with low-dose and high-dose BMP-2 the number of lineage-negative cells increased to 2.08 ± 0.36% and 5.74 ± 0.66%, respectively. Importantly, upon treatment with low-dose BMP-2 the fraction of both SSCs and BCSPs increased to 0.18 ± 0.007% and 0.14 ± 0.009%, respectively. Moreover, by increasing to high-dose BMP-2, the fraction of both SSCs and BCSPs was even further and significantly enhanced to 1.71 ± 0.23% and 0.4 ± 0.59%, respectively.

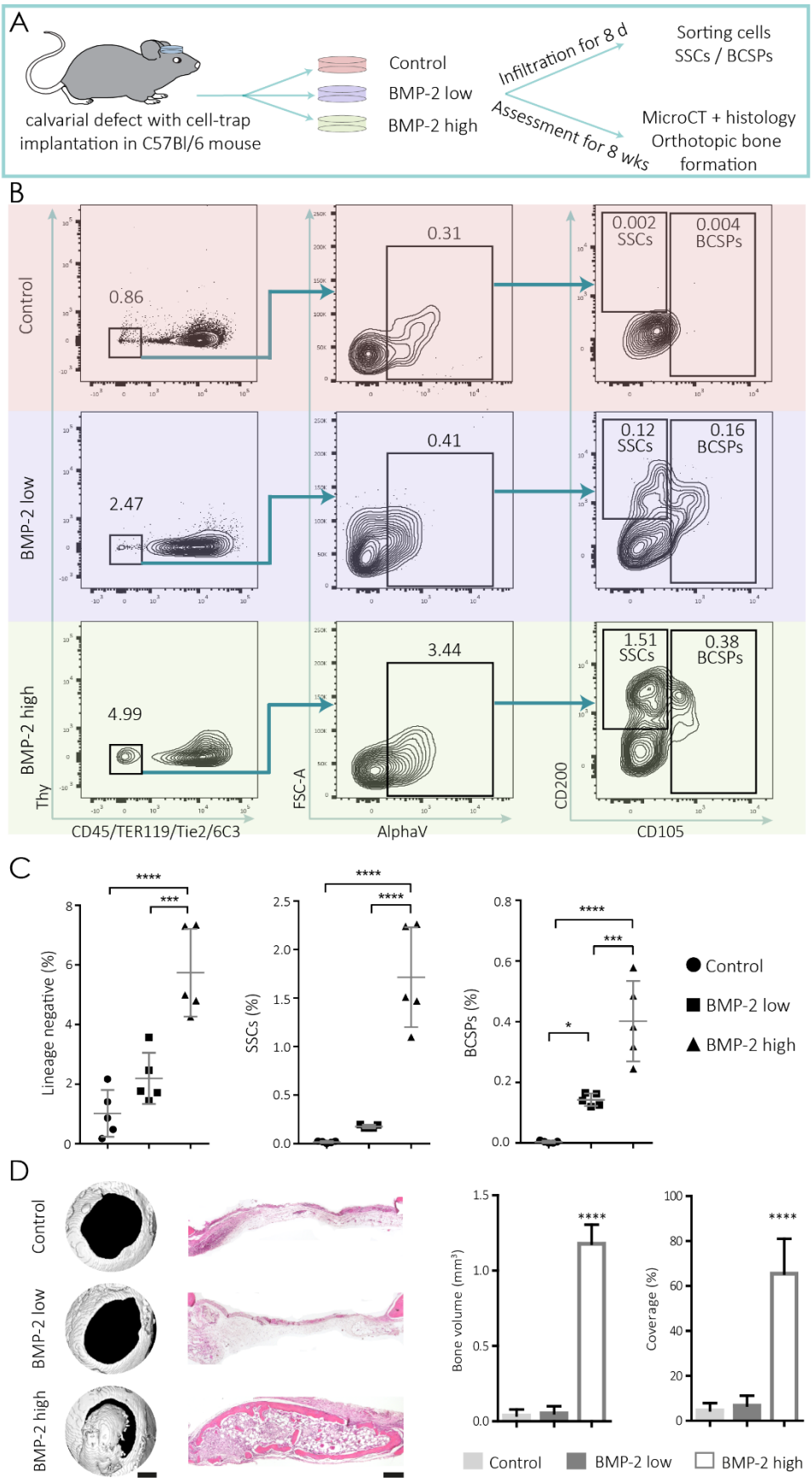

Figure 2. TG-PEG hydrogels promoted SSC and BCSP recruitment and bone healing

(**a**) Scheme of the experimental setup. TG-PEG hydrogels containing 0, 0.2 or 0.8 µg BMP-2 were implanted in murine critical-size calvarial defects. Fractions of infiltrating SSCs and BCSPs were determined by flow cytometry of enzymatically harvested

cells from day 8 implants. Bone formation was assessed at 8 weeks by microCT. (**b**) Representative FACS analysis of pre-gated live single cells from 8-day implants from each condition is shown. (**c**) Quantitative assessment of recruited healing-associated lineage-negative cells, SSCs and BCSPs. (**d**) Representative top views of 3D surface rendered microCT measurements after 8 weeks treatment with TG-hydrogels releasing different doses of BMP-2 (left panel, scale bar: 1 mm), corresponding H&E stained histological sections (middle panel, scale bar: 200 µm) and microCT quantifications showing bone volume and coverage (right panel). Data are depicted as mean ± SD, n = 5. One-way ANOVA Bonferroni's *post hoc* test * P < 0.05, ** P < 0.01 *** P < 0.001, **** P < 0.0001.

When bone defects were treated for up to 8 weeks with hydrogels containing no or low-dose BMP-2 they did not heal (Figure 2 d). In contrast, hydrogels containing high-dose BMP-2 elicited an efficient healing of bone defects. Together, these results demonstrate that hydrogel-delivered BMP-2 promoted the enrichment of SSCs and BCSPs in a dose-dependent manner and that the number of these cells and / or the available dose of BMP-2 needs to reach a critical threshold for bone healing to occur.

In vivo osteogenic potential of prospectively isolated SSCs and BCSPs

SSCs and BCSPs were shown to be involved in BMP-2 mediated healing of bone as well as in neonatal bone formation, indicating that in both processes they could have equivalent functions[30,41]. Therefore, we reasoned that sufficient quantities of these low-abundant SSCs and BCSPs for further *in vitro* and *in vivo* evaluations could be obtained by their isolation from neonatal mice. To allow the *in vivo* tracing of SSCs and BCSPs, they were isolated from limbs and sternum of P3 GFP- mice by mechanical and enzymatically-based release and prospective isolation using previously described marker panels (Figure 3 a, Figure S1 a)[30,41]. While this isolation procedure required a significant amount of time for fluorescence activated cell sorting (FACS), SSCs and BCSPs could be obtained reproducibly with high purity over 90% (Figure S1 b). When seeded at clonal dilution (110 cells cm^{-2}) for 9 days, both prospectively isolated cell fractions formed fibroblast colony forming units (CFU-F), though they were significantly higher for SSCs as compared to BCSPs (Figure 3 b, left panel). Both subpopulations showed spindle-shaped morphology and had strong proliferative potential (Figure 3 b, right panel).

Previous studies have demonstrated that SSCs and BCSPs spontaneously form bone when implanted beneath the renal capsule[30,41]. Here, prospectively isolated non-expanded SSCs and BCSPs spontaneously differentiated into bony tissues upon subcutaneous implantation as shown by histological sections stained with Movat's pentachrome or GFP-specific antibodies (Figure 3 c, and control GFP staining Figure S3 a).

Furthermore, to test the osteogenic potential of SSCs and BCSPs in a defect-mimicking model, they were encapsulated in biomimetic hydrogel discs of 4.4 mm diameter and 0.8 mm thickness (at a concentration of 10^7 cells per ml of hydrogel, optimized with human bone marrow stromal cells (Figure S2) and transplanted into segmental bone defects (Figure 3 d). In the absence of an osteogenic signal, both SSCs and BCSPs did not substantially support the healing of critical-sized

bone defects. However, micro computed tomography (microCT) revealed the presence of small bony particles and significantly improved bone healing upon SSC and BCSP transplantation as compared to treatment with murine embryonic fibroblasts (MEFs). Examination of decalcified tissue sections stained with Movat's pentachrome, GFP or macrophage (F4/80)-specific antibodies confirmed the spontaneous osteogenic differentiation of prospectively isolated SSCs and BCSPs (Figure 3 e, Figure S3 b). In contrast, co-treatments with low-dose BMP-2 (0.2 μg) and SSCs or BCSPs elicited a robust bone formation leading to a continuous shell of mineralized bone covering the defect as illustrated and quantified by microCT (Figure 3 d). Tissue sections revealed that the bone cortex encompassed trabecular bone elements and a hematopoietic compartment (Figure 3 e, bottom left panels). GFP-specific stained tissue sections revealed that transplanted SSCs and BCSPs had differentiated into bone-lining osteoblasts as well as matrix entrapped osteocytes (Figure 3 e, bottom right panel). While in control treatments with MEFs (10^7 cells per ml hydrogel), there were no signs of bone regeneration in absence of or low-dose BMP-2 (Figure S4 a). Treatments with mouse osteoblasts (MC3T3) resulted in bone formation only in presence of low-dose BMP-2, but not in its absence (Figure S4 b). Together, these data indicate that in the bone healing microenvironment both SSCs and BCSPs could spontaneously differentiate into osteogenic lineage cells. Moreover, in presence of low, but still subcritical dose of BMP-2, SSCs and BCSPs but not MEFs specifically participated in a robust bone formation.

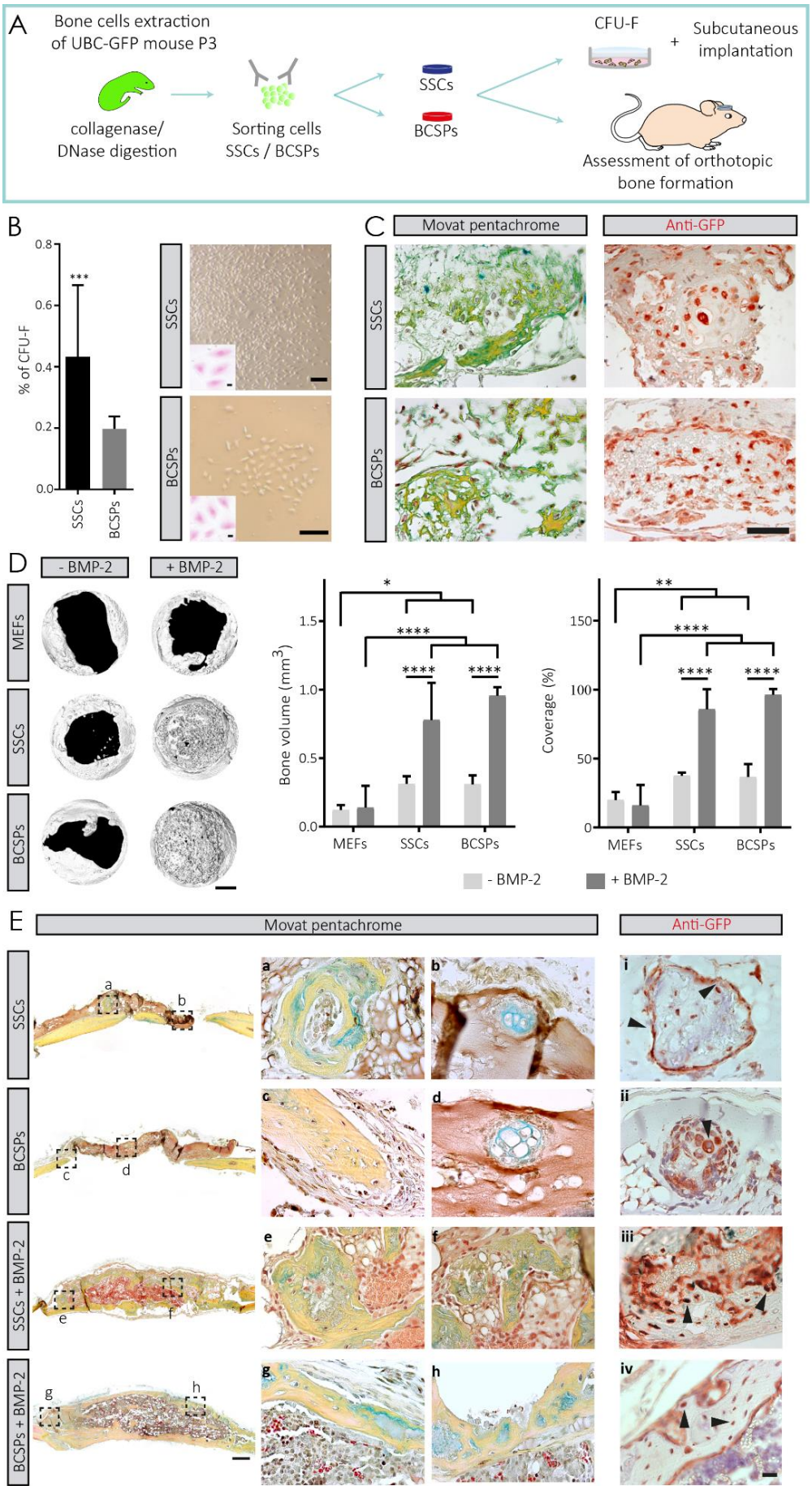

Figure 3. Characterization of prospectively isolated SSCs and BCSPs

(**a**) Scheme of murine SSC and BCSP prospective isolation and testing. SSCs and BCSPs were prospectively isolated from limbs and sternum of P3 GFP-mice. (**b**) *In vitro* colony formation of 110 freshly isolated cells cm-2 as observed after 4 days of seeding by brightfield microscopy of unstained (scale bar: 200 µm) and crystal violet stained samples (inlets, scale bar: 50 µm) as well as quantification of colonies (larger than 30 cells per colony) after 9 days of culture (left panel). Data are depicted as mean ± SD, for SSCs n = 18, for BCSPs n = 6, counted wells. Unpaired *t*-test *** $P < 0.001$. (**c**) Spontaneous differentiation of freshly isolated SSCs and BCSPs in mouse subcutaneous implants by Movat's pentachrome staining and anti-GFP stained histological sections (scale bar: 50 µm) (**d-e**) Healing of calvarial defects in immunocompromised mice after 4 weeks of implantation of TG-PEG hydrogels containing no or 0.2 µg BMP-2 as well as prospectively isolated SSCs, prospectively isolated BCSPs, or MEFs (10^7 cells per ml of hydrogel). (**d**) Representative top views of 3D surface rendered microCT reconstructions (left panel, scale bar: 1 mm) and microCT-based quantification of bone volume and defect coverage (right panels). Data are depicted as mean ± SD, MEFs ± BMP-2 n = 5, SSCs – BMP-2 n = 7, SSCs + BMP-2 n = 4 and BCSPs ± BMP-2 n = 7. Two-way ANOVA Bonferroni's *post hoc* test * $P < 0.05$, ** $P < 0.01$, *** $P < 0.001$, **** $P < 0.0001$. (**e**) Movat's pentachrome stained coronal cross sections of the full implant (left panel, scale bar: 200 µm) and (**a-h**) areas of the bone-implant interphase and from inside the healing implant. In red (fibrin) muscle/vascularized tissue; in yellow (reticular fibers/collagen) bone; in green/blue (mucin) cartilaginous tissue; and in black, nuclei and elastic fibers. (**i-iv**) GFP-specific stained tissue sections from the inside of the healing implant. In brown GFP cells; black triangles indicate SSCs and BCSPs in osteocyte-like positions within the remodeling healing area (scale bar: 20 µm).

Expanded SSCs and BCSPs maintain their *in vitro* osteogenic differentiation potential

To improve the availability of SSCs and BCSPs, both cell types were prospectively isolated from limbs and sternum of neonatal mice and expanded under standard culture conditions. To determine how rapid SSCs and BCSPs lose their phenotypic identity in *in vitro* culture, the expression of the cell surface markers CD105 and CD200 were reanalysed after two passages (Figure S5). Only 3.7% of expanded SSCs (e-SSCs) expressed CD200 (Figure S5 a), while 43.3% of the expanded BCSPs (e-BCSPs) remained CD105 positive (Figure S5 b). Interestingly, 33.7% of the e-SSCs acquired the expression of CD105 while they lost CD200 expression, exhibiting a phenotype comparable to prospectively isolated BCSPs (Figure S5 a). These data show a rapid loss of the initial marker profile in both e-SSCs and e-BCSPs and indicate their shift to a more differentiated phenotype upon *in vitro* culture.

To test the e-SSC's and e-BCSP's *in vitro* osteogenic differentiation potential they were encapsulated in TG-PEG hydrogels at a density of $3 \cdot 10^6$ cells per ml and cultured for 8 days in presence or absence of 100 ng ml^{-1} BMP-2. Their expression and activity of alkaline phosphatase (ALP), an intermediate marker of bone formation, were assessed. As in the *in vivo* assessments described above, MEFs and MC3T3 served as negative and positive (resp.) control cell types (Figure 4 a, b). While e-BCSPs and MC3T3 showed a basal ALP activity under control culture conditions, there was almost no ALP activity in MEFs and e-SSCs. To better mimic the differentiation microenvironment present in bone defects, all cell types were exposed to 100 ng ml^{-1} BMP-2 resulting in the significant upregulation of ALP in all osteogenic cell types but not in MEFs.

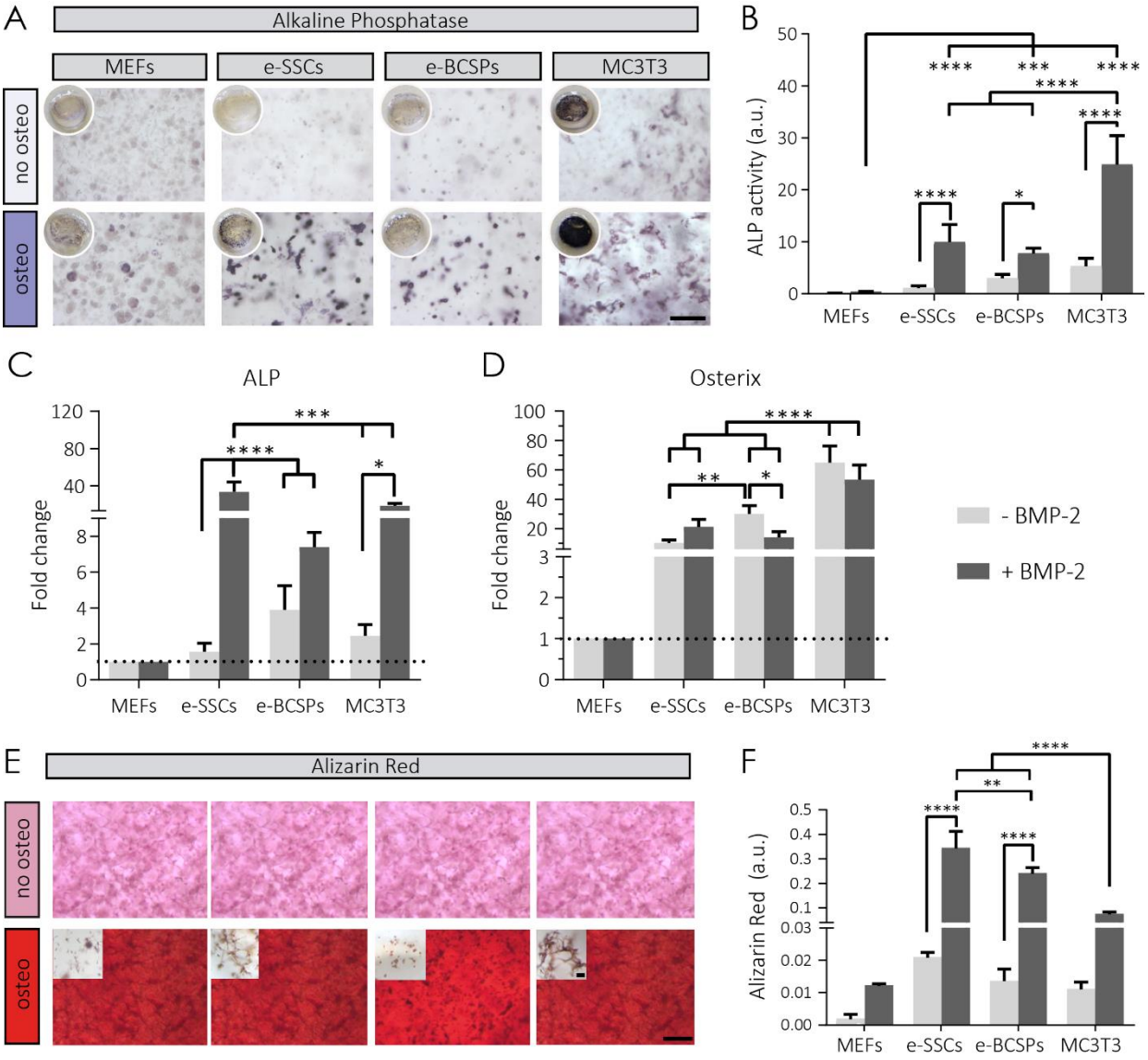

Figure 4. ***In vitro*** **osteogenic ability of e-SSCs and e-BCSPs**

e-SSCs and e-BCSPs as well as MEFs and MC3T3 cells were encapsulated at a seeding density of $3 \cdot 10^6$ cells per ml of TG-PEG hydrogel and cultured either in presence of 0 or 100 ng ml^{-1} BMP-2 medium. (**a-d**) The differentiation of the cell populations after 8 days of culture was determined by (**a**) alkaline phosphatase (ALP) staining (scale bar: 200 µm) and (**b**) quantitative evaluation of enzymatic ALP activity. ALP activity values were normalized to DNA content of the samples. Data are depicted as mean ± SD, n = 6. (**c**) Gene expression analysis of the early markers ALP and (**d**) osterix. For gene expression analysis Actb served as reference gene and the normalization was done upon MEFs. For CT values distribution of Actb gene see Figure S6. Data are depicted as mean ± SD, n = 4. (**e-f**) The differentiation of all cell populations after 14 days of culture was determined by (**e**) imaging of alizarin red stained (ARS) samples (scale bar: 50 µm) and by (**f**) quantification of ARS by absorbance at 405 nm. Data are depicted as mean ± SD, n = 4. Two-way ANOVA Bonferroni's *post hoc* test * $P < 0.05$, ** $P < 0.01$ *** $P < 0.001$, **** $P < 0.0001$.

To further confirm the osteogenic differentiation of 3D cultured cells, mRNA expression levels of the osteogenic markers alkaline phosphatase (ALP) and the transcription factor SP7 (osterix) were analyzed by RT-qPCR (Figure 4 c, d). In all osteogenic cells, ALP was significantly induced by BMP-2. In contrast, osterix was more abundant in calvarial preosteoblasts MC3T3 compared to

the e-SSC and e-BCSP populations and could not be further enhanced by BMP-2 treatment. This goes in line with previous reports which showed osterix to be required for craniofacial development and participate in the differentiation into mature osteoblasts[43].

We next investigated matrix mineralization, a late parameter of osteogenic differentiation, in an extracellular matrix (ECM) mimicking environment. Therefore, MEFs, e-SSCs, e-BCSPs, and MC3T3 cells were encapsulated in biomimetic hydrogels and cultured for 14 days under non-osteogenic or osteogenic conditions (supplemented with 100 ng ml^{-1} of BMP-2 and enriched with medium complements). Under non-osteogenic conditions, MEFs did not show any signs of mineralization. While under osteogenic conditions, e-SSCs, e-BCSPs and MC3T3 cells led to increasing numbers of mineralized nodules as observed by Alizarin Red S (ARS) stain (Figure 4 e). More importantly, e-SSCs and e-BCSPs cultured under osteogenic differentiation conditions significantly increased matrix mineralization in comparison to MEFs and MC3T3 cells (0.24 ± 0.01 and 0.34 ± 0.03 to 0.01 ± 0.0003 and 0.07 ± 0.005, respectively) as shown by ARS stain and absorbance measurements of extracted ARS (Figure 4 e, f). Taken together, these data suggest that e-SSCs and e-BCSPs maintained their osteogenic properties to a significant degree under standard culture conditions.

In vivo osteogenic differentiation potential of e-SSCs and e-BCSPs

In vitro differentiation does not sufficiently reproduce *in vivo* microenvironmental conditions and must be confirmed by *in vivo* evaluations[44]. Therefore, to confirm their osteogenic potential, GFP^+ e-SSCs and e-BCSPs were encapsulated (10^7 cells per ml of hydrogel) in biomimetic hydrogels that contained no or low-dose (0.2 μg) BMP-2 and implanted for four weeks in calvarial defects of immunocompromised mice (Figure 5 a) As shown by microCT evaluations, in the absence of BMP-2, both e-SSCs and e-BCSPs only minimally supported the healing of bone (Figure 5 b). In contrast, in the presence of low-dose BMP-2, e-SSCs and e-BCSPs significantly promoted bone healing (by an increase of bone volume) as compared to the MC3T3 controls. The bone healing accomplished by e-SSCs and e-BCSPs in presence of low BMP-2 doses, as determined by volumes of bone mineral deposition within the defect area, reached values of 1.308 ± 0.159 mm^3 and 1.198 ± 0.203 mm^3 respectively. These bone volumes are comparable to uninjured control calvarias which have a volume of 1.365 ± 0.132 mm^3. Histological evaluations of healing defects by Movat's pentachrome (Figure 5 c, left panels) and anti-GFP stainings (Figure 5 c, right panel) revealed that both e-SSCs and e-BCSPs localized to the margins of bone defects and actively participated in the formation of bone nodules by forming both osteoblasts and osteocytes (Figure 5 c). These results showed that expanded cells performed comparable to their freshly isolated cell populations. Together, these data indicate that e-SSCs and e-BCSPs retained their osteogenic potential during the process of passaging and time in culture but required additional effective osteogenic cues for the regeneration of large bone defects.

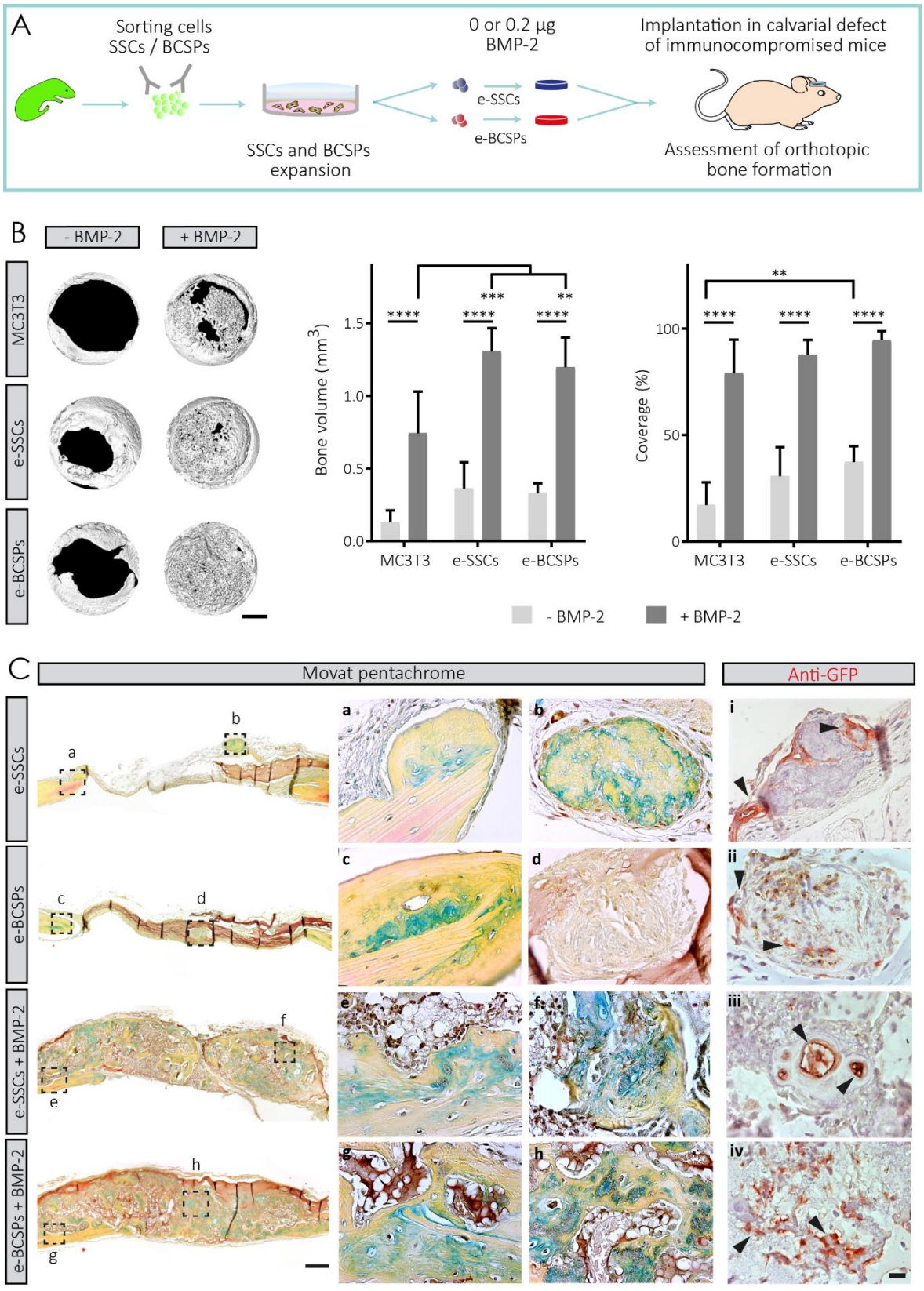

Figure 5. ***In vivo*** **osteogenic differentiation of expanded SSCs and BCSPs in orthotopic bone regeneration**

(**a**) GFP^{+} P3 limbs and sternum derived SSCs and BCSPs were expanded under standard cell culture conditions and encapsulated in TG-PEG hydrogels (10^{7} cells per ml of hydrogel) containing 0 or 0.2 µg BMP-2. Then, they were implanted into calvarial defects of immunocompromised receiver mice to assess bone formation and localization of the transplanted cells. (**b**) *Ex situ* microCT evaluations of bone healing 4 weeks post-craniotomy. Representative top view reconstructions of 3D surface rendered

microCT measurements (scale bar: 1 mm, left panels) and quantitative assessment of bone volume and coverage in the defect area. Data are depicted as mean ± SD, n = 5. Two-way ANOVA Bonferroni's *post hoc* test * P < 0.05, ** P < 0.01 *** P < 0.001, **** P < 0.0001. (**c**) Movat's pentachrome stained sections of coronal cross sections (scale bar on the left: 200 µm), middle panel, red (fibrin) indicates muscle/vascularized tissue; yellow (reticular fibers/collagen) indicates bone; green/blue (mucin) indicates cartilaginous tissue; and black, nuclei and elastic fibers. Contribution of e-SSCs and e-BCSPs to newly formed calvarial bone was assessed by immunohistochemistry. (**a-h**) Inlets of pentachrome stained coronal cross sections. (**i-iv**) Anti-GFP immunohistochemistry for localization of SSCs and BCSPs within the newly formed calvarial bone (scale bar: 20 µm, black triangles indicate stained cells in osteocyte-like positions within the remodeling healing area).

Discussion

Our study shows that the combination of low-dose BMP-2 and a sufficient number of skeletal stem or progenitor cells enables the efficient healing of bone defects, while the treatment with either cells alone or only low-dose BMP-2 remains ineffective. In the natural healing sequence of bone defects, it is challenging to dissect the effect of an osteogenic cue from the contribution of the mobilized skeletal stem and progenitor cell populations. Here, we employed biomimetic hydrogel niches to study the recruitment of endogenous SSCs and BCSPs as well as to locally deliver them in presence or absence of the osteogenic growth factor BMP-2 and evaluate bone regeneration. In previous work, chemical and physical properties of TG-PEG hydrogels were optimized to promote infiltration of host cells to heal calvarial defects[39]. Moreover, these provisional hydrogel niches have already been shown to enable the regeneration of bone in presence of high-dose BMP-2[39,40,45].

Bone regeneration requires BMP treatment that far exceeds physiological doses in both mice and human patients[46,47]. This could be due to the fact that delivered BMP either does not exert its full activity or that it does not encounter cellular entities that can promote or undergo osteogenesis[48,49]. Interestingly, biomimetic matrix-based release of low-dose BMP-2 significantly improved the mobilization of SSCs and BCSPs as compared to control treatments, despite the dose being subcritical to prompt bone regeneration by itself. This suggests that in this healing microenvironment the still low numbers of mobilized endogenous SSCs and BCSPs were insufficient to initiate bone formation. Additionally, it could also indicate that the delivered BMP-2 had dispersed by the time osteogenic cells were recruited[50]. Although high-dose BMP-2 more robustly mobilized SSCs and BCSPs, the efficient regeneration of bone defects could also be due to the improved availability of the osteogenic signal and therefore the enhanced differentiation of these recruited cells[46].

When transplanted beneath the renal capsule, neonatal murine bone-derived SSCs and BCSPs induced the formation of bone, cartilage, and a marrow cavity[30]. Therefore, we reasoned that the bone-healing microenvironment could provide sufficiently strong osteogenic cues to enable a purely cell-mediated bone healing. In fact, in the vicinity of regenerating bones, both SSCs and BCSPs spontaneously formed osteoblasts and even further differentiated into osteocytes. However, by the transplantation of 10^7 SSCs or BCSPs comprising approximately $2\text{-}5 \cdot 10^3$ colony forming units (CFU-F) per ml of hydrogel, only very few small cartilage or bone nodules were

formed inside the treated bone defects. This is consistent with earlier findings, where the number of colony forming units (CFU-F) of hBMSCs or adipose derived stem cells (hASCs) was shown to be a factor in determining the bone forming potential of cell-seeded scaffolds[51,52]. Together this suggests that within such healing microenvironments, SSCs and BCSPs can spontaneously differentiate into osteogenic cells, but for complete bone formation they would need to be present either in extremely high cell densities or further enriched in CFU-Fs.

Upon combined treatment of bone defects with hydrogels comprising prospectively isolated SSCs or BCSPs and low-dose BMP-2 we observed robust bone formation. Additionally, the progeny of the transplanted SSCs and BCSPs gave rise to osteoblasts and osteocytes within the regenerated bone as previously shown[53]. This data shows that subcritical doses of BMP-2 are sufficient to heal bone defects when bone stem or progenitor cells are enriched at the site of bone healing. It also indicates that most efficient bone regeneration treatments may rely on the mobilization or transplantation of skeletal stem or progenitor cells in addition to the release of adequate doses of osteogenic cues in a temporally controlled fashion[54]. Thus, it is key to employ a biomimetic 3D hydrogel that permits first the required migration and infiltration of cells, and second, their differentiation into bone matrix producing cells capable of remodeling their microenvironment by proteolysis. Here, we employed TG-PEG hydrogels containing RGD, the adhesion peptide found in fibronectin and other ECM proteins, as well as MMP-1 cleavable sites. Though the PEG backbone is chemically inert, it cannot be completely ruled out that incorporation of these cellular interaction sites directly influences the osteogenic differentiation of transplanted cells.

Prospectively isolated SSCs and BCSPs were assessed with intermediate expansion steps which, according to previous studies, might lead to selective expansion of cellular entities due to paracrine effects or culture-induced phenotypic changes[55]. While being a highly reproducible process, the prospective isolation of SSCs and BCSPs in sufficient quantities is a labor- and cost-intensive procedure limiting its utility for routine *in vivo* transplantation studies. Therefore, we aimed at expanding these cell populations while evaluating the oft-described loss of phenotypic properties and cell type-specific functions during expansion. Indeed, the expression of cell type-specific markers (CD105 and CD200) changed after only two passages during *in vitro* expansion resulting in a shift within the SSCs towards a BCSP-resembling phenotype. These data are consistent with earlier findings showing the partial loss of SSCs stem cell properties under standard *in vitro* culture[30]. However, *in vitro* assays revealed that both expanded cells (4-6 passages), e-SSCs and e-BCSPs, retained their osteogenic properties. Transplantations to the bone-healing microenvironment confirmed that both e-SSCs and e-BCSPs maintained their ability to spontaneously form osteogenic cells and regenerate bone in the presence of low-dose BMP-2. These data indicate that e-SSCs and e-BCSPs still comprise specific endogenous healing associated stem or progenitor cell populations. Therefore, these cells could be highly relevant for the study of healing dynamics including cellular and molecular functions both *in vitro* and *in vivo*. The recent discovery of human cell types[31] analogous to the murine cells used here should motivate follow-up studies and play a pivotal role in bringing this approach to the clinics for treating human patients.

The soft biomimetic hydrogels (about 400 Pa) used here are fully engineered substrates specifically tailorable by modular formulation of biological functionalities with synthetic polymers[39]. The flexibility of this system allows the adjustment of proteolytic degradability, integrin interactions, and growth factor binding and release[35,38,39,56]. We are convinced that, in combination with the e-SSCs and e-BCSPs, this system enables the establishment of 3D culture models where individual healing parameters can be studied in the absence of confounding matrix signaling as would be the case for naturally-derived biomaterials. More importantly, we propose that such models could be used to carefully evaluate the functionality of matrix-immobilized signals by tuning their sequential release, allowing the design of novel healing promoting materials and treatment regimens. Finally, the properties of the newly developed materials could be directly tested in animal models allowing for the correlation between *in vitro* and *in vivo* observations to further enable the efficient improvement of biomaterials.

While we showed that in the vicinity of healing bones SSCs and BCSPs spontaneously differentiate into osteogenic cells, we have not systematically evaluated the influence of cell and CFU-F density at the site of healing. In light of the decreased mobilization and differentiation capacity of SSCs and BCSPs in aged or diabetic animals[41,57,58], this will be an important parameter to establish clinically relevant models. Moreover, the fate and function of SSCs and BCSPs after *in vivo* transplantation, namely their osteogenic differentiation, their engraftment and survival as well as their role in paracrine signaling will need further analysis. In accordance with the diamond principle the prerequisite for functioning bone healing is a complex interaction between osteogenic cell populations, osteoinductive stimuli, an osteoconductive matrix and mechanical stimuli[59]. While paracrine signals seem to play an important role in bone healing, SSC progeny may positively regulate their own expansion, shifting from a stem population to a progenitor state, or participate in lineage specification[31]. Therefore, correlation of BMP-2 dosing and cell seeding density will also need further careful evaluation. Additionally, while we have shown that expanded fetal limb and sternum bone-derived cells have substantial osteogenic properties, their relative functional capacity compared to prospectively isolated SSCs and BCSPs from healing bones and from other fetal or adult bone tissues need to be elucidated in more detail. Finally, the comparison of murine and human SSCs would be an important next step to accurately appraise the predictive value of the cells and models presented here.

Conclusions

Taken together, in this study we have employed a biomimetic scaffold-based approach to investigate the role of osteogenic differentiation and mobilization of SSCs and BCSPs during bone regeneration. We provide evidence that the augmentation of SSCs and BCSPs at the healing site coupled with low-dose BMP-2 delivery most efficiently fosters bone healing. Additionally, we show that expanded e-SSCs and e-BCSPs retain the healing capacity of stem and progenitor cells. Their

relatively easy access enables the establishment and optimization of novel, well-defined skeletal stem and progenitor cells as well as innovative materials-based healing promoting strategies.

Acknowledgements

We thank Dr. Christopher Millan for his help and feedback in proofreading the manuscript, Dr. Paolo Cinelli for support with microCT, Flora Nicholls for help with animal experiments, Dr. Chafik Ghayor for providing MC3T3-E1 sc24 cells, Prof. Marcy Zenobi-Wong and Dr. Nicolas Broguière for support with rheology measurements. The research leading to these results has received funding from the People Programme (Marie Curie Actions) of the European Union's Seventh Framework Programme FP7/2007-2013/ under REA grant agreement No. 607868 (iTERM), and the Swiss National Science Foundation No. CR33I3_153316/1 and 310030_169808/1.

Experimental procedures

TG-PEG hydrogel formation. Matrix metalloprotease (MMP)-sensitive TG-PEG hydrogels that contained 50 μM RGD were formed with a final dry mass content of 1.7% (unless stated differently) in Tris buffer (50 mM, pH 7.6) containing calcium chloride (50 mM) as previously described[34,35]. Briefly, 8-arm PEG-VS (PEG-vinylsulfone, 40kDa MW; NOF, Germany) was functionalized with peptides (obtained with a purity of > 95% from Bachem AG, Switzerland) that contained an earlier described cysteine cassette (ERCG) optimized for its reaction with PEG-VS and either a factor XIII (FXIII) glutamine acceptor substrate sequence (Gln; H-NQEQVSPL-ERCG-NH_2) or a matrix metalloproteinase degradable (*in italics*) lysine donor substrate ($MMP_{sensitive}$-Lys; Ac-FKGG-*GPQGIWGQ*-ERCG-NH_2). A 1.2 molar excess of peptides over PEG-VS was reacted in TEA buffer (triethanolamine, pH 8.0) for 2 h at 37 °C. Resulting 8-PEG-Gln and 8-PEG-$MMP_{sensitive}$-Lys precursors were excessively dialyzed against pure water, lyophilized and stored at -20 °C until further use. FXIII (200 U ml^{-1}, Fibrogammin P, CSL Behring, Switzerland) was activated (FXIIIa) with thrombin (2 U ml^{-1}, Sigma–Aldrich, Switzerland) for 30 min at 37 °C and stored at -80 °C. Stoichiometrically balanced solutions of 8-PEG-Gln and 8-PEG-$MMP_{sensitive}$-Lys were prepared in Tris buffer (50 mM, pH 7.6) and calcium chloride (50 mM). Prior to the initiation of crosslinking 50 μM Gln-RGD (Ac-FKGG-RGDSPG-NH_2) and indicated amounts of growth factors and cells were added to the precursor solutions. The crosslinking of TG-PEG hydrogels was initiated by the addition of the transglutaminase FXIIIa (10 U ml^{-1}). FXIIIa catalyzes acyl-transfer reactions between the α-carboxamide group of the Gln glutaminyl residue and the ε-amino group of the Lys lysyl residue, resulting in the formation of ε-(α glutamyl) lysine isopeptide side-chain bridges between 8-PEG-Gln and 8-PEG-$MMP_{sensitive}$-Lys precursors[34]. Disc-shaped hydrogels were formed by casting droplets of crosslinking hydrogel formulations between two sterile hydrophobic glass microscopy slides (Sigma-Aldrich, SigmaCote) separated by 0.8 mm thick spacers, clamping with binder clips. Gels were incubated at 37 °C for 20 min. Hydrogel discs were released from the glass sides and transferred to cell culture medium or stored in humidified atmosphere until transplantation into cranial defects.

Rheological measurements. Hydrogel gelation was analyzed on a rheometer (MCR 301, Anton Paar) equipped with 20 mm plate–plate geometry (PP20, Anton Paar) at 37 °C in a humidified atmosphere. For measurements after swelling, TG-PEG hydrogels at different polymer concentrations (1.2%, 1.7%, 2.1% and 5% w/v) were prepared 24 h before measurements and incubated in Tris buffer at 37 °C. Swollen hydrogels were then loaded on the rheometer, compressed by 10% and measured with a frequency sweep at 1% strain. For *in situ* measurements gel mixtures were precisely loaded onto the center of the bottom plate. The upper plate was lowered to a measuring gap size of 0.2 mm, ensuring proper loading of the space between the plates and gel precursors, the dynamic oscillating measurement was then started. The evolution of storage and loss moduli at a constant angular frequency of 1 Hz and constant shear strain of 4% was recorded for 30 min when equilibrium was reached.

Animal care. All animal research procedures were approved by the Animal Experimentation Committee of the Veterinary Office of the Canton of Zurich, Switzerland and followed the guidelines of the Swiss Federal Veterinary Office for the use and care of laboratory animals. The cranial defect model was performed using 8-9-week-old female Crl:NMRI-*Foxn1*^{nu} mice (purchased from Charles River) or 8-9-week-old female wild-type C57BL/6 mice (purchased from Harlan). For the isolation of SSCs and BCSPs, postnatal day 3 (P3) transgenic mice that express enhanced Green Fluorescent Protein under direction of the human ubiquitin C promoter [C57BL/6-Tg(UBC-GFP)30Scha/J mice] (GFP-mice) maintained in our laboratory were employed. The use of GFP mice-derived cells enabled the *in vivo* tracking of transplanted cell populations into non-GFP nude mice by microscopy of fresh samples as well as GFP-specific immunostaining.

Calvarial defect healing model. TG-PEG hydrogels of 4.4 mm diameter (11 µl) that contained 0, 0.2, or 0.8 µg recombinant human BMP-2 (CHO cell derived, PeproTech), 10^7 cells per ml of hydrogel, or combinations thereof were casted between two sterile hydrophobic glass microscopy slides, completely released and stored in a humidified container until implantation. Craniotomies of 4 mm diameter were created in the parietal bones of the skull, one on each side of the sagittal suture. Pre-formed hydrogel discs were placed in the cranial defects and the skin was closed with 6.0 Vicryl sutures (Ethicon). Mice were euthanized after 4 to 8 weeks of treatment. Calvaria were excised, fixed overnight in 4% formalin, and stored in Tris buffer saline (TBS) before *ex vivo* endpoint analysis by microCT and histology.

Subcutaneous implantation. TG-PEG hydrogels (3 µl) containing 10^7 SSCs or BCSPs per ml of hydrogel were prepared. To create subcutaneous pouches in nude mice (Crl:NMRI-*Foxn1*^{nu}, Charles River), ca. 6 mm lateral skin incisions were made in four dorsal positions. Pre-formed hydrogel discs were placed in pouches and the skin was closed with 6.0 Vicryl sutures (Ethicon). Mice were euthanized after 4 weeks of implantation, samples were excised, fixed overnight in 4% formalin, and stored in TBS before *ex vivo* evaluations.

Prospective isolation and flow cytometry analysis (FACS) of SSCs and BCSPs. **For the isolation of SSCs and BCSPs**, we followed the protocol from the original publication where these cell populations were first defined[30]. Briefly, postnatal P3 GFP-labeled mice were euthanized by decapitation. Their skeletal tissue including limbs and sternum were dissected and carefully cleaned from soft tissue. Then transferred on ice in cell culture medium (minimum essential medium alpha, MEMα) containing 1% (v/v) penicillin/streptomycin and first mechanically dissociated with scissors, followed by mortar and pestle. Then a 2x solution of collagenase A (Roche) supplemented with DNase (Qiagen) was added, resulting in 1 mg ml^{-1} and 4 Kunitz ml^{-1} respectively, in culture medium and incubated for 40 min at 37 °C under constant agitation. After collagenase digestion and neutralization in FACS buffer (1 mM EDTA, 2% v/v fetal bovine serum in PBS pH 7.2), undigested materials were further dissociated by repeated gentle pipetting. Total dissociated tissues were filtered through 100 µm nylon mesh, resulting cell suspensions centrifuged at 400 g at 4 °C and resuspended in FACS buffer ready for staining.

Similarly, **for the analysis of SSC and BCSP accumulation** in healing bone, hydrogel implants were harvested from cranial defects after 8 days of treatment. As **for murine tissues**, they were first mechanically dissected followed by enzymatic digestion in 1 mg ml^{-1} collagenase A supplemented with 4 Kunitz ml^{-1} DNase in MEMα with 1% (v/v) penicillin/streptomycin solution for 40 min at 37 °C under gentle agitation. Collagenase was neutralized in FACS buffer and undigested materials were further dissociated by gentle pipetting. Total dissociated tissues were filtered through 100 μm nylon mesh, centrifuged at 400 g at 4 °C and resuspended in FACS buffer ready for staining.

For all aforementioned retrieved cells, red blood cells were lysed by incubation with RBC lysis buffer (Biolegend) for 10 min on ice before cells were washed and re-suspended in FACS buffer. Cells were stained with fluorochrome-conjugated antibodies against CD45- PE (Biolegend, 103105), Tie2- PE (Biolegend, 124007), TER119- PE (Biolegend, 116207), 6C3- PE (Biolegend, 108307), AlphaV integrin- biotin (Biolegend, 104104), CD105- Pacific Blue (Biolegend, 120412), CD90.2- PE-Cy7 (Biolegend, 140309) and CD200- PerCP-eFluor 710 (eBioscience, 46-5200-80) for 30 min at 4 °C. Cells were washed and stained with the secondary antibody streptavidin- APC-Cy7 (Biolegend, 405208) for 30 min at 4 °C. Sytox Red dead cell stain (ThermoFisher, S34859) was used according to the manufacturer's instructions to evaluate cell viability. Flow cytometric analysis and sorting were performed on the BD FACSAria III (BD Biosciences) instruments using BD FACSDiva software. For cell sorting 100 μm nozzle and 20 psi sheath pressure were applied. Gates were defined according to the fluorescence intensity of the fluorescence minus one (FMO) containing the isotype control conjugated to the same fluorochrome as the primary antibodies. Data was further analyzed using FlowJo software (FlowJo LLC).

MicroCT analysis of mouse calvarial specimens. X-ray microtomography (microCT) scans of fixed calvaria were performed with a Micro-CT40 (Scanco Medical AG). The X-ray tube was operating at an energy of 70 kVp and an intensity of 114 μA reconstructing three-dimensional images with an isotropic voxel size of 10 μm. A global threshold corresponding to 9.8% of the maximum grey values was used to separate bone from surrounding soft tissues. Regions of interest for the evaluation were selected by placing a cylinder of 3 mm diameter in the center of bone defects. Bone volume, connectivity, and trabecular thickness within this mask were measured using the ImageJ plugin BoneJ[60]. Bone coverage was measured in a dorso-ventral projection of the cylindrical mask.

Histological staining and immunohistochemistry of orthotopic bone formation. Formalin fixed calvaria were completely decalcified with 10% w/v EDTA (pH 7.14) and embedded in paraffin. For histological evaluations, 4 μm thin tissue sections were stained with hematoxylin & eosin (Sigma-Aldrich) and Movat's pentachrome. Briefly for Movat's pentachrome, sections were sequentially incubated with alcian blue (Fluka, 1 g in 100 ml in 1% glacial acetic acid) for 10 min, alkaline alcohol (10% v/v ammonium hydroxide in 95% EtOH) for 1 hour, Weigert's iron hematoxylin (Weigert reagent A and B in a ratio 1:1) for 20 minutes, brilliant crocein R-fuchsine (1

part Biebrich Scarlet-Acid Fuchsin and 1 part 0.2% acidic fuchsin in 0.5% acetic acid) for 20 minutes, 0.5% acetic acid for 30 seconds, 5% phosphotungsten acid (PWS) 15 min, 0.5% acetic acid for 2 minutes, washed 3 times with absolute ethanol for 5 minutes, safran dye (6 g safran powder in 100 ml absolute EtOH) overnight incubation and mounted in Eukit mounting medium (Kindler GmbH, Freiburg Germany). If not stated otherwise intermediate washing steps were conducted with H_2O. In Movat's pentachrome, red (fibrin) indicates muscle/vascularized tissue; yellow (reticular fibers/collagen) indicates bone; green/blue (mucin) indicates cartilaginous tissue; and black, nuclei and elastic fibers. For immunohistochemical localization of implanted GFP expressing cells in orthotopic bone formation, sections were deparaffinized, incubated in citrate buffer (20 mM citrate buffer pH 6, 95 °C) for 20 min for antigen retrieval, blocked in 5% albumin in PBS and incubated with anti-GFP antibody (Abcam, ab290) overnight at 4 °C. Next day, they were incubated with a biotinylated secondary goat anti-rabbit antibody for 1 hour at room temperature, followed by incubation with an avidin-biotin-peroxidase complex for 1 hour at room temperature, according to the manufacturer's instructions (Vector Laboratories Inc., PK-6101). Peroxidase was revealed by incubation with AEC (3-amino-9-ethylcarbazole) red substrate (Vector Laboratories Inc., SK-4200) prior blocking with 3% H_2O_2. Similarly, for macrophage staining anti-F4/80 antibody was used (BMA Biomedical, T-2028), sections were processed as previously stated with the only difference that Proteinase K retrieval was performed instead of heat-based.

Colony-forming unit fibroblast (CFU-F) assay. Prospectively isolated SSCs and BCSPs (110 cells cm^{-2}) were seeded on collagen-coated wells (Techno Plastic Products) and cultured for 9 days in MEMα containing 10% (v/v) fetal bovine serum (FBS) and 1% (v/v) penicillin/streptomycin at 37 °C with 5% CO_2. After fixation with 4% paraformaldehyde for 20 min, colonies were stained with 0.05% (w/v) crystal violet solution for 30 min. Cell clusters counting > 30 cells were scored as colony.

Cell culture. SSC and BCSP populations were seeded on collagen coated plates and cultured in maintenance medium consisting of MEMα (Gibco Life Technologies), 10% (v/v) FBS (Gibco Life Technologies) and 1% (v/v) penicillin/streptomycin solution (P/S, Gibco Life Technologies) under standard culture conditions (37 °C with 5% CO_2). K41 (wild type) murine embryonic fibroblasts (MEFs) were maintained in Dulbecco's modified eagle medium (DMEM low glucose, with Glutamax; Gibco Life Technologies), supplemented with 20% FBS and 1% v/v P/S as previously described[61]. The murine pre-osteoblastic cell line MC3T3-E1 sub-clone 24 (MC3T3) (ATCC, Manassas, VA) was maintained in MEMα with 10% (v/v) FBS and 1% (v/v) P/S. Human bone marrow-derived stromal cells (hBMSCs) were isolated from bone marrow aspirates of healthy donors obtained during orthopedic surgical procedures after informed consent and in accordance with the local ethical committee (University Hospital Basel; Prof. Dr. Kummer; approval date 26/03/2007 Ref. Number 78/07). They were maintained in MEMα with 10% (v/v) FBS and 1% (v/v) P/S. All cells were cultured at 37 °C in a humidified atmosphere at 5% CO_2 and used between passage 2 and 6. Brightfield images were acquired with Leica inverted microscope.

Osteogenic differentiation in 3D culture using ALP staining and quantification. To assess their osteogenic differentiation cells were encapsulated in TG-PEG hydrogels (1.7% PEG, 50 μM RGD) at a final concentration of $3 \cdot 10^6$ cells per ml (n = 6) and cultured for 8 days in the respective maintenance medium which was supplemented with 0 or 100 ng ml^{-1} BMP-2. Medium was changed every 4 days. After removal of the cell culture medium, gels were washed twice with PBS. For alkaline phosphatase (ALP) staining gels were incubated with ALP substrate solution (prepared from FAST BCIP/NBT tablets; Sigma-Aldrich) as recommended by the manufacturer. When visually sufficient color had developed in positive controls (8 min), the substrate solution in all conditions was replaced with PBS and cells within hydrogels were imaged with a Zeiss 200M inverted microscope. To measure ALP activity, gels were collected and digested in 2 mg ml^{-1} collagenase A in PBS solution for 30 min at 37 °C. Cells were pelleted and resuspended in lysis buffer (500 μL of 0.56 M 2-amino-2-methyl-1-propanol, 0.2% Triton X-100, pH 10 in H_2O) on ice and gently triturated by repeated pipetting and vortexing. The cell lysate was centrifuged for 10 min at 16000 rcf before the supernatant was collected. ALP substrate (50 μl of 20 mM 4-nitrophenyl phosphate disodium salt hexahydrate, 4 mM $MgCl_2$ in lysis buffer) was added to the cell lysates (50 μl) in a 96-well plate and incubated at 37 °C for 10 min before absorbance was measured at 410 nm with a microplate reader. ALP activity measurements were normalized on the relative DNA content that was measured in cell lysates by the CyQuant NF cell proliferation assay kit (Molecular Probes).

RT-qPCR analysis of 3D cultured cells. To determine their osteogenic capacity in 3D culture, cells were encapsulated in TG-PEG hydrogels (1.7% PEG, 50 μM RGD) at a final concentration of $3 \cdot 10^6$ cells per ml (n = 4). Gels were cultured for 8 days in MEMα with 10% (v/v) FBS and 1% (v/v) P/S supplemented with 0 and 100 ng ml^{-1} BMP-2 at 37 °C with 5% CO_2. Medium and growth factors were replaced after 4 days. Cells were harvested by digesting the hydrogels with collagenase A (2 mg ml^{-1}) for 30 min at 37 °C followed by 10 min centrifugation at 300 rcf. Total RNA was isolated from cell pellets by the RNeasy Micro Kit (Qiagen) according to the manufacturer's instructions. For reverse transcription quantitative PCR (RT-qPCR), 80 ng RNA were converted into 22 μl cDNA by means of the High-Capacity cDNA Reverse Transcription Kit (Applied Biosystems). RT-qPCR was carried out using TaqMan Universal PCR Master Mix (Applied Biosystems) and the ViiA™ 7 Real-Time PCR System (Applied Biosystems). The following TaqMan primer/probe sets were used for gene expression tests: Mm00475834_m1 (Alpl); Mm04209856_m1 (Sp7). Data were normalized to the mRNA levels of Mm02619580_g1 (Actb) and relative gene expression was presented as fold change according to the $2^{-\Delta\Delta CT}$ method.

Osteogenic differentiation in 3D culture using Alizarin Red Staining. To determine their ability for matrix mineralization, cells were encapsulated in TG-PEG hydrogels (1.7% PEG, 50 μM RGD) at final concentration of $5 \cdot 10^6$ cells per ml (n = 4), and cultured in maintenance medium or osteogenic induction medium consisting of DMEM high glucose (Gibco Life Technologies) with 10% (v/v) FBS and 1% (v/v) P/S modified with 10 mM HEPES, 1 mM sodium pyruvate, 2 mM L-glutamine, L-ascorbic acid (50 μg ml^{-1}), 10 mM β-glycerol phosphate

and 100 ng ml^{-1} BMP-2. The medium was changed every 3-4 days. Higher cell density and a highly supplemented medium was necessary for matrix mineralization as previously reported in the literature [62]. Hydrogels were fixed with 4% paraformaldehyde for 20 min, washed with water, and stained for 20 min with Alizarin Red S (40 mM) in ddH_2O (pH 4.1, adjusted with 0.1% NH_4OH) under gentle agitation. After extensive washing with water, hydrogels were imaged with a Zeiss 200M inverted microscope. For colorimetric quantification Alizarin Red S was extracted by incubating hydrogels with 10% (v/v) acetic acid in ddH2O at RT for 30 min under gentle agitation. The extracted solution was collected, incubated at 85 °C for 10 min, and kept on ice for 5 min. The resulting slurry was centrifuged at 16000 g for 15 min, 500 µl of the supernatant was transferred to a new tube where the pH was adjusted within the range of 4.1 - 4.5 before the absorbance was measured at 405 nm with a microplate reader.

Statistical Analysis. All statistical analyses were performed in GraphPad Prism (version 8.0.0, GraphPad Software). Data analyses were performed using one or two-way ANOVA and *post hoc* Bonferroni's correction or Student's *t*-test assuming two-tailed distribution and unequal variances. In all cases, a P-value of < 0.05 was considered statistically significant, and all data are depicted as mean ± SD.

References

1 Carragee, E. J., Hurwitz, E. L. & Weiner, B. K. A critical review of recombinant human bone morphogenetic protein-2 trials in spinal surgery: emerging safety concerns and lessons learned. *Spine J* **11**, 471-491, doi:10.1016/j.spinee.2011.04.023 (2011).

2 Charles, L. F. *et al.* Effects of low dose FGF-2 and BMP-2 on healing of calvarial defects in old mice. *Exp Gerontol* **64**, 62-69, doi:10.1016/j.exger.2015.02.006 (2015).

3 Zara, J. N. *et al.* High doses of bone morphogenetic protein 2 induce structurally abnormal bone and inflammation in vivo. *Tissue Eng Part A* **17**, 1389-1399, doi:10.1089/ten.TEA.2010.0555 (2011).

4 Carano, R. A. & Filvaroff, E. H. Angiogenesis and bone repair. *Drug Discov Today* **8**, 980-989 (2003).

5 Einhorn, T. A. & Gerstenfeld, L. C. Fracture healing: mechanisms and interventions. *Nat Rev Rheumatol* **11**, 45-54, doi:10.1038/nrrheum.2014.164 (2015).

6 Ai-Aql, Z. S., Alagl, A. S., Graves, D. T., Gerstenfeld, L. C. & Einhorn, T. A. Molecular mechanisms controlling bone formation during fracture healing and distraction osteogenesis. *J Dent Res* **87**, 107-118, doi:10.1177/154405910808700215 (2008).

7 Wang, X. *et al.* Role of mesenchymal stem cells in bone regeneration and fracture repair: a review. *Int Orthop* **37**, 2491-2498, doi:10.1007/s00264-013-2059-2 (2013).

8 Ratcliffe, E., Glen, K. E., Naing, M. W. & Williams, D. J. Current status and perspectives on stem cell-based therapies undergoing clinical trials for regenerative medicine: case studies. *Br Med Bull* **108**, 73-94, doi:10.1093/bmb/ldt034 (2013).

9 Mumme, M. *et al.* Nasal chondrocyte-based engineered autologous cartilage tissue for repair of articular cartilage defects: an observational first-in-human trial. *The Lancet* **388**, 1985-1994, doi:10.1016/S0140-6736(16)31658-0.

10 Sipp, D., Robey, P. G. & Turner, L. Clear up this stem-cell mess. *Nature* **561**, 455-457, doi:10.1038/d41586-018-06756-9 (2018).

11 Tollemar, V. *et al.* Stem cells, growth factors and scaffolds in craniofacial regenerative medicine. *Genes Dis* **3**, 56-71, doi:10.1016/j.gendis.2015.09.004 (2016).

12 Sundelacruz, S. & Kaplan, D. L. Stem cell- and scaffold-based tissue engineering approaches to osteochondral regenerative medicine. *Semin Cell Dev Biol* **20**, 646-655, doi:10.1016/j.semcdb.2009.03.017 (2009).

13 Bose, S., Roy, M. & Bandyopadhyay, A. Recent advances in bone tissue engineering scaffolds. *Trends Biotechnol* **30**, 546-554, doi:10.1016/j.tibtech.2012.07.005 (2012).

14 O'Brien, F. J. Biomaterials & scaffolds for tissue engineering. *Mater Today* **14**, 88-95, doi:Doi 10.1016/S1369-7021(11)70058-X (2011).

15 Freudenberg, U., Liang, Y., Kiick, K. L. & Werner, C. Glycosaminoglycan-Based Biohybrid Hydrogels: A Sweet and Smart Choice for Multifunctional Biomaterials. *Adv Mater* **28**, 8861-8891, doi:10.1002/adma.201601908 (2016).

16 Lutolf, M. P. & Hubbell, J. A. Synthetic biomaterials as instructive extracellular microenvironments for morphogenesis in tissue engineering. *Nat Biotechnol* **23**, 47-55, doi:10.1038/nbt1055 (2005).

17 Lienemann, P. S., Lutolf, M. P. & Ehrbar, M. Biomimetic hydrogels for controlled biomolecule delivery to augment bone regeneration. *Adv Drug Deliv Rev* **64**, 1078-1089, doi:10.1016/j.addr.2012.03.010 (2012).

18 Tibbitt, M. W., Rodell, C. B., Burdick, J. A. & Anseth, K. S. Progress in material design for biomedical applications. *Proc Natl Acad Sci U S A* **112**, 14444-14451, doi:10.1073/pnas.1516247112 (2015).

19 Spicer, C. D., Pashuck, E. T. & Stevens, M. M. Achieving Controlled Biomolecule-Biomaterial Conjugation. *Chem Rev* **118**, 7702-7743, doi:10.1021/acs.chemrev.8b00253 (2018).

20 Badeau, B. A., Comerford, M. P., Arakawa, C. K., Shadish, J. A. & DeForest, C. A. Engineered modular biomaterial logic gates for environmentally triggered therapeutic delivery. *Nat Chem* **10**, 251-258, doi:10.1038/nchem.2917 (2018).

21 Shekaran, A. *et al.* Bone regeneration using an alpha 2 beta 1 integrin-specific hydrogel as a BMP-2 delivery vehicle. *Biomaterials* **35**, 5453-5461, doi:10.1016/j.biomaterials.2014.03.055 (2014).

22 Lee, T. T. *et al.* Light-triggered in vivo activation of adhesive peptides regulates cell adhesion, inflammation and vascularization of biomaterials. *Nat Mater* **14**, 352-360, doi:10.1038/nmat4157 (2015).

23 Dimitriou, R., Tsiridis, E. & Giannoudis, P. V. Current concepts of molecular aspects of bone healing. *Injury* **36**, 1392-1404, doi:10.1016/j.injury.2005.07.019 (2005).

24 Longoni, A. *et al.* The impact of immune response on endochondral bone regeneration. *NPJ Regen Med* **3**, 22, doi:10.1038/s41536-018-0060-5 (2018).

25 Sacchetti, B. *et al.* Self-renewing osteoprogenitors in bone marrow sinusoids can organize a hematopoietic microenvironment. *Cell* **131**, 324-336, doi:10.1016/j.cell.2007.08.025 (2007).

26 Mendez-Ferrer, S. *et al.* Mesenchymal and haematopoietic stem cells form a unique bone marrow niche. *Nature* **466**, 829-834, doi:10.1038/nature09262 (2010).

27 Park, D. *et al.* Endogenous bone marrow MSCs are dynamic, fate-restricted participants in bone maintenance and regeneration. *Cell Stem Cell* **10**, 259-272, doi:10.1016/j.stem.2012.02.003 (2012).

28 Cancedda, R., Bollini, S., Descalzi, F., Mastrogiacomo, M. & Tasso, R. Learning from Mother Nature: Innovative Tools to Boost Endogenous Repair of Critical or Difficult-to-Heal Large Tissue Defects. *Front Bioeng Biotechnol* **5**, 28, doi:10.3389/fbioe.2017.00028 (2017).

29 Chen, K. G., Johnson, K. R., McKay, R. D. G. & Robey, P. G. Concise Review: Conceptualizing Paralogous Stem-Cell Niches and Unfolding Bone Marrow Progenitor Cell Identities. *Stem Cells* **36**, 11-21, doi:10.1002/stem.2711 (2018).

30 Chan, C. K. *et al.* Identification and specification of the mouse skeletal stem cell. *Cell* **160**, 285-298, doi:10.1016/j.cell.2014.12.002 (2015).

31 Chan, C. K. F. *et al.* Identification of the Human Skeletal Stem Cell. *Cell* **175**, 43-56 e21, doi:10.1016/j.cell.2018.07.029 (2018).

32 Liu, S. *et al.* Manufacturing Differences Affect Human Bone Marrow Stromal Cell Characteristics and Function: Comparison of Production Methods and Products from Multiple Centers. *Sci Rep* **7**, 46731, doi:10.1038/srep46731 (2017).

33 McGovern, J. A., Griffin, M. & Hutmacher, D. W. Animal models for bone tissue engineering and modelling disease. *Dis Model Mech* **11**, doi:10.1242/dmm.033084 (2018).

34 Ehrbar, M. *et al.* Biomolecular hydrogels formed and degraded via site-specific enzymatic reactions. *Biomacromolecules* **8**, 3000-3007, doi:10.1021/bm070228f (2007).

35 Ehrbar, M. *et al.* Enzymatic formation of modular cell-instructive fibrin analogs for tissue engineering. *Biomaterials* **28**, 3856-3866, doi:10.1016/j.biomaterials.2007.03.027 (2007).

36 Lienemann, P. S. *et al.* A versatile approach to engineering biomolecule-presenting cellular microenvironments. *Adv Healthc Mater* **2**, 292-296, doi:10.1002/adhm.201200280 (2013).

37 Lienemann, P. S. *et al.* Locally controlling mesenchymal stem cell morphogenesis by 3D PDGF-BB gradients towards the establishment of an in vitro perivascular niche. *Integr Biol (Camb)* **7**, 101-111, doi:10.1039/c4ib00152d (2015).

38 Metzger, S. *et al.* Modular poly(ethylene glycol) matrices for the controlled 3D-localized osteogenic differentiation of mesenchymal stem cells. *Adv Healthc Mater* **4**, 550-558, doi:10.1002/adhm.201400547 (2015).

39 Ehrbar, M. *et al.* Elucidating the role of matrix stiffness in 3D cell migration and remodeling. *Biophys J* **100**, 284-293, doi:10.1016/j.bpj.2010.11.082 (2011).

40 Lienemann, P. S. *et al.* Longitudinal in vivo evaluation of bone regeneration by combined measurement of multi-pinhole SPECT and micro-CT for tissue engineering. *Sci Rep* **5**, 10238, doi:10.1038/srep10238 (2015).

41 Marecic, O. *et al.* Identification and characterization of an injury-induced skeletal progenitor. *Proc Natl Acad Sci U S A* **112**, 9920-9925, doi:10.1073/pnas.1513066112 (2015).

42 Tevlin, R. *et al.* Pharmacological rescue of diabetic skeletal stem cell niches. *Sci Transl Med* **9**, doi:10.1126/scitranslmed.aag2809 (2017).

43 Baek, W. Y., Kim, Y. J., de Crombrugghe, B. & Kim, J. E. Osterix is required for cranial neural crest-derived craniofacial bone formation. *Biochem Biophys Res Commun* **432**, 188-192, doi:10.1016/j.bbrc.2012.12.138 (2013).

44 Bianco, P. *et al.* The meaning, the sense and the significance: translating the science of mesenchymal stem cells into medicine. *Nat Med* **19**, 35-42, doi:10.1038/nm.3028 (2013).

45 Lutolf, M. P. *et al.* Repair of bone defects using synthetic mimetics of collagenous extracellular matrices. *Nat Biotechnol* **21**, 513-518, doi:10.1038/nbt818 (2003).

46 Agrawal, V. & Sinha, M. A review on carrier systems for bone morphogenetic protein-2. *J Biomed Mater Res B Appl Biomater* **105**, 904-925, doi:10.1002/jbm.b.33599 (2017).

47 Ronga, M. *et al.* Clinical applications of growth factors in bone injuries: experience with BMPs. *Injury* **44 Suppl 1**, S34-39, doi:10.1016/S0020-1383(13)70008-1 (2013).

48 Boerckel, J. D. *et al.* Effects of protein dose and delivery system on BMP-mediated bone regeneration. *Biomaterials* **32**, 5241-5251, doi:10.1016/j.biomaterials.2011.03.063 (2011).

49 Uludag, H., Gao, T., Porter, T. J., Friess, W. & Wozney, J. M. Delivery systems for BMPs: factors contributing to protein retention at an application site. *J Bone Joint Surg Am* **83-A Suppl 1**, S128-135 (2001).

50 Cowan, C. M. *et al.* MicroCT evaluation of three-dimensional mineralization in response to BMP-2 doses in vitro and in critical sized rat calvarial defects. *Tissue Eng* **13**, 501-512, doi:10.1089/ten.2006.0141 (2007).

51 Muller, A. M. *et al.* Towards an intraoperative engineering of osteogenic and vasculogenic grafts from the stromal vascular fraction of human adipose tissue. *Eur Cell Mater* **19**, 127-135 (2010).

52 Walenda, T. *et al.* Synergistic effects of growth factors and mesenchymal stromal cells for expansion of hematopoietic stem and progenitor cells. *Exp Hematol* **39**, 617-628, doi:10.1016/j.exphem.2011.02.011 (2011).

53 Chan, C. K. *et al.* Clonal precursor of bone, cartilage, and hematopoietic niche stromal cells. *Proc Natl Acad Sci U S A* **110**, 12643-12648, doi:10.1073/pnas.1310212110 (2013).

54 Zhang, Y., Yang, W., Devit, A. & van den Beucken, J. Efficiency of coculture with angiogenic cells or physiological BMP-2 administration on improving osteogenic differentiation and bone formation of MSCs. *J Biomed Mater Res A* **107**, 643-653, doi:10.1002/jbm.a.36581 (2019).

55 Bara, J. J., Richards, R. G., Alini, M. & Stoddart, M. J. Concise review: Bone marrow-derived mesenchymal stem cells change phenotype following in vitro culture: implications for basic research and the clinic. *Stem Cells* **32**, 1713-1723, doi:10.1002/stem.1649 (2014).

56 Blache, U. *et al.* Notch-inducing hydrogels reveal a perivascular switch of mesenchymal stem cell fate. *EMBO Rep* **19**, doi:10.15252/embr.201845964 (2018).

57 Stolzing, A., Jones, E., McGonagle, D. & Scutt, A. Age-related changes in human bone marrow-derived mesenchymal stem cells: consequences for cell therapies. *Mech Ageing Dev* **129**, 163-173, doi:10.1016/j.mad.2007.12.002 (2008).

58 Katsara, O. *et al.* Effects of donor age, gender, and in vitro cellular aging on the phenotypic, functional, and molecular characteristics of mouse bone marrow-derived mesenchymal stem cells. *Stem Cells Dev* **20**, 1549-1561, doi:10.1089/scd.2010.0280 (2011).

59 Giannoudis, P. V., Einhorn, T. A. & Marsh, D. Fracture healing: the diamond concept. *Injury* **38 Suppl 4**, S3-6 (2007).

60 Doube, M. *et al.* BoneJ: Free and extensible bone image analysis in ImageJ. *Bone* **47**, 1076-1079, doi:10.1016/j.bone.2010.08.023 (2010).
61 Nakamura, K. *et al.* Functional specialization of calreticulin domains. *J Cell Biol* **154**, 961-972, doi:10.1083/jcb.200102073 (2001).
62 Marion, N. W. & Mao, J. J. Mesenchymal stem cells and tissue engineering. *Methods Enzymol* **420**, 339-361, doi:10.1016/S0076-6879(06)20016-8 (2006).

Supplementary data

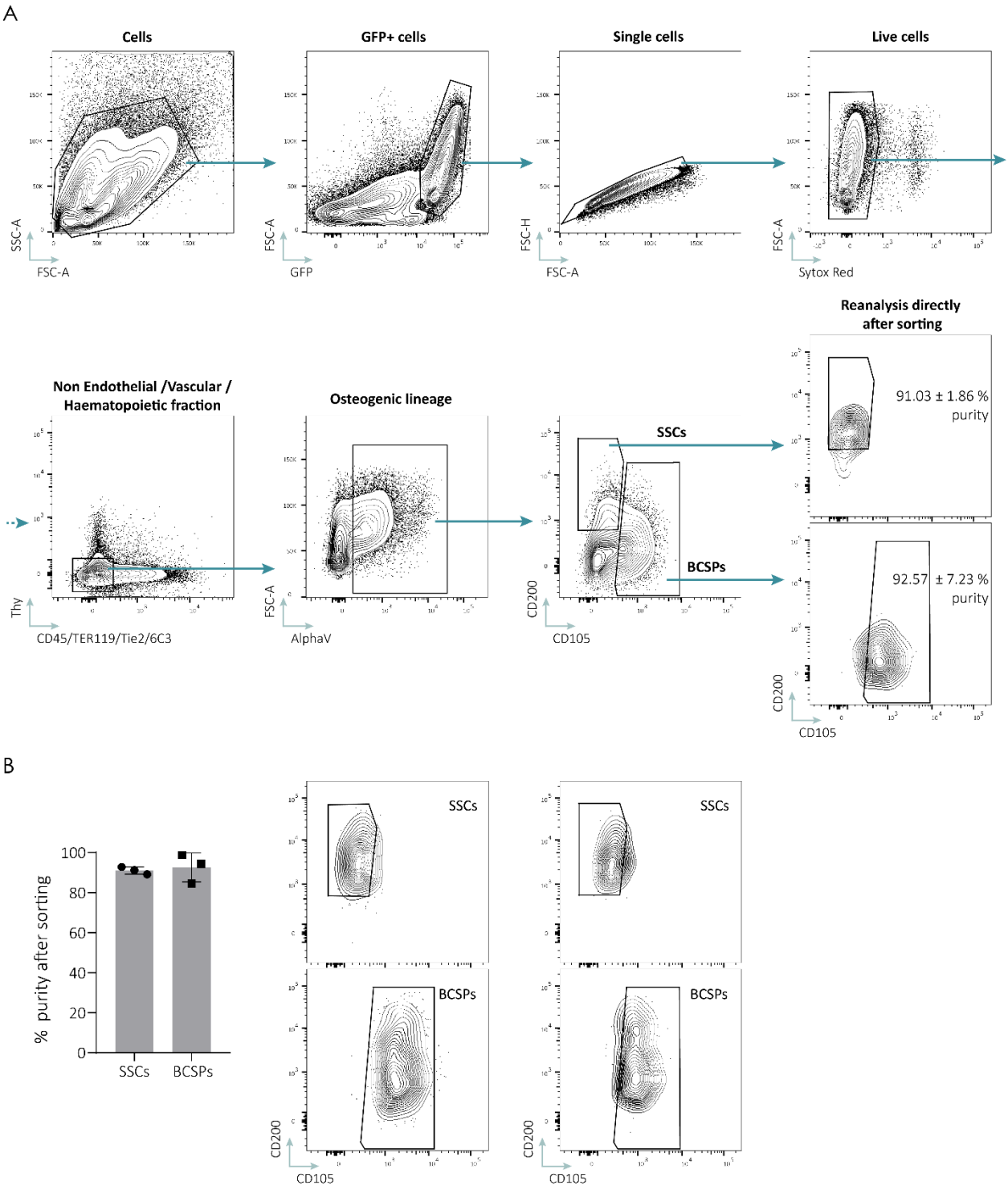

Figure S1. FACS gating strategy for isolation of SSCs and BCSPs

Cells were isolated from limbs and sternum digestion of GFP⁺ mice at P3 and stained for flow cytometry. (**a**) Representative FACS analysis of SSCs (CD45⁻ TER119⁻ Tie2⁻ AlphaV⁺ Thy⁻ 6C3⁻ CD105⁻ CD200⁺) and of BCSPs (CD45⁻ TER119⁻ Tie2⁻ AlphaV⁺ Thy⁻ 6C3⁻ CD105⁺) from cells that were stringently gated to only contain GFP⁺, single and live cells. Representative analysis of post-sort purity for SSCs (top right) and BCSPs (bottom right) is shown. (**b**) Post-sort purity evaluations of SSCs and BCSPs from two additional independent isolations and corresponding purities. Data are depicted as mean ± SD, n = 3.

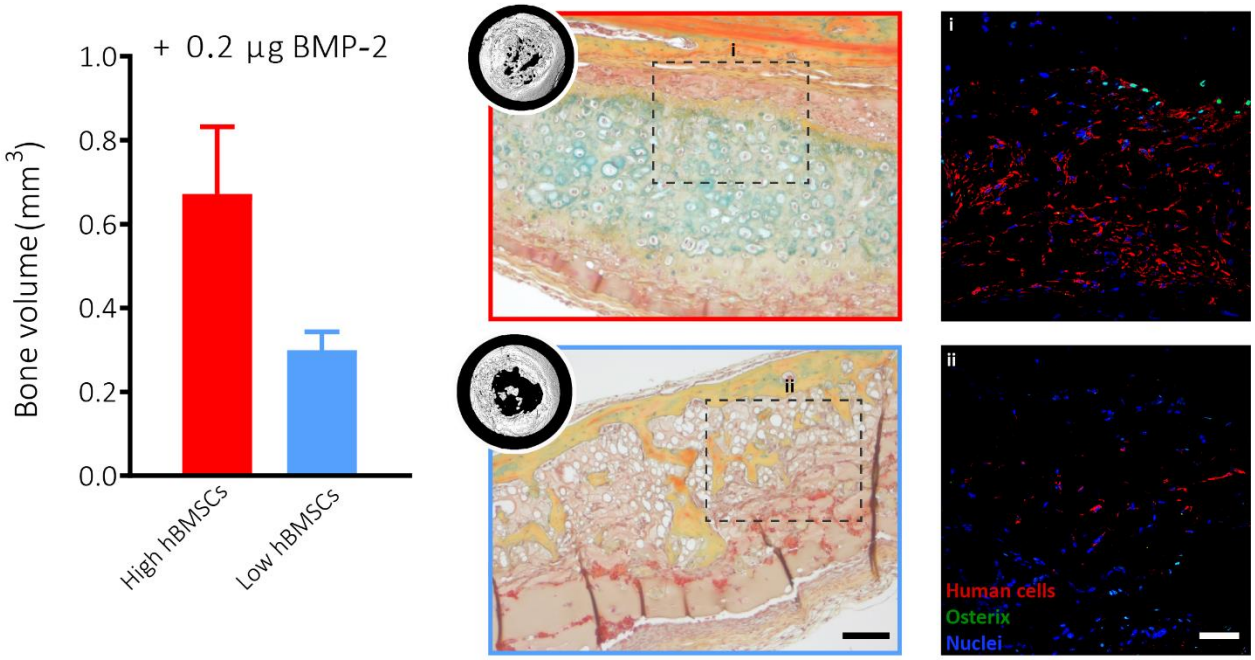

Figure S2. Effect of cell seeding density at a constant BMP-2 concentration of human bone marrow stromal cells (hBMSCs) in calvarial defects

Bone volume is increased in high hBMSC conditions as seen by microCT (inlet) and corroborated in histological evaluations (scale bars: 100 µm left and 50 µm right). Data are depicted as mean ± SD, n = 4.

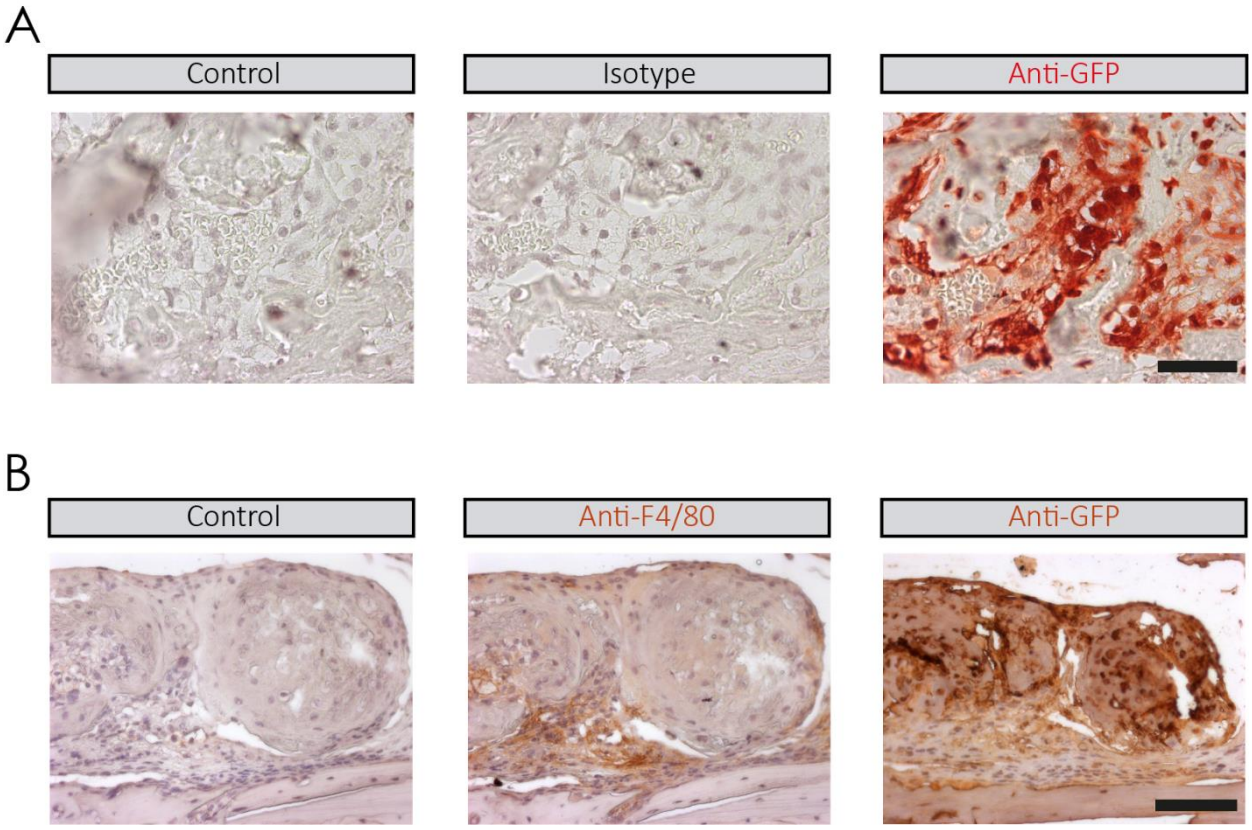

Figure S3. Specificity of GFP immunostaining

Calvarial defects were treated for 4-weeks with 0.2 µg BMP-2 and GFP$^+$ SSCs (10^7 cells per ml of hygrogel). Tissue sections were used to establish immunohistochemistry-based identification of GFP$^+$ positive cells. (**a**) The specificity of the immunostainings as shown by conducting the full staining procedure in absence of the GFP-specific first antibody (control), in presence of an unspecific isotype matched first antibody (isotype), and in presence of the GFP-specific first antibody (anti-GFP). Brown specific stain (scale bar: 20 µm). (**b**) Immunostainings in contiguous sections showing the lack of macrophages (F4/80) in areas containing GFP$^+$ cells, thus GFP$^+$ cells have not been phagocytosed by macrophages (scale bar: 100 µm).

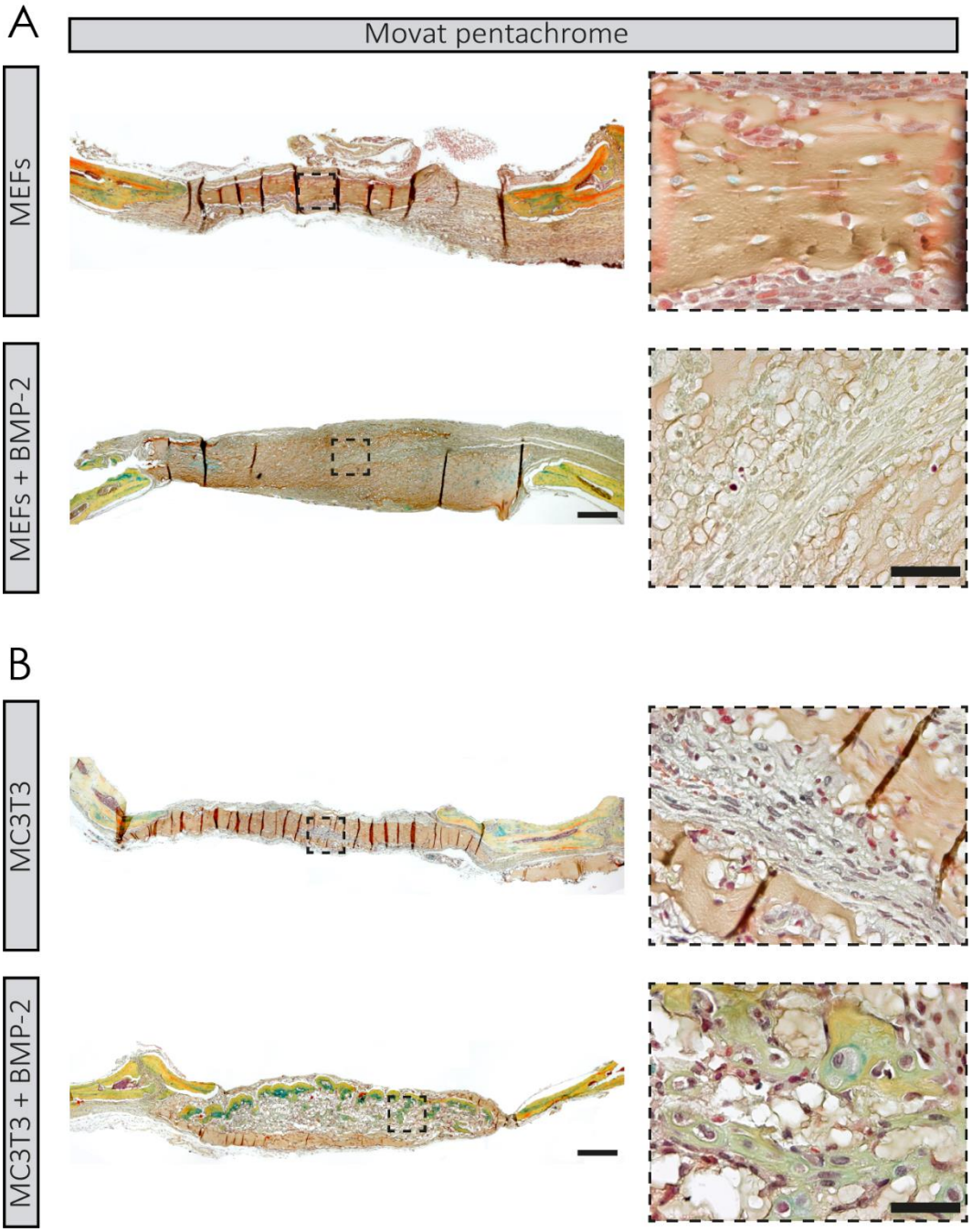

Figure S4. ***In vivo*** **osteogenic differentiation of MEFs and MC3T3 cells**

Healing of calvarial defects in immunocompromised mice using biomaterials containing no or 0.2 µg BMP-2 and (**a**) MEFs or (**b**) MC3T3 cells (10^7 cells per ml of hydrogel). Representative Movat's pentachrome stained coronal cross sections of the full implant after 4-weeks of transplantation (left panels, scale bars: 200 µm) and marked areas in higher magnification (right panels, scale bars: 20 µm). Red (fibrin) indicates muscle/vascularized tissue; yellow (reticular fibers/collagen) indicates bone; green/blue (mucin) indicates cartilaginous tissue; and black, nuclei and elastic fibers.

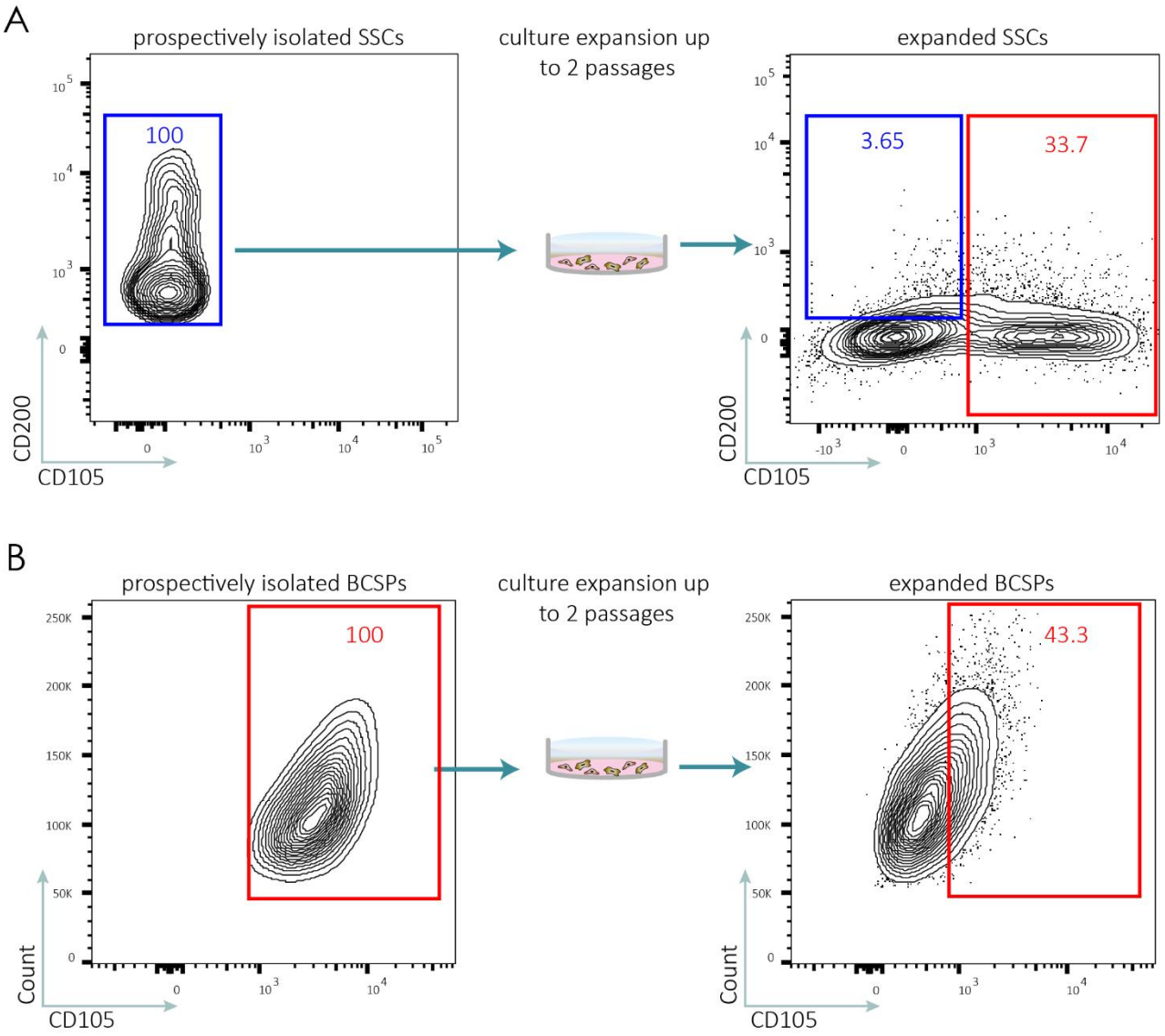

Figure S5. Shifting fates of SSCs and BCSPs upon culture expansion

(**a**) Prospectively isolated SSCs exhibit differential expression of CD105 and CD200 markers after culture expansion. (**b**) Expression of CD105 after culture expansion of prospectively isolated BCSPs. Cells were gated on live, GFP$^+$, lineage-negative, AlphaV$^+$, single cells.

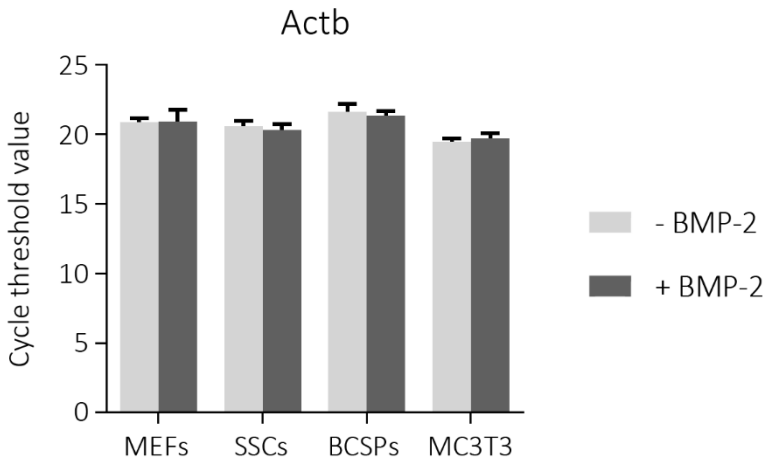

Figure S6. Actb distibution within the different subpopulations

No difference and an average CT mean of 20-fold increase was observed in presence of 0 (no osteoinduction) and 100 ng ml^{-1} BMP-2 (osteoinduction) treatment between the different subpopulations.

Si ens aixequem ben d'hora
i treballem sense retrets
som un país imparable.
– Pep Guardiola

Artwork by Pol Martín García
Girona, Catalunya

CHAPTER 3

Engineering microenvironments to interrogate human skeletal stem cell intrinsic function *in vivo*

Q Vallmajo-Martin[1,2], A Barbero[3], D Alpern[4], V Gardeux[4], I Martin[3], B Deplancke[4], M Lütolf[2], M Ehrbar[1]

The content of this chapter is part of a manuscript in preparation.

[1] Laboratory for Cell and Tissue Engineering, Department of Obstetrics, UniversitätsSpital Zürich, Switzerland;
[2] Laboratory of Stem Cell Bioengineering, Institute of Bioengineering, École Polytechnique Fédérale de Lausanne, Switzerland;
[3] Tissue Engineering, Department of Biomedicine, University Hospital Basel, University of Basel, Switzerland;
[4] Laboratory of Systems Biology and Genetics, Institute of Bioengineering, École Polytechnique Fédérale de Lausanne, Switzerland.

Statement of contributions

QVM designed, performed and analyzed all the experiments.

AB & IM isolated and cultured primary cells.

DA, VG & BD collaborated in the experiments related to RNA sequencing including experimental design, library preparation, and analysis.

ML collaborated with FACS evaluations, including experimental design and analysis.

ME designed experiments and supervised the whole project.

Abstract

Though the exact definition of skeletal stem cell remains controversial, it is understood that this classification can only be assessed *in vivo* under permissive conditions for an interrogated cell to differentiate along any and all of its lineages. A minimalistic *in vivo* setup free of external induction factors is essential for isolating the supposed stem cell's intrinsic capacity for differentiation. Such a setup is presented here featuring synthetic biomaterials rationally tailored by varying stiffness, degradability, and/or integration of bioactive ligands. We show its utility in assessing tissue and health status-dependent ability of human bone marrow-derived stromal cells (hBMSCs) to form bone and bone marrow *in vivo*. Interestingly, immunostaining supported by transcriptomics analysis revealed that differences in osteogenic differentiation capability were attributed to the cell's capacity to deposit extracellular matrix (ECM). The unique hydrogel system presented here allows systematical screening for the therapeutic potential of donor-specific hBMSCs in a clinically relevant *in vivo* model.

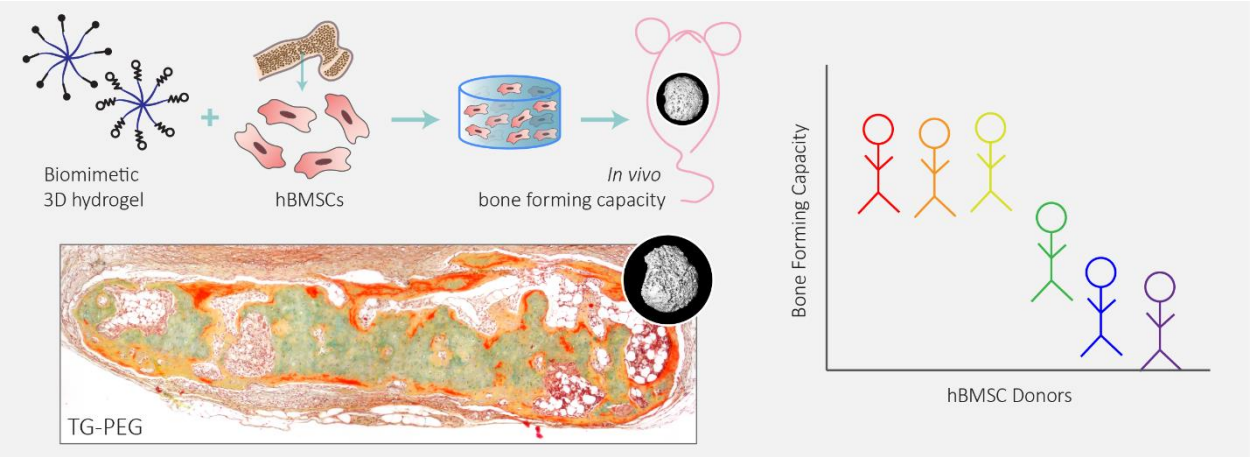

Keywords: Skeletal stem cell, human bone marrow stromal cell, engineered hydrogel, *in vivo* model

Brief communication

Human bone marrow stromal cells (hBMSCs) – despite promising regenerative functions observed in preclinical evaluations – have not yet met expectations in clinical trials. The lack of specific and reliable surface markers to accurately define them has hampered both the elucidation of the hBMSC basic biology and the establishment of their use in therapeutic protocols[1-3]. Indeed, to characterize hBMSC capacity, most studies have relied on *in vitro* differentiation protocols, which neither represent physiological nor treatment-relevant conditions[4]. To replace these *in vitro* assays there is an urgent need for highly reproducible *in vivo* tools to accurately evaluate stem cell function and potential. Ideally, stem cells would be embedded in a defined biomaterial that enables reciprocal, niche-recapitulating stem cell-material interactions, which synergistically dictate stem cell behavior[5]. Several materials have been tested as carriers for stem cell evaluation including hydroxyapatite/β-tricalcium phosphate (HA/TCP) ceramic scaffolds[6,7] or natural materials such as collagen[8], fibrin[9] and extracellular matrix-based scaffolds[10-12]. However, these biomaterials all bear osteoconductive or inherent biological properties that exogenously influence stem cell behavior and obscure elucidation of stem cell intrinsic functions. Until now, the biophysical properties and biochemical cues inherent in a scaffold material could not be disassociated. To overcome this, we employ a chemically defined poly(ethylene glycol)-based hydrogel that is crosslinked by transglutaminase FXIII (referred to as TG-PEG[13]) as a scaffold to support the stem cell niche. This highly tunable synthetic hydrogel serves for the first time as a powerful tool to study *in vivo* stem cell differentiation by facilitating an uncoupling of multiple individual microenvironmental and cellular parameters (Figure 1 a).

We first assessed the ability of TG-PEG to promote formation of ectopic bone marrow ossicle niches in mice and compared to the naturally-derived hydrogels collagen, fibrin, and ECM-based (named as ECMatrix). For this, soft hydrogels with similar stiffness (equivalent to a storage modulus of 50 Pa) (Figure S1 a) were used to encapsulate hBMSCs at an optimized concentration of $20 \cdot 10^6$ cells per ml of hydrogel (Figure S1 b), and immediately implanted in subcutaneous pouches of nude (*Foxn1^{nu}*) mice for 8 weeks. Micro-computed tomography (microCT) evaluations showed that collagen scaffolds failed to form bone, while small bony ossicles were formed in fibrin (0.187 ± 0.016 mm^3), ECMatrix (0.442 ± 0.467 mm3) and low stiffness TG-PEG (0.313 ± 0.129 mm^3) matrices (Figure 1 b). Histological evaluations revealed an 80 to 100% resorption of all hydrogels as seen by the loss in size of those gels (Figure 1 c, Figure S1 c).

We next hypothesized that stiffer hydrogels with higher crosslinking density would better promote ossicle development by providing more stability to the delivered cells. In contrast to natural hydrogels and owing to their synthetic nature, TG-PEG hydrogels are easily tuned over a wide range of 10 to 100-fold higher stiffness. Strikingly, TG-PEG hydrogels of intermediate stiffness (storage modulus of 500 Pa) (Figure S1 a) showed robust bone formation (2.089 ± 0.591 mm^3) (Figure 1 b). Histological evaluations revealed that hBMSCs remodeled the hydrogel into a bone marrow ossicle, while maintaining an integral scaffold (Figure 1 c). In the stiffest hydrogels tested

(owning a storage modulus of 5 kPa) (Figure S1 a), however, the capability of hBMSCs to efficiently remodel the hydrogel and deposit their own ECM was compromised resulting in variable bone formation (1.000 ± 1.160 mm^3). Modified Movat's pentachrome (MP) staining indicated that transplanted cells acquired a cartilage-like morphology and also highlighted the lack of infiltrated murine cells (Figure 1 b, c; Figure S1 c).

A cell's ability to physically anchor to its microenvironment and subsequently remodel it are two quintessential cell-matrix interactions. In particular, hBMSCs must continuously remodel their ECM, which they do primarily via secretion of matrix metalloproteinases (MMPs)[14]. Additionally, abundant ECM proteins - and currently used natural and synthetic biomaterials - contain the cell-adhesion peptide RGD to enable adhesion[15]. Therefore, to determine whether ossicle formation by hBMSCs depends on cell adhesion and matrix remodeling functions, we engineered TG-PEG hydrogels of intermediate stiffness that either lacked RGD sites or MMP-sensitive architecture. Bone volume was surprisingly not affected by either depriving encapsulated cells of RGD binding sites or excluding MMP-degradability, accomplishing 2.089 ± 0.591 and 2.456 ± 0.433 mm^3, respectively (Figure 1 b). However, histological evaluations revealed in the absence of RGD or MMP-degradable sites, the ossicles did not exhibit complete infiltration of a bone marrow population of murine cells. This was in stark contrast to robust marrow establishment observed in the TG-PEG hydrogels with cell adhesion and degradation sites (Figure 1 c, Figure S1 c). The incomplete bone marrow likely reflects the inability of transplanted and recruited host cells to invade and remodel the hydrogels. Concomitantly, in these conditions hBMSCs deposited an ECM rich in glycosaminoglycans (GAGs) and adapted a cartilage-like phenotype similar to what was observed for high stiffness hydrogels. Together, we show that individually tailoring of stiffness, MMP-sensitivity, and cell adhesion, which is only feasible in synthetic but not in natural biomaterials, is key for the evaluation and full exploration of hBMSC function.

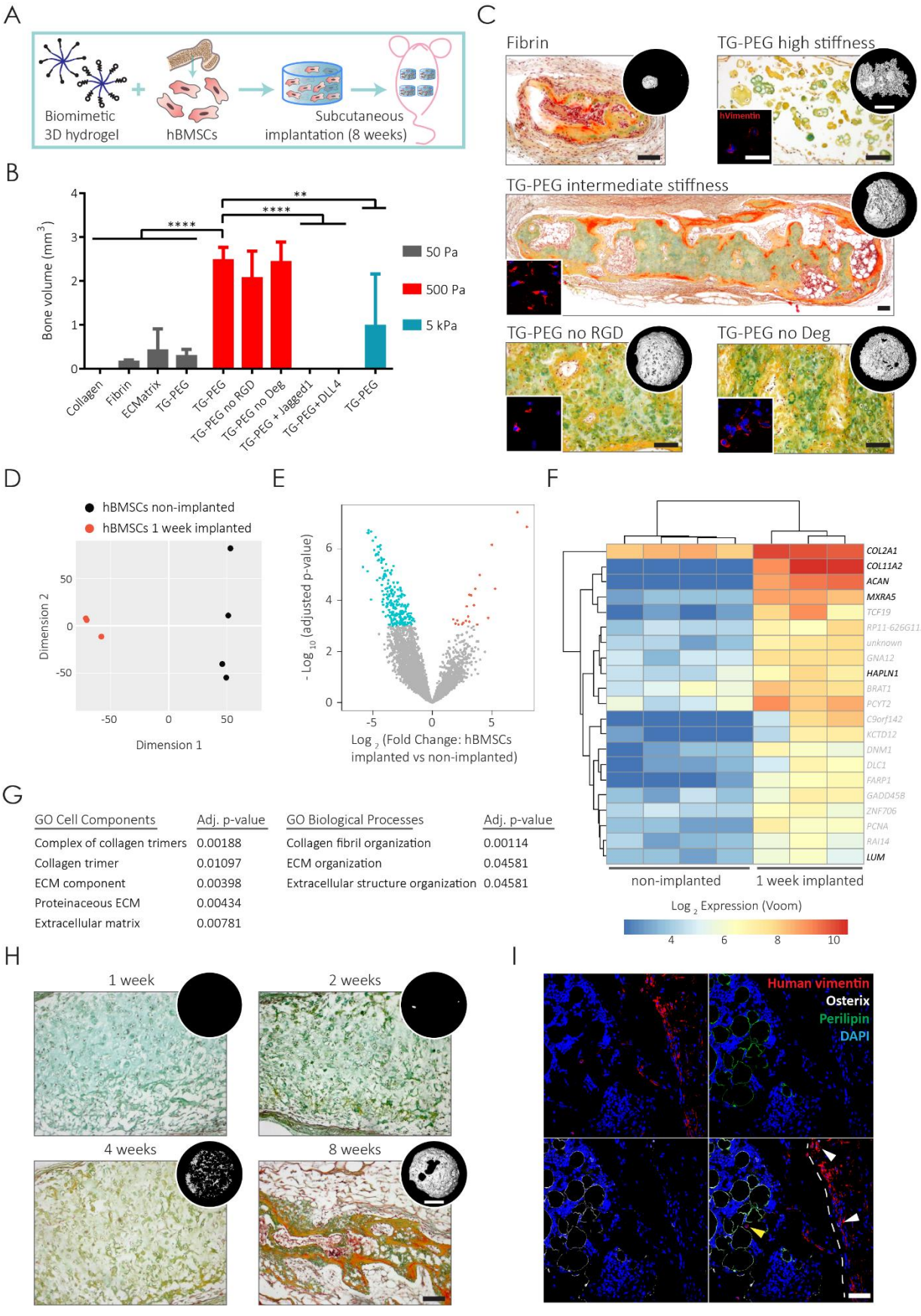

G

GO Cell Components	Adj. p-value	GO Biological Processes	Adj. p-value
Complex of collagen trimers	0.00188	Collagen fibril organization	0.00114
Collagen trimer	0.01097	ECM organization	0.04581
ECM component	0.00398	Extracellular structure organization	0.04581
Proteinaceous ECM	0.00434		
Extracellular matrix	0.00781		

Figure 1. Bioengineering scaffolds as bone and bone marrow models

(**a**) Human bone marrow stromal cells (hBMSCs, $20{\cdot}10^6$ cells per ml) were encapsulated in different 3D biomimetic hydrogels and subcutaneously implanted in nude mice. After 8 weeks ossicles were retrieved and bone volume was analyzed by micro computed tomography (microCT) followed by histological evaluations. (**b**) Low stiffness materials (50 Pa) showed limited bone volume (n = 4). Increased crosslinking density resulted in an intermediate stiffness (500 Pa) and induced robust bone formation (n = 4), and high stiffness (5 kPa) produced variable bone volume (n = 4). Next, the effect of matrix-immobilized molecules or biologically active moieties on niche development was assessed. While the absence of RGD adhesion or MMP-sensitive degradable sites did not alter bone formation (n = 4), the incorporation of Notch-ligands Jagged1 or DLL4 to the hydrogel backbone completely suppressed hBMSC osteogenic potential (n = 3). (**c**) Representative modified Movat's pentachrome (MP) stainings (mucin/glycosaminoglycans indicate cartilage in blue/green, collagen/reticular fibers indicative of bone in yellow, vascularized tissue and marrow in red, nuclei in black; scale bars: 100 µm) with corresponding inlets displaying the presence of human cells (scale bar: 20 µm) and microCT reconstructions (scale bar: 2 mm) of the explanted ossicles. All together indicated that soft hydrogels were reabsorbed by the host (top, fibrin), while stiffer hydrogels maintained their structure and allowed the implanted cells to remodel the hydrogel into an ossicle (middle, TG-PEG intermediate stiffness). Moreover, hBMSCs in TG-PEG hydrogels lacking the RGD adhesion peptide, the degradation sites or of high stiffness acquired a cartilage-like phenotype. (**d-g**) Human cells were retrieved 1 week post-implantation (n = 3) and compared to non-implanted hBMSCs (n = 4) by RNA sequencing analysis showing (**d**) two separated clusters in principal components analysis, (**e**) significantly differential expressed genes in a volcano plot, and (**f**) detailed upregulated genes in implanted cells represented in a heat map as normalized data by the Voom method, genes of interest ECM related have been highlighted. (**g**) Gene ontology revealed upregulated genes to be ECM-related. (**h**) Longitudinal evaluation of hBMSC-induced ossicles corroborated the remodeling of the hydrogel into an ossicle by ECM deposition shown by MP staining (scale bar: 100 µm) and bone formation by microCT reconstructions (scale bar: 2 mm). (**i**) By 8 weeks hBMSCs were found lining in bone areas (dotted white line) expressing osterix (indicated by white arrows) as well as in the marrow (indicated by yellow arrows, scale bar: 50 µm). Nuclei were stained by DAPI, human cells stained by human-specific vimentin in red, adipocytes stained by perilipin in green and osterix positive cells in white. All data are reported as mean ± standard deviation. ANOVA with Tukey's *post hoc* test ** $P < 0.01$, **** $P < 0.0001$.

Next, we tested if ossicle formation in optimized TG-PEG hydrogels (i.e. storage modulus of 500 Pa, 50 µM RGD and containing the MMP-1-sensitive degradable sequence) could be modulated by presentation in the microenvironment of cell-surface ligands known to inhibit or promote hBMSC differentiation. For this, Jagged1 or Delta-like-4 (DLL4), two Notch signaling ligands known to maintain the pool of mesenchymal progenitors in the bone marrow[16], were modularly incorporated into the hydrogel backbone using a high affinity protein A-based binding strategy[17]. When immobilized in the TG-PEG hydrogels, these ligands completely inhibited hBMSCs to form bone (Figure 1 b) via ligand-specific interactions in line with earlier *in vivo* reports[16]. In contrast, the addition of osteoconductive hydroxyapatite tricalcium phosphate (HA/TCP, 60/40, diameter < 75 µm) particles into the TG-PEG hydrogels did not augment bone formation by hBMSCs (Figure S2). These observations reinforce the fact that a minimalistic microenvironment sufficiently allows hBMSCs to fulfil their bone formation capacity.

To further investigate molecular events accompanying differentiation of hBMSCs encapsulated in TG-PEG *in vivo*, we performed transcription profiling of ossicles at two developmental stages: prior to and one week after subcutaneous implantation using bulk RNA barcoding and sequencing (BRB-seq)[18]. We observed a significant upregulation of endochondral pathway-associated ECM component genes such as collagen type II (*Col2a*), collagen type XI (*Col11a2*), aggrecan (*Acan*), matrix-remodeling-associated protein 5 (*Mxra5*), hyaluronan and proteoglycan link protein 1 (*Hapln1*), and lumican (*Lum*) upon implantation (Figure 1 d-g). Longitudinal MP stainings

corroborated the transcriptomics data by displaying the morphological ECM changes in these forming ossicles (Figure 1 h). Already after 1 week of implantation, hydrogels were rich in glycosaminoglycans that remodeled into calcified collagen fibers over time as seen by microCT reconstructions. Up to eight weeks after implantation, human cells were found in the ossicles (Figure 1 i, Figure S7 immunostaining controls) in endosteal and stromal niches supporting the bone marrow. Furthermore, some human cells were found to express osterix, a marker of osteogenic differentiation. Earlier, hBMSCs were shown to only undergo endochondral ossification after *in vitro* pre-differentiation with TGF-β3[8] or systemic supplementation with daily doses of human parathyroid hormone[10]. Remarkably, by the use of minimal PEG-based matrices we provide here the first evidence that hBMSCs can undergo *in situ* endochondral ossification in the absence of any biochemical cues.

We next sought to expand the clinical relevance of this system by further humanizing the bone marrow subniches within the ossicles. To do so, we systemically injected human hematopoietic stem progenitor cells (hHSPCs) after hBMSC-induced ossicle formation (> eight weeks post-subcutaneous transplantation) to induce a humanized hematopoietic system in NSG mice[19]. Histological analysis revealed that the ossicles were indeed humanized with hBMSCs in the bone forming regions, comprising a marrow with $hCD34^+$ HSPCs, indicating a functional niche (Figure S3). These results reinforce the use of this model as a valuable tool to study humanized bone-marrow related diseases.

In addition to use as a tool for studying ossicle formation, we also investigated whether our setup could be used as part of a therapeutic approach for healing critical-sized bone defects. To verify their osteogenic properties in the healing bone we treated murine calvarial bone defects with hBMSCs encapsulated in TG-PEG hydrogels of intermediate stiffness containing RGD and MMP-degradable sites (Figure S4 a). Using hBMSCs under such optimized delivery conditions resulted in a significant 2.7-fold increase in bone formation in the critical-sized calvarial defect as compared to hydrogel control (Figure S4 b, c). Implanted hBMSCs lined bony areas and were also found to express osterix (Figure S4 d, e; Figure S7 immunostaining controls). Thus, the healing of critical bone defects without the additional need of osteoinductive or osteconductive cues confirms the hBMSC's intrinsic bone forming capability and circumvents the need for BMP-2 induction, which has often been met with clinically deleterious effects[20].

To validate the functionality of our model, we tested the osteogenic potential of hBMSCs from multiple healthy donors (females or males from 17 to 39 years old, Table 1). We found significant differences in bone volumes ranging from 3.313 ± 0.265 mm^3 (BM donor 1) to 0.298 ± 0.327 mm^3 (BM donor 6) uncorrelated to age or sex (Figure 2 a). Importantly, hBMSC cell populations from different donors were indistinguishable by common FACS profile markers (Figure 2 e, Figure S5 a). Next, we used DNA quantification to evaluate whether hBMSC proliferation was related to the higher capacity to form bone *in vivo* (Figure 2 d). Results indicated that there was no correlation between proliferation rates of donor cells and bone volume observed *in vivo*. Furthermore,

histological analysis confirmed that samples corresponding to higher bone volumes exhibited collagen-rich fully developed bone marrow ossicles, while those with lower bone volumes did not despite persistence of human cells over the 8 weeks (Figure 2 c). Critically, the discrepancies between donors could only be detected because our system does not rely on osteoconductive or osteoinductive factors that otherwise mask the role of the cells. This was evidenced by co-encapsulating hBMSCs with BMP-2 in TG-gels. Osteogenic differences between donors were reduced and no longer significant (Figure 2 b; p-value BM D1 and BM D6 = 0.453) demonstrating that growth factor induction attenuates the intrinsic potential of the progenitor cells.

To further evaluate the system's ability to serve as a tool for discerning osteogenic capacity of various cell sources, we compared hBMSCs derived from osteoporotic patients, human adipose-derived stromal cells (hASCs), and fibroblasts. Similar to the hBMSCs with low osteogenic potential, hBMSCs from osteoporotic patients showed low bone volume (ranging from 0.671 ± 0.717 mm^3 for OP donor 1, to 0.079 ± 0.091 mm^3 for OP donor 2) and did not induce the formation of a bone marrow-like cavity, (Figure 2 a, Figure S5 b). Interestingly, hASCs were incapable of promoting any bone formation *de novo*, comparable to fibroblasts as a control cell type, though they remained in the hydrogels over a duration of 8 weeks (Figure 2 a, Figure S5 b).

Attempting to understand the underlying differences among these donors, we performed BRB-seq on hBMSCs from healthy and osteoporotic patients, as well as fibroblasts, retrieved from TG-PEG hydrogels. Principle component analysis (PCA) yielded three independently defined clusters comprising healthy-derived hBMSCs, osteoporotic-derived hBMSCs or fibroblasts (Figure 2 f). When comparing healthy vs. osteoporotic-derived hBMSCs, 127 genes were found significantly upregulated in healthy cells (Figure 2 g). Gene ontology analysis revealed that these upregulated genes were again ECM-related (Figure 2 h).

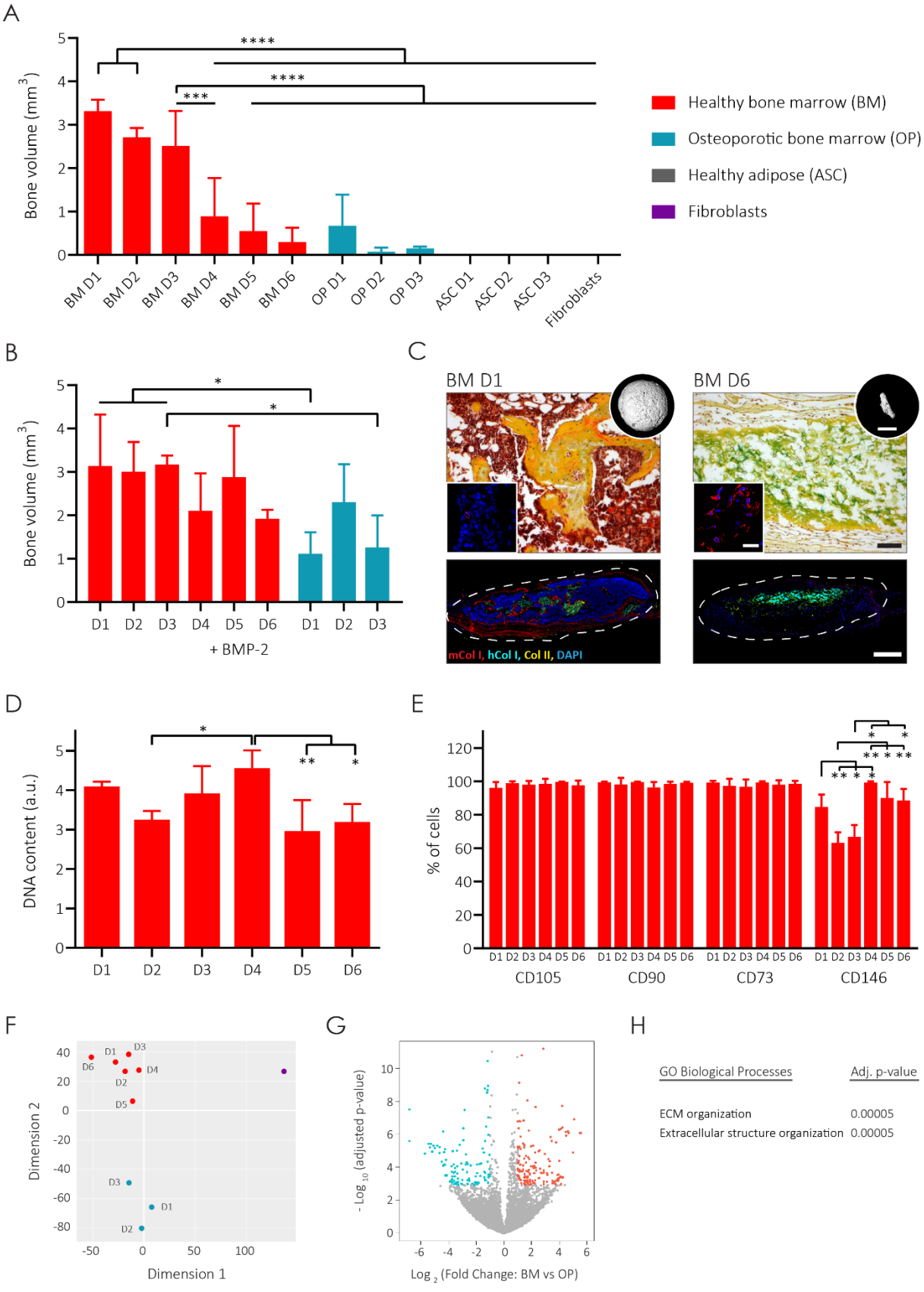
A
Bone volume (mm3)
****
****
***
BM D1
BM D2
BM D3
BM D4
BM D5
BM D6
OP D1
OP D2
OP D3
ASC D1
ASC D2
ASC D3
Fibroblasts
Healthy bone marrow (BM)
Osteoporotic bone marrow (OP)
Healthy adipose (ASC)
Fibroblasts
B
Bone volume (mm3)
D1 D2 D3 D4 D5 D6 D1 D2 D3
+ BMP-2
C
BM D1
BM D6
mCol I, hCol I, Col II, DAPI
D
DNA content (a.u.)
D1 D2 D3 D4 D5 D6
E
% of cells
D1 D2 D3 D4 D5 D6
CD105
CD90
CD73
CD146
F
Dimension 2
Dimension 1
G
- Log10 (adjusted p-value)
Log2 (Fold Change: BM vs OP)
H
GO Biological Processes
Adj. p-value
ECM organization
0.00005
Extracellular structure organization
0.00005

Figure 2. Screening differentiation capacity of different hBMSCs

(**a**) The presented model was employed to evaluate the effect of hBMSCs donors, health state and sources in cell capability to form bone *in vivo*. Bone marrow derived cells from healthy donors (BM; N = 6), osteoporotic patients (OP; N = 3) and human adipose-derived stromal cell from healthy donors (ASC; N = 3), as well as human fibroblasts as a control, were encapsulated in the optimized TG-PEG hydrogels and subcutaneously implanted in nude mice for 8 weeks. Bone volume was assessed by microCT (n = 4). (**b**) In the presence of a low concentration of BMP-2 (12.5 ng μl^{-1}), bone volume no longer showed differences between healthy donors (n = 4). (**c**) Histologies corroborated major differences among donors in the remodeling capacity of the implanted cells and recruitment of host cells. Representative MP staining (top, scale bar: 100 µm) with inlets displaying the presence of human cells (human-specific vimentin in red and DAPI, scale bar: 20 µm), and corresponding microCT reconstructions (scale bar: 2 mm). Superimposed projections of collagen specific stainings for murine type I (red), human type I (cyan) and type II (yellow) (bottom, scale bar: 500 µm) comparing BM donor 1 and 6. (**d**) Proliferation capacity of different healthy BM donors in TG-PEG hydrogels was assessed by DNA quantification (n = 4). (**e**) Flow cytometry comparison of expression of consensus surface markers (CD105, CD90, CD73 and CD146) on healthy hBMSCs (D1 to D6) showed no differences among donors (n ≥ 4). (**f-h**) Next, bulk RNA transcriptomics was performed on healthy, osteoporotic-derived hBMSCs and fibroblasts from cells encapsulated in TG-PEG hydrogels (n = 4 for each sample, represented average of technical replicates). (**f**) RNA sequencing analysis showed three defined clusters in the PCA separating healthy, osteoporotic and fibroblasts, respectively. (**g**) Further comparison of healthy-derived hBMSCs to osteoporotic underlined 93 downregulated and 127 upregulated genes, as represented in a volcano plot, (**h**) that were matched by gene ontology to extracellular matrix organization. All data are reported as mean ± standard deviation. ANOVA with Tukey's *post hoc* test * $P < 0.05$, ** $P < 0.01$, *** $P < 0.001$, **** $P < 0.0001$.

Finally, we tested whether osteogenic differentiation of hBMSCs prior to implantation could improve the formation of bone ossicles (Figure S6 a). Surprisingly, we observed that hBMSCs that had been pre-cultured in 2D for 8 days under osteogenic differentiation medium completely failed to form bone, while the osteogenic potential was only partially lost if pre-differentiation was performed in 3D culture (Figure S6 b-c). Together, our findings indicate that in our model only cells with a stem-like phenotype can spontaneously undergo endochondral ossification and deposition of *bona fide* bone marrow ECM in line with earlier findings[12]. The versatility of this unique platform is highlighted by its use to compare ossicle formation capacity of cells from various donors, cell sources, differentiation lineages, and disease states. We envision that the presented approach will be employed for testing novel skeletal stem cell populations[11] and pluripotent stem cells[21], among others, to widen the current knowledge about their potential and help bridge these key discoveries to successful clinical trials.

By optimizing a chemically-defined, modular synthetic hydrogel, we determined the minimal needs for hBMSCs to undergo differentiation *in vivo*. Hydrogels of intermediate stiffness (500 Pa) with RGD adhesion peptide and MMP-dependent degradable-sides are sufficient to develop into a humanized bone marrow ossicle. Indeed, as in the native microenvironment, hBMSC matrix deposition played a fundamental role in this process. Uncoupling biochemical and biophysical properties of the microenvironment shows that tuned biophysical properties are enough to direct stem cells. This versatile approach opens for the first time the possibility to screen donor-to-donor differences among stem cell capacity to form bone *in vivo*, that are undetectable *in vitro*. This minimal environment sets the new gold standard to predict stem cell potential for basic biology as well as for clinical applications.

Acknowledgements

We would like to acknowledge Dr. Christopher Millan (University of Zürich) for valuable discussion and help in editing the manuscript; Esther Kleiner (University Hospital Zürich) for technical assistance; Flora Nicholls (University of Zürich) for animal care; Dr. Paolo Cinelli (University of Zürich) for support with microCT; Tabea Leonie Stephan (University Hospital Zürich) for collagen stainings overlays; the Center for Microscopy and Image Analysis for SEM imaging (University of Zürich); Prof. Marcy Zenobi-Wong and Dr. Nicolas Broguiere (ETH Zürich) for support with rheological measurements; Dr. Malgorzata Kisielow and the Flow Cytometry Core Facility (ETH Zürich) for cell sorting assistance; Julie Russeil (EPF Lausanne) for RNA library preparation assistance. This work has been supported by the Swiss National Science Foundation (CR33I3_153316/1), and the Center for Clinical Research, University Hospital Zürich and University of Zürich.

Experimental procedures

All chemicals and materials were purchased from Sigma Aldrich or Thermo Fisher Scientific unless otherwise specified.

Human cell isolation and culture expansion. Human bone marrow-derived stromal cells (hBMSCs) were isolated as previously described[22] from bone marrow aspirates of healthy donors (n = 6) or osteoporotic patients (n = 3) obtained during orthopedic surgical procedures after informed consent and in accordance with the local ethical committee (University Hospital Basel; Prof. Dr. Kummer; approval date 26/03/2007 Ref Number 78/07). Age of healthy donors ranged from 17 to 39 as detailed in Table 1. Human adipose-derived stromal cells (hASCs) were isolated as previously reported[23,24] from adipose tissue obtained during routine surgical procedures of healthy donors (n = 3) after informed consent and in accordance with the local ethical committee (Ethikkommission beider Basel [EKKB], Ref Number 78/07). All cell types were cultured at 37 °C in a humidified atmosphere at 5% CO_2 in minimum essential medium alpha (MEMα, with nucleosides, Gibco) supplemented with fetal bovine serum (FBS, 10%, Gibco), penicillin (100 U ml^{-1}, Gibco), streptomycin (100 μg ml^{-1}, Gibco), and fibroblast growth factor-2 (FGF-2, 5 ng ml^{-1}, PeproTech). Cells were passaged before reaching 90% confluency, and medium was changed every 2-3 days.

Human cell characterization by flow cytometry analysis. As previously reported stromal cells were characterized by their plastic adherence and tri-differentiation potential *in vitro*[1,22]. Moreover, in here hBMSCs were profiled by the expression of consensus stem cell-like surface markers (CD29, CD44, CD105, CD90, CD73, CD146, CD49d, CD34 and CD45) detailed in Table 2. Briefly, cells were trypsinized, washed in phosphate buffer-saline (PBS) and resuspended in FACS buffer (1 mM ethylenediaminetetraacetic acid (EDTA) and 2% FBS in PBS) containing each antibody at an optimized concentration. Cells were stained for 30 min at 4 °C in the dark, washed, filtered through a 70 μm filter and analyzed by a BD FACSCanto flow cytometry analyzer. Dead cells were stained by SYTOX Blue dead cell stain and excluded from analysis like doublets. Data analysis was performed using FlowJo 10.0.8 software (TreeStar), and gates were assessed based on the corresponding isotype controls.

TG-PEG precursors synthesis and preparation. TG-PEG precursors were synthesized as previously described[13,25]. Briefly, 8-arm PEG-VS (PEG-vinylsulfone, 40 kDa MW; NOF) was functionalized with peptides (obtained with a purity of > 95% from Bachem AG) that contained an earlier described cysteine cassette (ERCG) optimized for its reaction with PEG-VS and either a factor XIII (FXIII) glutamine acceptor substrate sequence (Gln; H-NQEQVSPL-ERCG-NH_2) or a matrix metalloproteinase-degradable (*in italics*) lysine donor substrate ($MMP_{sensitive}$-Lys; Ac-FKGG-*GPQGIWGQ*-ERCG-NH_2), or instead a non-degradable lysine donor substrate (ND-Lys; Ac-FKGG-GDQGIAGF-ERCG-NH_2) for non-degradable TG-PEG gels. A 1.2 molar excess of peptides over PEG-VS was reacted in triethanolamine (TEA) at pH 8.0 for 2 h at 37 °C. Resulting

8-PEG-Gln and 8-PEG-$MMP_{sensitive}$-Lys or 8-PEG-ND-Lys precursors were excessively dialyzed against pure water, lyophilized and stored at -20 °C until further use. The crosslinking enzyme, transglutaminase FXIII (200 U ml^{-1}, Fibrogammin P, CSL Behring), was activated with thrombin (2 U ml^{-1}) for 30 min at 37 °C and stored in small aliquots at -80 °C until use.

3D biomimetic hydrogels for cell encapsulation. Cells were trypsinized and resuspended in 10% FBS/MEMα in the desired concentration and mixed in the corresponding precursor mixes.

3D TG-PEG hydrogel formation. Stoichiometrically balanced solutions of 8-arm PEG-Gln and 8-arm PEG-$MMP_{sensitive}$-Lys, or 8-arm PEG-Gln and 8-arm PEG-ND-Lys for non-degradable gels were prepared in Tris buffer (50 mM, pH 7.6) containing calcium chloride ($CaCl_2$, 50 mM). Additionally when stated, 50 μM Lys-RGD peptide (Ac-FKGG-RGDSPG-NH_2), indicated amounts of cells, 12.5 ng μl^{-1} BMP-2 (produced as previously described[26]) or indicated amounts of hydroxyapatite tricalcium phosphate (HA/TCP) particles (60/40, diameter < 75 μm, CAM Bioceramics) were added to the precursor solution. To immobilize recombinant human Jagged1–Fc protein (R&D Systems, 1277-JG-050) or recombinant human Delta-like-4 (DLL4)–Fc protein (Sino Biological, 10171-H02H) into TG-PEG hydrogels, these ligands (500 nM final concentration) were pre-incubated for 30 min with Gln-ZZ protein (5 μM final concentration, previously characterized [17]) to pre-form the Gln-ZZ/Fc-protein complex, and added to the gel precursor mix. Subsequently, hydrogel crosslinking of final dry mass content of 0.9% (corresponding to low stiffness), 1.7% (for intermediate stiffness) or 5% (for high stiffness) (w/v) was initiated by the addition of 10 U ml^{-1} of activated transglutaminase factor XIII, followed by vigorous mixing. Disc-shaped matrices were prepared between hydrophobic glass slides (treated with SigmaCote) and incubated for 30 min at 37 °C in a humidified atmosphere at 5% CO_2. After completed polymerization, hydrogels were released from glass slides and transferred to tissue-culture plates for *in vitro* experiments or stored in a humidified atmosphere for immediate *in vivo* implantation.

Natural matrices. hBMSCs (at final concentration of $20 \cdot 10^6$ cells per ml of hydrogel) were mixed in cold solutions of 3 mg ml^{-1} of collagen (PureCol EZ Gel solution, Sigma) or ECM-like matrix (referred as ECMatrix in the text, ECM625, Merck Millipore) following manufacturer's instructions. For fibrin gels as previously described[27], hBMSCs ($20 \cdot 10^6$ cells per ml of hydrogel) were added to a solution of 4 mg ml^{-1} of fibrinogen containing 2.5 mM $CaCl_2$. Next, FXIII (2 U ml^{-1}) and thrombin (2 U ml^{-1}) were incorporated to begin hydrogel crosslinking. Cell-laden hydrogels were then incubated for 30 min at 37 °C to enable complete polymerization prior to immediate (within 2 hours) *in vivo* implantation.

Hydrogel stiffness characterization by rheometry. Hydrogel gelation was analyzed on a rheometer (MCR 301, Anton Paar) equipped with 20 mm plate–plate geometry (PP20, Anton Paar) at 37 °C in a humidified atmosphere. For *in situ* measurements gel mixtures were precisely loaded onto the center of the bottom plate. The upper plate was lowered to a measuring gap size of 0.2 mm, ensuring proper loading of the space between the plates and gel precursors, the dynamic oscillating measurement was then started. The evolution of storage modulus (G') and loss modulus

(G") at a constant angular frequency of 1 Hz and constant shear strain of 4% was recorded for 30 min when equilibrium was reached. For measurements of TG-PEG hydrogels containing HA/TCP particles, to avoid particle precipitation during the rheological measurements, hydrogels were pre-formed. Hydrogels were prepared 24 h before measurements and incubated in Tris buffer at 37 °C. Swollen hydrogels were then loaded onto the rheometer, compressed by 10% and measured with a frequency sweep at 1% strain.

Scanning electron microscopy. For scanning electron microscopy (SEM), TG-PEG hydrogels containing HA/TCP particles were fixed in 50% osmium in phosphate buffered saline (PBS). After PBS washing, they were dehydrated by 30-minute period in 70% ethanol, followed by 80% and 100% ethanol and subsequently treated with hexamethyldisilazane (HMDS) for 1 hour, and then dried on air overnight. Lastly, samples were platinum sputter coated. Imaging was performed on a Zeiss Supra 50 VP at the UZH Center for Microscopy and Image Analysis (ZMB).

Proliferation assessment of encapsulated cells. hBMSCs ($3 \cdot 10^6$ cells per ml of hydrogel) from different donors were individually encapsulated in optimized TG-PEG hydrogels and maintained in MEMα + 10% FBS. To assess their proliferation, after 10 days in culture, medium was removed, hydrogels were washed with PBS and hBMSCs were retrieved by hydrogel digestion with collagenase A (100 µl, 2 mg ml^{-1} in PBS, Roche 11088793001) at 37 °C for 30 min. Subsequently, cells were collected in Hank's balanced salt solution (HBSS) buffer, and DNA content was assessed by the CyQuant NF Cell Proliferation kit assay (Invitrogen, C35006) following the manufacturer's instructions. Finally, fluorescence was recorded with excitation at 485 nm and emission at 530 nm using a microplate reader.

Osteogenic pre-differentiation of hBMSCs prior to implantation. To assess the effect that osteogenic differentiation had on hBMSC capacity to form bone *in vivo*, hBMSCs were cultured in 2D or in 3D optimized TG-PEG hydrogels (18 µl hydrogels, $20 \cdot 10^6$ cells per ml of hydrogel) with osteogenic medium composed of MEMα (with nucleosides), FBS (10%), penicillin (100 U ml^{-1}), streptomycin (100 µg ml^{-1}), 10 mM HEPES, 1 mM sodium pyruvate, 2 mM L-glutamine, 50 µg ml^{-1} L-ascorbic acid, 10 mM β-glycerol phosphate and 100 ng ml^{-1} BMP-2. Medium was replaced every 3 days. After 8 days, pre-differentiated hBMSCs in 2D were encapsulated in optimized TG-PEG hydrogels (18 µl, $20 \cdot 10^6$ cells per ml of hydrogel) and immediately (within 2 hours) subcutaneously implanted in nude mice. For 3D pre-differentiated hBMSCs, gels were washed in PBS, and subsequently implanted. hBMSCs that had not been pre-differentiated were also encapsulated and implanted as previously described to serve as positive controls.

Animal care. All animal procedures were approved by the veterinary offices of the Swiss cantons Zürich and Lausanne under the ethical license (Application No. ZH169/2015). Experiments and handling of mice were conducted in accordance with the Swiss law of animal protection. 6-8-week-old immunodeficient HsdCpb:NMRI-*Foxn1^{nu}* (nude) female mice (purchased from Envigo) or

NOD.Cg-*Prkdc*^{scid}*Il2rg*^{tm1Wjl}/SzJ (NSG) female mice (purchased from The Jackson Laboratory) were used for the following experiments.

Subcutaneous implantation of humanized hydrogels in mice. To create subcutaneous pouches in nude mice ca. 6 mm lateral skin incisions were made in four dorsal positions. Following randomization, pre-formed 18 µl gelled 3D scaffolds containing hBMSCs ($20 \cdot 10^6$ per ml of hydrogel) were placed in these pouches. Incisions were closed with 6.0 Vicryl sutures (Ethicon) and animals were closely monitored. One, two, four or eight weeks post-implantation unless stated otherwise, animals were euthanized via CO_2 asphyxiation, ossicles and specified murine organs were retrieved and immediately fixed in 4% (v/v) formalin solution for 12 h at 4 °C. After fixation they were washed in PBS and analyzed by microCT and histologies.

Calvarial defect healing model. Optimized TG-PEG hydrogels (intermediate stiffness, containing 50 µM RGD and MMP-degradable sites) of 11 µl containing hBMSCs ($20 \cdot 10^6$ per ml of hydrogel) were crosslinked and subsequently (within 2 hours) implanted. Craniotomies of 4 mm diameter were created in the parietal bones of the skull, one on each side of the sagittal suture. Pre-formed hydrogel discs were placed in the cranial defects and the skin was closed with 6.0 Vicryl sutures (Ethicon). Mice were euthanized 4 weeks post-implantation, calvaria were excised and immediately fixed in 4% (v/v) formalin solution for 12 h at 4 °C. After fixation they were washed in PBS and further analyzed by microCT and histologies.

NSG hematopoietic xenotransplantation. Primary human $CD34^+$ cells were isolated from umbilical cord blood collected from healthy donors at the University Hospital Zürich after obtaining informed consent. The study was approved by the ethics board of the canton Zürich, Switzerland (approval date 21/03/2007; Ref Number 07/07). Blood (typically between 30-70 ml) was subsequently centrifuged to enrich for mononuclear cells, which were in turn further magnetically sorted for $CD34^+$ cells using positive immunomagnetic selection ($CD34^+$ MicroBead Kit, Miltenyi Biotec) according to the manufacturer's instructions obtaining > 80% $CD34^+$ cells. Cells were directly frozen down until use. Upon NSG transplantation, cells were thawed in 50% IMDM 50% FBS, centrifuged 5 min at 300 g and subsequently resuspended in PBS. Then, NSG mice that had 8 weeks before received a subcutaneous implantation of hBMSC-laden TG-PEG scaffolds, received $0.6 \cdot 10^6$ human $CD34^+$ cells via tail vein injection (200 µl per animal). Animals were sacrificed 16 weeks post-$CD34^+$ human cells transplantation. Ossicles and organs were excised and immediately fixed in 4% (v/v) formalin solution for 12 h at 4 °C. After fixation they were washed in PBS and further analyzed by microCT and histologies.

Micro-computed tomography analysis at endpoints. After fixation in formalin and storage in PBS, ossicles were scanned in a microCT 40 (Scanco Medical AG) operated at an energy of 55 kVp and intensity of 72 µA at 4 W. Scans were executed at a high-resolution mode resulting in a voxel size of 10 µm. In reconstructed images bone tissue was segmented from background using a global threshold of 10% of maximum grey value. A cylindrical mask with a diameter of 5

mm was manually placed around the ossicle. Bone volume within the mask was measured using the ImageJ plugin BoneJ[28]. Reconstructions were assembled using the 3D Viewer plugin in ImageJ.

Histological and immunohistochemical studies. Next, samples were decalcified for 2 to 6 weeks in 10% EDTA solution with continuous shaking at 4 °C, followed by paraffin embedment and microtome sectioning at 4 μm. For histological stainings, hematoxylin & eosin (H&E) and modified Movat's pentachrome (MP)[29] stainings were performed using standard protocols. Briefly for MP staining, sections were sequentially incubated with alcian blue (Fluka, 1 g in 100 ml 1% glacial acetic acid) for 10 min, alkaline alcohol (10% ammonium hydroxide in 95% EtOH) for 1 hour, Weigert's iron hematoxylin (Weigert reagent A and B in a ratio 1:1) for 20 minutes, brilliant crocein R-fuchsine (1 part Biebrich Scarlet/Acid Fuchsin solution and 1 part 0.2% acidic fuchsin in 0.5% acetic acid) for 20 minutes, 0.5% acetic acid for 30 seconds, 5% phosphotungstic acid (PWS) for 15 min, 0.5% acetic acid for 2 minutes, washed 3 times with absolute ethanol for 5 minutes, 10 min in safran dye (6 g safran powder in 100 ml absolute EtOH), dehydrated and mounted in mounting medium. In MP, red (fibrin) indicates muscle/vascularized tissue; yellow (reticular fibers/collagen) indicates bone; green/blue (mucin) indicates cartilaginous tissue; and black, nuclei and elastic fibers. Images were acquired using a Zeiss 200M inverted microscope.

Immunohistochemistry (IHC). For IHC, slides were deparaffinized and rehydrated. Next, different antigen retrievals were performed based on the needs of each staining. Collagen stainings required enzymatic digestion with hyaluronidase (2 mg ml^{-1} in PBS) for 45 min, followed by 30 min incubation in pronase (1 mg ml^{-1} in PBS). For the rest of stainings heat antigen retrieval was performed, sections were incubated for 20 min at 90 °C in 10 mM sodium citrate, 0.05% Tween-20 at pH 6.0. All sections were then blocked for 1 h at room temperature in 1.5% bovine serum albumin (BSA) 0.5% Tween-20 in PBS, followed by 1ary antibody incubation overnight at 4 °C in PBS containing 1% BSA in a humidified chamber. Next day, sections were incubated with the corresponding 2ary antibody in PBS containing 1% BSA for 1 h at room temperature in the dark. Between individual incubation steps, sections were rinsed three times with PBS containing 0.1% Tween-20. Finally, fluorescent slides were washed and mounted with fluorescent mounting medium containing DAPI (Abcam, ab104139). Table 2 details the employed antibodies and their concentrations. For fluorescent stainings, inverted laser-scanning microscope Leica TCS SP5 was used, and images were further processed in Fiji and Adobe Photoshop CS6.

Isolation of human cells from implanted ossicles.

Ossicle isolation. Scaffolds were excised from the subcutaneous pockets at indicated times post-surgery and collected together with murine femurs in MEMα + 10% FBS on ice. Skin and connective tissue around the bones was carefully removed.

Ossicle digestion. Scaffolds and bones were first mechanically dissociated into small pieces in Eppendorf tubes, followed by addition of digestion medium (MEMα + 10% FBS + 1 mg ml^{-1} Collagenase A (Roche 11088793001) + 0.5 mg ml^{-1} DNase I (Roche 11284932001)), and were

incubated at 37 °C rocking for 1 h. Followed by trypsin (final conc. 0.025 %, Gibco) addition for 10 min at 37 °C, cells were washed with FACS buffer (PBS + 1 mM EDTA + 2% FBS) and filtered through a 70-μm cell strainer (BD Falcon 352350). When needed, red blood cells were lysed by incubation with RBC lysis buffer (Biolegend 420301) for 5 min at room temperature and cells were washed and re-suspended in FACS buffer. Next, cells were incubated for 10 min at 4 °C with mouse Fc block solution (1μg per 10^6 cells in 100 μl, BD Biosciences 553141) prior to receiving the antibody mix solution.

Flow cytometry sorting. To sort all human cells, despite their surface markers or differentiation state, a general anti-human HLA-ABC antibody (Table 2) was used. Cells were stained in FACS buffer for 30 min rocking at 4 °C in the dark. Cells were then washed and resuspended in FACS buffer to be analyzed in BD FACSAria III. Dead cells were stained by the Fixable Viability Dye and were, together with doublets, excluded from analysis. Gates were defined according to the fluorescence intensity of the isotype control and fluorescence minus one (FMO) staining. Next, human cells were sorted through a 100 μm nozzle with 20 psi sheath pressure directly into RNA lysis buffer.

RNA isolation and bulk mRNA sequencing. RNA was isolated from sorted cells from *in vivo* implanted ossicles or retrieved cells from hydrogels cultured *in vitro* following the Direct-zol RNA MiniPrep (Zymo Research, R2052). RNA sequencing libraries were prepared as previously described using BRB-seq method[18]. Data analysis and gene ontology enrichment was performed using the ASAP platform[30]. Briefly, genes were filtered based on count per million (CPM, 1 CPM in minimally 1 sample detected), followed by Voom normalization[31]. Differential expression was done using limma with adjusted p-value (FDR) ≤ 0.05 and fold change (FC) ≥ 2.

Statistical analysis. All data are reported as mean ± standard deviation. All statistical analyses were performed using GraphPad Prism (version 8.0.0, GraphPad Software). Mean values were compared by one-way or two-way analysis of variance (ANOVA) followed by Tukey's *post hoc* test for multiple comparisons. Statistical significance was accepted for $P < 0.05$, and reported as follows * $P < 0.05$, ** $P < 0.01$, *** $P < 0.001$, **** $P < 0.0001$. For experiments involving different biological donors, a distinction between N (biological donors) and n (technical replicates) was made. Further information is found in the particular figure legends.

Table 1. Demographic information from all the tested donors

Donor	Age (years)	Gender
BM D1	33	F
BM D2	23	M
BM D3	18	M
BM D4	17	M
BM D5	28	F
BM D6	39	M

Donor	Age (years)	Gender
OP D1	80	F
OP D2	91	F
OP D3	51	F
ASC D1	45	F
ASC D2	54	F
ASC D3	-	F

BM: healthy bone marrow; OP: osteoporotic bone marrow; ASC: healthy adipose; D: donor; F: female; M: male

Table 2. List of detailed antibodies used for flow cytometry and histological stainings

Antibody	Application & Dilution	Company	Catalog number
Mouse α hCD29 – PE	FC 1:300	BioLegend	303003
Mouse α hCD29 – APC	FC 1:300	BioLegend	303007
Mouse α hCD44 – APC	FC 1:100	BioLegend	338805
Mouse α hCD105 – FITC	FC 1:100	BioLegend	323204
Mouse α hCD90 – APC	FC 1:200	BD Biosciences	559869
Mouse α hCD73 – PE	FC 1:100	BD Biosciences	550257
Mouse α hCD73 – FITC	FC 1:100	BioLegend	344015
Mouse α hCD146 – PE	FC 1:100	BioLegend	361005
Mouse α hCD146 – FITC	FC 1:100	BioLegend	361011
Mouse α hCD49d – PE	FC 1:100	BD Biosciences	555503
Mouse α hCD49d – FITC	FC 1:100	BioLegend	304315
Mouse α hCD34 – FITC	FC 1:100	MACS	130-081-001
Mouse α hCD45 – eFluor 450	FC 1:100	eBioscience	48-0459-42
Mouse α HLA-ABC – PE	FC 1:200	BioLegend	311405
Isotype mouse IgG1 control – PE	FC 1:100	BD Biosciences	556650
Isotype mouse IgG1 control – APC	FC 1:100	BD Biosciences	345818
Isotype mouse IgG1 control – FITC	FC 1:100	BD Biosciences	555748
Isotype mouse IgG2a control – FITC	FC 1:100	BD Biosciences	555573
Isotype mouse IgG1 control – BV421	FC 1:100	BioLegend	400157
Isotype mouse IgG2a control – PE	FC 1:200	BioLegend	400213
SYTOX Blue Dead Cell Stain	FC 1:1500	ThermoFisher	S34857

Fixable Viability Dye – eFluor 780	FC 1:4000	eBioscience	65-0865-14
Rabbit α human CD34	IHC 1:50	Abcam	ab110643
Rabbit α human CD45	IHC 1:50	Abcam	ab40763
Rabbit α human CD31	IHC 1:50	Abcam	Ab76533
Rabbit α human collagen type 1	IHC 1:1000	Abcam	ab138492
Rabbit α mouse collagen type 1	IHC 1:50	Abcam	ab21286
Rabbit α collagen type 2	IHC 1:100	Abcam	ab34712
Rabbit α SP7 osterix	IHC 1:200	Abcam	ab22552
Goat α mouse perilipin	IHC 1:50	Abcam	ab61682
Mouse α human vimentin	IHC 1:200	Abcam	ab8069
Isotype rabbit IgG control	IHC 1:200	Abcam	ab172730
Isotype mouse IgG1 control	IHC 1:200	Abcam	ab18448
Goat α rabbit AF568	IHC 1:200	Abcam	ab175471
Goat α mouse DyLight 648	IHC 1:200	BioLegend	405312
Donkey α goat AF488	IHC 1:200	Abcam	ab150129

FC: flow cytometry; IHC: immunohistochemistry

References

1 Dominici, M. *et al.* Minimal criteria for defining multipotent mesenchymal stromal cells. The International Society for Cellular Therapy position statement. *Cytotherapy* **8**, 315-317 (2006).

2 Sipp, D., Robey, P. G. & Turner, L. Clear up this stem-cell mess. *Nature* **561**, 455-457 (2018).

3 Bianco, P. *et al.* The meaning, the sense and the significance: translating the science of mesenchymal stem cells into medicine. *Nature medicine* **19**, 35 (2013).

4 Bianco, P., Kuznetsov, S. A., Riminucci, M. & Robey, P. G. in *Methods in enzymology* Vol. 419 117-148 (Elsevier, 2006).

5 Murphy, W. L., McDevitt, T. C. & Engler, A. J. Materials as stem cell regulators. *Nature materials* **13**, 547 (2014).

6 Arinzeh, T. L., Tran, T., Mcalary, J. & Daculsi, G. A comparative study of biphasic calcium phosphate ceramics for human mesenchymal stem-cell-induced bone formation. *Biomaterials* **26**, 3631-3638 (2005).

7 Abarrategi, A. *et al.* In vivo ectopic implantation model to assess human mesenchymal progenitor cell potential. *Stem Cell Reviews and Reports* **9**, 833-846 (2013).

8 Scotti, C. *et al.* Recapitulation of endochondral bone formation using human adult mesenchymal stem cells as a paradigm for developmental engineering. *Proceedings of the National Academy of Sciences* **107**, 7251-7256 (2010).

9 Sacchetti, B. *et al.* Self-renewing osteoprogenitors in bone marrow sinusoids can organize a hematopoietic microenvironment. *Cell* **131**, 324-336 (2007).

10 Reinisch, A. *et al.* A humanized bone marrow ossicle xenotransplantation model enables improved engraftment of healthy and leukemic human hematopoietic cells. *Nature medicine* **22**, 812 (2016).

11 Chan, C. K. *et al.* Identification of the human skeletal stem cell. *Cell* **175**, 43-56. e21 (2018).

12 Reinisch, A. *et al.* Epigenetic and in vivo comparison of diverse MSC sources reveals an endochondral signature for human hematopoietic niche formation. *Blood* **125**, 249-260 (2015).

13 Ehrbar, M. *et al.* Enzymatic formation of modular cell-instructive fibrin analogs for tissue engineering. *Biomaterials* **28**, 3856-3866 (2007).

14 Mannello, F., Tonti, G. A., Bagnara, G. P. & Papa, S. Role and function of matrix metalloproteinases in the differentiation and biological characterization of mesenchymal stem cells. *Stem Cells* **24**, 475-481 (2006).

15 Ruoslahti, E. & Pierschbacher, M. D. New perspectives in cell adhesion: RGD and integrins. *Science* **238**, 491-497 (1987).

16 Hilton, M. J. *et al.* Notch signaling maintains bone marrow mesenchymal progenitors by suppressing osteoblast differentiation. *Nature medicine* **14**, 306 (2008).

17 Lienemann, P. S. *et al.* A versatile approach to engineering biomolecule-presenting cellular microenvironments. *Advanced healthcare materials* **2**, 292-296 (2013).

18 Alpern, D. *et al.* BRB-seq: ultra-affordable high-throughput transcriptomics enabled by bulk RNA barcoding and sequencing. *Genome biology* **20**, 71 (2019).

19 Fritsch, K. *et al.* Engineered humanized bone organs maintain human hematopoiesis in vivo. *Experimental hematology* **61**, 45-51. e45 (2018).

20 Mesfin, A. *et al.* High-dose rhBMP-2 for adults: major and minor complications: a study of 502 spine cases. *JBJS* **95**, 1546-1553 (2013).

21 Chin, C. J. *et al.* Transcriptionally and functionally distinct mesenchymal subpopulations are generated from human pluripotent stem cells. *Stem cell reports* **10**, 436-446 (2018).

22 Papadimitropoulos, A. *et al.* Expansion of human mesenchymal stromal cells from fresh bone marrow in a 3D scaffold-based system under direct perfusion. *PloS one* **9**, e102359 (2014).

23 Guven, S. *et al.* Engineering of large osteogenic grafts with rapid engraftment capacity using mesenchymal and endothelial progenitors from human adipose tissue. *Biomaterials* **32**, 5801-5809, doi:10.1016/j.biomaterials.2011.04.064 (2011).
24 Osinga, R. *et al.* Generation of a Bone Organ by Human Adipose-Derived Stromal Cells Through Endochondral Ossification. *Stem cells translational medicine* **5**, 1090-1097, doi:10.5966/sctm.2015-0256 (2016).
25 Ehrbar, M. *et al.* Biomolecular hydrogels formed and degraded via site-specific enzymatic reactions. *Biomacromolecules* **8**, 3000-3007 (2007).
26 Weber, F. E. *et al.* Disulfide bridge conformers of mature BMP are inhibitors for heterotopic ossification. *Biochemical and Biophysical Research Communications* **286**, 554-558 (2001).
27 Schense, J. C. & Hubbell, J. A. Cross-linking exogenous bifunctional peptides into fibrin gels with factor XIIIa. *Bioconjugate chemistry* **10**, 75-81 (1999).
28 Doube, M. *et al.* BoneJ: free and extensible bone image analysis in ImageJ. *Bone* **47**, 1076-1079 (2010).
29 Garvey, W., Fathi, A., Bigelow, F., Carpenter, B. & Jimenez, C. Improved Movat pentachrome stain. *Stain technology* **61**, 60-62 (1986).
30 Gardeux, V., David, F. P., Shajkofci, A., Schwalie, P. C. & Deplancke, B. ASAP: a web-based platform for the analysis and interactive visualization of single-cell RNA-seq data. *Bioinformatics* **33**, 3123-3125 (2017).
31 Ritchie, M. E. *et al.* limma powers differential expression analyses for RNA-sequencing and microarray studies. *Nucleic acids research* **43**, e47-e47 (2015).

Supplementary data

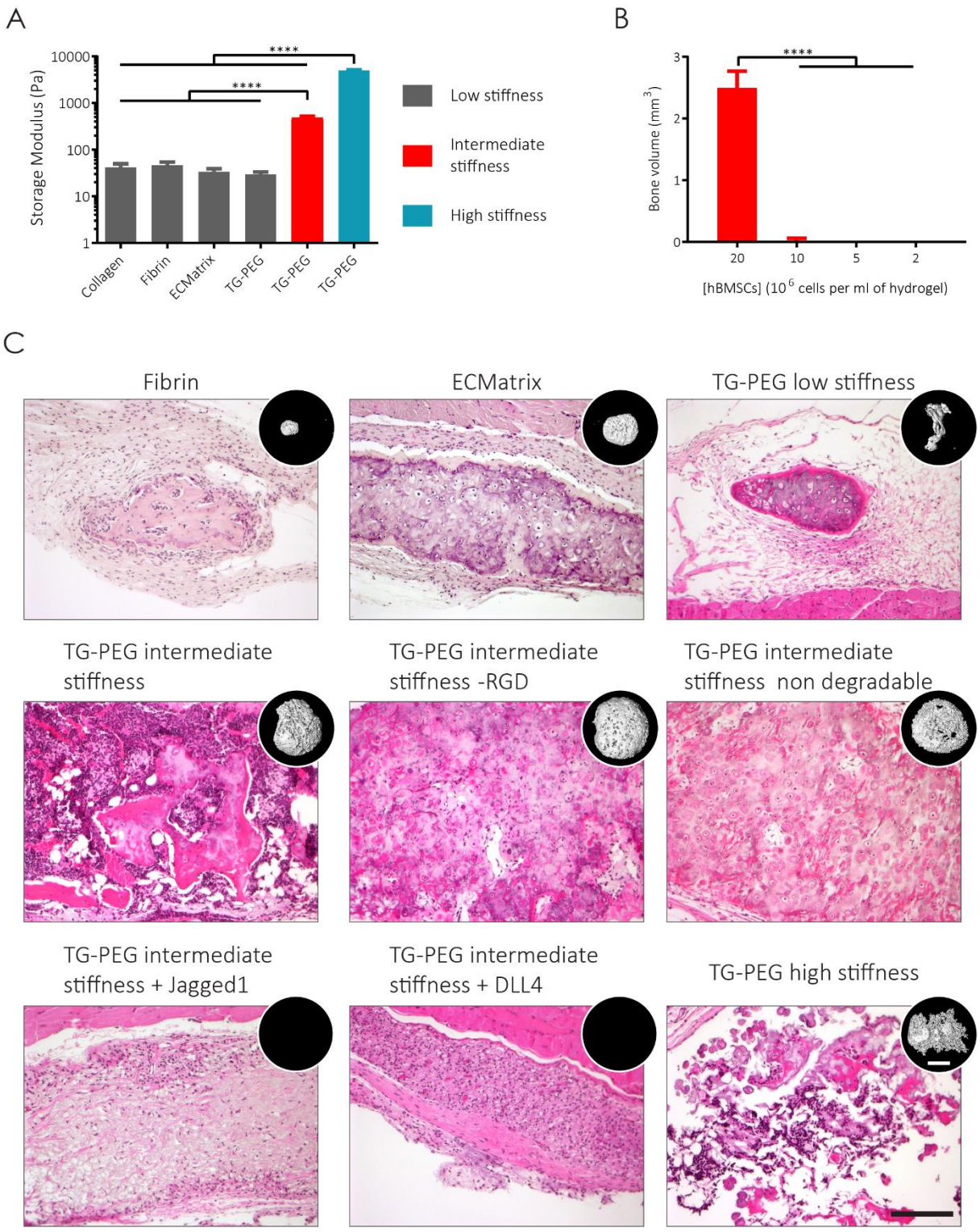

Figure S1. Scaffold influences bone and bone marrow formation

(**a**) Storage moduli of different hydrogels measured by *in situ* rheology showing low stiffness hydrogels of 50 Pa, and the tuning of TG-PEG hydrogels to intermediate and high stiffness of 500 Pa and 5 kPa, respectively (n = 3, graphic repeated in Chapter 4, Figure 1 b for clarity). (**b**) Titration of hBMSCs encapsulated in intermediate stiffness TG-PEG hydrogels at different concentrations prior to implantation showed that $20{\cdot}10^6$ cells per ml of hydrogel is the minimum needed to induce bone formation in the absence of any osteoinductive or osteoconductive factors (n = 4). (**c**) Representative H&E stainings (scale bar:

200 µm) and microCT reconstruction (scale bar: 2 mm, some microCT images are repeated from Figure c) of all conditions. All data are reported as mean ± standard deviation. ANOVA with Tukey's *post hoc* test **** P < 0.0001.

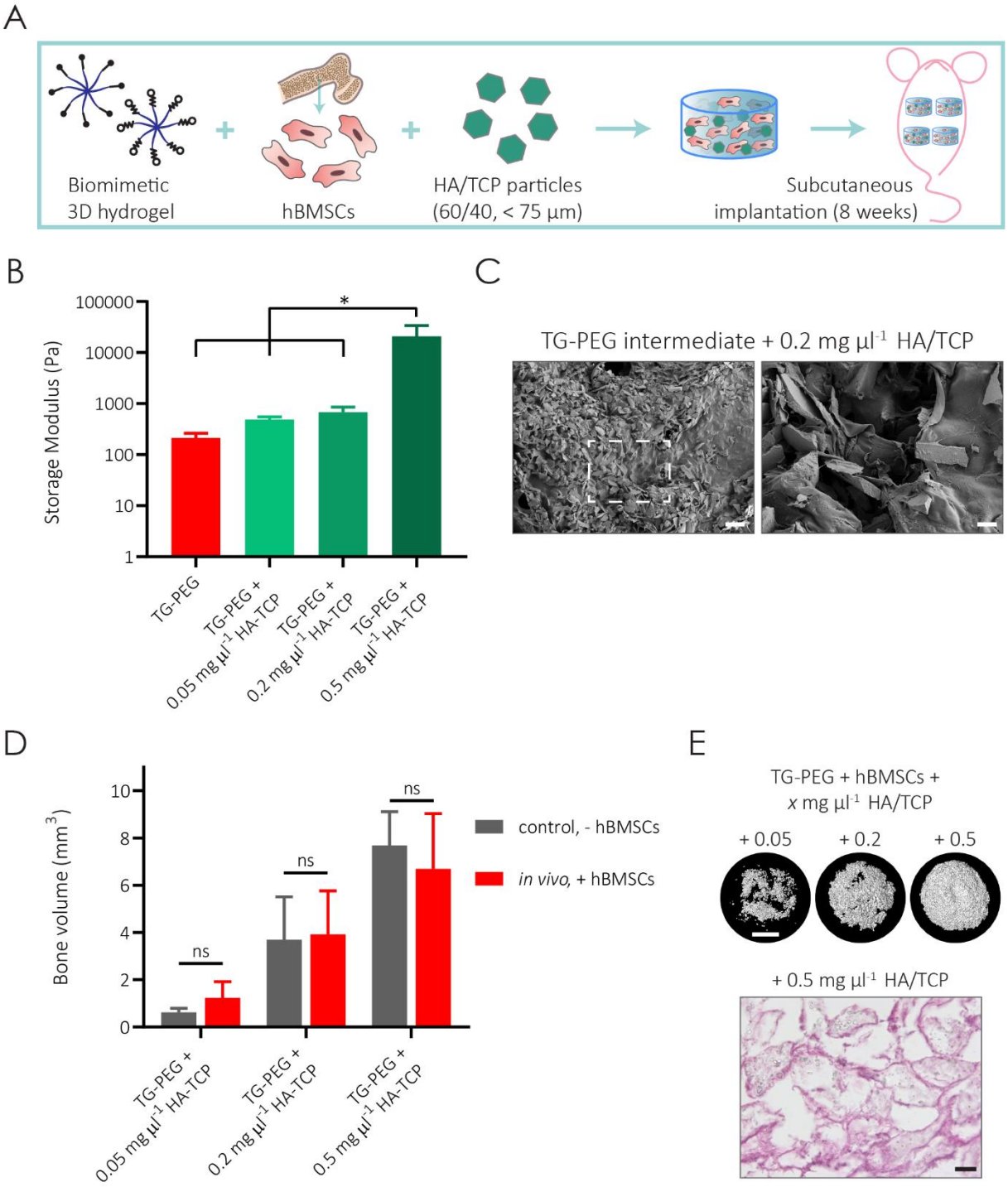

Figure S2. HA/TCP osteoconductive particles encapsulated in TG-PEG hydrogels inhibits hBMSC bone formation

(**a**) Diverse amounts of osteoconductive hydroxyapatite tricalcium phosphate (HA/TCP, 60/40, diameter < 75 µm) particles were added in TG-PEG hydrogels of intermediate stiffness combined with hBMSCs prior to transplantation in nude mice. (**b**) Encapsulation of particles in the hydrogel significantly increased the storage modulus of TG-PEG hydrogels as seen by rheological tests (n = 3). (**c**) SEM imaging revealed important structural changes in the hydrogel by the addition of HA/TCP

particles (scale bar left: 200 µm, zoom in right: 40 µm). (**d**) After 8 weeks of being subcutaneously implanted in mice bone volume showed no differences to non-implanted control hydrogels (n = 4). (**e**) H&E staining (scale bar: 20 µm) and microCT reconstructions (scale bar: 2 mm) corroborated lack of bone formation. All data are reported as mean ± standard deviation. ANOVA with Tukey's *post hoc* test * $P < 0.05$, ns: no significant.

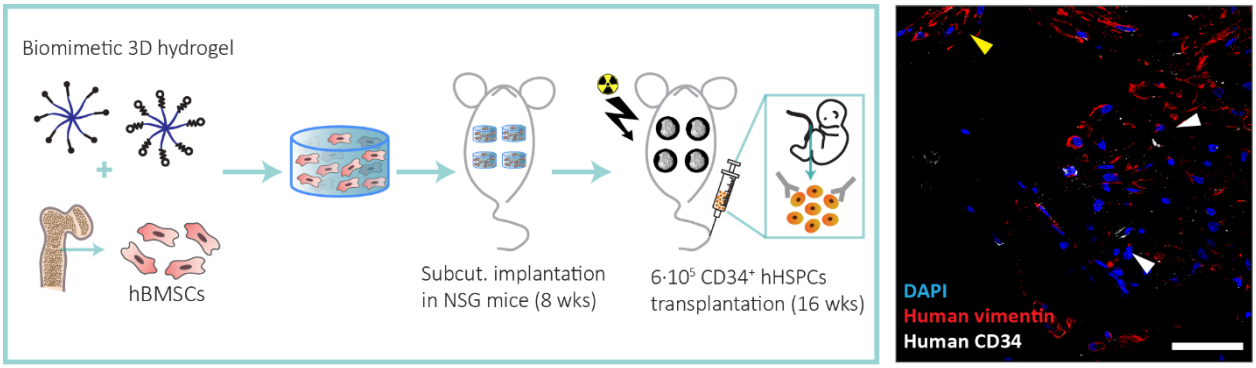

Figure S3. Human hematopoietic stem/progenitor cells and hBMSCs co-develop bone marrow-like structures

Schematics of the workflow. hBMSCs were encapsulated in TG-PEG hydrogels, after ossicle formation in NSG mice, human hematopoietic stem/progenitor cells (hHSPCs) were systemically disseminated via tail vein injection. Dual humanization was observed 16 weeks post-hHSPC transplantation by localizing hBMSCs residing in bony areas (yellow arrow) and $CD34^+$ hHSPCs in the marrow (indicated by white arrows, scale bar: 50 µm). Nuclei were stained by DAPI, human cells stained by human-specific vimentin in red, and human CD34 cells in white.

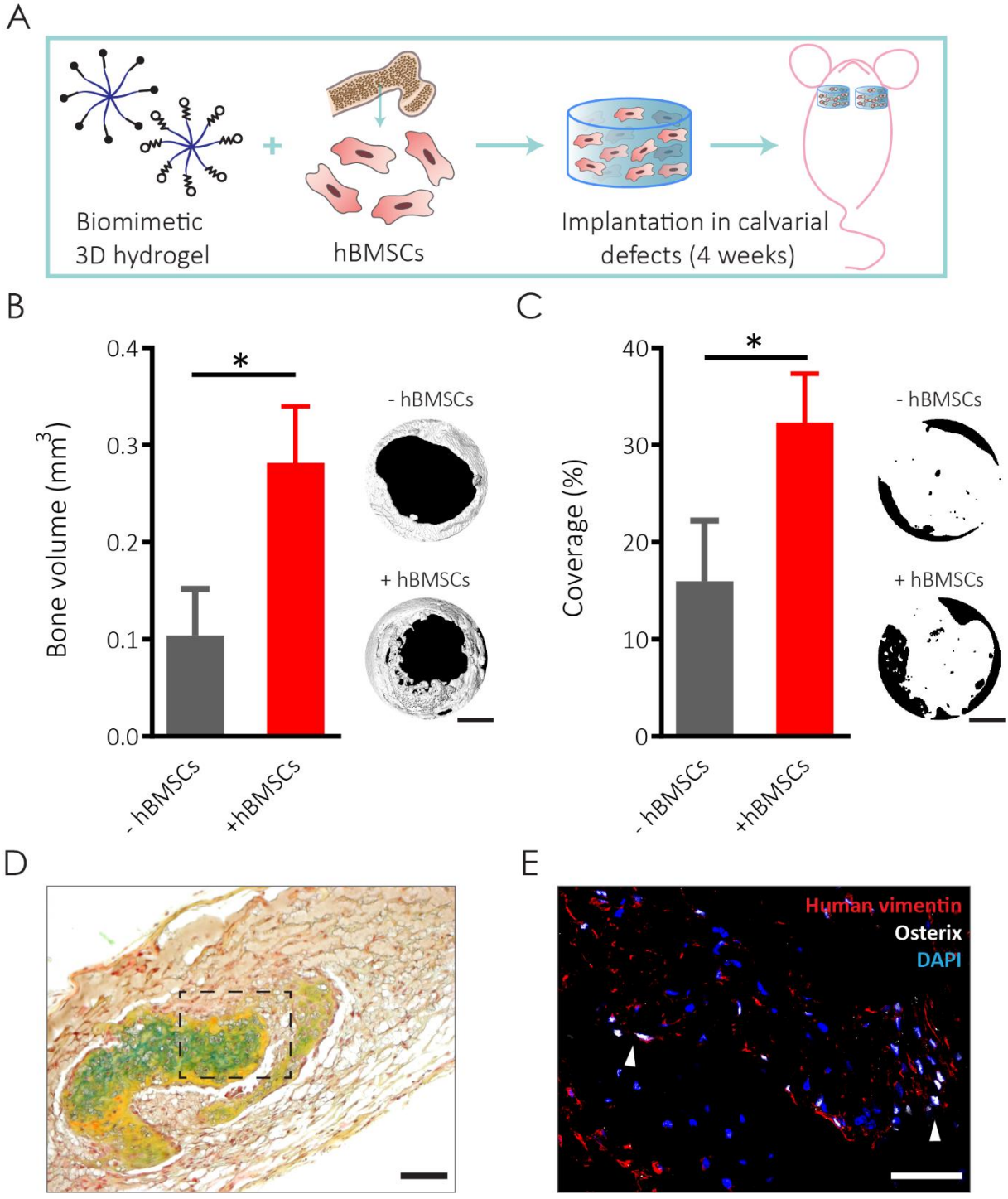

Figure S4. Calvarial defects

(**a**) Optimized TG-PEG hydrogels (intermediate stiffness, containing RGD adhesion and MMP-sensitive degradable sides) containing high density of hBMSCs ($20{\cdot}10^6$ cells per ml of hydrogel) were implanted in murine calvarial defects for 4 weeks. (**b**) MicroCT revealed higher bone volume and (**c**) total coverage in hydrogels containing hBMSCs compared to control gels not containing cells (n = 3, scale bars: 2 mm). (**d**) Histological analysis corroborated the presence of bony-structures (MP staining; scale bar: 100 µm), (**e**) which in turn contained hBMSCs. Some co-expressed osterix (indicated by white arrows; scale bar: 50 µm). Nuclei were stained by DAPI, human cells stained by human-specific vimentin in red and osterix positive cells in white. All data are reported as mean ± standard deviation. ANOVA with Tukey's *post hoc* test * $P < 0.05$.

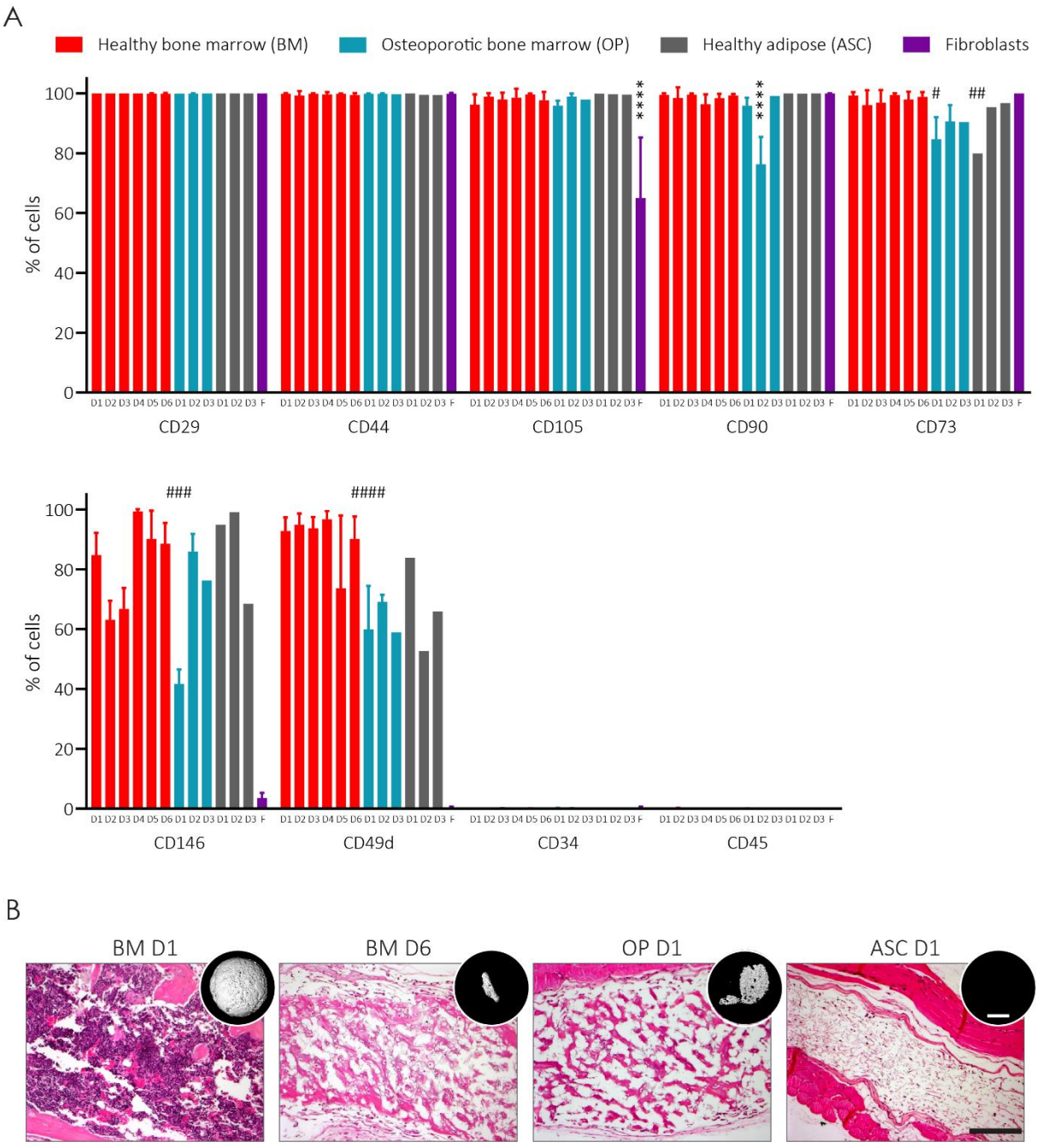

Figure S5. hBMSCs characterization by surface markers and *in vivo* performance

(**a**) Flow cytometry comparison of expression of consensus surface markers similarly expressed among cell types (CD29, CD44, CD105, CD90 and CD73), absent in fibroblasts (CD146, CD49d) and absent in all cell types (CD34, CD45) showed no correlation to *in vivo* bone formation capacity of these cells ($1 \leq n \leq 6$; #, ##, ###, #### referring to multiple comparison statistics which are specified in Table S1). (**b**) Representative H&E staining (scale bar: 200 µm) and microCT reconstruction (scale bar: 2 mm) for each tested donor type highlighted major differences in ECM remodeling and host cell infiltration. All data are reported as mean ± standard deviation. ANOVA with Tukey's *post hoc* test **** $P < 0.0001$.

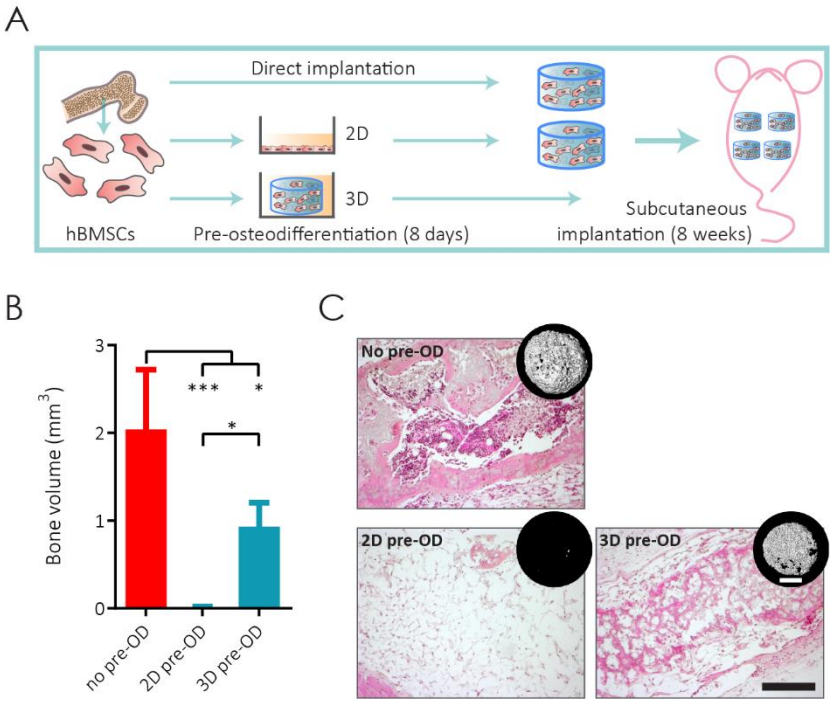

Figure S6. hBMSC osteogenic differentiation *in vitro* prior to implantation limits hBMSC bone formation capacity *in vivo*

(**a**) hBMSCs were cultured either in 2D or in 3D (TG-PEG hydrogels) in osteogenic medium for 8 days. 2D cells were then encapsulated and 3D hydrogels were directly subcutaneously implanted in nude mice for 8 weeks. (**b**) MicroCT measurements revealed loss of bone volume in hBMSCs pre-osteodifferentiated *in vitro* (pre-OD) compared to hBMSCs directly implanted (i.e. not differentiated) (n = 4). (**c**) H&E stainings (scale bar: 200 µm) and microCT reconstructions (scale bar: 2 mm) showed bone and marrow for unprimed hBMSCs, while 2D pre-differentiated cells retained a fibrotic-like phenotype, and 3D pre-differentiated cells condensed and deposited minimal ECM but did not contain a marrow. All data are reported as mean ± standard deviation. ANOVA with Tukey's *post hoc* test * $P < 0.05$, *** $P < 0.001$.

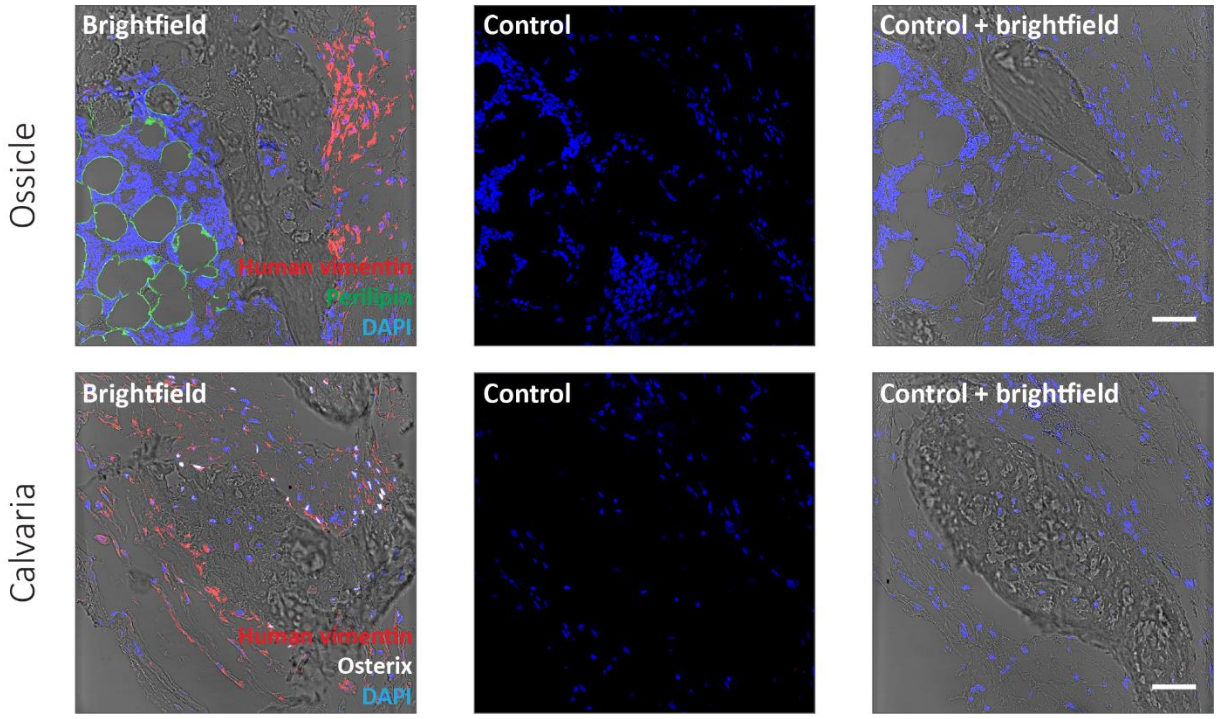

Figure S7. Control immunostainings

Brightfield image combined with immunostaining to better localize the human cells within the ossicles (top left) and control staining with isotype-matched control antibodies for subcutaneously implanted ossicles (top right; scale bar: 50 µm). For ossicles implanted in calvarial defects (bottom), brightfield imaging combined with immunostaining to better localize the human cells (left) and control staining with isotype antibodies (right; scale bar: 50 µm). Nuclei were stained by DAPI, human cells stained by human-specific vimentin in red, adipocytes stained by perilipin in green and osterix positive cells in white.

Table S1. Detailed statistics from hBMSC surface characterization by flow cytometry

Tukey's multiple comparisons test	Mean Diff.	95.00% CI of diff.	Summary	Adjusted P Value
# CD73 OP D1				
BM D1 vs. OP D1	14.65	5.931 to 23.37	****	<0.0001
BM D2 vs. OP D1	11.38	2.664 to 20.10	**	0.0014
BM D3 vs. OP D1	12.15	3.148 to 21.16	***	0.0008
BM D4 vs. OP D1	14.75	5.748 to 23.76	****	<0.0001
BM D5 vs. OP D1	13.28	3.866 to 22.70	***	0.0003
BM D6 vs. OP D1	14.13	5.414 to 22.85	****	<0.0001
OP D1 vs. Fibroblasts	-15.33	-25.40 to -5.266	****	<0.0001
## CD73 ASC D1				
BM D1 vs. ASC D1	19.42	6.098 to 32.74	***	0.0002
BM D2 vs. ASC D1	16.15	2.832 to 29.47	**	0.0047

BM D3 vs. ASC D1	16.92	3.413 to 30.43	**	0.0028
BM D4 vs. ASC D1	19.52	6.013 to 33.03	***	0.0002
BM D5 vs. ASC D1	18.05	4.264 to 31.84	**	0.0013
BM D6 vs. ASC D1	18.9	5.582 to 32.22	***	0.0003
ASC D1 vs. Fibroblasts	-20.1	-34.34 to -5.862	***	0.0003
### CD146				
BM D1 vs. BM D3	17.98	4.401 to 31.57	**	0.0013
BM D1 vs. BM D2	21.65	8.912 to 34.39	****	<0.0001
BM D1 vs. BM D4	-14.59	-27.33 to -1.845	*	0.011
BM D1 vs. OP D1	43.03	28.15 to 57.91	****	<0.0001
BM D1 vs. Fibroblasts	81.23	66.35 to 96.11	****	<0.0001
BM D3 vs. BM D4	-32.57	-46.69 to -18.45	****	<0.0001
BM D3 vs. BM D5	-23.35	-38.23 to -8.471	****	<0.0001
BM D3 vs. BM D6	-21.78	-36.65 to -6.896	***	0.0002
BM D3 vs. OP D2	-19.18	-35.25 to -3.112	**	0.0063
BM D3 vs. OP D1	25.05	8.979 to 41.12	****	<0.0001
BM D3 vs. ASC D1	-28.15	-51.68 to -4.624	**	0.0061
BM D3 vs. ASC D2	-32.35	-55.88 to -8.824	***	0.0007
BM D3 vs. Fibroblasts	63.24	47.17 to 79.31	****	<0.0001
BM D2 vs. BM D4	-36.24	-49.55 to -22.93	****	<0.0001
BM D2 vs. BM D5	-27.02	-41.14 to -12.90	****	<0.0001
BM D2 vs. BM D6	-25.45	-39.56 to -11.33	****	<0.0001
BM D2 vs. OP D2	-22.85	-38.22 to -7.486	***	0.0001
BM D2 vs. OP D1	21.38	6.013 to 36.75	***	0.0005
BM D2 vs. ASC D1	-31.82	-54.87 to -8.770	***	0.0006
BM D2 vs. ASC D2	-36.02	-59.07 to -12.97	****	<0.0001
BM D2 vs. Fibroblasts	59.57	44.21 to 74.94	****	<0.0001
BM D4 vs. OP D1	57.62	42.25 to 72.99	****	<0.0001
BM D4 vs. ASC D3	30.82	7.770 to 53.87	**	0.0011
BM D4 vs. Fibroblasts	95.81	80.45 to 111.2	****	<0.0001

BM D5 vs. OP D1	48.4	32.33 to 64.47	****	<0.0001
BM D5 vs. Fibroblasts	86.59	70.52 to 102.7	****	<0.0001
BM D6 vs. OP D1	46.83	30.75 to 62.90	****	<0.0001
BM D6 vs. Fibroblasts	85.02	68.95 to 101.1	****	<0.0001
OP D2 vs. OP D1	44.23	27.05 to 61.41	****	<0.0001
OP D2 vs. Fibroblasts	82.43	65.25 to 99.61	****	<0.0001
OP D1 vs. OP D3	-34.6	-58.90 to -10.30	***	0.0003
OP D1 vs. ASC D1	-53.2	-77.50 to -28.90	****	<0.0001
OP D1 vs. ASC D2	-57.4	-81.70 to -33.10	****	<0.0001
OP D1 vs. ASC D3	-26.8	-51.10 to -2.503	*	0.0175
OP D1 vs. Fibroblasts	38.19	21.01 to 55.37	****	<0.0001
OP D3 vs. Fibroblasts	72.79	48.50 to 97.09	****	<0.0001
ASC D1 vs. Fibroblasts	91.39	67.10 to 115.7	****	<0.0001
ASC D2 vs. ASC D3	30.6	0.8420 to 60.36	*	0.0379
ASC D2 vs. Fibroblasts	95.59	71.30 to 119.9	****	<0.0001
ASC D3 vs. Fibroblasts	64.99	40.70 to 89.29	****	<0.0001
#### CD49d				
BM D1 vs. BM D5	19.09	4.970 to 33.20	***	0.0009
BM D1 vs. OP D2	23.66	8.293 to 39.03	****	<0.0001
BM D1 vs. OP D1	32.83	17.46 to 48.19	****	<0.0001
BM D1 vs. OP D3	33.76	10.71 to 56.81	***	0.0002
BM D1 vs. ASC D2	40.06	17.01 to 63.11	****	<0.0001
BM D1 vs. ASC D3	26.86	3.810 to 49.91	**	0.0088
BM D1 vs. Fibroblasts	92.35	76.98 to 107.7	****	<0.0001
BM D3 vs. BM D5	20.01	5.890 to 34.12	***	0.0004
BM D3 vs. OP D2	24.58	9.213 to 39.95	****	<0.0001
BM D3 vs. OP D1	33.75	18.38 to 49.11	****	<0.0001
BM D3 vs. OP D3	34.68	11.63 to 57.73	***	0.0001
BM D3 vs. ASC D2	40.98	17.93 to 64.03	****	<0.0001
BM D3 vs. ASC D3	27.78	4.730 to 50.83	**	0.0055

BM D3 vs. Fibroblasts	93.27	77.90 to 108.6	****	<0.0001
BM D2 vs. BM D5	21.2	6.321 to 36.08	***	0.0003
BM D2 vs. OP D2	25.78	9.704 to 41.85	****	<0.0001
BM D2 vs. OP D1	34.94	18.87 to 51.01	****	<0.0001
BM D2 vs. OP D3	35.87	12.35 to 59.40	****	<0.0001
BM D2 vs. ASC D2	42.17	18.65 to 65.70	****	<0.0001
BM D2 vs. ASC D3	28.97	5.449 to 52.50	**	0.004
BM D2 vs. Fibroblasts	94.46	78.39 to 110.5	****	<0.0001
BM D4 vs. BM D5	23.05	8.171 to 37.93	****	<0.0001
BM D4 vs. OP D2	27.63	11.55 to 43.70	****	<0.0001
BM D4 vs. OP D1	36.79	20.72 to 52.86	****	<0.0001
BM D4 vs. OP D3	37.72	14.20 to 61.25	****	<0.0001
BM D4 vs. ASC D2	44.02	20.50 to 67.55	****	<0.0001
BM D4 vs. ASC D3	30.82	7.299 to 54.35	**	0.0015
BM D4 vs. Fibroblasts	96.31	80.24 to 112.4	****	<0.0001
BM D5 vs. BM D6	-16.43	-30.54 to -2.310	**	0.0089
BM D5 vs. Fibroblasts	73.26	57.19 to 89.33	****	<0.0001
BM D6 vs. OP D2	21	5.633 to 36.37	***	0.0007
BM D6 vs. OP D1	30.17	14.80 to 45.53	****	<0.0001
BM D6 vs. OP D3	31.1	8.050 to 54.15	***	0.0009
BM D6 vs. ASC D2	37.4	14.35 to 60.45	****	<0.0001
BM D6 vs. ASC D3	24.2	1.150 to 47.25	*	0.0305
BM D6 vs. Fibroblasts	89.69	74.32 to 105.1	****	<0.0001
OP D2 vs. Fibroblasts	68.69	51.51 to 85.87	****	<0.0001
OP D1 vs. Fibroblasts	59.52	42.34 to 76.70	****	<0.0001
OP D3 vs. Fibroblasts	58.59	34.29 to 82.89	****	<0.0001
ASC D1 vs. ASC D2	31.2	1.442 to 60.96	*	0.031
ASC D1 vs. Fibroblasts	83.49	59.19 to 107.8	****	<0.0001
ASC D2 vs. Fibroblasts	52.29	27.99 to 76.59	****	<0.0001
ASC D3 vs. Fibroblasts	65.49	41.19 to 89.79	****	<0.0001

Been wondering for days
How you felt me slip your mind
Leave behind your wanton ways
I want to learn to love in kind
Cause you were all I ever longed for.
– Mumford and Sons

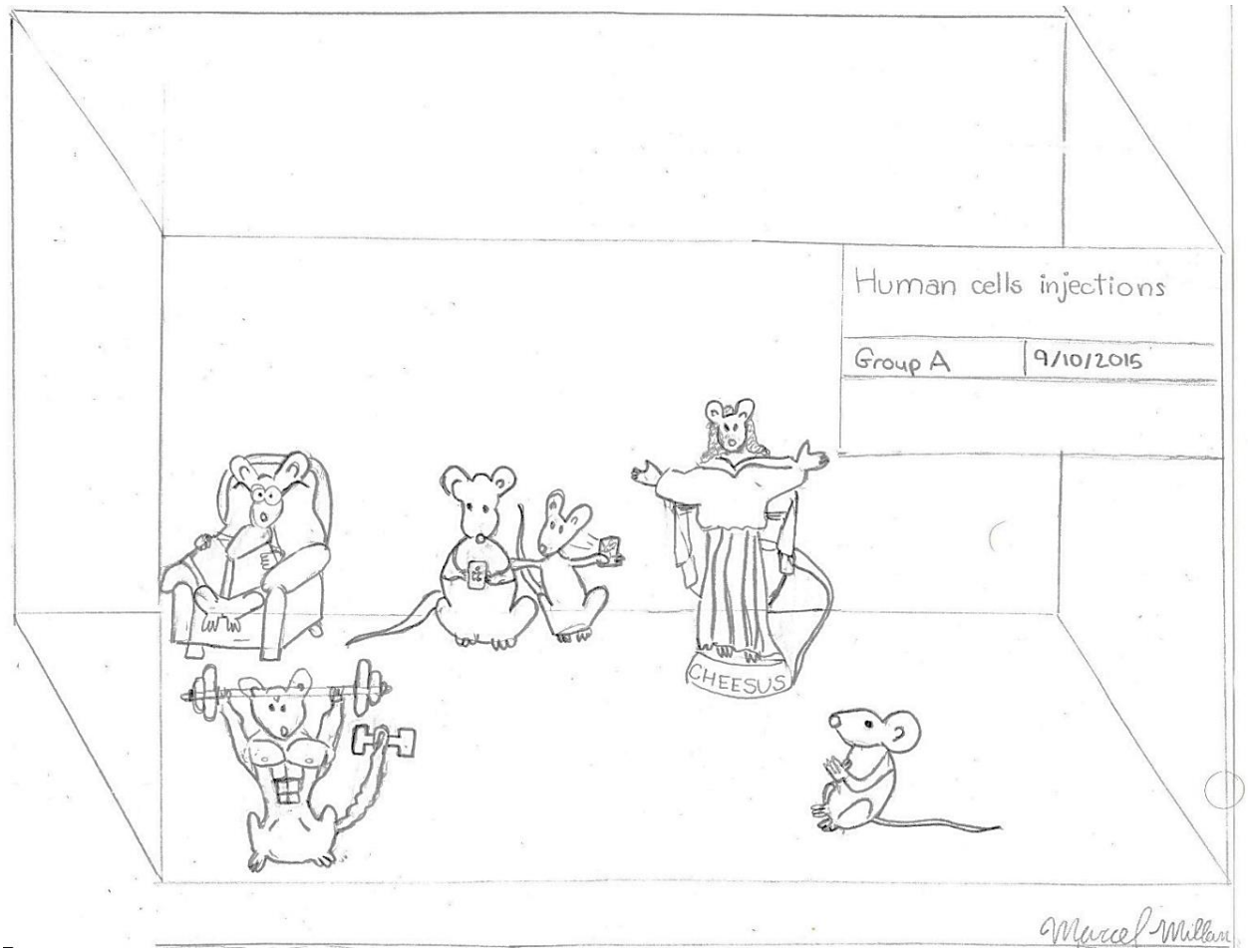

Artwork by Marcel Millan
Philadelphia, PA, USA

CHAPTER 4

Engineered humanized bone marrow organoids for investigating cancer osteotropism *in vivo*

Q Vallmajo-Martin[1,2], A Chiou[3], M Whitman[3], S Rojas-Sutterlin[4], ND Tavakol[4], S Giger[2], D Capron[5], G Zuchtriegel[5], F Weber[6], B Bornhauser[5], O Naveiras[4], C Fischbach[3], M Lütolf[2], M Ehrbar[1]

The content of this chapter is part of a manuscript in preparation.

[1] Laboratory for Cell and Tissue Engineering, Department of Obstetrics, UniversitätsSpital Zürich, Switzerland;
[2] Laboratory of Stem Cell Bioengineering, Institute of Bioengineering, École Polytechnique Fédérale de Lausanne, Switzerland;
[3] Nancy E. & Peter C. Meinig School of Biomedical Engineering, University Hospital Basel, Cornell University, USA;
[4] Laboratory of Regenerative Hematopoiesis, Institute of Bioengineering, École Polytechnique Fédérale de Lausanne, Switzerland;
[5] Department of Oncology, University Children's Hospital of Zürich, Zürich, Switzerland;
[6] Department of Cranio-Maxillofacial Surgery, Oral Biotechnology and Bioengineering, UniversitätsSpital Zürich, Switzerland.

Statement of contributions

QVM designed, performed and analyzed all the experiments.

AC, MW & CF collaborated in the experiments related to breast cancer metastasis *in vivo* including experimental design, *in vivo* experiments and bioluminescence data analysis.

SRS, NDT & ON performed the HSC transplantation to NSG mice carrying ossicles.

SG & ML assisted in flow cytometry analysis.

DC, ZG & BB supplied leukemic cells and performed transplantation to NSG mice carrying ossicles.

FW synthesized and purified the BMP-2 used in this project.

ME designed experiments and supervised the whole project.

Abstract

The bone marrow (BM) orchestrates the hematopoietic system throughout a lifetime. Disruptions of bone marrow regulatory processes can give rise to deleterious pathologies including, among others, leukemia. It is also the common site of metastasis for several types of cancer including breast and prostate. Models to independently decipher the contribution of different cell types, extracellular matrix and soluble cues involved in these events are needed. Towards this aim, we have established a synthetic 3D hydrogel-based model to create humanized functional bone marrow niches. Exploiting the modularity of this well-defined system, microenvironmental parameters were optimized for BM niche formation to overcome limitations of the currently employed natural-based matrices. By encapsulation of human bone marrow stromal cells (hBMSCs) and titrating low doses of bone morphogenetic protein-2 (BMP-2), poly(ethylene glycol) (PEG)-based hydrogels remodeled into functional BM organoids upon 8 weeks of subcutaneous implantation. The newly formed humanized organoids comprised murine hematopoietic stem cells (HSCs) and enabled homing of human hematopoietic stem progenitor cells (hHSPCs) or human leukemic cells. Furthermore, MDA-MB-231 breast cancer cells, when systemically disseminated in mice homed to humanized ossicles demonstrating a preferential breast cancer metastasis to bone undergoing remodeling. Together, we believe that our rationally engineered humanized bone organoids hold tremendous promise to mimic healthy and pathological bone marrow niches. Therefore, it will likely unmask patient-specific factors involved in leukemia as well as osteotropic metastasis of breast cancer.

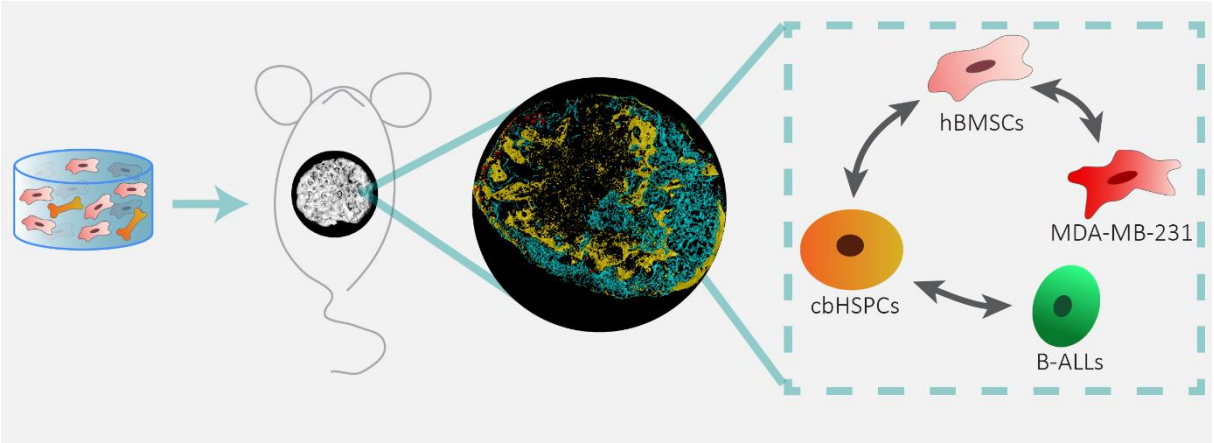

Keywords: Bone marrow niche, human bone organoid, synthetic matrices, cancer, osteotropic cancer, bone metastasis

Introduction

Detrimental shifts from homeostasis in the bone marrow microenvironment, or niche, significantly contribute to the propagation of various types of cancer. Elucidating individual contributions of altered niche factors in promoting malignancy is a considerable challenge owing to the dynamic complexity of the bone marrow[1-3]. Models that capture the interplay between marrow resident cells and their niche, and which permit the systematic study of niche component roles in the dissemination of cancer cells, could provide quintessential clinical benefit. Though it is well known that bone is the preferential homing site for metastatic breast and prostate cancer, at that stage the diseases remain largely incurable with only palliative treatment options[4]. This clinical void can be partially attributed to the lack of suitable animal models that mimic key features of metastasis of human tumor cells to the human bone microenvironment. Despite tremendous advances in more complex transgenic humanized mouse models that, for instance, would recapitulate a set of human cytokines[5], the successful engraftment of human tumor cells in the murine bone and bone marrow remains a challenge.

To overcome these species-related incompatibilities, the development of heterotopic humanized bone marrow ossicles has raised significant interest in the recent years[6-11]. Combining bioengineering tools and thorough characterization of the human stromal stem and progenitor cell populations have enabled the development of biomimetic constructs that, upon subcutaneous implantation in mice, can undergo the formation of functional humanized bone. Results have shown that these systems dramatically improve engraftment of healthy hematopoietic and leukemic cells[6] as well as prostate cancer metastatic cells[7], and shed light onto specific interactions among human stromal and human tumor cells involved in metastasis[12].

The microenvironment of the bone marrow niche plays a key role in balancing maintenance, proliferation and differentiation of its resident stem cells[13]. It follows, therefore, that 3D bioengineered scaffolds employed for its study play a paramount role in dictating specific behaviors of the encapsulated cells. Scaffolds tested to date include a myriad of natural 3D hydrogel matrices such as collagen[8,9], fibrin[10] or extracellular matrix (ECM)-based[6]. Even though natural materials are biocompatible and promote cell infiltration, their complex and variable compositions feature inherent bioactivity that is difficult to control. Synthetic analogues that permit systematic modifications of biophysical and biochemical properties have emerged as promising alternatives for the rational engineering of complex organs allowing uncoupled interrogation of specific biological processes[14,15].

Here we explore the use of a synthetic hydrogel based on poly(ethylene glycol) that is enzymatically crosslinked by transglutaminase factor XIII (referred to as TG-PEG[16,17]), as a well-defined 3D matrix for the development of a functional human bone marrow organoid. Playing on the substrate reactivity of FXIII, RGD peptides for cell adhesion or MMP-cleavable peptides for cell-mediated degradability can be modularly crosslinked into the hydrogel at precise concentrations independent

of the overall PEG concentration. This permitted systematic variation of hydrogel stiffness, degradability, and cell adhesion, which was exploited to engineer a provisional microenvironment with sufficient stability to support engraftment of human bone marrow-derived stromal cells (hBMSCs) and bone morphogenetic protein (BMP)-2 delivery. By titrating the seeding density and dose of hBMSCs and BMP-2 (resp.) within the constructs, we identified the optimal parameters to form robust and reproducible humanized bone marrow organoids in mice. The functionality of engineered humanized bone marrows was validated by studying the homing of systemically injected healthy hematopoietic stem and progenitor cells (hHSPCs). Ultimately, the functional bone marrows were employed to study the engraftment of leukemic cells and the metastasis of human breast cancer cells (Figure 1 a).

Results

Mechanically matched natural and synthetic hydrogels support bone and bone marrow formation

First, we sought to compare the efficiency of bone and bone marrow organoid induction between natural hydrogel materials (i.e. collagen, fibrin and ECM-like matrix referred to as ECMatrix) with that of TG-PEG. Since the mechanical properties of the microenvironment play such a critical role in directing stem cell behaviors, it was essential to determine the elastic moduli of the natural materials and then use a corresponding formulation of TG-PEG. Collagen, fibrin, and ECMatrix were all found to have stiffness between 30-50 Pa (Figure 1 b) as measured by rheology. Unlike the natural materials, the stiffness of TG-PEG hydrogels could be tuned easily by changing the polymer concentration (w/v). TG-PEG hydrogels of 0.9% (w/v) were found to have stiffness of 40.66 ± 15.86 Pa which was within the range of the natural materials. For formation of bony ossicles, hydrogels were prepared from each of the natural materials and for low stiffness TG-PEG, and each hydrogel was loaded with a high concentration of bone morphogenetic protein 2 (BMP-2, 50 ng μl^{-1}). Loaded hydrogels were then implanted subcutaneously in nude mice for eight weeks. Micro-computed tomography (microCT) confirmed the presence of bone organoids for all implanted hydrogels (Figure 1 c). However, the volume of the ossicles after eight weeks for all conditions was lower than the initial volume of the subcutaneous implants as seen by gross morphology and histological evaluations (Figure 1 c), indicating rapid remodeling of the materials *in vivo*.

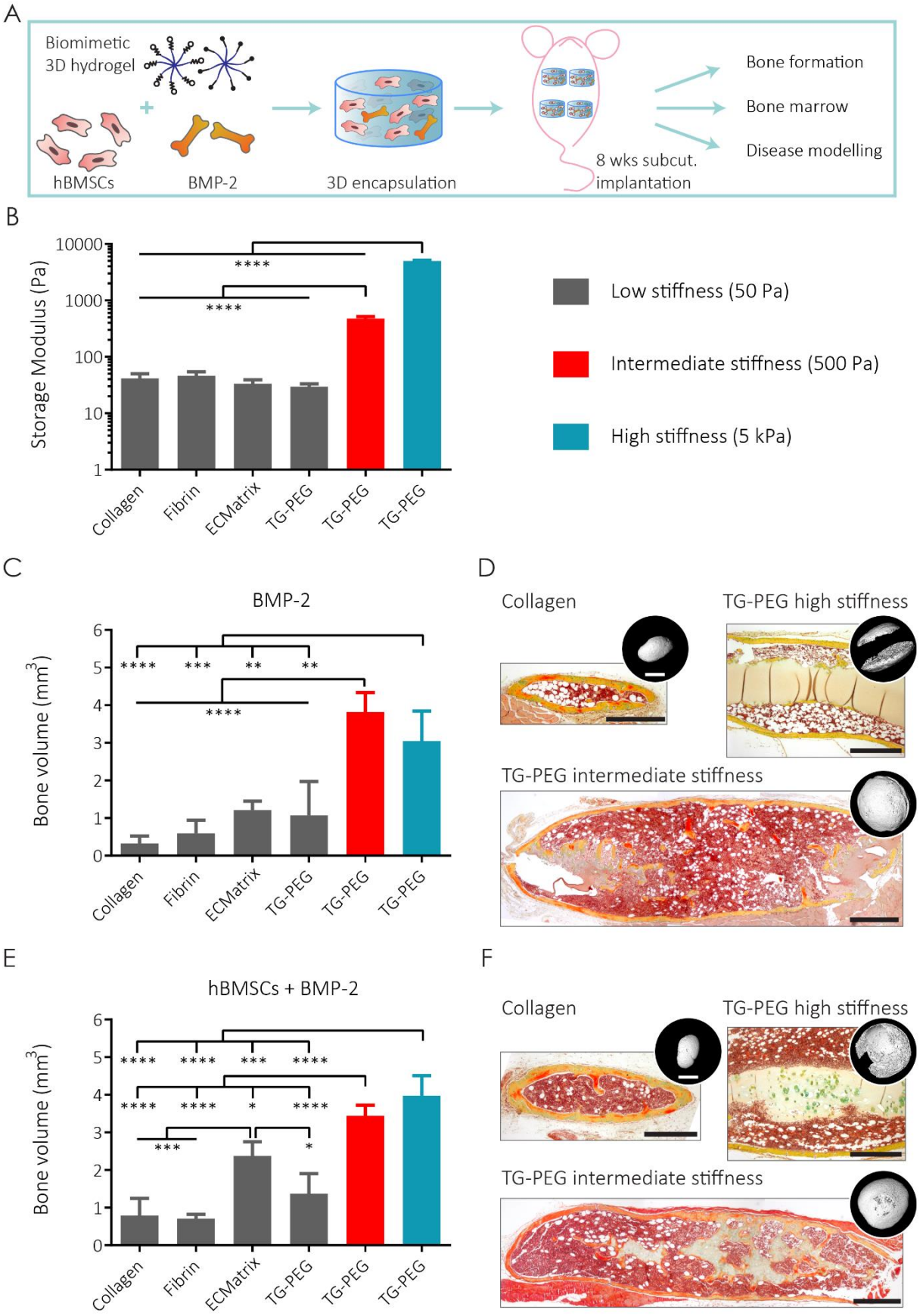

Figure 1. Bioengineered scaffolds as bone marrow models

(**a**) Experimental scheme. hBMSCs and/or osteogenic growth factor BMP-2 are combined in biomimetic 3D hydrogels before subcutaneous implantation in nude mice. This xenograft model allows the study of bone and bone marrow formation, and serves as disease modeling. (**b**) Storage moduli measured by *in situ* rheometry of different natural hydrogels including collagen, fibrin and ECMatrix, and synthetic TG-PEG hydrogels at different formulations (n = 3, graphic repeated in Chapter 3, Figure S1 a, for clarity). (**c** to **f**) Bone organoid formation in subcutaneous pouches of immunocompromised mice 8 weeks after implantation of differently formulated hydrogels comprising (**c** and **d**) BMP-2 only and (**d** and **e**) BMP-2 (12.5 ng μl^{-1}) and hBMSCs ($20{\cdot}10^6$ cells per ml of hydrogel). (**c** and **e**) MicroCT-based quantification of bone mineral content (n = 4) and (**d** and **f**) representative Movat's pentachrome stained histological sections (scale bars: 500 µm) with their corresponding microCT reconstructions (scale bars: 2 mm). All data are reported as mean ± standard deviation. ANOVA with Tukey's *post hoc* test * $P < 0.05$, ** $P < 0.01$, *** $P < 0.001$, **** $P < 0.0001$.

Engineered synthetic hydrogels with tuned stiffness outperform natural materials

We next reasoned that hydrogels with higher stiffness would confer *in vivo* stability and improve the formation of bone organoids. Therefore, TG-PEG hydrogels with intermediate (1.7% w/v; 478.52 ± 40.62 Pa) and high stiffness (5% w/v; 4995.59 ± 147.76 Pa) containing BMP-2 (50 ng μl^{-1}) were used as subcutaneous implants. MicroCT evaluations showed that maximum bone volume was achieved in intermediate stiffness TG-PEG hydrogels. Intermediate stiffness TG-PEG hydrogels exhibited significantly different bone volume (3.818 ± 0.520 mm^3) compared to all other low-stiffness hydrogels, and including a nearly 12-fold higher bone volume than collagen hydrogels (Figure 1 c). Interestingly, the stiffest hydrogels tested resulted in slightly lower bone volumes than the intermediate condition. Histologies corroborated these findings. Reduced ossicle size in the lower stiffness hydrogels was attributed to reabsorption of the hydrogel material by the host (Figure 1 d). For high stiffness conditions, on the other hand, histologies showed that bone formation primarily occurred at the outer perimeter of the implanted hydrogels, likely due to diffusion of BMP-2 from the loaded construct. Infiltration of host cells is critical for robust ossicle formation and seems to have been significantly impeded by high stiffness hydrogels.

Ossicle humanization would logically provide heightened clinical relevance to such models with intended utility in investigation of human malignancies. Towards that goal, we next studied how the introduction of hBMSCs to the hydrogels impacts ossicle formation. hBMSCs ($10{\cdot}10^6$ per ml hydrogel) were loaded together with BMP-2 for each natural and TG-PEG material as before. Bone volumes after eight weeks of subcutaneous implantation were similar to values observed without cells, with the exception of ECMatrix that significantly outperformed the other soft materials (Figure 1 e). Histological evaluations revealed that collagen and fibrin gels were substantially reabsorbed (Figure 1 f). Though bone volumes were again comparable between high and intermediate stiffness TG-PEG hydrogels, histologies revealed that remodeling of high stiffness gels into robust bone marrow tissue was limited and again occurred only in the outer perimeter. Intermediate stiffness TG-PEG hydrogels of 500 Pa provided the optimal conditions for concomitantly preserving bone volume while permitting recruitment of host cells and, ultimately, robust self-organization into bone marrow-like tissue. This was true for both conditions, with or

without cells, and makes the intermediate TG-PEG hydrogels a superior choice for ossicle formation over previously described natural materials.

Specific interactions with the ECM are well known to regulate cell behaviors[18]. To determine their role in bone and bone marrow development, we investigated the impact upon omission of cell-ECM adhesion or MMP-specific degradability in intermediate stiffness TG-PEG matrices. Importantly, storage moduli were not affected by either exclusion from the TG-PEG matrices (Figure S1 a). Absence of RGD cell binding sites did not impact bone volumes of hydrogels regardless of whether hBMSCs were present (Figure S1 b, c). MMP-specific degradability of the gels, on the other hand, was shown to play a key role in bone organoid development. When non-degradable gels containing RGD were implanted without hBMSCs, they resulted in bone volumes of 0.792 ± 0.857 mm^3 (Figure S1 b), significantly lower than their degradable counterparts. Histologies clearly pointed to the inability of host cells to infiltrate and populate the marrow compartment in non-degradable hydrogels (Figure S1 d). Conversely, if hBMSCs were encapsulated in non-degradable gels, then higher bone volumes were achieved reaching 6.618 ± 1.446 mm^3 (Figure S1 c). H&E displayed that non-degradable constructs resulted in formation of a cortical bone shell around the implants enclosing a marrow adjacent to the hydrogels (Figure S1 d). This indicates that murine cells were not able to penetrate the non-degradable hydrogels but the diffusion of BMP-2, and likely hBMSC paracrine signaling, did induce recruitment of murine cells to the hydrogel surrounding. Thus, murine cells developed the cortical bone, while hBMSCs underwent calcification within the hydrogels (Figure S1 e). These data highlight the necessity of proteolytic degradable sites within the scaffolds to form a complete ossicle with human cells supporting host hematopoietic marrow derived from host cell recruitment. Thus, TG-PEG matrices of an intermediate stiffness containing RGD and MMP-sensitive degradable sites were established as minimal environments for bone organoid formation.

Bone marrow organoid formation is tuned by molecular and cellular contributions

In previous studies involving hydrogels and ossicle formation, a high concentration of BMP-2 has always been used (> 0.5 ng μl^{-1})[7,8,11]. The use of such high BMP-2 doses, however, may mask the role of co-implanted cells preventing elucidation of their contribution to ossicle formation. Thus, building upon the optimized microenvironmental parameters presented earlier, we sought to identify the optimal BMP-2 dose to accompany delivery of hBMSCs.

To address this issue, we compared TG-PEG hydrogels with or without hBMSCs ($20 \cdot 10^6$ per ml of hydrogel) at different BMP-2 concentrations ranging from 100 to 6.25 ng µl-1. Eight weeks after subcutaneous implantation we evaluated bone volume formation by microCT. As expected, higher amounts of BMP-2 induced higher bone volumes (Figure 2 a). Below the threshold BMP-2 concentration of 12.5 ng μl^{-1} and in the absence of hBMSCs, bone formation did not occur (Figure 2 a, b). Strikingly, however, the presence of hBMSCs was sufficient to overcome this and induce development of bony ossicles at lower BMP-2 concentrations. These results speak to the paramount role of hBMSCs in the formation of the bone organoids, and confirms that use of high

BMP-2 doses makes it nearly impossible to discern contributions of the growth factor from those of the delivered cells. To validate the hypothesis that bone formation was cell-dependent, a titration of hBMSC seeding densities was evaluated at a fixed low dose of BMP-2. Below $0.5 \cdot 10^6$ hBMSCs per ml of hydrogel, ossicles did not form (Figure 2 c). The capacity of hBMSCs to form bone *in vivo* under low BMP-2 conditions was corroborated for several hBMSC donors (Figure 2 d). And lastly, primary fibroblast cells served as a negative control where no bone formation was seen.

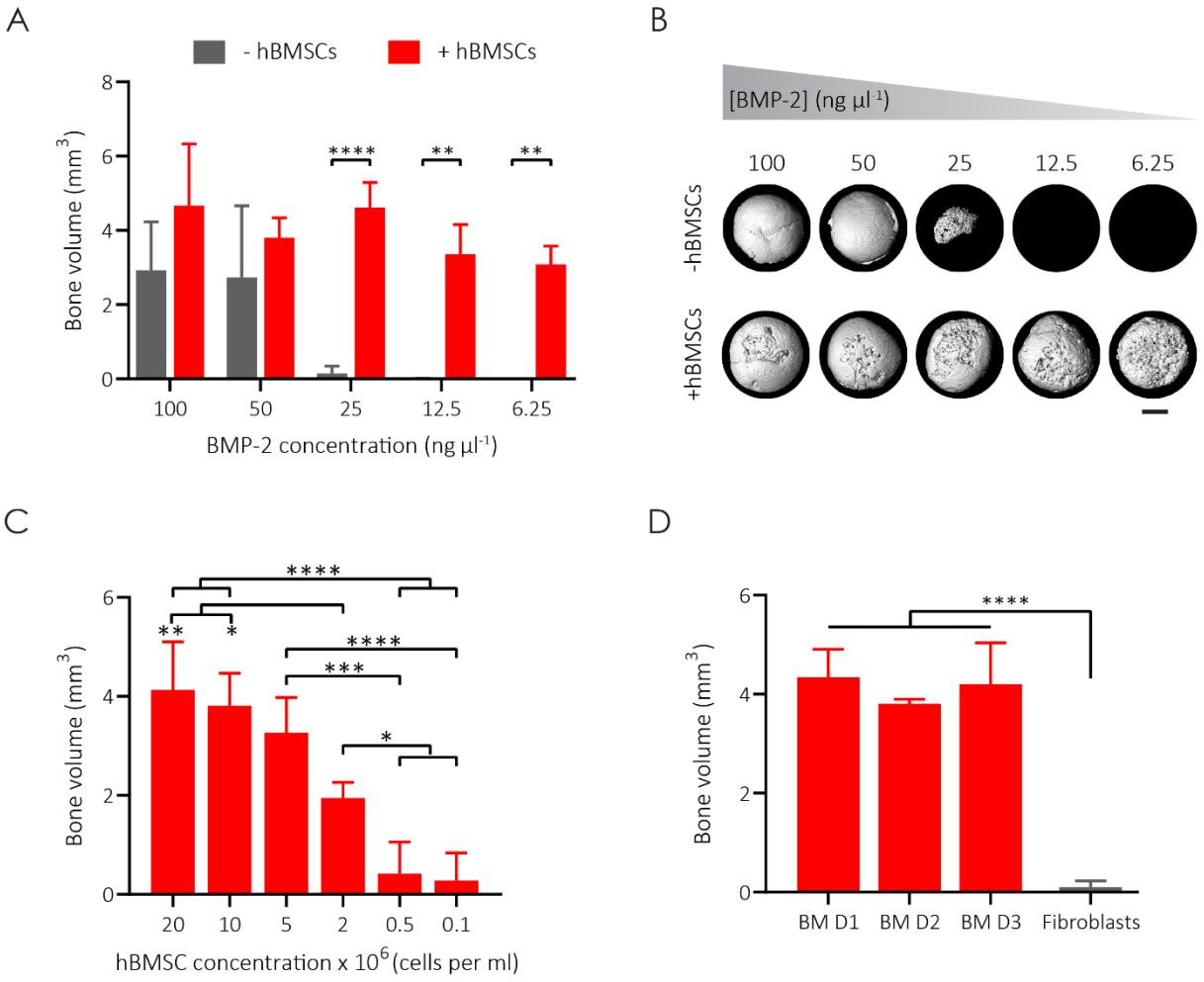

Figure 2. Molecular and cellular contributions to bone marrow organoid formation

(**a**) MicroCT quantification of bone volume formation when different BMP-2 concentrations are incorporated in optimized TG-PEG systems in absence or presence of hBMSCs ($20 \cdot 10^6$ cells per ml of hydrogel) (n = 4). (**b**) Representative microCT reconstructions of ossicles 8 weeks post-implantation with decreasing BMP-2 concentrations with or without hBMSCs (scale bar: 2 mm). (**c**) Bone volumes of varying hBMSC cell concentrations at fix BMP-2 concentration (low, 12.5 ng μl^{-1}) (n = 4). (**d**) Bone volumes of different donors at $20 \cdot 10^6$ cells per ml of hydrogel containing low BMP-2 concentrations, human fibroblasts were used as controls (n = 4). All data are reported as mean ± standard deviation. ANOVA with Tukey's *post hoc* test * $P < 0.05$, ** $P < 0.01$, *** $P < 0.001$, **** $P < 0.0001$.

The system's versatility was further tested for use in comparing different growth factors known to impact stem cell behaviors. Growth factors involved in either proliferation or migration have been linked controversially to hBMSC bone formation[19,20]. Here, we encapsulated hBMSCs with either fibroblast growth factor-2 (FGF-2) or platelet-derived growth factor BB (PDGF-BB). After eight weeks of subcutaneous implantation we found that presence of either growth factor resulted in inhibited bone formation as seen via microCT (Figure S2 a), despite the persistence of human cells throughout the incubation period (Figure S2 b). Thus, in the presented approach hBMSC osteogenic differentiation capacity seems to necessitate presence of osteogenic factors in low amounts whereas proliferative stimuli are insufficient. Taken all together, starting from a non-inductive and chemically-defined 3D biomaterial, we can customize bone organoids on demand by seamlessly altering microenvironmental parameters, supplementation of growth factors, and cell-specific contributions.

hBMSCs undergo endochondral ossification and are found in the hematopoietic bone marrow niche

To gain further insight into the manner which hBMSC-laden hydrogels undergo ossification, we evaluated ossicle development longitudinally at 1, 2, 4, and 8 weeks post-implantation via histological analysis. Movat's Pentachrome staining revealed high ECM turnover from glycosaminoglycans to collagenous structures during the first weeks after implantation (Figure 3 a). This remodeling was accompanied of bone formation as seen by microCT. Specifically, hBMSCs adapted morphologies characteristic of chondrocyte-like cells during week 1 and 2 post-transplantation (Figure 3 b). Furthermore, active participation of hBMSCs in ECM remodeling was verified by human-specific staining of collagen type I deposition (Figure 3 c). Abundance of collagen type II at week 4 implicates endochondral ossification as the mode of bone formation by these human cells. By week 8, bone and bone marrow organoids contained cortical and trabecular bone appearing well supported and richly vascularized (Figure 3 d). The onset of the HSC niche was at week 4, when host-derived murine hematopoietic stem and progenitor cells (Lin^- c-Kit^+ $Sca\text{-}1^+$) started infiltrating the ossicles evolving into a full bone marrow by week 8 (Figure 3 e).

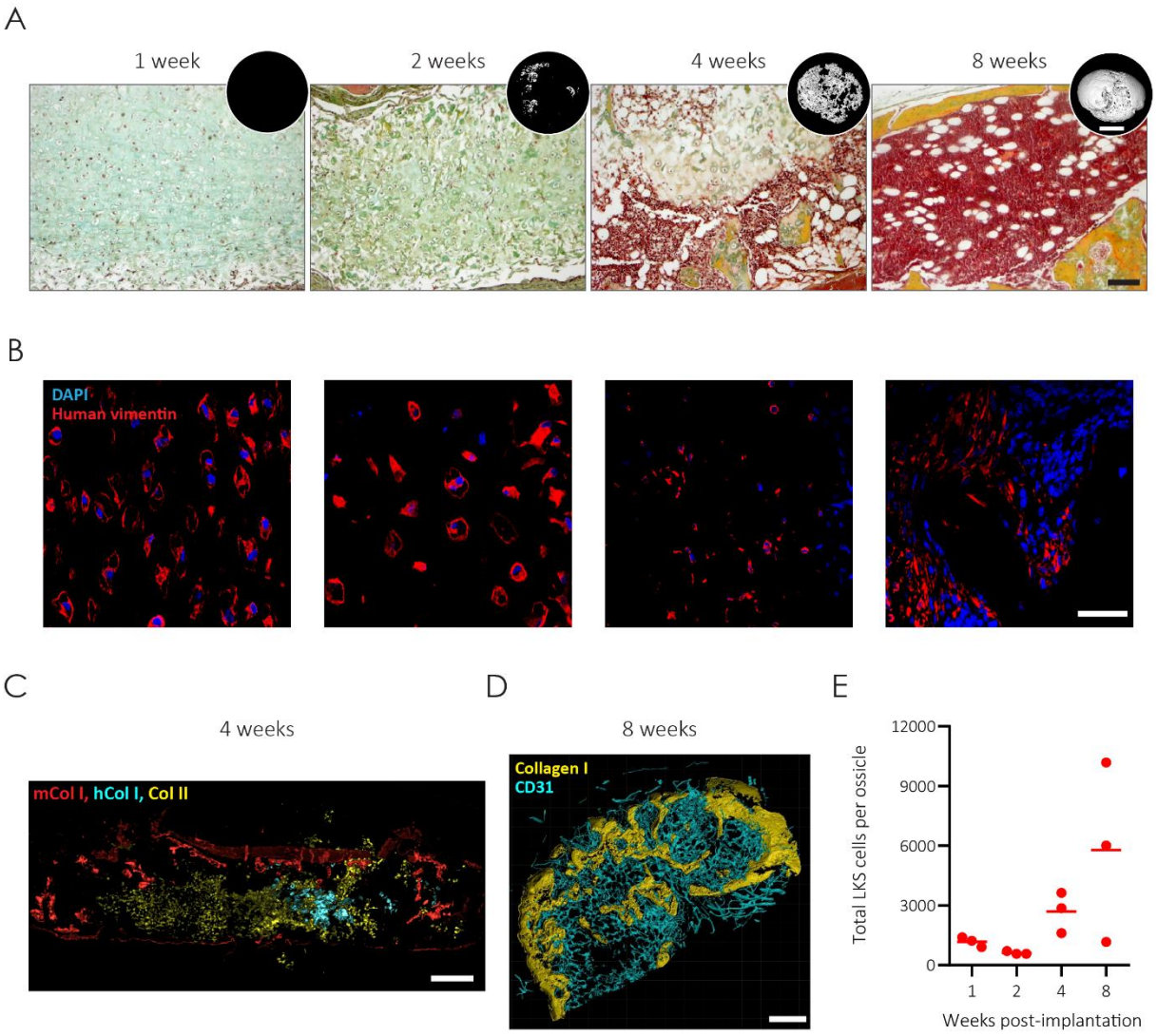

Figure 3. Humanized bone marrow organoid *in vivo* formation

Longitudinal evaluation of bone organoid formation after the subcutaneous implantation of TG-PEG hydrogels comprising BMP-2 (12.5 ng μl^{-1}) and hBMSCs ($20{\cdot}10^6$ cells per ml) into immunocompromised mice. (**a**) Representative Movat's pentachrome stained histological sections revealed high ECM turnover from glycosaminoglycans to collagenous structures during the first weeks of implantation, and the development of a rich bone marrow by week 8 post-implantation (scale bar: 100 µm). MicroCT reconstructions showed that remodeling was accompanied of calcium deposition first from trabecular areas, and last at 8 weeks forming cortical bone (scale bar: 2 mm). (**b**) Zoomed images from indicated regions in (a). Specific human vimentin staining showed that in early weeks post-implantation hBMSCs acquired a chondrocyte-like morphology, while later they were found in bone lining structures (scale bar: 50 µm). (**c**) Superimposed projections of collagen specific stainings for murine type I (red), human type I (cyan) and type II (yellow), show active hBMSC participation in ECM-deposition and remodeling (scale bar: 500 µm). (**d**) Ossicles were ossified and highly vascularized at 8 weeks (scale bar: 1 mm). Vascular structures stained by CD31 in cyan, and ECM collagen I in yellow. (**e**) Total number of murine hematopoietic stem and progenitor cells (immunophenotypically defined as LKS, Lin^- $c\text{-}Kit^+$ $Sca\text{-}1^+$) recruited in implants at different times post-implantation (n = 3, mean plotted).

In vivo engineered organoids sustain a humanized bone marrow niche

The next step in building complexity into the system was to investigate whether these bone organoids could also recruit and maintain a humanized hematopoietic system. To do so, hematopoietic stem and progenitor cells were sorted based on $CD34^+$ expression from human umbilical cord blood (cbHSPCs), and subsequently injected into sublethally irradiated NSG mice that were carrying hBMSC-containing ossicles (Figure 4 a). We first corroborated that these hBMSC-laden constructs could still undergo ossification in this mouse strain as previously observed in nude mice. Bone volume evaluations by microCT and histological analysis revealed that hBMSCs with low BMP-2 amounts could develop into bony structures over 8 weeks of implantation, while samples lacking cells did not elicit any bone formation (Figure 4 b). Eight weeks after scaffold implantation and ossicle development, cbHSPCs ($0.6 \cdot 10^6$ cells per animal) were systemically injected. cbHSPC phenotype prior to implantation was confirmed by their *in vitro* differentiation capacity in CFU assays (Figure S3 a). We then monitored hematopoietic humanization by analyzing the number of human $CD45^+$ cells found in the mouse blood over time by flow cytometry (Figure S3 b). Humanization reached a level of 80% at 16 weeks post-$CD34^+$ cell transplantation, in keeping with earlier reports[6]. Mice were sacrificed and it was confirmed that other organs such as murine bone marrow, spleen, liver and thymus were also highly humanized as indicated by flow cytometry and histological analysis (Figure S3 c). Further phenotypical analysis of the $hCD45^+$ cells found in the different organs confirmed that human hematopoietic cells were able to undergo commitment into the different lineages *in vivo* substantiating that the mice had a functional human hematopoietic system (Figure S3 d). Specific immunostainings for $hCD34^+$ cells within hBMSC induced-ossicles highlighted the recruitment of hHSPCs to the newly formed bone marrow (Figure 4 c). Co-localization with human vimentin showed that hBMSCs were present in the humanized marrow lining in the trabecular areas. The recruitment and subsequent maintenance of human hematopoietic cells in these hBMSC-induced ossicles indicates the formation of a functional humanized bone marrow.

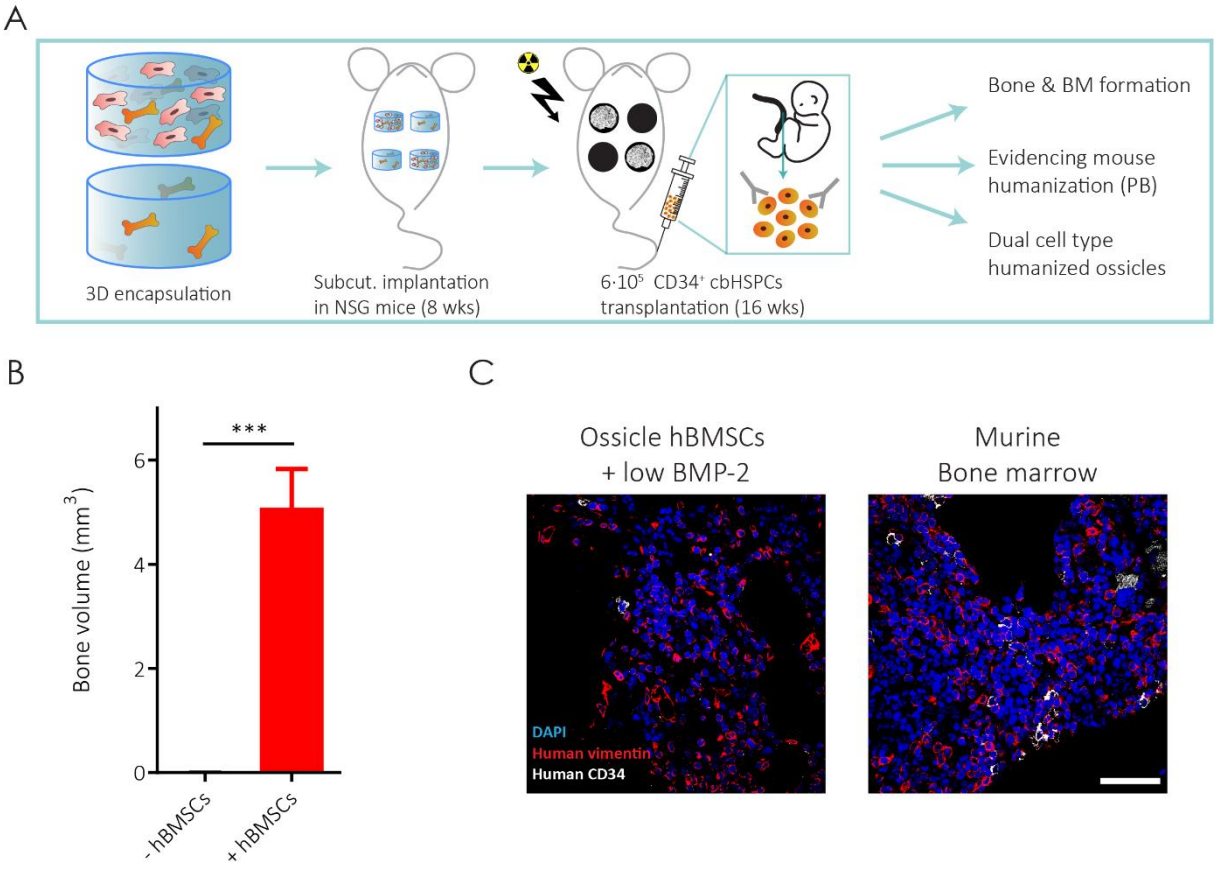

Figure 4. Bone marrow organoids as pillars of a human hematopoietic niche

(**a**) Schematics of the workflow. TG-PEG hydrogels containing hBMSCs and low amounts of BMP-2, or control gels without cells, were implanted in NSG mice to allow ossicle formation for 8 weeks. Next, human hematopoietic stem/progenitor cells (cbHSPCs) were systemically disseminated via tail vein injection. (**b**) Bone volume of ossicles 8 weeks post-scaffold implantation (n = 3). All data are reported as mean ± standard deviation. Unpaired *t*-test *** $P < 0.001$. (**c**) Histological evaluations revealed the presence of CD34⁺ hHSPCs in the marrow of hBMSC-induced ossicles as well as in murine BM counterparts (scale bar: 50 µm). Nuclei were stained by DAPI, human cells stained by human-specific vimentin in red, and human CD34 cells in white.

Human leukemia cells engrafted in synthetic bone organoids

We next proceeded to employ this robust system as a model to study leukemic cell dissemination in the bone marrow. Hydrogels containing hBMSCs and low BMP-2 were subcutaneously implanted for 8 weeks in NSG mice to allow ossicle formation. Control hydrogels without cells were used to corroborate that the BMP-2 could not *per se* elicit leukemic cell recruitment. Then, acute B lymphoblastic leukemia (B-ALL) patient derived cells transduced with Luc-GFP were systemically injected ($1 \cdot 10^6$ cells per animal), and their dissemination was monitored over time by bioluminescence tracking (Figure 5 a). Peculiarly, leukemic cells appeared specifically and exclusively in humanized ossicles at 7 days post-transplantation, corroborating that leukemic cell recruitment was not induced by the loaded BMP-2 (Figure 5 b). By day 16 leukemic cells had spread in tissues throughout the mice including the femur and spine and, thus, the experiment was

terminated. Ossicles were excised and bioluminescence was quantified showing that hBMSC-induced ossicles had significantly higher leukemic cell engraftment than ossicles without cells (Figure 5 c). Ultimately, leukemic cells were found to grow within the ossicles as clusters in trabecular areas, whilst hBMSCs remained in cortical regions (Figure 5 d). Follow-up studies are under way to elucidate the dependency of this effect on deposition of human-specific ECM within the ossicles.

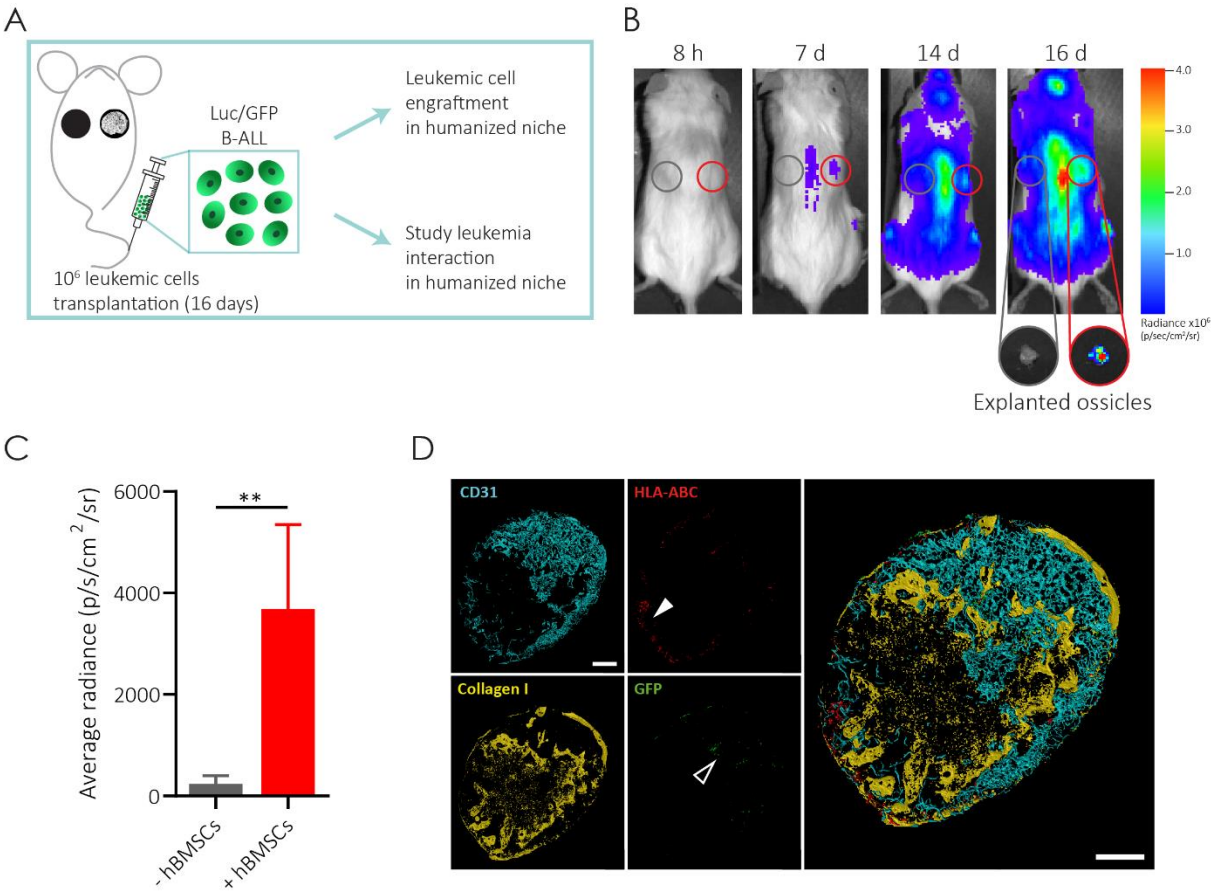

Figure 5. Leukemic cancer model

(**a**) Scheme of the experimental workflow. Optimized TG-PEG hydrogels laden with hBMSCs and low BMP-2 concentrations, or control gels without cells, were implanted in NSG mice. 8 weeks after ossicle formation, B-ALL leukemic cells (10^6 cells per mouse), containing Luc/GFP constructs, were intravenously injected. This model enables the study of leukemic cell engraftment and evaluation of tumor and stroma cell interactions. (**b**) Leukemic cell engraftment was monitored by *in vivo* bioluminescence imaging at different time points after cell transplantation. Representative mouse with increasing BLI signal over time. (**c**) At endpoint, 16 days post-leukemic cell delivery, ossicles were retrieved and average radiance was measured (n = 4). All data are reported as mean ± standard deviation. Unpaired *t*-test ** $P < 0.01$. (**d**) Histological evaluations of ossicles containing hBMSCs and leukemic cells showed that while hBMSCs were found lining in the cortical area of the ossicles (filled white arrow), leukemic cells were mostly in trabecular areas forming distinct cell lusters (hollow white arrow). Ossicles were highly vascularized and contained fully developed bone and bone marrow structures (scale bars: 1 mm). Vascular structures stained by CD31 in cyan, human cells stained by HLA-ABC in red, ECM collagen I in yellow and GFP^+ leukemic cells in green.

Human breast cancer cells metastasize preferentially at early stages of bone formation

While leukemia is a bone marrow-specific cancer, we also sought to evaluate the *in vivo* human bone organoids as potential models for studying osteotropic metastasis of breast cancer cells. As before, TG-PEG hydrogels containing hBMSCs and BMP-2 were implanted subcutaneously in nude mice. To mimic cancer progression in different stages of bone development, human breast cancer cells (MDA-MB-231) were systemically injected at 2, 4 or, 8 weeks post-ossicle implantation (Figure 6 a). Using bioluminescent imaging, cell dissemination to the humanized ossicles could be tracked longitudinally. Strikingly, cancer cell engraftment and progression were more pronounced in ossicles undergoing morphological changes (i.e. early stage), rather than fully-developed ones (Figure 6 b).

Next, to rule out that human cancer cells metastasize to the remodeling bone with higher preference than mature bone simply due to higher vascularization and, therefore, more general exposure to circulating cells during early-stage ossicle formation, we performed intraossicle injections at the same time points. Similarly, cancer cells engrafted better and grew more rapidly in ossicles at early-stage of bone formation compared to after 8 weeks (Figure 6 c). Ultimately, endpoint evaluations of bone volumes formed in the constructs showed a significant reduction in bone volume for ossicles challenged with breast cancer cells at 2 weeks (Figure 6 d). This could be due to the fact that these samples were evaluated at an overall earlier time point as the amount of time between cancer cell injection and ossicle excision was kept constant. However, the lower bone volume in ossicles that received intraossicle injections, compared to those where cancer cells were injected systemically indicate a likely direct correlation between higher cancer cell flux and lower bone volume, especially when comparing the 2-week timepoint for each group. Follow-up histological evaluations are currently in progress to assess this further.

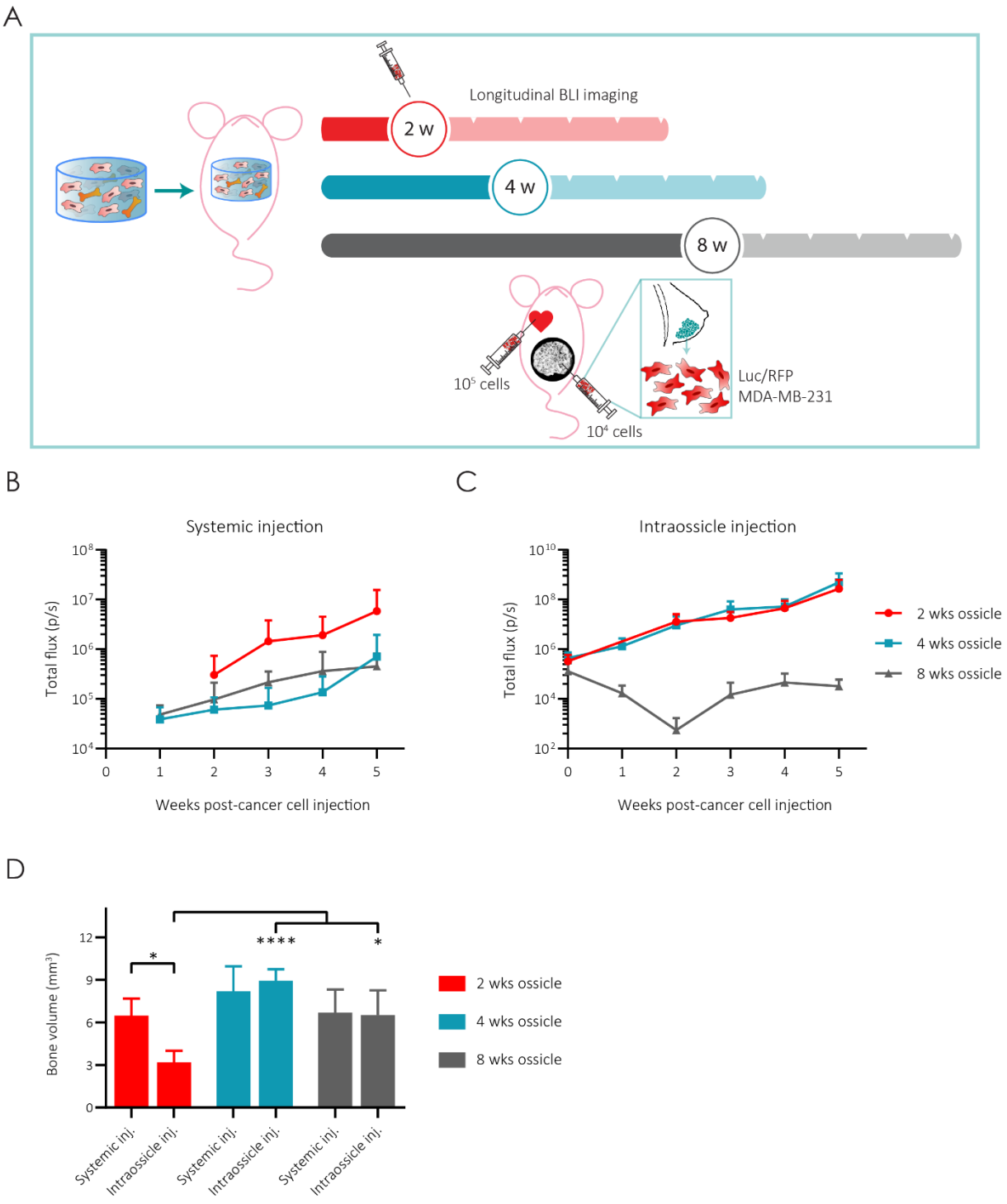

Figure 6. Bone metastasis cancer model

(**a**) Scheme of the experimental workflow. Optimized TG-PEG hydrogels laden with hBMSCs and low BMP-2 concentrations were subcutaneously implanted in nude mice. 2, 4 or 8 weeks after hydrogel implantation, MDA-MB-231 breast cancer cells, containing the Luc/RFP constructs, were injected in those mice, either systemically by intracardiac injection (10^5 cells per mouse), or intraossicle (10^4 cells per mouse). Longitudinal bioluminescence imaging (BLI) was performed. (**b-c**) Longitudinal evaluation of total BLI flux detected in the ossicles over the course of 5 weeks post-cancer cell delivery, for (**b**) systemic and (**c**) intraossicle injections. (**d**) Bone volume was measured by microCT evaluations at endpoint, 5 weeks post-cancer cell injection (n = 4 for 2 wks ossicle, and n = 5 for 4 and 8 wks ossicles). All data are reported as mean ± standard deviation. ANOVA with Tukey's *post hoc* test * $P < 0.05$, **** $P < 0.0001$.

Discussion

We report for the first time, to our knowledge, the use of a fully synthetic matrix for the humanization of a functional bone marrow model with application in cancer modelling. Notably, the modularity of TG-PEG facilitates uncoupling of key parameters for systematically assessing their contribution to the formation of bone marrow organoids *in vivo*. This permits fine-tuning and optimization of scaffold design at a resolution not possible with other materials. Additionally, we have provided thorough evidence that hBMSCs encapsulated in optimized TG-PEG hydrogels participate in robust remodeling and ECM deposition leading to production of bone-marrow like structures. Ultimately its use as a model for osteotropic leukemia and breast cancer metastasis rendered the system particularly suited for exploring whether cancer cells preferentially engraft at a particular stage during ossification and bone development. Taken all together, this sophisticated yet simplistic humanized bone organoid holds tremendous promise to mimic the bone marrow niche in health and pathology, and may help to unmask the factors involved in osteotropic metastasis of various cancers in a clinically-relevant *in vivo* setting that captures human physiology.

Conventional murine models are fraught with limitations from species incompatibility of tested compounds or just significant interspecies differences, as well as difficulty to isolate individual study parameters[21]. Xenografts models have emerged as promising alternatives to combine a native microenvironment provided by the host with the addition of human cells and other factors to study in a humanized *in vivo* environment.[6-8] In parallel, to understand cooperative effects in the bone marrow microenvironment, we need to have control over these single parameters[22]. This is accomplished here via a bottom-up approach that allows controllable modulation of the local microenvironment through the use of intrinsic materials properties. These include stiffness and degradability, biologically active moieties such as growth factor delivery or presentation of ligands and cell-adhesion sites, and a great deal of versatility regarding cell type. Remarkably, in this study we showed that primary hBMSCs with low BMP-2 amounts can form robust bone marrow organoids in TG-PEG hydrogels, which represent a blank-slate in terms of ECM proteins or other endogenous signaling factors. The possibility to reduce the BMP-2 concentration to the low dose achieved here without sacrificing bone formation is of paramount importance. High doses of growth factors as used routinely until now[8,23] not only are potentially harmful in a clinical setting[24], but additionally can mask the very biological processes that our studies are aimed at interrogating.

The relative ease of manipulation (i.e. no need of pre-differentiation of the stromal cells for long culture periods unlike previous studies[9,11]), batch-to-batch reproducibility, and animal-free nature of components makes the presented system especially attractive for utility in on-demand patient-xenograft models. We envision that stromal, endothelial, hematopoietic and tumor cells from a single donor could be combined to assess the effect of potential drugs in tumor suppression, mitigation of metastasis, and even interaction/activation of the immune system.

Due to the dynamic development of the presented human bone organoids into a full bone over the course of 8 weeks in mouse, we could closely recapitulate different stages of bone development, healing and remodeling. Our results confirm that osteotropic metastasis occurs more efficiently in developing bone than in mature bone. These findings could explain reported observations that bone metastasis is often associated with bone injuries or osteoporosis, situations in which bone is undergoing remodeling and therefore more vulnerable to tumor cell engraftment[25,26].

Collectively, this intricate xenograft model featuring humanized bone microenvironments and human tumor cells has potential to be a powerful tool for studying osteotropic metastasis. It can be utilized to study the molecular cargo that may be involved in homing cancer cells to bone[27], priming the pre-metastatic site for secondary lesions[28], and mapping out morphological changes in the bone microenvironment that contribute to disease progression[29]. Furthermore, it may prove valuable as preclinical tool for screening novel therapeutics that combat metastatic processes allowing for earlier intervention and vastly improved patient outcomes.

Outlook

Humanized bone marrow organoids served as a fundamental niche tool to study processes that no other current approaches, neither *in vitro* nor murine models, could have assessed. Yet some questions remain unanswered. Are there physical interactions among the hBMSCs and the human cancer cells? Do the cancer cells engraft in a particular region (endosteal, perivascular, stromal) of those bone marrow organoids? Are the cancerous lesions involved in the bone loss? Does the human-specific ECM deposited by encapsulated hBMSCs play a key role in allowing or facilitating metastasis? To answer these questions, further evaluation is currently underway of the herein harvested ossicles to determine whether there are interactions between human stromal and cancer cells, and to assess in more detail where cancer cells home within the ossicles (i.e. endosteal, perivascular or stromal areas). To do so, we are collaborating with the group of Prof. Schroeder (ETH Zürich) that has recently established a 3D imaging technology optimized for imaging and quantification of bone marrow sections[30,31].

Acknowledgements

We would like to deeply thank Dr. Christopher Millan (University of Zürich) for his valuable feedback and help in editing the manuscript; Esther Kleiner (University Hospital Zürich) for technical assistance in histological analysis and $CD34^+$ cells isolation; Flora Nicholls (University of Zürich) for animal care; Dr. Paolo Cinelli (University of Zürich) for support with micro-CT; Tabea Leonie Stephan (University Hospital Zürich) for collagen staining overlays; Dr. Norman Russkamp

(University Hospital Zürich) for BLI imaging support; Prof. Marcy Zenobi-Wong and Dr. Nicolas Broguière (ETH Zürich) for support with rheological measurements; Prof. Ivan Martin (University Hospital of Basel) for isolation of BMSCs. This work has been supported by the Swiss National Science Foundation (CR33I3_153316/1), and the Center for Clinical Research, University Hospital Zürich and University of Zürich.

Experimental procedures

All chemicals and materials were purchased from Sigma Aldrich or Thermo Fisher Scientific unless otherwise specified.

Human cell isolation and culture expansion. Human bone marrow-derived stromal cells (hBMSC) were isolated as previously described[32] from bone marrow aspirates of healthy donors (n = 3) obtained during orthopedic surgical procedures after informed consent and in accordance with the local ethical committee (University Hospital Basel; Prof. Dr. Kummer; approval date 26/03/2007 Ref Number 78/07). Cells were cultured at 37 °C in a humidified atmosphere at 5% CO_2 in minimum essential medium alpha (MEMα, with nucleosides, Gibco) supplemented with fetal bovine serum (FBS, 10%, Gibco), penicillin (100 U ml^{-1}, Gibco), streptomycin (100 µg ml^{-1}, Gibco), and fibroblast growth factor-2 (FGF-2, 5 ng ml^{-1}, PeproTech). Cells were passaged before reaching 90% confluency, and medium was changed every 2-3 days.

TG-PEG precursors synthesis and preparation. TG-PEG precursors were synthesized as previously described[16,17]. Briefly, 8-arm PEG-VS (PEG-vinylsulfone, 40 kDa MW; NOF) was functionalized with peptides (obtained with a purity of > 95% from Bachem AG) that contained an earlier described cysteine cassette (ERCG) optimized for its reaction with PEG-VS and either a factor XIII (FXIII) glutamine acceptor substrate sequence (Gln; H-NQEQVSPL-ERCG-NH_2) or a matrix metalloproteinase-degradable (*in italics*) lysine donor substrate ($MMP_{sensitive}$-Lys; Ac-FKGG-*GPQGIWGQ*-ERCG-NH_2), or instead a non-degradable lysine donor substrate (ND-Lys; Ac-FKGG-GDQGIAGF-ERCG-NH_2) for non-degradable TG-PEG gels. A 1.2 molar excess of peptides over PEG-VS was reacted in triethanolamine (TEA) at pH 8.0 for 2 h at 37 °C. Resulting 8-PEG-Gln and 8-PEG-$MMP_{sensitive}$-Lys or 8-PEG-ND-Lys precursors were excessively dialyzed against pure water, lyophilized and stored at -20 °C until further use. The crosslinking enzyme, transglutaminase FXIII (200 U ml^{-1}, Fibrogammin P, CSL Behring), was activated with thrombin (2 U ml^{-1}) for 30 min at 37 °C and stored in small aliquots at −80 °C until use.

3D biomimetic hydrogels. When needed, cells were trypsinized and resuspended in 10% FBS/MEMα in the desired concentration and mix in the corresponding precursor mixes.

3D TG-PEG hydrogel formation. Stoichiometrically balanced solutions of 8-arm PEG-Gln and 8-arm PEG-$MMP_{sensitive}$-Lys, or 8-arm PEG-Gln and 8-arm PEG-ND-Lys for non-degradable gels were prepared in Tris buffer (50 mM, pH 7.6) containing calcium chloride ($CaCl_2$, 50 mM), as previously described[16]. Additionally when stated, 50 µM Lys-RGD peptide (Ac-FKGG-RGDSPG-NH_2), indicated amounts of cells and BMP-2 (produced as previously described[33]) were added to the precursor solution. Subsequently, hydrogel crosslinking of final dry mass content of 0.9% (corresponding to low stiffness), 1.7% (for intermediate stiffness) or 5% (for high stiffness) (w/v) was initiated by the addition of 10 U ml^{-1} of activated transglutaminase factor XIII, followed by vigorous mixing. Disc-shaped matrices were prepared between hydrophobic glass slides (treated

with SigmaCote), and incubated for 30 min at 37 °C in a humidified atmosphere at 5% CO_2. After completed polymerization, hydrogels were released from glass slides and transferred to tissue-culture plates for *in vitro* experiments or stored in a humidified atmosphere for immediate *in vivo* implantation.

Natural matrices. BMP-2 (50 ng μl^{-1}) and/or hBMSCs ($10 \cdot 10^6$ cells per ml of hydrogel) were mixed in cold solutions of 3 mg ml^{-1} of collagen (PureCol EZ Gel solution, Sigma) or ECM-like matrix (referred as ECMatrix in the text, ECM625, Merck Millipore) following manufacturer's instructions. For fibrin gels as previously described [34], growth factor and/or cells were added to a solution of 4 mg ml^{-1} of fibrinogen containing 2.5 mM $CaCl_2$. Next, FXIII (2 U ml^{-1}) and thrombin (2 U ml^{-1}) were incorporated to begin hydrogel crosslinking. Cell-laden hydrogels were then incubated for 30 min at 37 °C to enable complete polymerization prior to immediate (within 2 hours) *in vivo* implantation.

Hydrogel stiffness characterization by *in situ* rheometry. Hydrogel gelation was analyzed on a rheometer (MCR 301, Anton Paar) equipped with 20 mm plate–plate geometry (PP20, Anton Paar) at 37 °C in a humidified atmosphere. Gel mixtures were precisely loaded onto the center of the bottom plate. The upper plate was lowered to a measuring gap size of 0.2 mm, ensuring proper loading of the space between the plates and gel precursors, the dynamic oscillating measurement was then started. The evolution of storage modulus (G') and loss modulus (G") at a constant angular frequency of 1 Hz and constant shear strain of 4% was recorded for 30 min when equilibrium was reached.

Animal care. All animal procedures were approved by the veterinary offices of the Swiss cantons Zürich and Lausanne under the ethical license (Application No. ZH169/2015). Experiments and handling of mice were conducted in accordance with the Swiss law of animal protection. 6-8-week-old immunodeficient HsdCpb:NMRI-*Foxn1*^{nu} (nude) female mice (purchased from Envigo) or NOD.Cg-*Prkdc*^{scid}*Il2rg*^{tm1Wjl}/SzJ (NSG) female mice (purchased from The Jackson Laboratory) were used for the followed experiments.

Subdermal implantation of humanized hydrogels in mice. For establishment experiments, 18 µl gelled scaffolds containing growth factors and/or cells were subsequently implanted into 4 subcutaneous pockets of nude or NSG mice. For leukemic and metastasis experiments, 30 µl gelled scaffolds containing optimized conditions, intermediate stiffness TG-PEG with hBMSCs ($20 \cdot 10^6$ cells per ml of hydrogel) supplemented with low amounts of BMP-2 (12.5 ng µl) and control gels (with only low amounts of BMP-2) were implanted. Ossicles were retrieved after 1, 2, 4 or 8 weeks post-OP, unless otherwise stated.

Hematopoietic xenotransplantation. Primary human $CD34^+$ cells were isolated from umbilical cord blood collected from healthy donors at the University Hospital Zürich after obtaining informed consent. The study was approved by the ethics board of the canton Zürich, Switzerland (approval date 21/03/2007; Ref Number 07/07). Blood (typically between 30-70 ml)

was subsequently centrifuged to enrich for mononuclear cells, which were in turn further magnetically sorted for $CD34^+$ cells using positive immunomagnetic selection ($CD34^+$ MicroBead Kit, Miltenyi Biotec) according to the manufacturer's instructions obtaining a >80% $CD34^+$ cells. Cells were directly frozen down until use. Upon NSG transplantation, cells (containing CD34 81.41 %, CD3 2.17%, CD19 16.17%, Lin^- $CD34^+$ $CD38^-$ 58.28% and Lin^- $CD34^+$ $CD38^-$ $CD45RA^-$ $CD90^+$ 10.83%) were thawed in 50% IMDM 50% FBS, centrifuged 5 min at 300 g and subsequently resuspended in phosphate buffer saline (PBS). Then, NSG mice that had 8 weeks before received a subcutaneous implantation of hBMSCs laden TG-PEG scaffolds were sub-lethally irradiated (1x, 200 cGy) 4 hours prior receiving $0.6 \cdot 10^6$ human $CD34^+$ cells via tail vein injection (200 µl per animal). Engraftment was monitored by longitudinal bleeding of the mice and assessment of human $CD45^+$ over total blood cells. At 16 weeks after human $CD34^+$ cells transplantation animals reached > 80% humanization on blood (Figure S3 b), so they were euthanized. Organs were excised and used for human engraftment evaluation by flow cytometry or fix for histologies, while ossicles were immediately fixed in 4% (v/v) formalin solution for 12 h at 4 °C. After fixation they were washed in PBS and further analyzed by microCT and histologies to assess human cell localization.

Assessment of human engraftment. At 6 and 16 weeks mice were bled via tail vein to analyze humanization by presence of $hCD45^+$ cells in peripheral blood (PB). At endpoint, 16 weeks post-transplantation, spleen, bone marrow, thymus and liver were digested and analyzed by flow cytometry for human engraftment. Detailed used antibodies are in Table 1.

Leukemic xenotransplantation. Leukemic cells were isolated from B-ALL high-risk patients. Cells were then transduced with a Luc-GFP construct using lentivirus, the positive population was sorted, and further expanded in NSG mice as xenografts. As previously mentioned, NSG mice carrying 8-week implanted bone organoids (40 µl TG-PEG hydrogels of intermediate stiffness with hBMSCs and low BMP-2 amounts) received $1 \cdot 10^6$ human leukemic cells via tail vein injection (100 µl per animal). Animals were closely monitored, and leukemic cell progression was assessed by bioluminescence tracking twice a week. 16 days post-leukemic cell injection, animals were sacrificed, ossicles and organs collected and immediately fixed in 4% (w/v) formaldehyde solution methanol-free for 12 h at 4 °C. After fixation they were washed in PBS and further analyzed by microCT and histologies to assess human cell localization.

Bioluminescence imaging. Mice were anesthetized by isoflurane inhalation before receiving an intraperitoneal injection of 100 µl of RediJect D-Luciferin (150 mg kg^{-1}, 770504, Perkin). Bioluminescence images were acquired using a IVIS 200 imaging system (VivoVision), and analyzed by Living Imaging software (v 4.0).

Cancer cell xenotransplantation. Human breast cancer MDA-MB-231 cells, transduced with the Luc-RFP construct, were resuspended in PBS for injection. Nude mice carrying 2, 4 or 8-week implanted bone organoids (40 µl TG-PEG hydrogels of intermediate stiffness with hBMSCs and

low BMP-2 amounts) received $1 \cdot 10^5$ human breast cancer cells systemically via intracardiac injection (100 µl per animal), or $1 \cdot 10^4$ human breast cancer cells via intraossicle injection (2 µl per ossicle). Control animals received sham injections of PBS only. Injections were monitored via ultrasound imaging. Animals were closely monitored, and breast cancer cell progression was assessed by bioluminescence tracking once a week. 5 weeks post-cancer cell injection, animals were sacrificed, ossicles and organs collected and immediately fixed in 4% (w/v) formaldehyde solution methanol-free for 12 h at 4 °C. After fixation they were washed in PBS and further analyzed by microCT and histologies to assess human cell localization.

Micro-computed tomography analysis at endpoints. After fixation in formalin and storage in PBS, ossicles were scanned in a microCT 40 (Scanco Medical AG) operated at energy of 55 kVp and intensity of 72 µA at 4 W. Scans were executed at a high-resolution mode resulting in a voxel size of 10 µm. In reconstructed images bone tissue was segmented from background using a global threshold of 10% of maximum grey value. A cylindrical mask with a diameter of 5 mm was manually placed around the ossicles. Bone volume within the mask was measured using the ImageJ plugin BoneJ[35]. Reconstructions were assembled using the 3D Viewer plugin in ImageJ.

Histological and immunohistochemical studies. Next, samples were decalcified for 2 to 6 weeks in 10% ethylenediaminetetraacetic acid (EDTA) solution with continuous shaking at 4 °C, followed by paraffin embedment and microtome sectioning at 4 µm. For histological stainings, hematoxylin & eosin (H&E) and modified Movat's pentachrome (MP)[36] stainings were performed using standard protocols. Briefly for MP staining, sections were sequentially incubated with alcian blue (Fluka, 1 g in 100 ml in 1% glacial acetic acid) for 10 min, alkaline alcohol (10% ammonium hydroxide in 95% EtOH) for 1 hour, Weigert's iron hematoxylin (Weigert reagent A and B in a ratio 1:1) for 20 minutes, brilliant crocein R-fuchsine (1 part Biebrich Scarlet/Acid Fuchsin solution and 1 part 0.2% acidic fuchsin in 0.5% acetic acid) for 20 minutes, 0.5% acetic acid for 30 seconds, 5% phosphotungstic acid (PWS) for 15 min, 0.5% acetic acid for 2 minutes, washed 3 times with absolute ethanol for 5 minutes, 10 min in safran dye (6g safran powder in 100 ml absolute EtOH), dehydrated and mounted in mounting medium. In MP, red (fibrin) indicates muscle/vascularized tissue; yellow (reticular fibers/collagen) indicates bone; green/blue (mucin) indicates cartilaginous tissue; and black, nuclei and elastic fibers. Images were acquired using a Zeiss 200M inverted microscope.

Immunohistochemistry (IHC). For IHC, slides were deparaffinized and rehydrated. Next different antigen retrievals were performed based on the needs of each staining. Collagen stainings required enzymatic digestion with hyaluronidase (2 mg ml^{-1} in PBS) for 45 min, followed by 30 min incubation in pronase (1 mg ml^{-1} in PBS). For the rest of stainings heat antigen retrieval was performed, sections were incubated for 20 min at 90 °C in 10 mM sodium citrate, 0.05% Tween-20 at pH 6.0. All sections were then blocked for 1 h at room temperature in 1.5% bovine serum albumin (BSA) 0.5% Tween-20 in PBS, followed by 1ary antibody incubation overnight at 4 °C in PBS containing 1% BSA in a humidified chamber. Next day, sections were incubated with the

corresponding 2ary antibody in PBS containing 1% BSA for 1h at room temperature in the dark. Between individual incubation steps, sections were rinsed three times with PBS containing 0.1% Tween-20. Finally, fluorescent slides were washed and mounted with fluorescent mounting medium containing DAPI (Abcam, ab104139). Table 1 details the employed antibodies and their concentrations. For fluorescent stainings, inverted laser-scanning microscope Leica TCS SP5 was used, and images were further processed in Fiji and Adobe Photoshop CS6.

Isolation and flow cytometry analysis of implanted ossicles and murine bones.

Ossicle isolation. Scaffolds were excised from the subcutaneous pockets at indicated times post-surgery and collected together with murine femurs in MEMα + 10% FBS on ice. Skin and connective tissue around the bones was carefully removed with tissue.

Ossicle digestion. Scaffolds and bones were first mechanically dissociated into small pieces in eppendorfs, followed by addition of digestion medium (MEMα + 10% FBS + 1 mg ml^{-1} Collagenase A (Roche 11088793001) + 0.5 mg ml^{-1} DNase I (Roche 11284932001)), and were incubated at 37 °C rocking for 1 h. Followed by trypsin (final conc. 0.025%, Gibco) addition for 10 min at 37 °C, cells were washed with FACS buffer (PBS + 1 mM EDTA + 2% FBS) and filtered through a 70-µm cell strainer (BD Falcon 352350). When needed, red blood cells were lysed by incubation with RBC lysis buffer (Biolegend 420301) for 5 min at room temperature and cells were washed and re-suspended in FACS buffer. Next, cells were incubated for 10 min at 4 °C with mouse Fc block solution (1µg per 10^6 cells in 100µl, BD Biosciences 553141) prior to receiving the antibody mix solution.

Flow cytometry staining. Cells were stained with the titrated monoclonal antibody mix in FACS buffer for 30min rocking at 4 °C in the dark. Table 1 details the employed antibodies and their concentrations. Cells were washed and resuspended in FACS buffer to be analyzed in BD LSR II Fortessa. Compensation beads (AbC Total Antibody Compensation Bead Kit, Invitrogen A10497) were used to calculate color compensation. Dead cells were stained by SYTOX Blue dead cell stain and were, alongside doublets, excluded from analysis. Gates were defined according to the fluorescence intensity of the isotype controls and fluorescence minus one (FMO) stainings. Data was analyzed using FlowJo Software (version 10.0.8, TreeStar) and shown as contour plots or histograms of fluorescent intensity.

Statistical analysis. All data are reported as mean ± standard deviation. All statistical analyses were performed using GraphPad Prism (version 8.0.0, GraphPad Software). Mean values were compared by one-way or two-way analysis of variance (ANOVA) followed by Tukey's *post hoc* test for multiple comparisons. Statistical significance was accepted for $P < 0.05$, and reported as follows * $P < 0.05$, ** $P < 0.01$, *** $P < 0.001$, **** $P < 0.0001$. Further information is found in the particular figure legends.

Table 1. List of detailed antibodies used for flow cytometry and histological stainings

Antibody	Application & Dilution	Company	Catalog number
Rabbit α human CD45	IHC 1:50	Abcam	ab40763
Rabbit α human CD34	IHC 1:50	Abcam	ab110643
Rabbit α human collagen type 1	IHC 1:1000	Abcam	ab138492
Rabbit α mouse collagen type 1	IHC 1:50	Abcam	ab21286
Rabbit α collagen type 2	IHC 1:100	Abcam	ab34712
Rabbit α SP7 osterix	IHC 1:200	Abcam	ab22552
Goat α mouse perilipin	IHC 1:50	Abcam	ab61682
Mouse α human vimentin	IHC 1:200	Abcam	ab8069
Isotype rabbit IgG control	IHC 1:200	Abcam	ab172730
Isotype mouse IgG1 control	IHC 1:200	Abcam	ab18448
Goat α rabbit AF568	IHC 1:200	Abcam	ab175471
Goat α mouse DyLight 648	IHC 1:200	BioLegend	405312
Donkey α goat AF488	IHC 1:200	Abcam	ab150129
Mouse α hCD2 – PE-Cy5	FC 1:100	BioLegend	300209
Mouse α hCD3 – PE-Cy5	FC 1:100	BioLegend	300309
Mouse α hCD4 – PE-Cy5	FC 1:100	BioLegend	317411
Mouse α hCD8 – PE-Cy5	FC 1:100	BioLegend	300909
Mouse α hCD10 – PE-Cy5	FC 1:100	BioLegend	312206
Mouse α hCD11b – PE-Cy5	FC 1:100	BioLegend	301307
Mouse α hCD14 – PE-Cy5	FC 1:100	eBioscience	15-0149-41
Mouse α hCD19 – PE-Cy5	FC 1:100	BioLegend	302209
Mouse α hCD20 – PE-Cy5	FC 1:100	BioLegend	302307
Mouse α hCD56 – PE-Cy5	FC 1:100	BioLegend	304607
Mouse α hCD235a – PE-Cy5	FC 1:100	BD Biosciences	561776
Mouse α hCD45 – eFluor 450	FC 1:100	eBioscience	48-0459-42
Mouse α hCD34 – PE-Cy7	FC 1:50	BD Biosciences	561107
Mouse α hCD34 – AF700	FC 1:40	eBioscience	36-9459-41
Mouse α hCD38 – FITC	FC 1:25	BD Biosciences	555459
Mouse α hCD45RA – APC-eFluor 780	FC 1:100	eBioscience	47-0458-42
Mouse α hCD90 – PE	FC 1:25	BD Biosciences	555596
Zombie Aqua Fixable Viability kit	FC 1:1000	BioLegend	423101

Mouse α hCD335 – BV786	FC 1:50	BD Bioscience	563329
Mouse α hCD33 – BV711	FC 1:100	BioLegend	303424
Rat α mCD45 – PE	FC 1:500	BioLegend	103105
Mouse α hCD14 – APC-Cy7	FC 1:100	BioLegend	301820
Mouse α hCD19 – APC	FC 1:50	BioLegend	302211
Rat α Lin cocktail – biotin	FC 1:100	BioLegend	133307
Streptavidin – PO	FC 1:400	Thermofisher	S32365
Rat α c-Kit – PE-Cy7	FC 1:300	BioLegend	105813
Rat α Sca-1 –APC	FC 1:1000	BioLegend	108111

IHC: immunohistochemistry; FC: flow cytometry

References

1 Arai, F. *et al.* Tie2/angiopoietin-1 signaling regulates hematopoietic stem cell quiescence in the bone marrow niche. *Cell* **118**, 149-161 (2004).

2 Méndez-Ferrer, S. *et al.* Mesenchymal and haematopoietic stem cells form a unique bone marrow niche. *Nature* **466**, 829-834 (2010).

3 Morrison, S. J. & Scadden, D. T. The bone marrow niche for haematopoietic stem cells. *Nature* **505**, 327-334 (2014).

4 Buijs, J. T. & van der Pluijm, G. Osteotropic cancers: from primary tumor to bone. *Cancer letters* **273**, 177-193 (2009).

5 Rongvaux, A. *et al.* Development and function of human innate immune cells in a humanized mouse model. *Nature biotechnology* **32**, 364 (2014).

6 Reinisch, A. *et al.* A humanized bone marrow ossicle xenotransplantation model enables improved engraftment of healthy and leukemic human hematopoietic cells. *Nature medicine* **22**, 812 (2016).

7 Holzapfel, B. M. *et al.* Species-specific homing mechanisms of human prostate cancer metastasis in tissue engineered bone. *Biomaterials* **35**, 4108-4115 (2014).

8 Abarrategi, A. *et al.* Versatile humanized niche model enables study of normal and malignant human hematopoiesis. *The Journal of clinical investigation* **127**, 543-548 (2017).

9 Scotti, C. *et al.* Engineering of a functional bone organ through endochondral ossification. *Proceedings of the National Academy of Sciences* **110**, 3997-4002 (2013).

10 Sacchetti, B. *et al.* Self-renewing osteoprogenitors in bone marrow sinusoids can organize a hematopoietic microenvironment. *Cell* **131**, 324-336 (2007).

11 Martine, L. C. *et al.* Engineering a humanized bone organ model in mice to study bone metastases. *Nature protocols* **12**, 639 (2017).

12 Thibaudeau, L. *et al.* New mechanistic insights of integrin β1 in breast cancer bone colonization. *Oncotarget* **6**, 332 (2015).

13 Adams, G. B. & Scadden, D. T. The hematopoietic stem cell in its place. *Nature immunology* **7**, 333 (2006).

14 Gjorevski, N. *et al.* Designer matrices for intestinal stem cell and organoid culture. *Nature* **539**, 560 (2016).

15 Cruz-Acuña, R. *et al.* Synthetic hydrogels for human intestinal organoid generation and colonic wound repair. *Nature cell biology* **19**, 1326 (2017).

16 Ehrbar, M. *et al.* Enzymatic formation of modular cell-instructive fibrin analogs for tissue engineering. *Biomaterials* **28**, 3856-3866, doi:10.1016/j.biomaterials.2007.03.027 (2007).

17 Ehrbar, M. *et al.* Biomolecular hydrogels formed and degraded via site-specific enzymatic reactions. *Biomacromolecules* **8**, 3000-3007, doi:10.1021/bm070228f (2007).

18 Werb, Z. ECM and cell surface proteolysis: regulating cellular ecology. *Cell* **91**, 439-442 (1997).

19 Ito, K. & Suda, T. Metabolic requirements for the maintenance of self-renewing stem cells. *Nature reviews Molecular cell biology* **15**, 243 (2014).

20 Lieberman, J. R., Daluiski, A. & Einhorn, T. A. The role of growth factors in the repair of bone: biology and clinical applications. *JBJS* **84**, 1032-1044 (2002).

21 Rangarajan, A. & Weinberg, R. A. Comparative biology of mouse versus human cells: modelling human cancer in mice. *Nature Reviews Cancer* **3**, 952 (2003).

22 Di Maggio, N. *et al.* Toward modeling the bone marrow niche using scaffold-based 3D culture systems. *Biomaterials* **32**, 321-329 (2011).

23 Torisawa, Y.-s. *et al.* Bone marrow–on–a–chip replicates hematopoietic niche physiology in vitro. *Nature methods* **11**, 663-669 (2014).

24 Mesfin, A. *et al.* High-dose rhBMP-2 for adults: major and minor complications: a study of 502 spine cases. *JBJS* **95**, 1546-1553 (2013).

25 Brown, J. *et al.* Bone resorption predicts for skeletal complications in metastatic bone disease. *British journal of cancer* **89**, 2031 (2003).
26 Brown, J. E. *et al.* Bone turnover markers as predictors of skeletal complications in prostate cancer, lung cancer, and other solid tumors. *Journal of the National Cancer Institute* **97**, 59-69 (2005).
27 Hoshino, A. *et al.* Tumour exosome integrins determine organotropic metastasis. *Nature* **527**, 329 (2015).
28 Keklikoglou, I. *et al.* Chemotherapy elicits pro-metastatic extracellular vesicles in breast cancer models. *Nature cell biology* **21**, 190 (2019).
29 Roodman, G. D. Mechanisms of bone metastasis. *New England journal of medicine* **350**, 1655-1664 (2004).
30 Coutu, D. L., Kokkaliaris, K. D., Kunz, L. & Schroeder, T. Three-dimensional map of nonhematopoietic bone and bone-marrow cells and molecules. *Nature biotechnology* **35**, 1202 (2017).
31 Coutu, D. L., Kokkaliaris, K. D., Kunz, L. & Schroeder, T. Multicolor quantitative confocal imaging cytometry. *Nature methods* **15**, 39 (2018).
32 Papadimitropoulos, A. *et al.* Expansion of human mesenchymal stromal cells from fresh bone marrow in a 3D scaffold-based system under direct perfusion. *PloS one* **9**, e102359 (2014).
33 Weber, F. E. *et al.* Disulfide bridge conformers of mature BMP are inhibitors for heterotopic ossification. *Biochemical and Biophysical Research Communications* **286**, 554-558 (2001).
34 Schense, J. C. & Hubbell, J. A. Cross-linking exogenous bifunctional peptides into fibrin gels with factor XIIIa. *Bioconjugate chemistry* **10**, 75-81 (1999).
35 Doube, M. *et al.* BoneJ: free and extensible bone image analysis in ImageJ. *Bone* **47**, 1076-1079 (2010).
36 Garvey, W., Fathi, A., Bigelow, F., Carpenter, B. & Jimenez, C. Improved Movat pentachrome stain. *Stain technology* **61**, 60-62 (1986).

Supplementary data

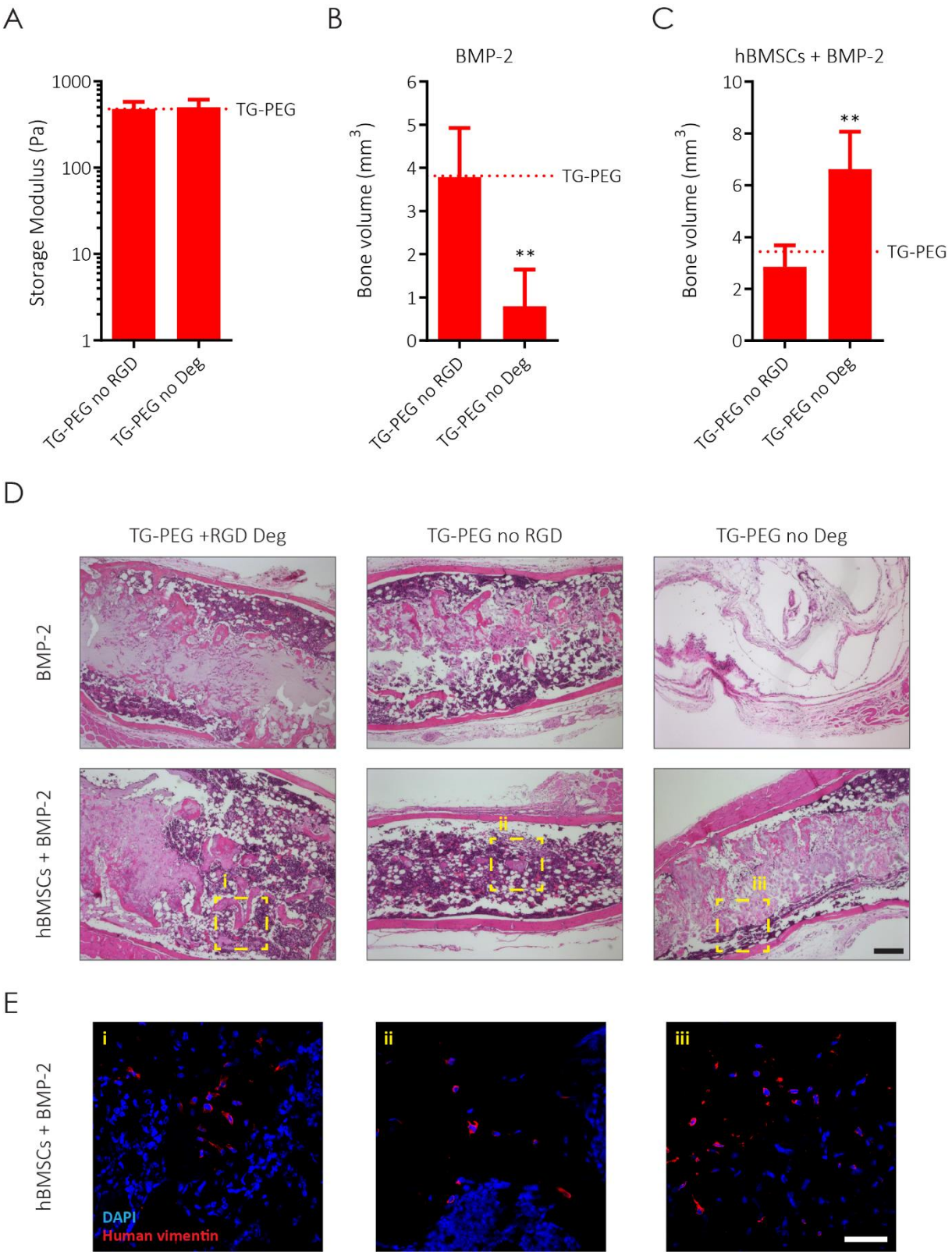

Figure S1. The role of cell adhesion and degradability in organoid formation *in vivo*

(**a**) Storage moduli of TG-PEG hydrogels of intermediate stiffness without the cell-adhesion RGD peptide, or lacking MMP-degradable sites (n = 3). Dotted line indicates the average storage modulus of intermediate stiffness TG-PEG containing RGD peptide and degradable sites for reference. (**b**) Bone volume of these hydrogels with only BMP-2 supplementation 8 weeks post-implantation, or (**c**) BMP-2 and hBMSCs condition (n = 4). Dotted line indicates average bone volume of the reference TG-PEG (TG-PEG +RGD Degradable). (**d**) H&E staining of the aforementioned conditions (scale bar: 200 µm), (**e**) and specific human vimentin staining (scale bar: 50 µm). All data are reported as mean ± standard deviation. ANOVA with Tukey's *post hoc* test ** $P < 0.01$.

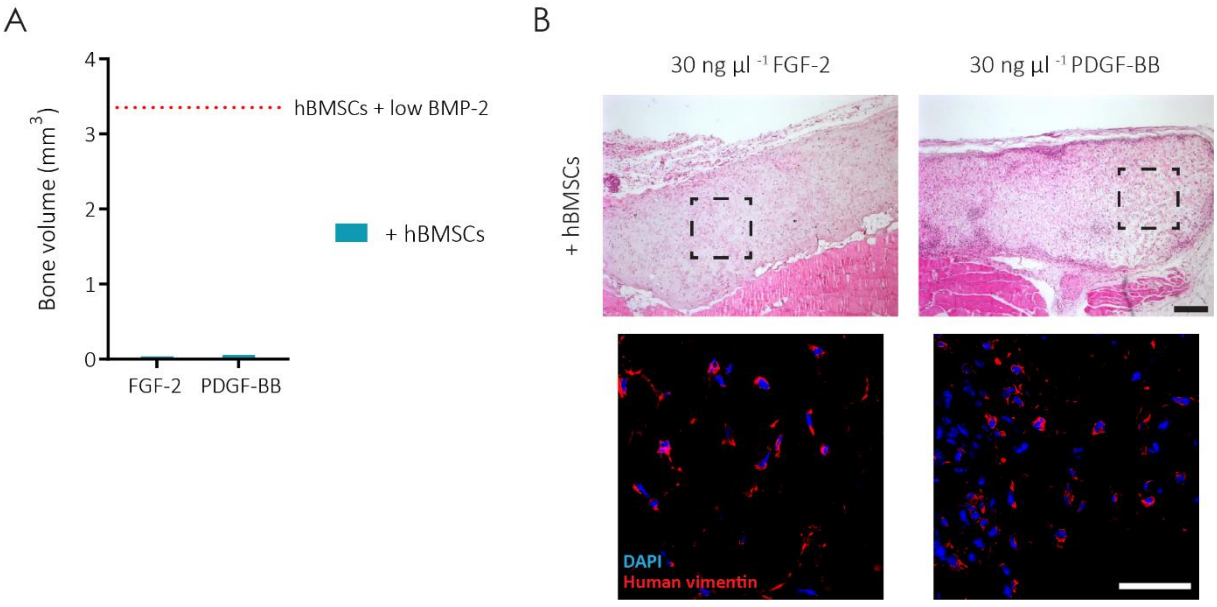

Figure S2. Effect of proliferation and migration induction in organoid formation

(**a**) Bone volume was absent after 8 weeks of hBMSCs encapsulation in hydrogels containing either FGF-2 or PDGF-BB (n = 4). Dotted line indicates the average bone volume of hBMSCs with low BMP-2 amounts for reference. (**b**) Histological analysis revealed hydrogels are maintained and human cells remain in the hydrogel as seen by H&E (scale bar: 200 µm) and specific human vimentin staining (scale bar: 50 µm). All data are reported as mean ± standard deviation.

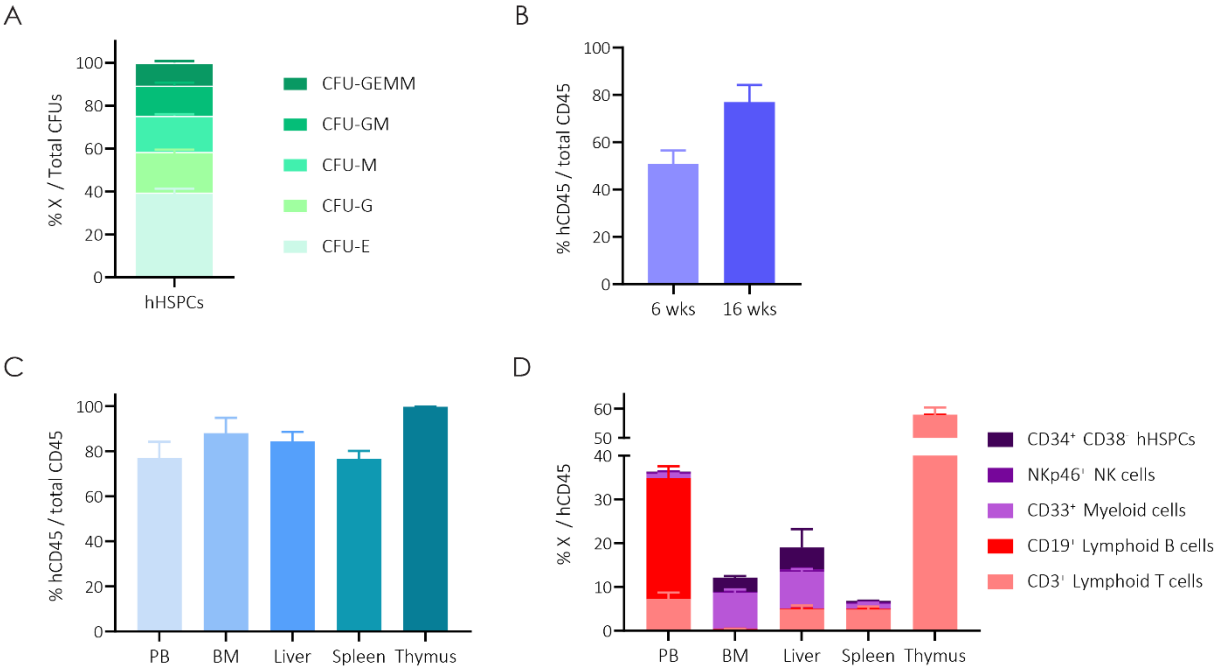

Figure S3. NSG mice humanization

(**a**) Distribution of different types of colonies based on their morphology formed from cord blood-derived cbCD34$^+$ HSPCs (n = 3). (**b**) Percentage of hCD45$^+$ cells of total CD45$^+$ (hCD45 + mCD45) found in peripheral blood (PB) of NSG mice up 6 and 16 weeks post-cbHSPC transplantation (n = 3). (**c**) Percentage of hCD45$^+$ cells of total CD45$^+$ (hCD45 + mCD45) found in PB, bone marrow (BM), liver, spleen or thymus of NSG mice transplanted with cbHSPCs at 16 weeks (n = 3). (**d**) Analysis of the human subpopulations found in the different organs at 16 weeks (n = 3). All data are reported as mean ± standard deviation.

Heu parat una furgoneta aprofitant la vista privilegiada d'una ciutat.
Tu assenyales l'absis romànic d'una catedral i sou joves i forts!
I sentiu l'eternitat al vostre davant! – Manel

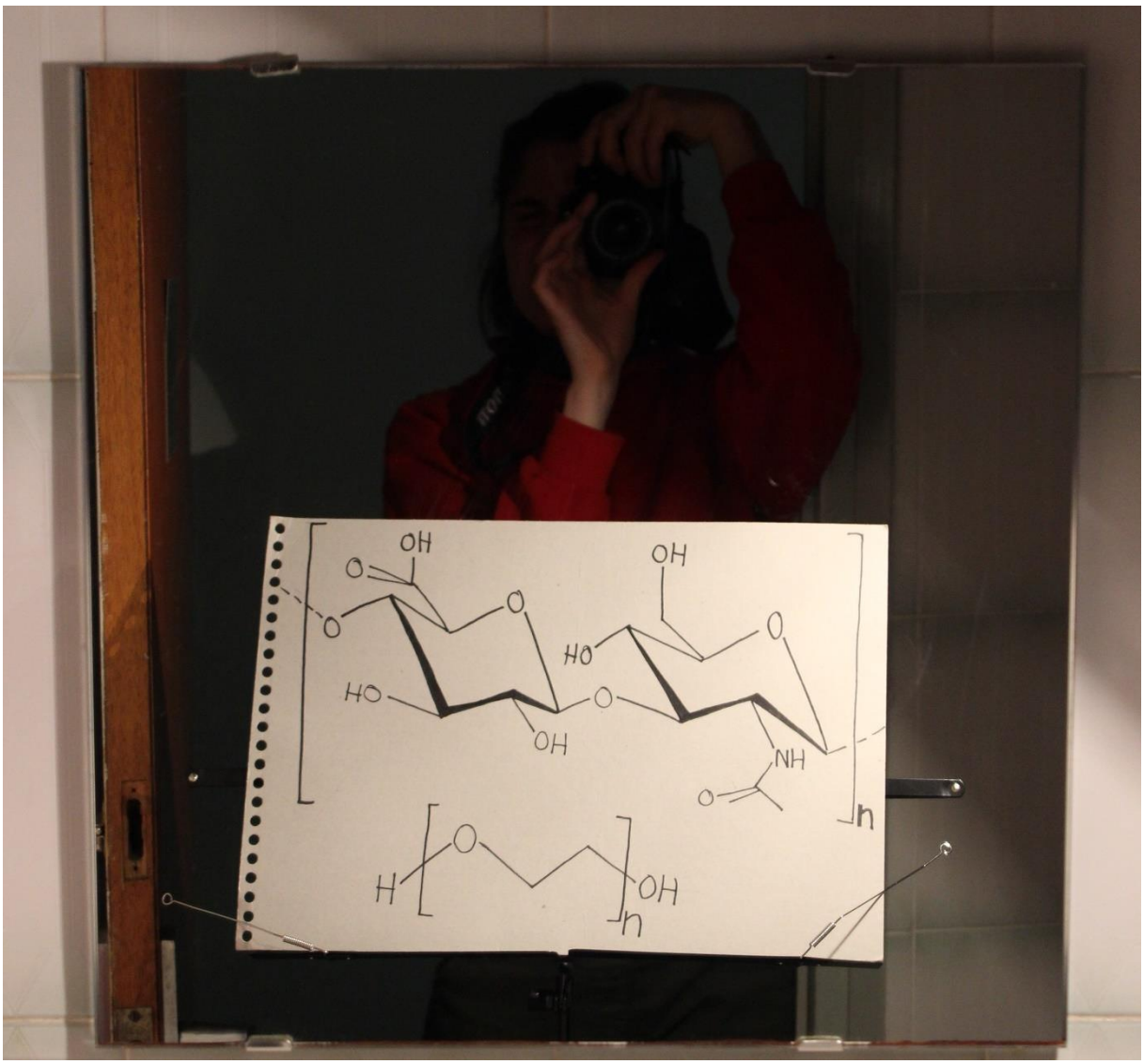

Artwork by Anna Rodrigo Albertí
Girona, Catalunya

CHAPTER 5

PEG/HA hybrid hydrogels for biologically and mechanically tailorable bone and bone marrow stem cell niches

Q Vallmajo-Martin[1,2], N Broguiere[2,3], C Millan[4], M Zenobi-Wong[3], M Ehrbar[1]

The content of this chapter is part of a manuscript in preparation.

[1] Laboratory for Cell and Tissue Engineering, Department of Obstetrics, UniversitätsSpital Zürich, Switzerland;
[2] Laboratory of Stem Cell Bioengineering, Institute of Bioengineering, École Polytechnique Fédérale de Lausanne, Switzerland;
[3] Tissue Engineering and Biofabrication Laboratory, Department of Health Science and Technology, Eidgenössische Technische Hochschule Zürich, Switzerland;
[4] Laboratory for Urologic Tissue Engineering and Stem Cell Therapy, Department of Urology, UniversitätsSpital Zürich, Switzerland.

Statement of contributions

QVM designed, performed and analyzed all the experiments.

NB & MZW developed and manufactured HA-TG.

CM collaborated with histological evaluations, including experimental setup and analysis.

ME designed experiments and supervised the whole project

Abstract

Therapeutic applications involving human bone marrow stromal cells (hBMSCs) have not yet been met with significant clinical success due to inefficient engraftment in the skeletal system following injury. Overcoming this necessitates the development of novel biomaterials that shield the delivered cells from adverse reaction from the host while enabling their full regenerative capacity to recapitulate the bone marrow niche. Here we show that enzymatically crosslinked hydrogels can function *in vivo* to support both the osteogenic differentiation of hBMSCs, and also the maintenance of human hematopoietic stem and progenitor cells (hHSPCs). Hydrogels based on poly(ethylene glycol) (PEG), hyaluronic acid (HA), or combinations thereof, with matched stiffness of approximately 260 Pa, were compared. Interestingly, HA-based hydrogels elicited higher proliferation for both cell types. Furthermore, when implanted in nude mice with only high amounts of bone morphogenetic protein 2 (BMP-2), all these scaffolds remodeled into a fully developed bone marrow-like structure after eight weeks, facilitating recruitment of murine host cells. Similarly, hydrogels containing hBMSCs with low amounts of BMP-2 transplanted *in vivo* also formed ossicles enclosing host hematopoietic cells, and moreover supporting human stromal cells. Though micro-computed tomography (microCT) indicated similar total volumes of bone tissue formation in all conditions, immunostaining revealed a significantly lower number of macrophages in HA-containing hydrogels, which coincided with an overall higher retention of human cells and thus, higher degree of humanization. Such modular hydrogel platforms were shown to mimic the bone marrow stem cell niche and serve as a vehicle for the delivery of hBMSCs in an *in vivo* model.

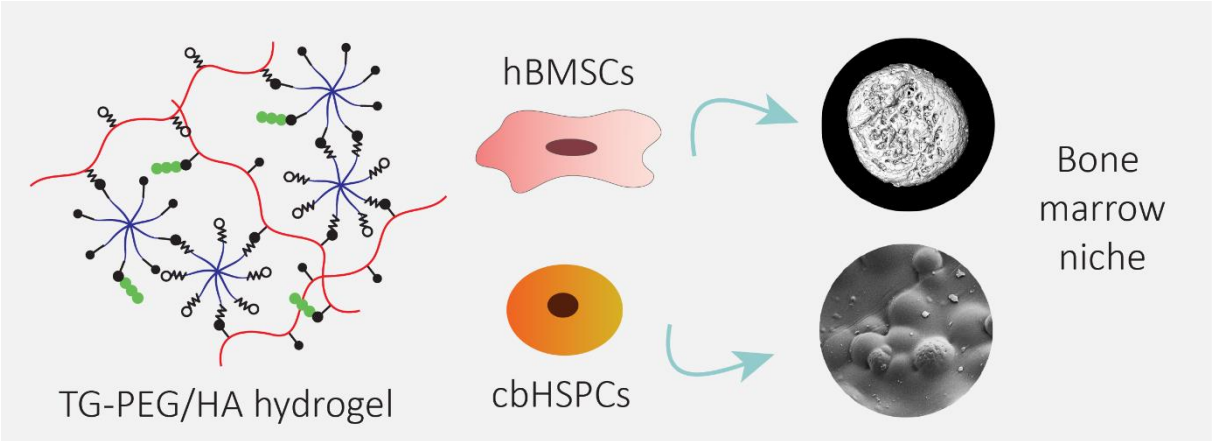

Keywords: Hydrogel, enzymatic crosslinking, osteogenesis, hematopoietic stem cell, bone marrow niche

Introduction

The regenerative capacity of human bone marrow-derived stromal cells (hBMSCs) has been highly touted and, together with the recent discovery of human skeletal stem cells (SSCs)[1], should drive successful clinical application. Ideally, these stromal/stem cells could be delivered to the injury site to treat degenerative, post-traumatic or post-surgical skeletal disorders, and participate in tissue regeneration via *de novo* bone deposition and stimulation of host cells by paracrine signaling. Despite advances in tissue engineering and rapid development of novel biomaterials, the ideal stem cell carrier for such an application has yet to be characterized stunting clinical translation[2].

hBMSCs reside in the bone marrow stem cell microenvironment, often referred to as the bone marrow niche, together with hematopoietic stem and progenitor cells (hHSPCs), among other cell types[3,4]. While hBMSCs direct the connective tissue regeneration, hHSPCs continuously renew the whole hematopoietic system throughout life. One of the bottlenecks of culturing hHSPCs *ex vivo* is their rapid lineage commitment and, thus, loss of long-term reconstitution capacity of the hematopoietic system[5]. It is key to develop novel expansion conditions that enable proliferation of these cells while maintaining the progenitor and stem cell populations without inducing their irreversible commitment.

Mimicking key *in vivo* microenvironments in simplified yet accurate models is crucial for successful tissue engineering approaches. Certain biomaterials have been shown to faithfully recapitulate fundamental features of these *in vivo* niches[6]. Biomaterials have additionally been shown to support cell transplantation for the regeneration of organs such as skin[7] or bladder[8], among others. However, many developed stem cell-based therapies, especially for more complex skeletal tissues, have failed in clinical translation[9,10]. A primary reason for this is the low yield of viable transplanted cells that ultimately can participate in tissue healing[11]. In one clinical trial on patients with osteogenesis imperfecta, it was shown that less than 1% of donor transplanted cells engrafted in the host[12]. To overcome this, the ideal cell delivery scaffold should elicit minimal immune response, allow inosculation of host vasculature, and provide biomechanical balance between initial stability upon delivery of the cells whilst still degrading over time to allow for remodeling and engraftment. Thus, the carrier biomaterial for transplanted cells is perhaps equally important as the type and characteristics of the transplanted cells.

Hydrogels, due to their high water content and viscoelastic properties mirroring important architectural qualities of native tissues, stand out among other biomaterials as optimal cell carriers for tissue engineering[13]. Some hydrogel materials have been developed based on proteins and naturally-derived extracellular matrix (ECM) components such as collagen, fibrin, laminin, chitosan, hyaluronic acid (HA) and alginate among others[14]. These materials exhibit biocompatibility and promote many cellular functions, yet their inherent biological activity and batch-to-batch variability often limit their application. In the attempt to obtain highly reproducible quality of these materials, recombinant synthesis and purification from bacteria has been

established for HA[15]. HA-based hydrogels have emerged as a highly promising semi-synthetic approach to mimic the high levels of endogenous HA found in the ECM of certain tissue types especially when undergoing remodeling[16]. Yet limited ability to tune their physical and chemical properties has motivated the development of hydrogels composed of synthetically-derived components[17]. Synthetic hydrogels have enabled an orthogonal design allowing independent modification of stiffness and/or presentation of biologically active moieties. Due to its high hydrophilicity, one of the most widely used non-natural polymers for hydrogel design has been poly(ethylene glycol) (PEG)[18].

Our lab pioneered the development of an enzymatically crosslinked PEG-based hydrogel, named TG-PEG[19]. Enzymatically-mediated polymerization can overcome many of the limitations of other crosslinking mechanisms by enabling cell encapsulation at physiological pH and temperature, while excluding toxic byproducts of, for example, free-radical polymerization. Transglutaminase factor XIII crosslinks the ends of functionalized 8-arm PEG precursor molecules – with either a glutamine-acceptor (Gln-PEG) or a lysine-donor substrate sequence (Lys-PEG) – into a stable TG-PEG hydrogel[19]. This biomimetic 3D PEG hydrogel can readily incorporate cell-adhesion sites, protease-sensitive degradable moieties, as well as growth factors[20,21]. Recently, FXIII-crosslinked HA hydrogels (TG-HA) were developed and used to support the formation of neuronal networks[22] and cartilage tissue[23].

In recent years we and others have incorporated glycosaminoglycans (GAGs) into TG-PEG-based enzymatically crosslinked matrices resulting in hybrid hydrogels, for instance with chondroitin sulfate (CS) for MSCs[24] or HA for cancer and myoblasts culture[25]. However, the systems presented until now relied on stoichiometrically balanced formulations of reciprocally functionalized GAG and PEG precursors (Lys-CS and Gln-PEG[24] or Gln-HA and Lys-PEG[25]), such that GAG and PEG equally contribute to the formation of the hydrogel backbone. A major limitation of this approach is that even minimal deviations from the optimal PEG to GAG ratio lead to hydrogel imperfections and thus a reduction of the hydrogel stiffness.

Here, we present an alternative strategy to form TG-PEG/HA hybrid hydrogels to facilely tune their backbone composition without affecting hydrogel stiffness. These hybrid hydrogels rely on the seamless integration of TG-PEG and TG-HA hydrogels, which, due to the presence of stoichiometrically balanced Gln and Lys functionalities, enable the formation of hydrogels with any desirable HA to PEG ratio without significantly altering mechanical properties and abrogating the need to adapt the crosslinking conditions. First, we established TG-PEG and TG-HA hydrogels with matched, cell culture-compatible stiffness. Then, we formulated stiffness-matched TG-PEG and TG-HA at different ratios, resulting in various TG-PEG/HA hybrid hydrogels. Rheological analysis confirmed that all TG-PEG/HA hybrid hydrogels maintained similar mechanical properties as TG-PEG and TG-HA alone. These TG-PEG/HA hybrid hydrogels were employed to recapitulate the bone and bone marrow microenvironment.

Proliferation and differentiation behaviors of encapsulated hBMSCs and hHSPCs showed that HA-containing hydrogels better supported the proliferation of both cell types, while pure TG-PEG hydrogels better maintained the HSC phenotype. Next, *in vivo* transplantations were performed of TG-PEG, TG-HA, or TG-PEG/HA hybrid hydrogels. The hydrogels were loaded with either a high concentration (50 ng μl^{-1}) of BMP-2 without cells or a combination of ($20 \cdot 10^6$ cells per ml) hBMSCs and low concentration (10 ng μl^{-1}) of BMP-2. The formation of bone compartments was observed in all conditions, though fully endowed bone marrow compartments were exclusively found in hydrogels containing hBMSCs with low BMP-2 amounts. Finally, immunohistochemical evaluations of the induced bone and bone marrow compartments showed that hBMSCs engraft significantly more and recruitment of macrophages is significantly reduced in HA-comprising hydrogels compared to pure PEG hydrogels. These observations suggest that, by combining PEG engineering and biological HA functions, TG-PEG/HA hybrid hydrogels could serve as highly effective stem cell carriers for clinical translation.

Results

Hybrid TG-PEG/HA hydrogels exhibit mechanical properties comparable to pure TG-PEG and TG-HA hydrogels

To elucidate the role of HA in the bone marrow niche, we engineered a method to seamlessly integrate HA into otherwise fully defined PEG-based hydrogels. We have previously reported on a PEG-based system that modifying the ends of an 8-arm PEG to contain either a Gln-acceptor or a Lys-donor enables crosslinking by the transglutaminase FXIII at physiological conditions[19]. Taking advantage of a recently described modified HA that enables the same enzymatic crosslinking mechanism[22], we rationally combined TG-PEG and TG-HA precursors that both contained a balanced ratio of Gln- or Lys-substrates (Figure 1). Inspired by the native ECM that permits dynamic interactions between cells and matrix[26], we inserted a matrix metalloproteinase (MMP)-1 sensitive domain in both PEG and HA-Lys donor substrates to enable MMP-mediated degradation of the scaffolds. Finally, to closely mimic the fundamental cell-ECM interactions in the bone marrow, the cell-adhesion peptide RGD (50 μM) was tethered to the glutamine acceptors.

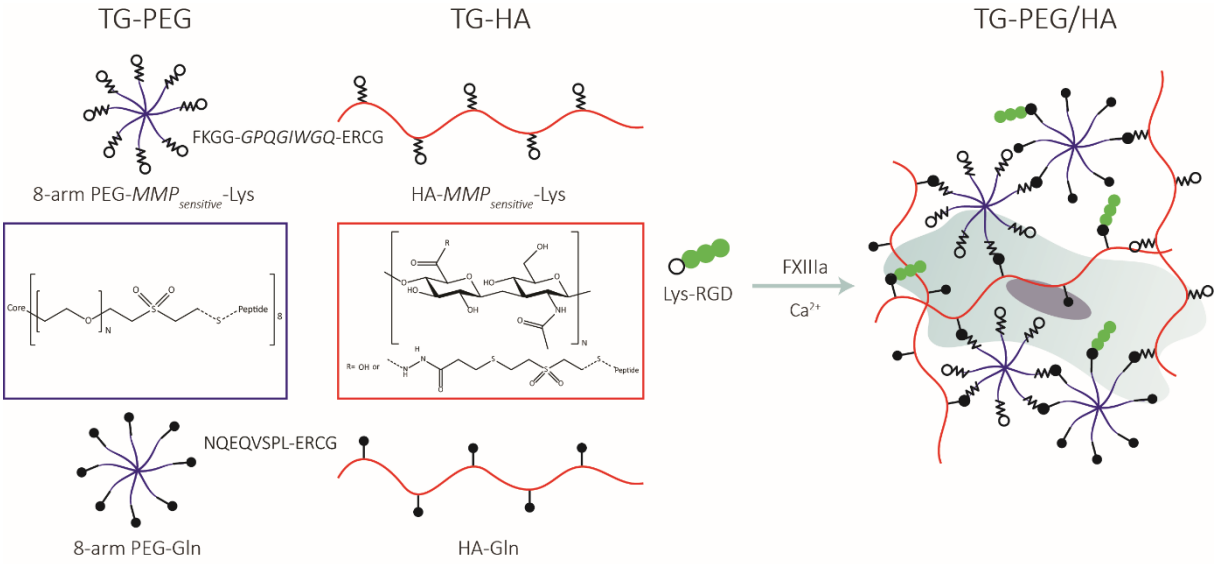

Figure 1. Scheme of the enzymatically crosslinked seamless TG-PEG/HA hybrid hydrogel system

TG-PEG hydrogels are formed by equimolar concentrations of 8-arm PEG-Gln and 8-arm PEG-MMPsensitive-Lys, whereas TG-HA hydrogels are formed by equimolar concentrations of HA-Gln and HA-MMPsensitive-Lys. Mixing of TG-PEG and TG-HA hydrogel precursors at any desirable ratio allows the seamless integration of both systems. Hydrogel precursors can be formulated at different initial polymer concentrations, supplemented with Lys-RGD (50 µM) and crosslinked under physiological conditions by transglutaminase FXIIIa (7.5 U ml^{-1}) in the presence of Ca^{2+}. Cells and growth factors can be added to hydrogel formulations before crosslinking.

In order to begin with hydrogels of similar stiffness in a range that would enable cell invasion and spreading, we determined the storage moduli of different crosslinking densities of TG-PEG (ranging from 1.2% to 1.8% w/v solution) and TG-HA (ranging from 0.75% to 1% w/v solution) via *in situ* rheological analysis. Results showed that 1.5% (w/v) TG-PEG and 0.75% (w/v) TG-HA had comparable storage moduli of 243.2 ± 38.58 Pa and 254.6 ± 31.32 Pa, respectively (Figure S1 a). Thus, we proceeded to evaluate the properties of the mixtures of these two hydrogels that, despite containing different backbone chemistries, shared similar mechanical properties and FXIII substrate sequences. Mixtures of 50/50, 25/75 or 75/25 of the aforementioned crosslinking densities of TG-HA and TG-PEG were prepared (i.e. 50/50 means equal volumes of 1.5% (w/v) TG-PEG and 0.75% (w/v) TG-HA) (Table 1). Storage moduli of all hybrid hydrogels remained similar within the range of 250 to 320 Pa and exhibited no statistically significant differences (Figure 2 a, b). However, hydrogels did differ significantly in onset of polymerization ranging from under one minute for hydrogels containing mainly HA to up to 3 minutes for TG-PEG gels (Figure 2 c). The presence of HA drastically reduced the polymerization time likely due to the fact that HA, owing to its high molecular weight (on the order of 1 MDa), features a large number of functional groups (on the order of 250) for the herein used substitution rate of 10% of the disaccharide repeat units.

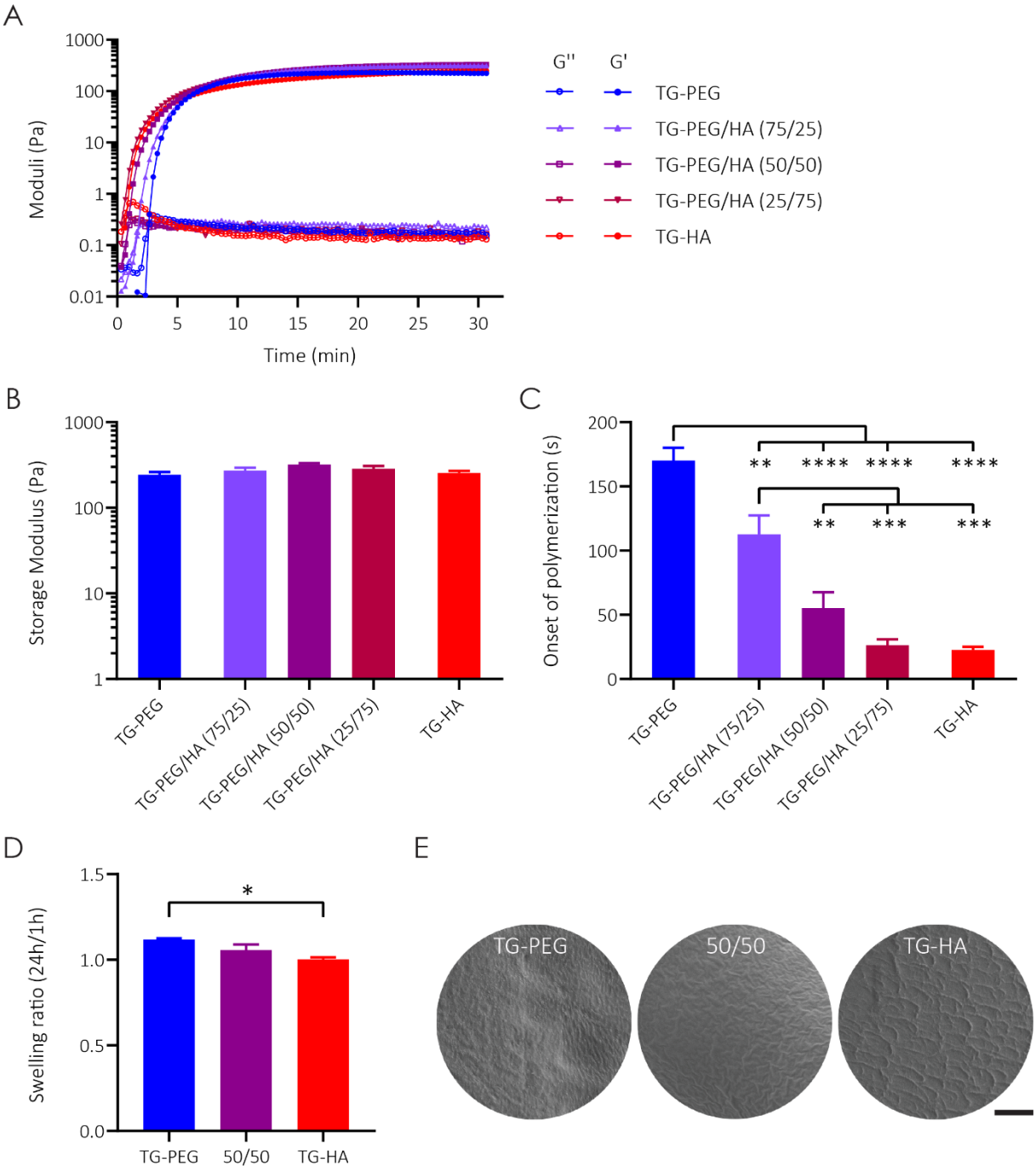

Figure 2. Mechanical and physical characterization of TG-PEG/HA hybrid hydrogels

(**a-c**) Rheological characterization of pure TG-PEG, pure TG-HA, and TG-PEG/HA hybrid hydrogels. (**a**) Representative mechanical profile consisting of storage modulus (G') and loss modulus (G''). (**b**) Storage moduli of hydrogels after reaching a plateau in storage moduli at 30 min (n = 4). (**c**) The onset of polymerization was significantly reduced by the addition of HA in the hydrogel mix (n = 4). (**d**) Swelling ratio (mass swollen/ initial mass) of hydrogels after 24 h in soaking buffer (n = 3). (**e**) Representative scanning electron microscopy (SEM) images showing no apparent differences in the surface microstructures of TG-PEG, TG-PEG/HA (50/50) hybrid or TG-HA hydrogels (scale bar: 5 µm). All data are reported as mean ± standard error. ANOVA with Tukey's *post hoc* test * P < 0.05, ** P < 0.01, *** P < 0.001, **** P < 0.0001.

Swelling ratios, calculated as hydrogel mass after 24 hours compared to 1 hour after polymerization, showed that HA-containing hydrogels did not swell, whereas PEG hydrogels did undergo very

mild swelling (1.1 x over 24 hours) (Figure 2 d). We next assessed the storage moduli of swollen hydrogels to ensure that these mild differences in swelling did not result in significant changes on their mechanical properties. Rheological tests of swollen hydrogels revealed that the mechanical properties were still conserved upon swelling (Figure S1 b). Ultimately, it was corroborated by SEM imaging that there were no major differences among the ultrastructures of hybrid hydrogels and the corresponding pure TG-PEG and TG-HA hydrogels, all having a homogeneous microstructure (Figure 2 e).

HA-comprising hydrogels enhance *in vitro* hBMSC proliferation while maintaining stem cell differentiation capacity

Utilizing hydrogels with matched mechanical properties, we proceeded to evaluate the effect of material composition on hBMSCs function *in vitro* (Figure 3 a). hBMSCs were encapsulated in the hydrogels at $2 \cdot 10^6$ cells per ml and cells were fixed 3 days post-encapsulation followed by actin and DAPI staining to evaluate cell spreading. When encapsulated in pure moderately stiff (260 Pa), either TG-PEG or TG-HA hydrogels, hBMSCs were shown to interact with both materials as seen by cell spreading (Figure 3 b). However, cell spreading was hindered in stiffer hydrogels (equivalent to 1200 Pa storage modulus[23]) (Figure S2 a). Similarly, hydrogels lacking RGD adhesion sites did not enable cell spreading (Figure S2 b).

Interestingly, hBMSCs encapsulated in TG-HA hydrogels exhibited significantly higher proliferation than in TG-PEG hydrogels (Figure 3 c). The presence of the RGD adhesion peptide also increased hBMSC proliferation in both TG-HA and TG-PEG hydrogels. There was an additive effect seen when a maximum cell proliferation was achieved in TG-HA hydrogels containing RGD. Thus, hydrogels more closely resembling the natural ECM conferred an advantage to hBMSCs regarding proliferation capacity. Importantly, the seamless TG-PEG/HA hybrid hydrogel systems showed increasing proliferation of hBMSCs in hydrogels containing increasing concentrations of HA. Therefore, TG-PEG/HA hybrid hydrogels enable to tune the contribution of HA and RGD on cell functions, such as proliferation.

Intriguingly, when cultured in osteogenic differentiation medium for 12 days, all hBMSCs underwent osteogenic differentiation irrespective of substrate material as seen by ALP activity (Figure 3 d, e). Thus, despite the increased proliferation of hBMSCs in RGD- and/or HA-containing hydrogels, our data shows that osteogenic differentiation proceeds equally well in absence of both components.

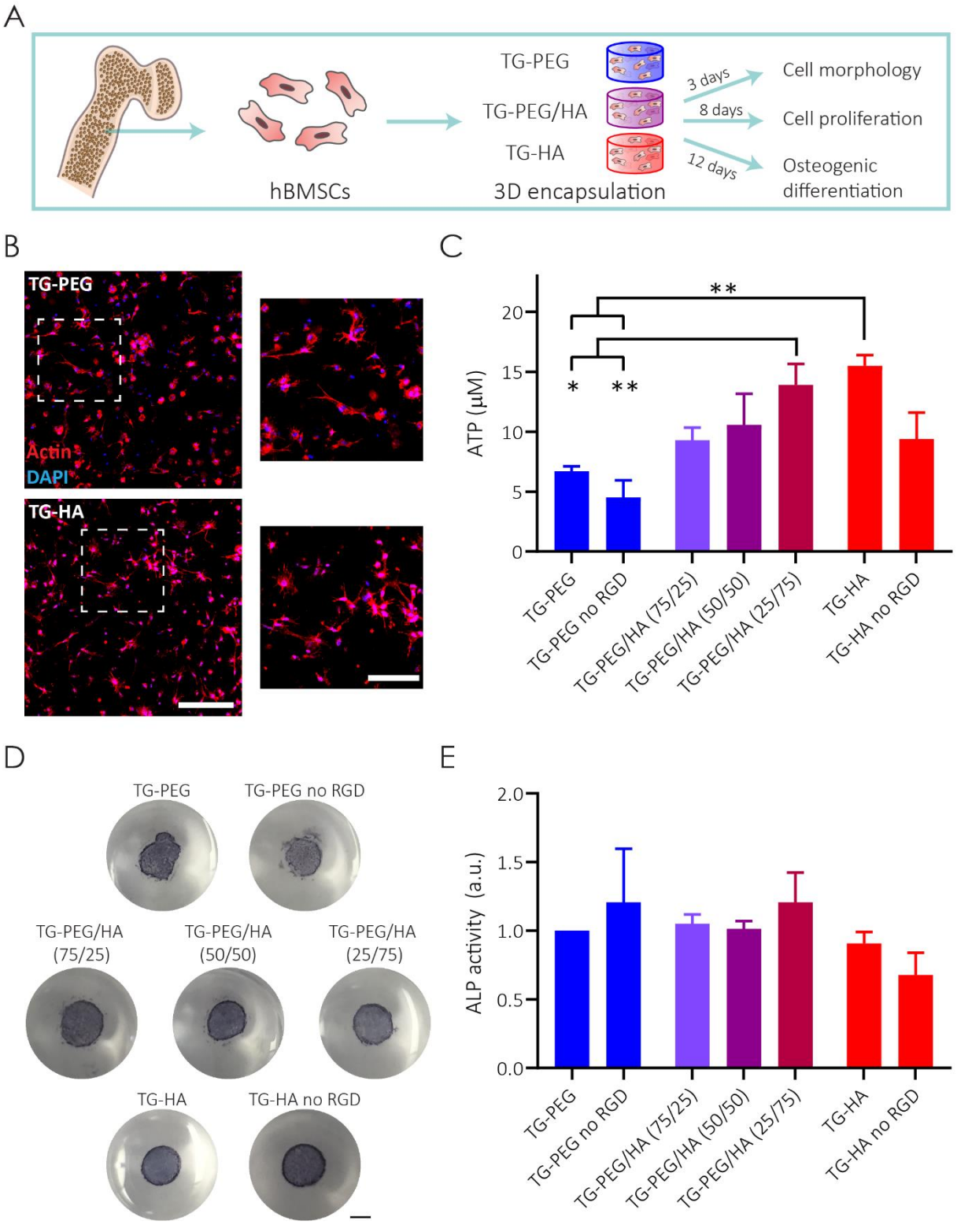

Figure 3. HA-comprising hydrogels enhance *in vitro* hBMSC proliferation while maintaining stem cell osteogenic differentiation capacity

(**a**) Scheme of hBMSC isolation, hydrogel encapsulation, proliferation and osteogenic differentiation. (**b-d**) hBMSCs were encapsulated in TG-PEG, TG-HA and TG-PEG/HA hydrogels at $2 \cdot 10^6$ cells per ml of hydrogel. (**b**) Actin and DAPI staining displaying hBMSC morphology after 3 days in culture (left, scale bar: 200 µm; right zoom in, scale bar: 400 µm). (**c**) Proliferation of encapsulated hBMSCs in the different hydrogels at day 8 was assessed by ATP content (N = 3). (**d**) hBMSCs were differentiated in osteogenic medium for 12 days and evaluated by ALP staining (scale bar: 2 mm) or (**e**) quantification of ALP activity (N = 3). All data are reported as mean ± standard error. ANOVA with Tukey's *post hoc* test * $P < 0.05$, ** $P < 0.01$.

hHSPCs retain higher stem cell phenotype when encapsulated in TG-hydrogels than in 2D cultures

Next, we evaluated the role of HA in supporting the function of hHSPCs, the stem/progenitor cell populations within the bone marrow microenvironment responsible for the maintenance of the hematopoietic system. For this, cells were isolated from human umbilical cord blood by $CD34^+$ selection and encapsulated at $1.5 \cdot 10^6$ cells per ml in either pure TG-PEG, pure TG-HA or the 50/50 TG-PEG/HA hybrid hydrogels (Figure 4 a). As seen by brightfield and SEM imaging, $CD34^+$ cells cultured for up to 16 days grew similarly in clusters in all hydrogels contrasting starkly with single-cell morphologies observed in the 2D culture control (Figure 4 b, Figure S3 a, b). However, while total cell proliferation was slightly increased in 50/50 TG-PEG/HA hybrid hydrogels, it was significantly increased in TG-HA hydrogels compared to TG-PEG only (Figure 4 c), as similarly seen for hBMSCs.

Assessing the phenotypes of encapsulated cells in more detail after 2 weeks in culture, immunocytochemistry revealed that some of the cell clusters observed in hydrogels were shown to contain $CD34^+$ cells, a characteristic marker of undifferentiated hHSPCs (Figure 4 d, Figure S3 c). To rigorously classify the cell populations present in the different conditions, we used a set of 16 surface markers analyzed by flow cytometry characterizing HSPCs (Lin^- $CD34^+$ $CD38^-$) and myeloid progenitors (MyelP, Lin^- $CD34^+$ $CD38^+$) based on their CD38 and CD34 expression within the lineage-negative subset (Figure S4). All hydrogel conditions contained similar percentages of HSPCs as compared to standard 2D culture conditions (Figure 4 e). Then, HSPCs were further restricted into hematopoietic stem cells (HSCs, Lin^- $CD34^+$ $CD38^-$ $CD45RA^-$ $CD90^+$) and their immediate progeny comprising multipotent progenitors (MPPs, Lin^- $CD34^+$ $CD38^-$ $CD45RA^-$ $CD90^-$) and multilymphoid progenitors (MLPs, Lin^- $CD34^+$ $CD38^-$ $CD45RA^+$ $CD90^-$) based on their CD90 and CD45RA expression. Remarkably, HSPC populations cultured in hydrogels were significantly enriched with HSCs after 16 days compared to 2D cultures (Figure 4 f). Strikingly, TG-PEG hydrogels, despite restricting proliferation, significantly maintained the highest HSC population over this time in culture. Lastly, no significant differences were seen between hydrogels or 2D conditions for the subpopulations of MyelP cells containing common myeloid progenitors/megakaryocyte-erythrocyte progenitors (CMP/MEP, Lin^- $CD34^+$ $CD38^+$ $CD45RA^-$) and B-/Natural Killer-cell progenitors/granulocyte-macrophage progenitors (B/NK/ GMP, Lin^- $CD34^+$ $CD38^+$ $CD45RA^+$) (Figure 4 g). In conclusion, all 3D hydrogel formulations were able to maintain HSPCs in a more stem cell-like phenotype than 2D cultures.

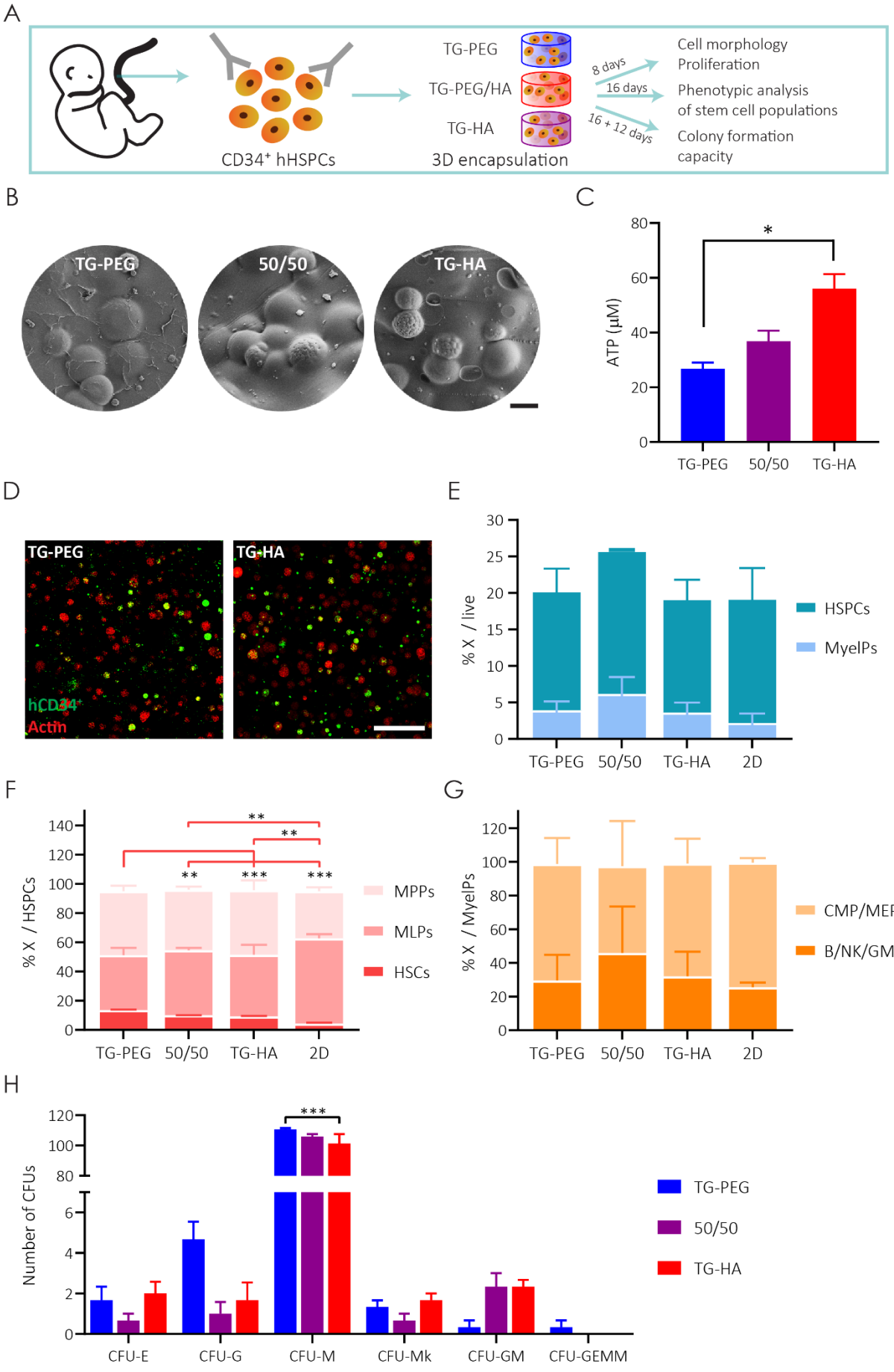
A
TG-PEG
TG-PEG/HA
TG-HA
8 days
16 days
16 + 12 days
Cell morphology
Proliferation
Phenotypic analysis
of stem cell populations
Colony formation
capacity
CD34⁺ hHSPCs
3D encapsulation
B
TG-PEG
50/50
TG-HA
C
ATP (µM)
TG-PEG
50/50
TG-HA
D
TG-PEG
TG-HA
hCD34⁺
Actin
E
% X / live
HSPCs
MyeIPs
TG-PEG
50/50
TG-HA
2D
F
% X / HSPCs
MPPs
MLPs
HSCs
TG-PEG
50/50
TG-HA
2D
G
% X / MyeIPs
CMP/MEP
B/NK/GMP
TG-PEG
50/50
TG-HA
2D
H
Number of CFUs
TG-PEG
50/50
TG-HA
CFU-E
CFU-G
CFU-M
CFU-Mk
CFU-GM
CFU-GEMM

Figure 4. TG-PEG/HA hybrid hydrogels maintain stem cell phenotype of hHSPCs *in vitro*

(**a**) Scheme of workflow. hHSPCs were isolated from umbilical cord blood, selected based on $CD34^+$ expression, and encapsulated at $1.5 \cdot 10^6$ cells per ml in pure TG-PEG, pure TG-HA, or in TG-PEG/HA (50/50) hybrid hydrogels. Cell proliferation, phenotypic stem cell populations and functional colony formation assay were assessed. (**b**) Representative SEM images of hHSPCs after 16 days of culture in different hydrogels (scale bar: 30 µm). (**c**) Proliferation of encapsulated hHSPCs at day 8 by assessment of ATP content (n = 3). (**d**) Immunostaining of encapsulated hHSPCs after 16 days in culture illuminated maintenance of $CD34^+$ hHSPCs (scale bar: 200 µm). (**e-g**) Phenotypic characterization by flow cytometry of hHSPCs after culture for 16 days in different hydrogels. Employing a set of 16 surface markers enabled the strict characterization of retrieved cells into (**e**) HSPCs or MyelPs, (**f**) in-turn HSPCs further subdivided in HSCs, MLPs and MPPs, and (**g**) MyelPs into CMP/MEP and B/NK/GMP (N = 4 for pure hydrogels, and N = 2 for hybrid). (**h**) To assess lineage commitment of hydrogel retrieved cells, they were cultured for 12 days in a differentiation cocktail of cytokines and colony-formation units (CFUs) were analyzed based on their morphology into erythrocytes (CFU-E), granulocytes (CFU-G), macrophages (CFU-M), granulocytes and macrophages (CFU-GM) or granulocytes, erythrocytes, macrophages and megakaryocytes (CFU-GEMM) (n = 3). All data are reported as mean ± standard error. ANOVA with Tukey's *post hoc* test * $P < 0.05$, ** $P < 0.01$, *** $P < 0.001$. For stacked graphics, statistics are color-coded to correspond to the specific population.

To assess the effect that encapsulation in different hydrogels has on the capacity of cells for lineage commitment, we performed the colony-formation unit (CFU) assay. Cells were retrieved from the TG-PEG, TG-HA or 50/50 hybrid scaffolds after 16 days in culture, and further plated in 2D for 12 days in a differentiation cocktail medium to stimulate hHSPC differentiation into different lineages. Based on their morphology, CFUs were then classified into different groups depending on whether they contained erythrocytes (CFU-E), granulocytes (CFU-G), macrophages (CFU-M), granulocytes and macrophages (CFU-GM) or granulocytes, erythrocytes, macrophages and megakaryocytes (CFU-GEMM). All cells expanded in the various 3D hydrogels were still able to differentiate into the different lineages, with a tendency that cells that had been cultured in TG-PEG were able to form more colonies (Figure 4 h). This demonstrates that in all hydrogels some of the encapsulated cells can retain their stem cell capacity after 16 days of culture.

Proliferation and differentiation of hHSPCs in TG-HA hydrogels is CD44 independent

CD44 is a cell surface protein involved in matrix adhesion that is present in many cell types, including hBMSCs[27] and hHSPCs[28], whose primary ligand is hyaluronic acid. It has been previously reported that a specific interaction between CD44 and hyaluronic acid is involved in HSPC trafficking to the bone marrow *in vivo* [29]. However, in our static setup, we did not observe significant differences between culture with or without HA in terms of cell morphology, stemness or differentiation. This led us to hypothesize that hHSPC differentiation into the corresponding lineages and maintenance of HSC stemness was CD44 independent in the presented biomimetic 3D hydrogels. To validate this hypothesis, we blocked CD44 on cells cultured in 3D ($1.5 \cdot 10^5$ cells per ml of TG-PEG or TG-HA) or 2D conditions over 2 weeks by the addition of an anti-CD44 antibody (Figure S5 a). Blockage of CD44 did not alter cell proliferation and resulted in similar HSPC population patterns. Even though, CD44 blocking slightly reduced the HSC population for both hydrogel conditions, there was not a stronger effect in the HA-containing hydrogels, confirming that the interaction of CD44 with HA is not key in the described system (Figure S5 b,

c, d). Once more, it was corroborated that HSCs differentiated towards an MLP-like phenotype when cultured in 2D, while in 3D HSC-like phenotypes were observed (Figure S5 c). Therefore, hHSPC culture and differentiation seems to not rely on CD44 interaction with the supporting microenvironment.

Hybrid hydrogels induce and maintain a bone marrow niche *in vivo*

After showing the potential of 50/50 TG-PEG/HA hybrid or pure TG-PEG and TG-HA hydrogels to recapitulate the stem cell niche *in vitro*, we set out to validate their use for *in vivo* applications. First, hydrogels were subcutaneously implanted for eight weeks in nude mice containing only a high concentration of BMP-2 (50 ng μl^{-1}) (Figure 5 a top). We carefully evaluated their stability over time, as well as their ability to recruit host cells and to remodel into a bone marrow-like structure, all key factors with which to comply in order to be further used as stem cell carriers. Similar bone volumes were accomplished among all the conditions as seen by micro-computed tomography (microCT) (Figure 5 b, c). As seen by histological evaluations, all hydrogels maintained their structure, were not reabsorbed, and allowed murine cell infiltration. In more detail, safranin-o/fast-green staining revealed that a bone shell was formed in all conditions, and that this shell was enclosing a marrow cavity (Figure 5 d). Interestingly, some hydrogel areas remained intact especially in the center of the implanted constructs, as seen by lack of cells in those areas. This absence of remodeling in the center of the all hydrogels shows that cells approached from the borders of the implant and infiltrated inwards, most likely by MMP-mediated degradation, in a similar manner for all hydrogel conditions.

Next, to augment the complexity of the setup and to better mimic a clinical setting where cells and growth factors are both delivered to the site of injury, we implanted hydrogels containing $20 \cdot 10^6$ hBMSCs per ml of hydrogel and a low BMP-2 concentration (10 ng μl^{-1}) for eight weeks subcutaneously in mice (Figure 5 a bottom). Similarly, all hydrogels formed comparable bone volumes and the presence of hBMSCs enabled bone formation despite supplying low BMP-2 amounts (Figure 5 b). While total bone volume was similar with or without cells, it was clear from microCT reconstructions and histology sections that ossicles with high BMP-2 formed a defined bone shell but little or no trabecular bone (Figure 5 c, d). Conversely, hydrogels containing hBMSCs with low BMP-2, likely due to the presence of embedded hBMSCs, were fully remodeled and did not contain any remaining hydrogel material after the eight weeks *in vivo*. In addition, the presence of human cells also led to high recruitment of host cells as seen by the presence of densely populated marrows. This shows that the implanted human cells, together with low BMP-2 supplementation, could more efficiently remodel the hydrogel backbone into a functional extracellular matrix structure for host cells (Figure 5 d). Immunostaining for human-specific collagen type I deposition revealed that in all hydrogels, human cells actively participated in forming bone matrix (Figure S6 a, b). This data shows that both hybrid similarly to completely synthetic hydrogels can serve as good bone marrow niche models.

TG-HA-containing hydrogels elicit lower murine immune cell infiltration

Successful clinical translation of any material requires its low immunogenicity upon implantation. As important and connected to the low immune response is the efficient delivery and engraftment of cells into the host. Thus, by specific immunostainings we evaluated both the number of host macrophages recruited and the number of human cells remaining in the different constructs eight weeks after implantation. In both conditions *in vivo*, either without cells and high BMP-2 or with hBMSCs and low BMP-2, a significantly lower number of F4/80 macrophages was found in pure TG-HA compared to pure TG-PEG hydrogels (Figure 5 e, f). Not surprisingly, the presence of macrophages was higher in both hydrogels when human cells were transplanted. Interestingly, in 50/50 TG-PEG/HA hydrogels the presence of macrophages was comparably low as in pure TG-HA hydrogels, indicating that the presence of even minimal concentrations of HA could reduce the mobilization of macrophages.

Furthermore, significantly more human cells persisted after eight weeks *in vivo* in pure TG-HA compared to pure TG-PEG hydrogels (Figure 5 e, g). Surprisingly, in the 50/50 TG-PEG/HA hydrogels, the number of human cells was not significantly higher compared to TG-PEG hydrogels. The higher number of human cells found in TG-HA hydrogels could be linked to the lower number of murine macrophages. Together, these observations indicate that TG-HA hydrogels are a better choice for delivery of hBMSCs, while pure TG-PEG are superior for the maintenance of hHSCs. Consequently, TG-PEG/HA hybrid hydrogels by adjusting the content of PEG and HA can likely be tailored for the optimized transplantation and engraftment of both stem cell types.

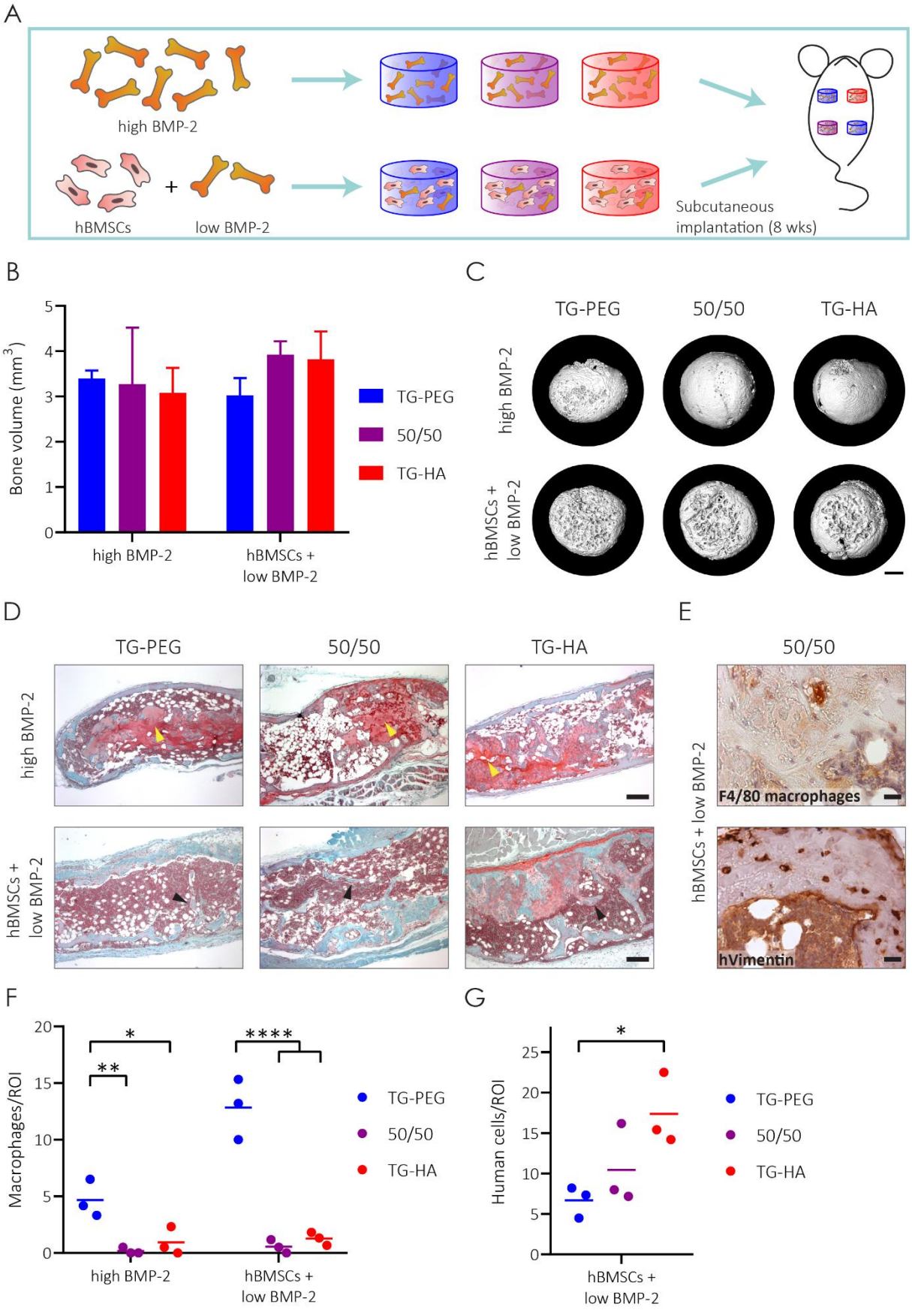

Figure 5. TG-PEG/HA hybrid hydrogels induce bone marrow niches *in vivo*

(**a**) TG-PEG, TG-PEG/HA (50/50) hybrid or TG-HA hydrogels containing either high BMP-2 concentrations (50 ng μl^{-1}) or hBMSCs ($20 \cdot 10^6$ cells per ml of hydrogel) and low BMP-2 concentrations (10 ng μl^{-1}) were subcutaneously implanted in nude mice for 8 weeks. (**b**) Evaluation of total bone volume of excised ossicles by microCT (n = 3). (**c**) Representative microCT reconstructions (scale bar: 1 mm) and (**d**) safranin-o/fast-green staining showing trabecular bone (black triangles) in hydrogels containing hBMSCs, and regions of un-remodeled hydrogel (yellow triangles) in high BMP-2 conditions (scale bars: 200 µm). (**e**) Representative immunohistochemistry staining of TG-PEG/HA (50/50) hybrid hydrogels with hBMSCs and low BMP-2 for F4/80 macrophages (top) and human specific vimentin (bottom) (scale bars: 20 µm). Quantification of (**f**) macrophages and (**g**) human cells per selected region of interests (ROI) for all the conditions (n = 3). All data are reported as mean ± standard error. ANOVA with Tukey's *post hoc* test * $P < 0.05$, ** $P < 0.01$, **** $P < 0.0001$.

Discussion

In this study, we presented a clinically-relevant seamless TG-PEG/HA hybrid hydrogel system that could be used to recapitulate the bone and bone marrow niche *in vitro* and was also validated as a growth factor or stem cell carrier *in vivo*. Starting from a fully synthetic PEG-based material we engineered a hybrid hydrogel by incorporating HA, a nonsulfated linear GAG highly abundant in many tissues and already used in the clinics for a few applications[11,30]. Compared to previously described GAG-based hybrid hydrogels[24,25], we present a simplistic method to tune the ratio of GAG present in the hydrogel while maintaining its stiffness. This approach overcomes limitations of earlier approaches that required synthesis of various hydrogel precursor batches with varying degrees of modification. The ability to seamlessly tune the GAG:PEG ratio is made possible here because both TG-HA and TG-PEG are equally functionalized and therefore participate equally in the enzymatic crosslinking of the hydrogel. A potential drawback of this setup, though, may be that the less controlled chemistry could potentially result in a heterogeneous scaffold. This, however, did not appear to be true as SEM imaging indicated similar microstructures among hydrogels. Even though for the present study we compared all hydrogel formulations at a consistently conserved stiffness, for other applications the gels can be easily customized on demand by simply altering their respective w/v concentrations without the need of further chemical modifications of the precursors.

It is important to remark that mechanical properties of the presented hydrogels were comparable, so that the results obtained could be attributed solely to the biological differences between the hydrogels and, thus, minimize the effect of mechanical influences. Also of high relevance is that all presented hydrogels had the same enzymatic crosslinking mechanism, which enabled their direct comparison, and foremost allowed facile hybrid hydrogel formation, making it in turn possible to observe dose-dependent effects such as HA-promoted proliferation. It is important to mention though, that despite the careful normalization of parameters, TG-PEG and TG-HA macromers have different structures and molecular weights. Even though the mechanical stress sensed by the encapsulated cells should be the same in all conditions as evidenced by matching storage moduli, we cannot discard that other effects could affect the cells. To completely rule out polymer topology effects, one would need low molecular weight 8-arm hyaluronan, but no synthesis is known for such a precursor and the biological recognition would risk being affected instead. Linear high

molecular weight PEG is also not readily side-functionalized. Apart from stiffness and biological signaling, well controlled in this study, there might be relevant differences in physicochemical properties and resulting interactions with cells and deposited matrix, due to the very different electrical charge, water organizing properties, hydrogen bonding, and polymer-polymer interactions that are provided by PEG versus HA. The effects observed here warrant further exploration and side-by-side comparison of various hydrogel backbones as a mean to fine-tune biological responses.

When recapitulating microenvironments *in vitro*, synthetic hydrogels have been of paramount importance to mimic these niches in a controllable and precise manner[31]. In this work we show that completely synthetic PEG-based hydrogels can host two fundamental stem cell types, hBMSCs and hHSPCs. Addition of hyaluronic acid enhanced proliferation of both cell types, an effect of HA that has been previously studied thoroughly and shown to hold true for several types of stem cells[32]. Moreover the additive proliferative effect between HA and the RGD adhesion peptide observed here aligned with previous results described for mouse cells[33].

However, higher proliferation did not translate into higher differentiation capacity in our setup. In the case of hBMSCs, we propose that upon osteogenic differentiation, cells reduce their proliferation[34], and thus, the HA proliferative effect is no longer noted. On the other hand, the higher cell proliferation of hHSPCs has been shown to result in differentiation of these cells towards more committed lineages[35].

The intriguing results showing a lack of CD44-specific effect of HA on the behavior of hHSPCs are at first glance contradictory with previous results[29]. HA has been reported to be involved in the trafficking of hematopoietic stem cells to the bone marrow, and thus associated with early changes of these cells towards a spindle-like morphology that translates into a change in their stemness and differentiation balance. However, in our setup cells are encapsulated and afforded little-to-no mobility in these small-pore hydrogels. Therefore, if CD44-HA interactions are involved in trafficking HSPCs to the bone marrow as previously reported, it can well be that our system does not mimic such *in vivo* situation, thus potentially explaining lack of CD44-specific effects seen here. Furthermore, in the previously mentioned findings, it was shown that the trafficking of HSPCs was synergistically regulated by CD44 availability along with the chemokine stromal cell-derived factor-1 (SDF-1), which is lacking in our setup and thus potentially a contributing reason to the lack of either morphological changes in our hHSPCs or other phenotypical differences. Another possibility that we cannot exclude is that encapsulated hHSPCs might deposit their own ECM (even low amounts of HA) in TG-PEG hydrogels as previously reported for hBMSCs[36], and thus closely interact with their own ECM instead of the given microenvironment. This could explain the observed reduction in the HSC population, when blocking with CD44, independent of the biomaterial used.

Key to clinical translation of any biomaterial is their lack of inducing an immunogenic response. Though all presented hydrogels elicited a low immunogenic response when implanted *in vivo*, the

significantly lower number of macrophages found in HA-containing hydrogels makes them a promising candidate for clinical use. These results aligned with other studies where they elegantly demonstrated an improvement in survival of transplanted retinal stem cells[37] or chondrogenic cells[38] when delivered in HA-based hydrogels. This effect could be explained by the use here of high molecular weight HA, which has previously been shown to downregulate inflammatory genes in macrophages, unlike low molecular weight HA[39,40]. Together with reduced immune response, the higher engraftment of human cells in HA-containing hydrogels overcomes undoubtedly one of the major limitations in clinical trials, the survival of transplanted cells[11]. To complement and validate this system towards clinical utility, future evaluations on less immunocompromised animal and injury models should be undertaken since it is also known that the T_H2-mediated immune response mediates tissue healing and regeneration[41].

In addition to the previously stated, lack of vascularization is a hindrance for tissue engineering success[42]. The need for cells to exchange nutrients, dissolved gases and waste is obvious. If scaffolds are not well vascularized, hypoxic conditions will first change the fate of the transplanted stem cells, and can even induce their death. We and others have previously shown that this cell-laden synthetic construct can be vascularized *in vitro* with the addition of endothelial cells[43,44], and that smart biomaterials functionalized with growth factors (e.g. VEGF) can *per se* elicit vascularization *in vivo*[45]. So ultimately taking the system complexity one step further, we envision the combination of the herein described tools with endothelial cells or functionalized smart materials. This could dramatically improve human cell survival and function *in vivo* by enabling more efficient vascularization within the host environment.

Without compromising biological performance, we could show vast improvements in reduced immunogenicity and donor cell engraftments, two parameters that are highly desirable for successful clinical translation of the proposed materials. The TG-PEG/HA hybrid hydrogel presents the benefits of both worlds. On one side the synthetic PEG part can be tuned to higher stiffness unlike HA, with controllable gelling times allowing easier use of the biomaterial, while the HA part confers higher cell proliferation and lower immunogenicity resulting in higher cell engraftment. With the increasing demand for personalized medicine, seamless tuning of biomaterials together with better characterization and understanding of stem cell populations holds great promise for successful clinical translation.

Conclusions

Concomitantly, we showed the tunability of synthetic hydrogels towards a more biological phenotype without loss of their physical or mechanical properties. Incorporation of hyaluronic acid in PEG hydrogels increased proliferation both for hBMSCs and hHSPCs. However, this increase in proliferation did not translate in higher osteogenic differentiation potential for hBMSCs *in vitro* nor *in vivo*. Strikingly, all 3D platforms significantly enhanced the maintenance of HSCs *in vitro*

compared to 2D cultures, and *in vivo* remodeled into a bone marrow-like environment. Crucially, hBMSC-laden hydrogels containing hyaluronic acid elicited a lower immunogenic response as seen by lower number of macrophages, which in turn resulted in higher number of remaining human cells. The easy tuning of the proposed 3D biomaterial and key higher human cell engraftment upon transplantation endow its use for a wide range of clinical applications.

Acknowledgements

We would like to thank Eva Avilla-Royo (University Hospital Zürich) for helpful discussions and manuscript editing; Esther Kleiner (University Hospital Zürich) for technical assistance in $CD34^+$ cell isolation and histological analysis; Lisa Krattiger (University Hospital Zürich) for technical assistance in CFUs and brightfield imaging; Prof. Franz Weber (University of Zürich) for the synthesis and purification of BMP-2; Flora Nicholls (University of Zürich) for animal care; Dr. Paolo Cinelli (University of Zürich) for support with microCT; the Center for Microscopy and Image Analysis for SEM imaging (University of Zürich); Prof. Ivan Martin (University Hospital of Basel) for isolation of hBMSCs. This work has been supported by the Swiss National Science Foundation (CR33I3_153316/1), and the Center for Clinical Research, University Hospital Zürich and University of Zürich.

Experimental procedures

All chemicals and materials were purchased from Sigma Aldrich or Thermo Fisher Scientific unless otherwise specified.

Hydrogel precursor synthesis and 3D hydrogel formation. TG-PEG and TG-HA precursors were synthesized as previously described [19] and [23], respectively.

Briefly, for **TG-PEG**, 8-arm PEG-VS (PEG-vinylsulfone, 40 kDa MW; NOF) was functionalized with peptides (obtained with a purity of > 95% from Bachem AG) that contained an earlier described cysteine cassette (ERCG) optimized for its reaction with PEG-VS and either a factor XIII (FXIII) glutamine acceptor substrate sequence (Gln; H-NQEQVSPL-ERCG-NH_2) or a matrix metalloproteinase degradable (*in italics*) lysine donor substrate ($MMP_{sensitive}$-Lys; Ac-FKGG-*GPQGIWGQ*-ERCG-NH_2). A 1.2 molar excess of peptides over PEG-VS was reacted in triethanolamine (TEA) at pH 8.0 for 2 h at 37 °C. Resulting 8-arm PEG-Gln and 8-arm PEG-$MMP_{sensitive}$-Lys precursors were excessively dialyzed against pure water, lyophilized and stored at -20 °C until further use.

For **TG-HA**, hyaluronic acid sodium salt (Lifecore Biomedical, 1.01-1.8 MDa) was substituted on its carboxylates with 3,3'-dithiobis(propanoic dihydrazide) (Frontier Scientific) using 1-ethyl-3-(3-dimethylaminopropyl)carbodiimide (EDC) couplings in MES buffer, initially pH 4.1 and evolving to pH 4.5 during the reaction, with molarities adjusted to provide substitution on 10% of the disaccharide repeat units (as monitored by NMR). The disulfides were then reduced with TCEP-HCl (Fluorochem), and the resulting thiolated HA was dialyzed against pure water. After reaction with a large excess of divinyl sulfone in TEA buffer, the resulting vinylsulfonated HA was again purified by dialysis, and finally substituted with either $MMP_{sensitive}$-Lys or Gln peptides with a second Michael addition in TEA buffer. After a final dialysis, the product was lyophilized and stored at -20° C until further use.

The crosslinking enzyme, transglutaminase FXIII (200 U ml^{-1}, Fibrogammin P, CSL Behring), was activated (FXIIIa) with thrombin (2 U ml^{-1}) for 30 min at 37 °C and stored in small aliquots at -80 °C until use.

3D TG-hydrogels formation. Stoichiometrically balanced solutions of 8-PEG-Gln and 8-PEG-$MMP_{sensitive}$-Lys or HA-Gln and HA-$MMP_{sensitive}$-Lys were prepared in Tris buffer (50 mM, pH 7.6) containing calcium chloride ($CaCl_2$, 50 mM). TG-PEG/HA hybrids were synthesized by combining different ratios of 1.5% (w/v) TG-PEG and 0.75% (w/v) TG-HA, resulting in the mixtures detailed in Table 1. Additionally, 50 μM Lys-RGD peptide (Ac-FKGG-RGDSPG-NH_2) and indicated amounts of cells and BMP-2 (produced as previously described[46]) were added to the precursor solution. Subsequently, hydrogel crosslinking containing the % in w/v indicated in Table 1 was initiated by the addition of 7.5 U ml^{-1} of activated transglutaminase factor XIII, followed by vigorous mixing. Disc-shaped matrices were prepared between hydrophobic glass slides (treated

with SigmaCote), and incubated for 30 min at 37 °C in a humidified atmosphere at 5% CO_2. After completed polymerization, hydrogels were released from glass slides and transferred to tissue-culture plates for *in vitro* experiments or stored in a humidified atmosphere for immediate *in vivo* implantation.

Table 1. Detailed percentages (w/v) selected per every hydrogel mixture

Nomenclature	% (w/v) TG-PEG	% (w/v) TG-HA
TG-PEG	1.5	0
TG-PEG/HA (75/25)	1.125	0.1875
TG-PEG/HA (50/50)	0.75	0.375
TG-PEG/HA (25/75)	0.375	0.5625
TG-HA	0	0.75

Hydrogel stiffness characterization by rheometry. Hydrogel gelation was analyzed on a rheometer (MCR 301, Anton Paar) equipped with 20 mm plate–plate geometry (PP20, Anton Paar) at 37 °C in a humidified atmosphere.

***In situ* rheology.** For *in situ* measurements gel mixtures were precisely loaded onto the center of the bottom plate. The upper plate was lowered to a measuring gap size of 0.2 mm, ensuring proper loading of the space between the plates and gel precursors, the dynamic oscillating measurement was then started. The evolution of storage modulus (G') and loss modulus (G") at a constant angular frequency of 1 Hz and constant shear strain of 4% was recorded for 30 min when equilibrium was reached. **Onset of polymerization** was determined as the time when the storage modulus would become higher than the loss modulus.

Swollen gels rheology. For measurements after swelling, hydrogels were prepared 24 h before measurements and incubated in Tris buffer at 37 °C. Swollen hydrogels were then loaded onto the rheometer, compressed by 10% and measured with a frequency sweep at 1% strain.

Swelling. Hydrogel mass was recorded immediately after gelation. Then gels were allowed to swell for 24 hours in Tris buffer at 37 °C and their mass was recorded again. Swelling was calculated as the ratio of swollen hydrogel mass at 24 h vs. just after gelation (1 h).

Scanning electron microscopy. For scanning electron microscopy (SEM), hydrogels were fixed in 50% osmium in phosphate buffered saline (PBS). After PBS washing, they were dehydrated by 30-minute incubation in 70% ethanol, followed by 80% and 100% ethanol and subsequently treated with hexamethyldisilazane (HMDS) for 1 hour, and then dried on air overnight. Lastly, samples were platinum sputter coated. Imaging was performed on a Zeiss Supra 50 VP at the UZH Center for Microscopy and Image Analysis (ZMB).

Human BMSC isolation and culture. Human bone marrow-derived stromal cells (hBMSCs) were isolated as described previously[47] from bone marrow aspirates of healthy donors obtained during orthopedic surgical procedures after informed consent and in accordance with the local ethical committee (University Hospital Basel; Prof. Dr. Kummer; approval date 26/03/2007 Ref Number 78/07). Cells were cultured at 37 °C in a humidified atmosphere at 5% CO_2 in MEMα (with nucleosides, Gibco) supplemented with fetal bovine serum (FBS, 10%, Gibco), penicillin (100 U ml^{-1}, Gibco), streptomycin (100 μg ml^{-1}, Gibco), and fibroblast growth factor 2 (FGF-2, 5 ng ml^{-1}, PeproTech). Cells were passaged before reaching 90% confluency, and medium was changed every 2-3 days.

Human $CD34^+$/hHSPC isolation and culture. Primary human $CD34^+$ cells were isolated from umbilical cord blood collected from healthy donors at the University Hospital Zürich after obtaining informed consent. The study was approved by the ethics board of the canton Zürich, Switzerland (approval date 21/03/2007; Ref Number 07/07). Blood (typically between 30-70 ml) was subsequently centrifuged to enrich for mononuclear cells, which were in turn further magnetically sorted based on their positive CD34 expression using positive immunomagnetic selection ($CD34^+$ MicroBead Kit, Miltenyi Biotec) according to the manufacturer's instructions. Cells were directly used or frozen down for future use. If frozen, cells were thawed in 50% IMDM 50% FBS, centrifuged 5 min at 300 g and subsequently cultured in 2D or encapsulated in hydrogels ($1.5 \cdot 10^6$ cells per ml of TG-PEG or TG-HA) as indicated. Cells were cultured in StemSpan SFEM (StemCell Technologies) complemented with penicillin (10 U ml^{-1}), streptomycin (10 μg ml^{-1}), human low density lipoprotein (hLDL, 10 μg ml^{-1}, StemCell Technologies), stem cell factor (hSCF, 100 ng ml^{-1}, PeproTech), thrombopoietin (hTPO, 100 ng ml^{-1}, Peprotech) and FMS-like tyrosine kinase 3 ligand (hFlt3L, 100 ng ml^{-1}, Peprotech). Cells were maintained in culture for up to 16 days at 37 °C in a humidified atmosphere at 5% CO_2. Medium was exchanged every 4 days.

CD44 blocking experiment. Cell pellets were incubated for 30 min with the antibody rat α-human CD44 antibody (clone Hermes-1), prior to being encapsulated in the different hydrogel conditions or plated as 2D controls. Lower cell concentration ($1.5 \cdot 10^5$ cells per ml of TG-PEG or TG-HA) were used in order to have more efficient antibody blocking. The antibody was later added in the cell medium at 5 μg ml^{-1} and changed every 4 days.

Cell Proliferation. Eight days post-encapsulation cell-laden hydrogels were washed with PBS and adenosine triphosphate (ATP) was measured using the CellTiter-Glo® luminescent cell viability assay (Promega) following the manufacturer's protocol.

Osteogenic differentiation of hBMSCs in 3D hydrogels. To assess hBMSC osteogenic differentiation in different hydrogels, hBMSCs from 3 different biological donors were encapsulated at $2 \cdot 10^6$ cells per ml of hydrogel. Encapsulated cells were then cultured for 12 days in osteogenic medium composed of MEMα (with nucleosides), FBS (10%), penicillin (100 U ml^{-1}), streptomycin (100 μg ml^{-1}), 10 mM HEPES, 1mM sodium pyruvate, 2 mM L-glutamine, 50 μg ml^{-}

[1] L-ascorbic acid, 10 mM β-glycerol phosphate and 100 ng ml^{-1} BMP-2. Medium was replaced every 4 days.

ALP staining. ALP staining was performed to whole hydrogels after 12 days in osteogenic differentiation medium using SIGMA*FAST* BCIP/NBT tablets. Briefly, medium was removed and hydrogels were washed with PBS and 200 µl of ALP substrate solution diluted according to the manufacturer's instructions was added. After 5 min the solution was removed, hydrogels were washed with PBS once and fixed with 4% paraformaldehyde (PFA) for 20 min at RT. Whole hydrogels were imaged with a digital camera (HDR XR 500, Sony).

ALP quantification. To measure ALP activity 12 days post-encapsulation, medium was removed, hydrogels were washed with PBS and hBMSCs were retrieved by digestion with collagenase A (100 µl, 2 mg ml^{-1} in PBS, Roche) at 37 °C for 30 min. Subsequently, cells were collected in 500 µl lysis buffer (0.56 M 2-amino-2-methyl-1-propanol, 0.2% Triton X-100, pH 10.0 in H_2O) and incubated for 30 min on ice. The cell lysate was then centrifuged at 16000 g for 10 min and the supernatant was collected. 50 µl ALP reagent (20 mM 4-nitrophenyl phosphate disodium salt hexahydrate, 4 mM $MgCl_2$ in lysis buffer) was added to 50 µl cell lysate in 96-wells and incubated at 37 °C for 10 min before the reaction was stopped by the addition of 100 µl NaOH (1 M). Finally, absorbance was measured at 410 nm with a microplate reader.

Immunocytochemistry of cells encapsulated in TG hydrogels.

Actin and DAPI. hBMSC-laden hydrogels were fixed in 4% paraformaldehyde for 30 min at room temperature (RT), followed by several washes of PBS and stored at 4 °C until staining. Cells were permeabilized in 0.1% Triton X-100 in 1% bovine serum albumin (BSA)/PBS at RT for 1 h. Next, samples were incubated with phalloidin-rhodamine (1:400) and 4',6-diamidino-2-phenylindole (DAPI, 1 µg ml^{-1}) in 1% BSA/PBS at RT for 3 hours followed by overnight washing.

CD34$^+$, actin and DAPI. Similarly, hHSPC-laden hydrogels were fixed in 4% paraformaldehyde for 30min at room temperature (RT), followed by washes of PBS and stored at 4 °C until staining. Cells were permeabilized in 0.1% Triton X-100 in 1% BSA/PBS at RT for 1 h. Next, samples were incubated with anti-human CD34 antibody overnight at 4 °C. Next day, hydrogels were washed three times for 1 h under shaking. Followed by incubation with secondary antibody, phalloidin-rhodamine (1:400) and 4',6-diamidino-2-phenylindole (DAPI, 1 µg ml^{-1}) in 1% BSA/PBS at RT for 4 hours followed by overnight washing. Detailed information about the used antibodies can be found in in Table 2. Gels were imaged with Leica TCS SP5 confocal microscope. Image analysis and processing were performed using Fiji.

hHSPC retrieval and preparation for flow cytometry analysis. To recover the encapsulated hHSPCs ($1.5 \cdot 10^6$ cells per ml of hydrogel), hydrogels were digested with collagenase A (100 µl, 2 mg ml^{-1}, Roche) at 37 °C for 30 min. In order to record adequate event numbers per sample during flow cytometry, the replicates (typically n = 3 unless differently stated) were pooled

for each condition and pelleted by centrifugation. The resulting pellet was resuspended in pre-warmed trypsin- ethylenediaminetetraacetic acid (EDTA) (100 µl per pellet) and incubated for 2 min at 37 °C to dissociate cell aggregates before being washed with FACS buffer (1 mM EDTA and 2% FBS in PBS). From the resulting suspension cells were ready for flow cytometry analysis and CFU assays.

Flow cytometry analysis. Cells were characterized by their surface expression of the following human markers: lineage (CD2, CD3, CD4, CD8, CD10, CD11b, CD14, CD19, CD20, CD56, CD235), CD45, CD34, CD38, CD90 and CD45-RA. Cells were stained for 30 min at 4 °C in the dark, washed, filtered through a 70 µm filter and analyzed by BD LSRFortessa. Dead cells were stained by Zombie Aqua AmCyan viability dye and were, alongside doublets, excluded from analysis. Data analysis was performed using FlowJo 10.0.8 software (TreeStar), and fluorescence minus one (FMO) control stainings were used for stringent gating. Detailed information about the used antibodies is in Table 2 and gating strategy example in Figure S4.

Colony forming units assay. To evaluate the functional potential of cells cultured in hydrogels, a colony forming unit (CFU) assay was performed[48]. Briefly, 1000 cells from each sample were resuspended in 1 ml of methylcellulose media (MethoCult H4230, StemCell Technologies) with 200 µl of IMDM + GlutaMAX supplemented with penicillin (10 U ml^{-1}), streptomycin (10 µg ml^{-1}), human interleukin 3 (hIL-3, 100 ng ml^{-1}, PeproTech), interleukin 6 (hIL-6, 50 ng ml^{-1}, PeproTech), stem cell factor (hSCF, 50 ng ml^{-1}, PeproTech), granulocyte macrophage colony stimulating factor (hGM-CSF, 250 ng ml^{-1}, PeproTech), thrombopoietin (hTPO, 250 ng ml^{-1}, PeproTech), FMS-like tyrosine kinase 3 ligand (hFlt3L, 50 ng ml^{-1}, R&D Systems), interleukin 11 (hIL-11, 50 ng ml^{-1}, PeproTech) and erythropoietin (hEPO, 20 U ml^{-1}, EPREX). Cells were then cultured in 9 cm^2 (6 well plate) for 12 days at 37 °C in a humidified atmosphere at 5% CO_2. At this time, CFUs were counted and categorized into the subcolonies containing erythrocytes (CFU-E), granulocytes (CFU-G), macrophages (CFU-M), granulocytes and macrophages (CFU-GM) or granulocytes, erythrocytes, macrophages and megakaryocytes (CFU-GEMM).

Animal care. All animal procedures were approved by the veterinary offices of the Swiss cantons Zürich under the ethical license (Application No. ZH169/2015). Experiments and handling of mice were conducted in accordance with the Swiss law of animal protection. 7-week-old immunodeficient HsdCpb:NMRI-*Foxn1^{nu}* (nude) female mice (purchased from Envigo) were used for the following experiments.

Subdermal implantation of hydrogels in mice. To create subcutaneous pouches in nude mice ca. 6 mm lateral skin incisions were made in four dorsal positions. Following randomization, pre-formed 20 µl gelled scaffolds (TG-PEG, TG-HA or 50/50 hybrid) containing high BMP-2 (50 ng $µl^{-1}$) or hBMSCs ($20 \cdot 10^6$ per ml of hydrogel) and low BMP-2 (10 ng $µl^{-1}$) were placed in these pouches. Incisions were closed with 6.0 Vicryl sutures (Ethicon) and animals were closely

monitored. Eight weeks post-implantation, animals were euthanized via CO_2 asphixiation, ossicles were retrieved and immediately fixed in 4% (v/v) formalin solution for 12 h at 4 °C.

Micro-computed tomography analysis at endpoints. After fixation in formalin and storage in PBS, ossicles were scanned in a microCT 40 (Scanco Medical AG). The X-ray tube was operated at an energy of 55 kVp and intensity of 72 μA at 4 W. Scans were executed at a high-resolution mode resulting in a voxel size of 10 μm. In reconstructed images bone tissue was segmented from background using a global threshold of 10% of maximum grey value. A cylindrical mask with a diameter of 5 mm was manually placed around the ossicle. Bone volume within the mask was measured using the ImageJ plugin BoneJ[49]. Reconstructions were assembled using the 3D Viewer plugin in ImageJ.

Histological and immunohistochemical studies. Next, samples were decalcified for 2 to 6 weeks in 10% EDTA solution with continuous shaking at 4 °C, followed by paraffin embedment and microtome sectioning at 4 μm. For histological stainings, hematoxylin & eosin (H&E) and safranin-o/fast-green stainings were performed using standard protocols.

Immunohistochemistry (IHC). For IHC, slides were deparaffinized and rehydrated. Next, different antigen retrievals were performed based on the needs of each staining. Collagen staining required enzymatic digestion with hyaluronidase (2 mg ml^{-1} in PBS) for 45 min, followed by 30 min incubation in pronase (1 mg ml^{-1} in PBS). Macrophage staining needed proteinase K-based retrieval (20 μg ml^{-1} in 50 mM Tris base, 1 mM EDTA, 5 mM $CaCl_2$, 0.5% Triton X-100 at pH 8.0), consisting of 15 min incubation at 37 °C. And last, for vimentin staining, heat antigen retrieval was performed, sections were incubated for 20 min at 90 °C in 10 mM sodium citrate, 0.05% Tween-20 at pH 6.0. All sections were then blocked for 1 h at room temperature in 1.5% BSA 0.5% Tween-20 in PBS, followed by 1ary antibody incubation overnight at 4 °C in PBS containing 1% BSA in a humidified chamber. Next day, sections were incubated with the corresponding 2ary antibody in PBS containing 1% BSA for 1 h at room temperature in the dark. Between individual incubation steps sections were rinsed three times with PBS containing 0.5% Tween-20. Finally, fluorescent slides were washed and mounted with fluorescent mounting medium containing DAPI (Abcam, ab104139). While for immunohistochemistry, DAB substrate chromagen (Abcam, ab64238) was applied to the slides for 5 minutes, followed by hematoxylin counterstaining and mounting in mounting medium (Abcam, ab128982). Table 2 details the employed antibodies and their concentrations. Images of histological staining and immunohistochemistry were acquired using a Zeiss 200M inverted microscope. For fluorescent stainings, Leica BM550B or inverted laser-scanning microscope Leica TCS SP5 were used. Images were processed in Fiji and Adobe Photoshop CS6. For cell quantification at least five different regions of interests (ROIs) from each section were selected and the number of cells was manually counted.

Statistical analysis. All data are reported as mean ± standard error. All statistical analyses were performed using GraphPad Prism (version 8.0.0, GraphPad Software). Mean values were compared by one-way or two-way analysis of variance (ANOVA) followed by Tukey's *post hoc* test

for multiple comparisons. Statistical significance was accepted for $P < 0.05$, and reported as follows * $P < 0.05$, ** $P < 0.01$, *** $P < 0.001$, **** $P < 0.0001$. For experiments involving different biological donors, a distinction between N (biological donors used) and n (technical replicates) was made. Further information is found in the particular figure legends.

Table 2. List of detailed antibodies used for flow cytometry and histological stainings

Antibody	Application & Dilution	Company	Catalog number
Mouse α hCD2 – PE-Cy5	FC 1:100	BioLegend	300209
Mouse α hCD3 – PE-Cy5	FC 1:100	BioLegend	300309
Mouse α hCD4 – PE-Cy5	FC 1:100	BioLegend	317411
Mouse α hCD8 – PE-Cy5	FC 1:100	BioLegend	300909
Mouse α hCD10 – PE-Cy5	FC 1:100	BioLegend	312206
Mouse α hCD11b – PE-Cy5	FC 1:100	BioLegend	301307
Mouse α hCD14 – PE-Cy5	FC 1:100	eBioscience	15-0149-41
Mouse α hCD19 – PE-Cy5	FC 1:100	BioLegend	302209
Mouse α hCD20 – PE-Cy5	FC 1:100	BioLegend	302307
Mouse α hCD56 – PE-Cy5	FC 1:100	BioLegend	304607
Mouse α hCD235a – PE-Cy5	FC 1:100	BD Biosciences	561776
Mouse α hCD45 – eFluor 450	FC 1:100	eBioscience	48-0459-42
Mouse α hCD34 – PE-Cy7	FC 1:50	BD Biosciences	561107
Mouse α hCD38 – FITC	FC 1:25	BD Biosciences	555459
Mouse α hCD45RA – APC-eFluor 780	FC 1:100	eBioscience	47-0458-42
Mouse α hCD90 – PE	FC 1:25	BD Biosciences	555596
Zombie Aqua Fixable Viability kit	FC 1:1000	BioLegend	423101
Rabbit α human CD34	IF 1:50	Abcam	ab81289
Rabbit α human collagen type 1	IHC 1:1000	Abcam	ab138492
Mouse α human vimentin	IHC 1:200	Abcam	ab8069
Rat α macrophage F4/80	IHC 1:50	BMA Biomedicals	T-2028
Isotype rabbit IgG control	IHC 1:200	Abcam	ab172730
Isotype mouse IgG1 control	IHC 1:200	Abcam	ab18448
Isotype rat IgG2 control	IHC 1:50	eBioscience	14-4321
Goat α rabbit AF488	IHC 1:200	Abcam	ab150077
Goat α rabbit HRP	IHC 1:200	Dako	P 0448
HRP Polymer α mouse	IHC kit	Dako	K 4006

Goat α rat HRP	IHC 1:200	Zymed	81-9520
Rat α human CD44	Neutralization	ThermoFisher	MA4400

FC: flow cytometry; IF: immunofluorescence; IHC: immunohistochemistry

References

1 Chan, C. K. *et al.* Identification of the human skeletal stem cell. *Cell* **175**, 43-56. e21 (2018).

2 Aguado, B. A., Grim, J. C., Rosales, A. M., Watson-Capps, J. J. & Anseth, K. S. Engineering precision biomaterials for personalized medicine. *Science translational medicine* **10**, eaam8645 (2018).

3 Méndez-Ferrer, S. *et al.* Mesenchymal and haematopoietic stem cells form a unique bone marrow niche. *Nature* **466**, 829 (2010).

4 Morrison, S. J. & Scadden, D. T. The bone marrow niche for haematopoietic stem cells. *Nature* **505**, 327 (2014).

5 Sorrentino, B. P. Clinical strategies for expansion of haematopoietic stem cells. *Nature Reviews Immunology* **4**, 878 (2004).

6 Hubbell, J. A. Biomaterials in tissue engineering. *Nature Biotechnology* **13**, 565-576 (1995).

7 Yannas, I., Lee, E., Orgill, D. P., Skrabut, E. & Murphy, G. F. Synthesis and characterization of a model extracellular matrix that induces partial regeneration of adult mammalian skin. *Proceedings of the National Academy of Sciences* **86**, 933-937 (1989).

8 Atala, A., Bauer, S. B., Soker, S., Yoo, J. J. & Retik, A. B. Tissue-engineered autologous bladders for patients needing cystoplasty. *The Lancet* **9518**, 1241-1246 (2006).

9 Marks, P., Witten, C. & Califf, R. Clarifying Stem-Cell Therapy's Benefits and Risks. *The New England journal of medicine* **376**, 1007-1009 (2017).

10 Ratcliffe, A. Difficulties in the translation of functionalized biomaterials into regenerative medicine clinical products. *Biomaterials* **32**, 4215-4217 (2011).

11 Wang, X., Rivera-Bolanos, N., Jiang, B. & Ameer, G. A. Advanced Functional Biomaterials for Stem Cell Delivery in Regenerative Engineering and Medicine. *Advanced Functional Materials*, 1809009 (2019).

12 Phinney, D. G. & Prockop, D. J. Concise review: mesenchymal stem/multipotent stromal cells: the state of transdifferentiation and modes of tissue repair—current views. *Stem cells* **25**, 2896-2902 (2007).

13 Lee, K. Y. & Mooney, D. J. Hydrogels for tissue engineering. *Chemical reviews* **101**, 1869-1880 (2001).

14 Caliari, S. R. & Burdick, J. A. A practical guide to hydrogels for cell culture. *Nature methods* **13**, 405 (2016).

15 Rehm, B. H. Bacterial polymers: biosynthesis, modifications and applications. *Nature Reviews Microbiology* **8**, 578 (2010).

16 Burdick, J. A. & Prestwich, G. D. Hyaluronic acid hydrogels for biomedical applications. *Advanced materials* **23**, H41-H56 (2011).

17 Lutolf, M. & Hubbell, J. Synthetic biomaterials as instructive extracellular microenvironments for morphogenesis in tissue engineering. *Nature biotechnology* **23**, 47-55 (2005).

18 Seliktar, D. Designing cell-compatible hydrogels for biomedical applications. *Science* **336**, 1124-1128 (2012).

19 Ehrbar, M. *et al.* Enzymatic formation of modular cell-instructive fibrin analogs for tissue engineering. *Biomaterials* **28**, 3856-3866 (2007).

20 Ehrbar, M. *et al.* Biomolecular hydrogels formed and degraded via site-specific enzymatic reactions. *Biomacromolecules* **8**, 3000-3007 (2007).

21 Lienemann, P. S. *et al.* A versatile approach to engineering biomolecule-presenting cellular microenvironments. *Advanced healthcare materials* **2**, 292-296 (2013).

22 Broguiere, N., Isenmann, L. & Zenobi-Wong, M. Novel enzymatically cross-linked hyaluronan hydrogels support the formation of 3D neuronal networks. *Biomaterials* **99**, 47-55 (2016).

23 Broguiere, N., Cavalli, E., Salzmann, G. M., Applegate, L. A. & Zenobi-Wong, M. Factor XIII cross-linked hyaluronan hydrogels for cartilage tissue engineering. *ACS Biomaterials Science & Engineering* **2**, 2176-2184 (2016).

24 Anjum, F. *et al.* Enzyme responsive GAG-based natural-synthetic hybrid hydrogel for tunable growth factor delivery and stem cell differentiation. *Biomaterials* **87**, 104-117 (2016).

25 Ranga, A., Lutolf, M. P., Hilborn, J. n. & Ossipov, D. A. Hyaluronic acid hydrogels formed in situ by transglutaminase-catalyzed reaction. *Biomacromolecules* **17**, 1553-1560 (2016).

26 Fuchs, E., Tumbar, T. & Guasch, G. Socializing with the neighbors: stem cells and their niche. *Cell* **116**, 769-778 (2004).

27 Pittenger, M. F. *et al.* Multilineage Potential of Adult Human Mesenchymal Stem Cells. *Science*, 143-147 (1999).

28 Dimitroff, C. J., Lee, J. Y., Rafii, S., Fuhlbrigge, R. C. & Sackstein, R. CD44 is a major E-selectin ligand on human hematopoietic progenitor cells. *The Journal of cell biology* **153**, 1277-1286 (2001).

29 Avigdor, A. *et al.* CD44 and hyaluronic acid cooperate with SDF-1 in the trafficking of human CD34+ stem/progenitor cells to bone marrow. *Blood* **103**, 2981-2989 (2004).

30 Park, Y. B., Ha, C. W., Lee, C. H., Yoon, Y. C. & Park, Y. G. Cartilage regeneration in osteoarthritic patients by a composite of allogeneic umbilical cord blood-derived mesenchymal stem cells and hyaluronate hydrogel: Results from a clinical trial for safety and proof-of-concept with 7 years of extended follow-up. *Stem cells translational medicine* **6**, 613-621 (2017).

31 Madl, C. M., Heilshorn, S. C. & Blau, H. M. Bioengineering strategies to accelerate stem cell therapeutics. *Nature* **557**, 335 (2018).

32 Sherman, L., Sleeman, J., Herrlich, P. & Ponta, H. Hyaluronate receptors: key players in growth, differentiation, migration and tumor progression. *Current opinion in cell biology* **6**, 726-733 (1994).

33 Lei, Y., Gojgini, S., Lam, J. & Segura, T. The spreading, migration and proliferation of mouse mesenchymal stem cells cultured inside hyaluronic acid hydrogels. *Biomaterials* **32**, 39-47 (2011).

34 Jaiswal, N., Haynesworth, S. E., Caplan, A. I. & Bruder, S. P. Osteogenic differentiation of purified, culture-expanded human mesenchymal stem cells in vitro. *Journal of cellular biochemistry* **64**, 295-312 (1997).

35 Ogawa, M. Differentiation and proliferation of hematopoietic stem cells. *Blood* **81**, 2844-2853 (1993).

36 Blache, U. *et al.* Notch-inducing hydrogels reveal a perivascular switch of mesenchymal stem cell fate. *EMBO reports* **19**, e45964 (2018).

37 Ballios, B. G. *et al.* A hyaluronan-based injectable hydrogel improves the survival and integration of stem cell progeny following transplantation. *Stem Cell Reports* **4**, 1031-1045 (2015).

38 Cavalli, E. *et al.* A comparative study of cartilage engineered constructs in immunocompromised, humanized and immunocompetent mice. *Journal of Immunology and Regenerative Medicine* **2**, 36-46 (2018).

39 McKee, C. M. *et al.* Hyaluronan (HA) fragments induce chemokine gene expression in alveolar macrophages. The role of HA size and CD44. *The Journal of clinical investigation* **98**, 2403-2413 (1996).

40 Rayahin, J. E., Buhrman, J. S., Zhang, Y., Koh, T. J. & Gemeinhart, R. A. High and low molecular weight hyaluronic acid differentially influence macrophage activation. *ACS biomaterials science & engineering* **1**, 481-493 (2015).

41 Sadtler, K. *et al.* Developing a pro-regenerative biomaterial scaffold microenvironment requires T helper 2 cells. *Science* **352**, 366-370 (2016).

42 Rouwkema, J., Rivron, N. C. & van Blitterswijk, C. A. Vascularization in tissue engineering. *Trends in biotechnology* **26**, 434-441 (2008).

43 Blache, U. *et al.* Dual Role of Mesenchymal Stem Cells Allows for Microvascularized Bone Tissue-Like Environments in PEG Hydrogels. *Advanced healthcare materials* **5**, 489-498 (2016).
44 Levenberg, S. *et al.* Engineering vascularized skeletal muscle tissue. *Nature biotechnology* **23**, 879 (2005).
45 Zisch, A. H. *et al.* Cell-demanded release of VEGF from synthetic, biointeractive cell ingrowth matrices for vascularized tissue growth. *The FASEB journal* **17**, 2260-2262 (2003).
46 Weber, F. E. *et al.* Disulfide bridge conformers of mature BMP are inhibitors for heterotopic ossification. *Biochemical and Biophysical Research Communications* **286**, 554-558 (2001).
47 Papadimitropoulos, A. *et al.* Expansion of human mesenchymal stromal cells from fresh bone marrow in a 3D scaffold-based system under direct perfusion. *PloS one* **9**, e102359 (2014).
48 Miller, C. L. & Lai, B. in *Basic Cell Culture Protocols* 71-89 (Springer, 2005).
49 Doube, M. *et al.* BoneJ: free and extensible bone image analysis in ImageJ. *Bone* **47**, 1076-1079 (2010).

Supplementary data

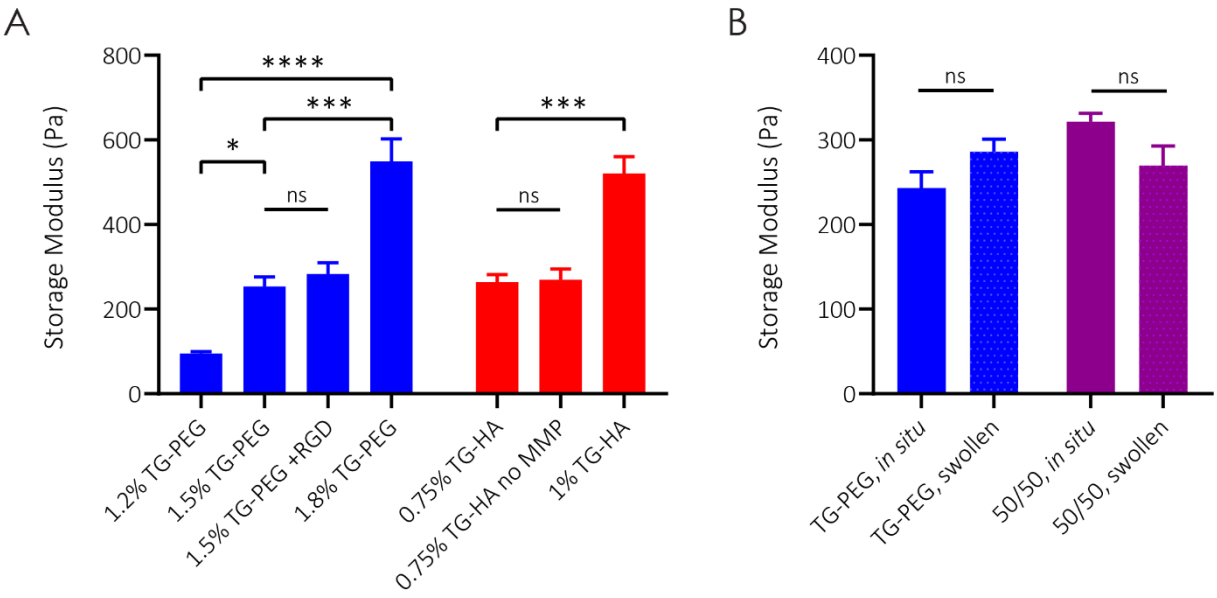

Figure S1. Mechanical characterization of TG-hydrogels

(**a**) Storage moduli of different crosslinking densities of TG-PEG and TG-HA measured by *in situ* rheological analysis after reaching equilibrium at 30 minutes, and effect on stiffness of cell-adhesion peptide RGD or MMP-degradable site incorporation in the hydrogel backbone (n = 3). (**b**) Storage moduli of swollen hydrogels compared to *in situ* measurements (n = 4). All data are reported as mean ± standard error. ANOVA with Tukey's *post hoc* test * $P < 0.05$, *** $P < 0.001$, **** $P < 0.0001$, ns: no significant.

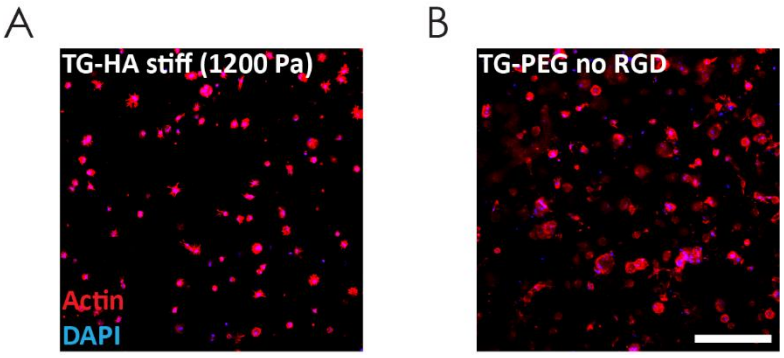

Figure S2. Spreading of hBMSCs in TG-hydrogels

Actin and DAPI staining at day 3 of hBMSCs encapsulated at $2 \cdot 10^6$ cells per ml of hydrogel in (**a**) high stiffness TG-HA hydrogels (1200 Pa of storage modulus, equivalent to 2% (w/v) TG-HA), or in (**b**) TG-PEG hydrogels (280 Pa of storage modulus, equivalent to 1.5% (w/v) TG-PEG) lacking the cell-adhesion RGD peptide (scale bar: 200 µm).

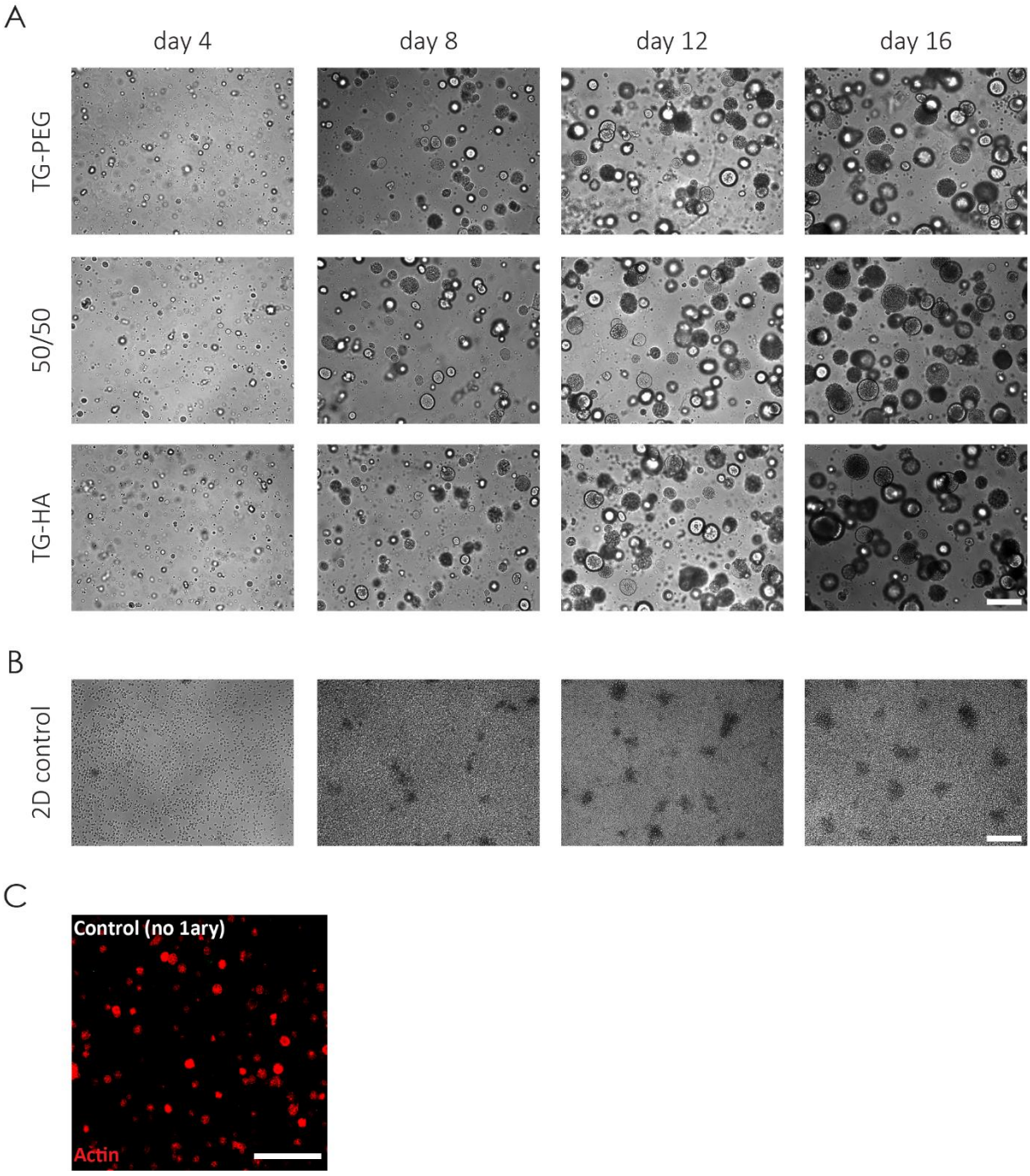

Figure S3. Assessment of hHSPCs cultured in TG-hydrogels

(**a**) Brightfield imaging of longitudinal growth and morphological changes of hHSPCs encapsulated at $1.5 \cdot 10^6$ cells per ml in pure TG-PEG or TG-HA or in hybrid TG-PEG/HA hydrogels over 16 days culture (scale bar: 200 µm). (**b**) Brightfield images of hHSPCs cultured in 2D (scale bar: 200 µm). (**c**) Immunostaining control of $CD34^+$ and actin, lacking the primary antibody (scale bar: 200 µm).

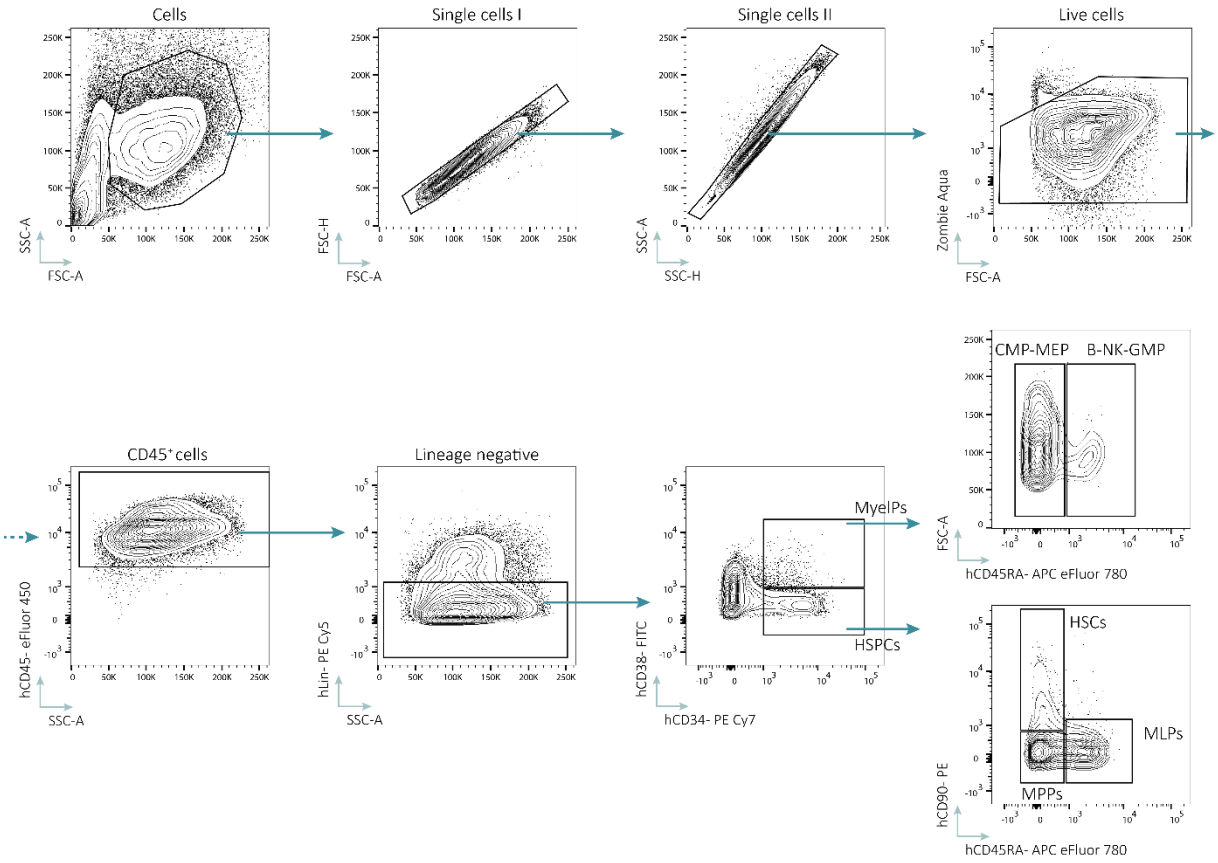

Figure S4. Flow cytometry gating strategy to characterize hHSPCs subpopulations

Cells retrieved from hydrogels after 16 days in culture were analyzed by a set of 16 surface markers. Single and live cells were pre-selected and further classified into hematopoietic stem and progenitor cells (HSPCs, Lin$^-$ CD34$^+$ CD38$^-$), myeloid progenitors (MyelP, Lin$^-$ CD34$^+$ CD38$^+$), hematopoietic stem cells (HSCs, Lin$^-$ CD34$^+$ CD38$^-$ CD45RA$^-$ CD90$^+$), multipotent progenitors (MPPs, Lin$^-$ CD34$^+$ CD38$^-$ CD45RA$^-$ CD90$^-$), multilymphoid progenitors (MLPs, Lin$^-$ CD34$^+$ CD38$^-$ CD45RA$^+$ CD90$^-$), common myeloid progenitors/ megakaryocyte-erythrocyte progenitors (CMP/MEP, Lin$^-$ CD34$^+$ CD38$^+$ CD45RA$^-$) or B-/Natural Killer- cell progenitors/granulocyte-macrophage progenitors (B/NK/GMP, Lin$^-$ CD34$^+$ CD38$^+$ CD45RA$^+$). Fluorescence minus one (FMO) and isotype controls were used to design the gates.

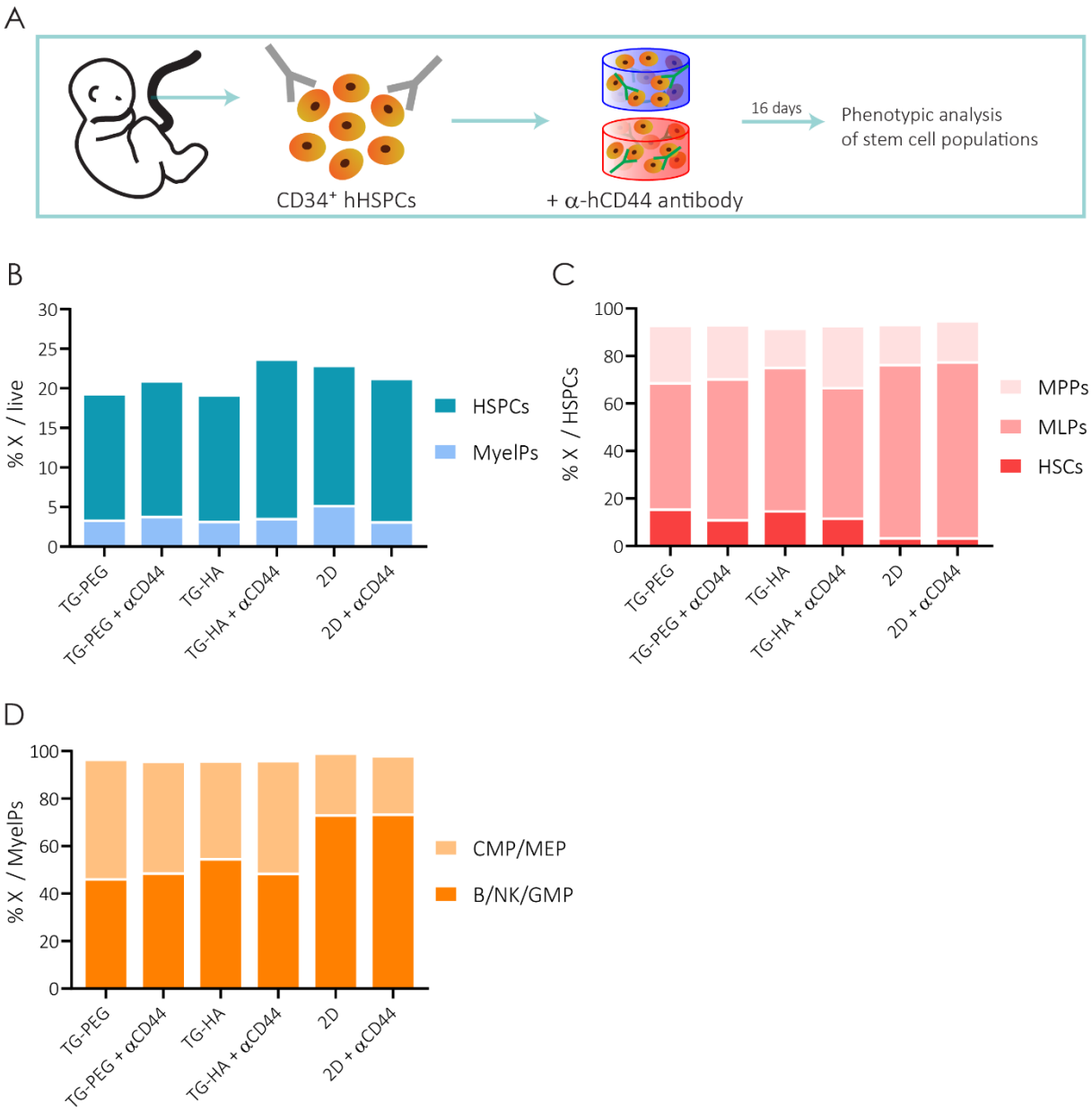

Figure S5. Culture of hHSPCs *in vitro* in TG-HA hydrogels is CD44 independent

(**a**) Scheme of hHSPC isolation from umbilical cord blood, followed by selection based on CD34⁺, and their encapsulation at $1.5 \cdot 10^5$ cells per ml of TG-PEG or TG-HA hydrogel with continuous addition of anti-hCD44 antibody. After 16 days in culture, cells were retrieved from 3D hydrogels or collected from 2D controls, and phenotypic stem cell populations were characterized into (**b**) HSPCs or MyelPs, and in turn HSPCs subdivided in (**c**) HSCs, MLPs and MPPs, while MyelPs were further restricted into (**d**) CMP/MEP and B/NK/GMP (N = 1).

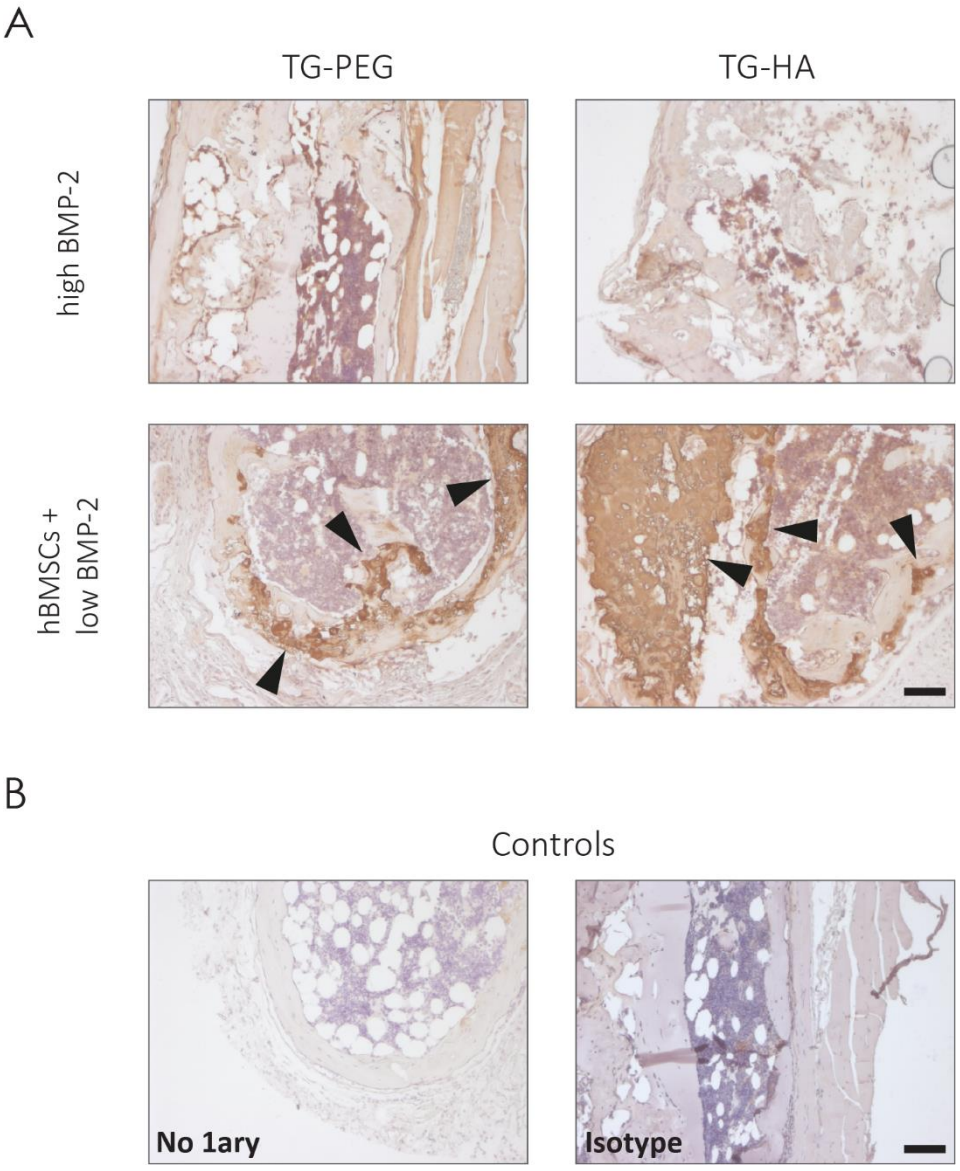

Figure S6. Transplanted hBMSC remodeling and ECM deposition

(**a**) Immunostaining for human-specific collagen type I in implanted hydrogels revealed that when hBMSCs are transplanted in TG-hydrogels, cells participated in forming a bone-like ECM structure (scale bar: 100 µm). (**b**) Control staining with no primary antibody or isotype antibody (scale bar: 100 µm).

We are inspired by one another
to accomplish things far greater
than what we could ever do on our own.
– Drew Brees

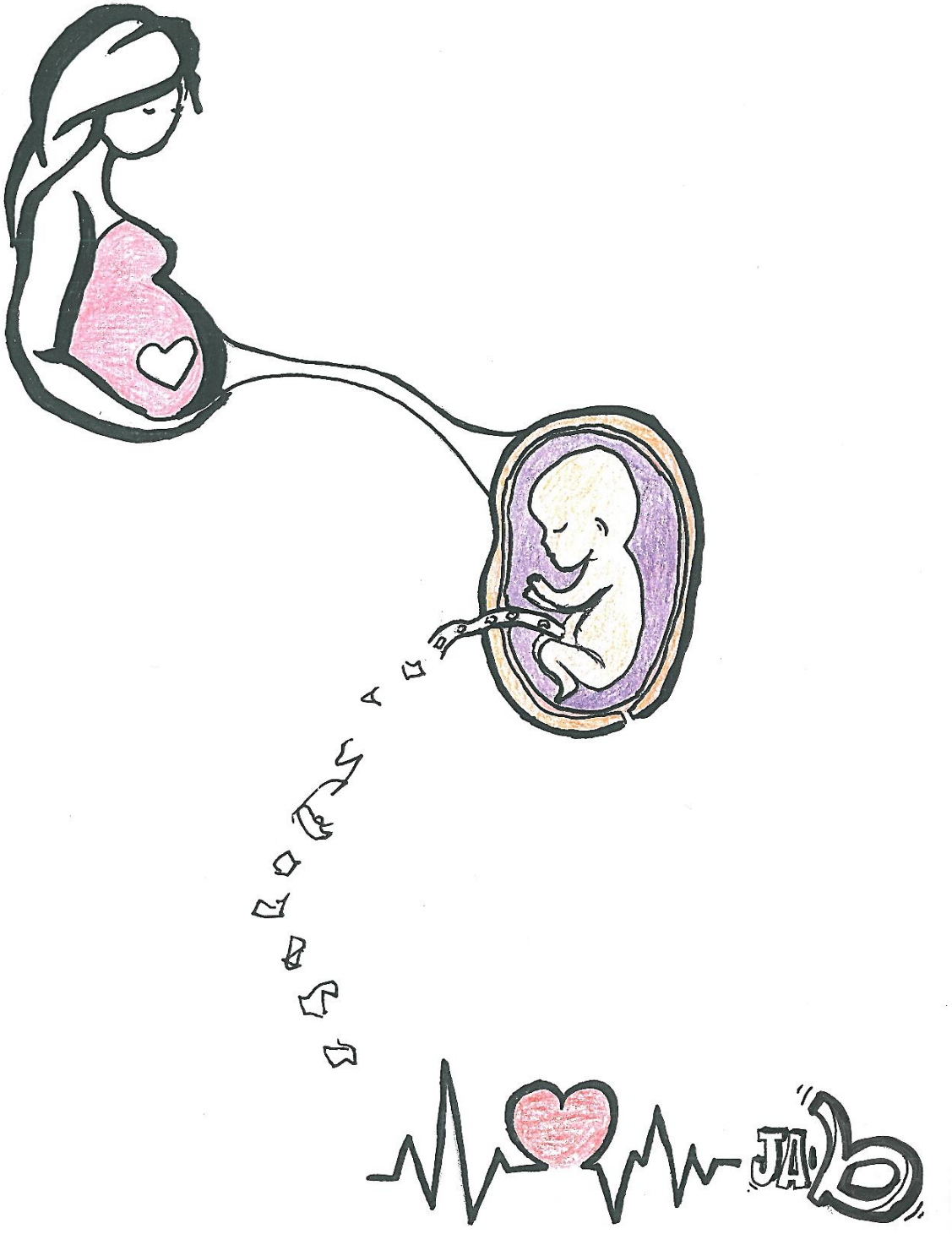

Artwork by Anna Noguer Vallmajó, Joan Presas Palet and Biel Presas Noguer
La Bisbal d'Empordà, Catalunya

CHAPTER 6

Synthetic modular hydrogels foster functional expansion of human hematopoietic stem cells

Q Vallmajo-Martin[1,2], V Lysenko[3], L Krattiger[1], A Theocharides[3], M Ehrbar[1]

The content of this chapter is part of a manuscript in preparation.

[1] Laboratory for Cell and Tissue Engineering, Department of Obstetrics, UniversitätsSpital Zürich, Switzerland;
[2] Laboratory of Stem Cell Bioengineering, Institute of Bioengineering, École Polytechnique Fédérale de Lausanne, Switzerland;
[3] Laboratory of Experimental Hematology, Department of Hematology, UniversitätsSpital Zürich, Switzerland.

Statement of contributions

QVM designed, conducted, and analyzed all the experiments.

VL & AT assisted and performed the NSG transplantation experiments.

LK performed and analyzed rheological experiments and collected flow cytometry data from stiffness experiments.

ME designed experiments and supervised the whole project.

Abstract

Deficiency in the number of hematopoietic stem cells (HSCs) available for bone marrow transplants remains a major challenge in medicine today. HSCs grown *in vitro* rapidly lose their regenerative capacity likely due to the lack of niche-derived signals comprising molecular and cellular components. Identification of critical hematopoietic niche components necessitates the generation of more tractable *in vitro* platforms. Here, we engineered blank synthetic poly(ethylene glycol)-based (TG-PEG) hydrogels to recapitulate the hematopoietic niche *in vitro*. Owing to the modular design of these hydrogels, we could systematically assess how individual niche parameters guide human HSC proliferation and stemness. While RGD-mediated adhesion was found to not play a role, inhibition of matrix-metalloproteinases (MMPs) halted HSC expansion in 3D hydrogels. Cultures in soft matrices resulted in greater expansion of phenotypic HSCs when compared to stiff hydrogels. Additionally, the presentation of hydrogel-immobilized Notch ligands in soft hydrogels significantly enhanced the expansion of HSCs, but failed ensure their long-term reconstitution capacity. Strikingly, long-term *in vivo* multipotency of cultured HSCs could be obtained by three-dimensional culture in unmodified TG-PEG hydrogels. This minimalistic human bone marrow analogue presents a potent tunable platform for the discovery of critical hematopoietic stem cell niche factors.

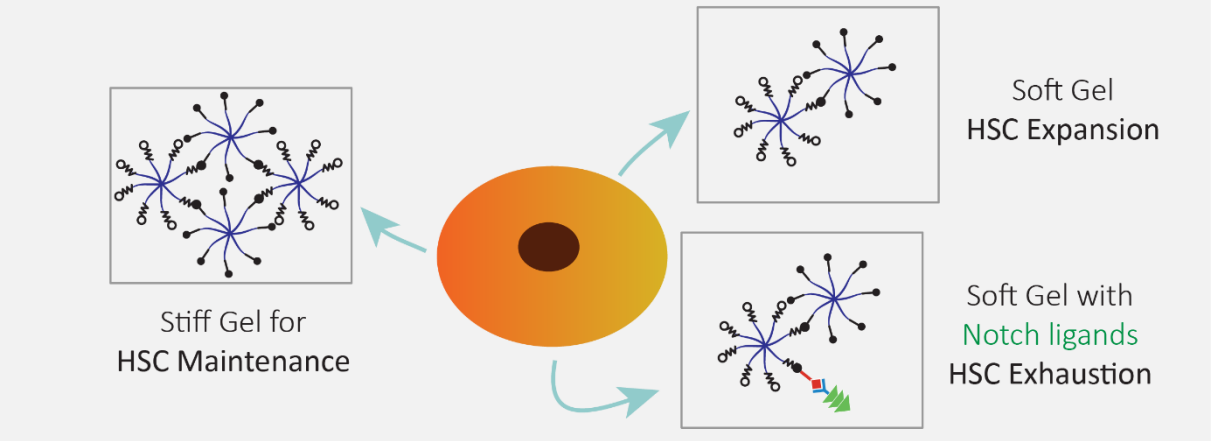

Keywords: Hematopoietic stem cell, bone marrow niche, 3D *in vitro* model, biomedical engineering

Introduction

Hematopoietic stem cells (HSCs) are the seed of continually differentiating and self-renewing multipotent cells that eventually give rise to all mature blood and immune cells for an entire lifetime[1,2]. The marked regenerative capacity of these cells has enabled the success of bone marrow transplantations to treat patients with life-threatening hematological disorders since the 1960s[3]. However, the full clinical potential of HSCs has been hampered by the failure of host engraftment, limited host regeneration, and lack of successful HSC *ex vivo* expansion techniques that would facilitate and promote their applicability. HSCs rapidly lose their potential and, therefore, their healing capacity when removed from their microenvironment (i.e. the hematopoietic stem cell niche)[4,5]. Consequently, a deeper understanding of the contributing factors within this niche could open up the possibilities for broader therapeutic use of these cells.

Sophisticated *in vivo* models have shown that the HSC niche exists as a dynamically orchestrated milieu of complex cellular, molecular and mechanical factors that tightly control HSC proliferation, self-renewal, differentiation, quiescence and dormancy[5,6]. Some of the fundamental components of the niche comprise osteoblasts[7,8], stromal cells[9,10], endothelial cells[11] and the sympathetic nervous system[12], as well as molecular factors including growth factors, cytokines and chemokines[13,14]. Despite the value of wholistic *in vivo* models comprising the full complexity of the bone marrow niche, the need for dissecting the individual contributions has urged the development of more simplistic *ex vivo* strategies.

This has prompted recent attempts to use 3D bioengineered scaffolds to recapitulate the HSC niche *in vitro*. For instance, co-culture of human bone marrow stromal cells (hBMSCs) and HSCs in macroporous biomaterials highlighted the importance of stromal cells to maintain HSC functionality[15,16]. Hydrogels have also been essential in explicating HSC fate decisions in both natural[17,18] and synthetic[19,20] approaches, with the latter offering the advantage to uncouple biophysical and biochemical factors for individual study[20-22].

Motivated by these findings, we employed a previously reported fully defined 3D hydrogel based on poly(ethylene glycol) (PEG)[23,24] crosslinked by the transglutaminase factor XIII (TG-PEG). Its biomimetic modular design and lack of inherent biological properties has made TG-PEG an ideal substrate to evaluate a variety of biological processes including bone regeneration[25], muscle stem cell-renewal[26], cardioprogenitor differentiation[27], perivascular niche interactions[28], single cell murine HSC fate choices[21,22] and recently, intestinal organoid development[29]. Here, we sought to tailor TG-PEG hydrogels to explore the effect of different parameters including stiffness, cell-matrix interaction, proteolytic degradability, and presentation of specific bone marrow niche ligands on human HSCs.

Our data indicate that stiffer hydrogels maintain a significantly higher population of phenotypic HSC-like cells (Lin^- $CD34^+$ $CD38^-$ $CD90^+$ $CD45RA^-$) at the cost of limiting their expansion, while cells cultured in soft conditions significantly expand to higher numbers, yet undergo lineage

commitment towards a multilymphoid progenitor (MLP)-like phenotype (MLPs, Lin^- $CD34^+$ $CD38^-$ $CD45RA^+$ $CD90^-$). However, this can be altered by the addition of Notch signaling-related ligands such as Jagged1 or Delta-like-canonical Notch ligand 4 (DLL4) which, while promoting cell proliferation, serve to maintain their stem-like phenotype as validated in CFU-experiments. Intriguingly, upon transplantation into irradiated NSG mice, $CD34^+$ hematopoietic cells cultured in TG-PEG surrogates containing the Jagged1-ligand could only successfully reconstitute the hematopoietic system for up to 4 months, indicating the presence of short-term HSCs (ST-HSCs) in this condition, but not long-term (LT-HSCs) counterparts. $CD34^+$ hematopoietic cells retrieved from either soft or stiff TG-PEG hydrogels, in contrast, engrafted at least up to 6 months indicating the presence of functional LT-HSCs in synthetic hydrogels. Taken all together, this tunable TG-PEG platform holds promise to serve as a model to screen and evaluate novel HSC niche participants.

Results

Synthetic hydrogels support the expansion of cbHSPCs

To establish basic conditions for the expansion of HSCs *in vitro,* we encapsulated human umbilical cord blood-derived $CD34^+$ hematopoietic stem and progenitor cells, herein referred to as cbHSPCs, in TG-PEG hydrogels ($1.5 \cdot 10^6$ cells per ml). To facilitate the reciprocal interaction of cbHSPCs with their microenvironment, hydrogels contained matrix metalloproteinase (MMP)-sensitive sites and were endowed with RGD adhesion peptides (50 μM) (Figure 1 a). cbHSPCs encapsulated in 3D hydrogels acquired a distinctive morphology, and often grew as individual sphere-shaped cell clusters already visible after 8 days in culture, as observed by scanning electron microscope (SEM) imaging and confocal imaging of actin/DAPI staining (Figure 1 b). Indeed, quantification of DNA content showed that cbHSPCs significantly proliferated over time in these minimal microenvironments (Figure 1 c).

We next wondered whether immunophenotypically defined HSCs (Lin^- $CD34^+$ $CD38^-$ $CD45RA^-$ $CD90^+$) and their immediate progeny comprising multipotent progenitors (MPPs, Lin^- $CD34^+$ $CD38^-$ $CD45RA^-$ $CD90^-$) and multilymphoid progenitors (MLPs, Lin^- $CD34^+$ $CD38^-$ $CD45RA^+$ $CD90^-$) were present after 16 days in culture in these synthetic matrices, as previously reported for natural analogues[17,18]. Stiffness of the materials was matched in order to exclude substrate stiffness as a source of any observed differences. For this, the crosslinking density of PEG precursors was tuned to obtain TG-PEG hydrogels featuring a storage modulus of 30 Pa, like 3D natural matrices (i.e. collagen, fibrin and Matrigel) (Figure S1 a). When cbHSPCs were encapsulated in these various hydrogels for 16 days, no significant differences in overall proliferation were observed (Figure S1 a). Subsequently, cells were retrieved and rigorously characterized by flow cytometry (Figure S2: gating strategy, Table 1: specified cell phenotypes, Table 2: list of used antibodies). Even though all conditions contained HSCs, MLPs and MPPs, there was a notably higher percentage of HSCs

and lower MLPs in TG-PEG hydrogels, highlighting the potential use of fully defined synthetic matrices for cbHSPCs culture (Figure S1 b).

Next, to determine if integrin-mediated adhesion was required for expansion of cbHSPCs in TG-PEG hydrogels, we compared the populations of cells after 16 days in culture in hydrogels lacking vs. containing the RGD sequence. Strikingly, the absence of cell attachment sites did not affect cell population distributions nor expansion potential (Figure 1 d–f). This shows that cbHSPCs do not depend on matrix adhesion for their maintenance and expansion. Intrigued to elucidate whether these cells remodel their microenvironment, we added GM6001, a broad spectrum MMP inhibitor (50 μM), to the cultures. Notably, MMP inhibition shifted cells towards a lineage-committed phenotype dramatically reducing myeloid progenitors (MyelP, Lin^- $CD34^+$ $CD38^+$) and mildly diminishing HSPCs (Lin^- $CD34^+$ $CD38^-$) (Figure 1 g). However, the distribution of phenotypes within the HSPC population was maintained, and HSCs were still present (Figure 1 h). Remarkably though, the expansion of HSPCs and HSCs were both reduced to less than half (Figure 1 i), showing that these cells do need MMPs to proliferate.

Microenvironmental stiffness modulates HSPC stemness and expansion balance

Previously, the use of PEG-heparin hybrid hydrogels for 3D culture of HSPCs indicated a positive correlation between the number of long-term culture-initiating cells and the heparin concentration in the hydrogel[20]. In that study, however, it could not be determined whether the effects on HSPCs were attributed to presence of higher amounts of biologically active heparin, or to increased stiffness of the hydrogel due to higher heparin concentrations. To determine if hydrogel stiffness alone impacts HSPC behavior, we formed TG-PEG hydrogels with identical composition but increasing crosslinking density. Rheological measurements showed that by varying the concentration of TG-PEG precursors, hydrogels with at least 2 orders of magnitude in storage moduli (i.e. ranging from 0.04 ± 0.01 kPa to 9.61 ± 0.51 kPa) could be formed (Figure 2 a). We next encapsulated equal numbers of cbHSPCs in hydrogels of increasing stiffness, and observed that cells rapidly adapted very different morphologies depending on the substrate stiffness (Figure S3). Even though in all conditions, cells developed into characteristic clusters, the size and number of clusters were considerably distinct. Cells grown in soft substrates formed more and bigger clusters compared to stiff hydrogels, likely due to physical constraints. Total cell proliferation over 16 days in culture was reduced in hydrogels with increased stiffness, as assessed by DNA content quantification (Figure 2 a).

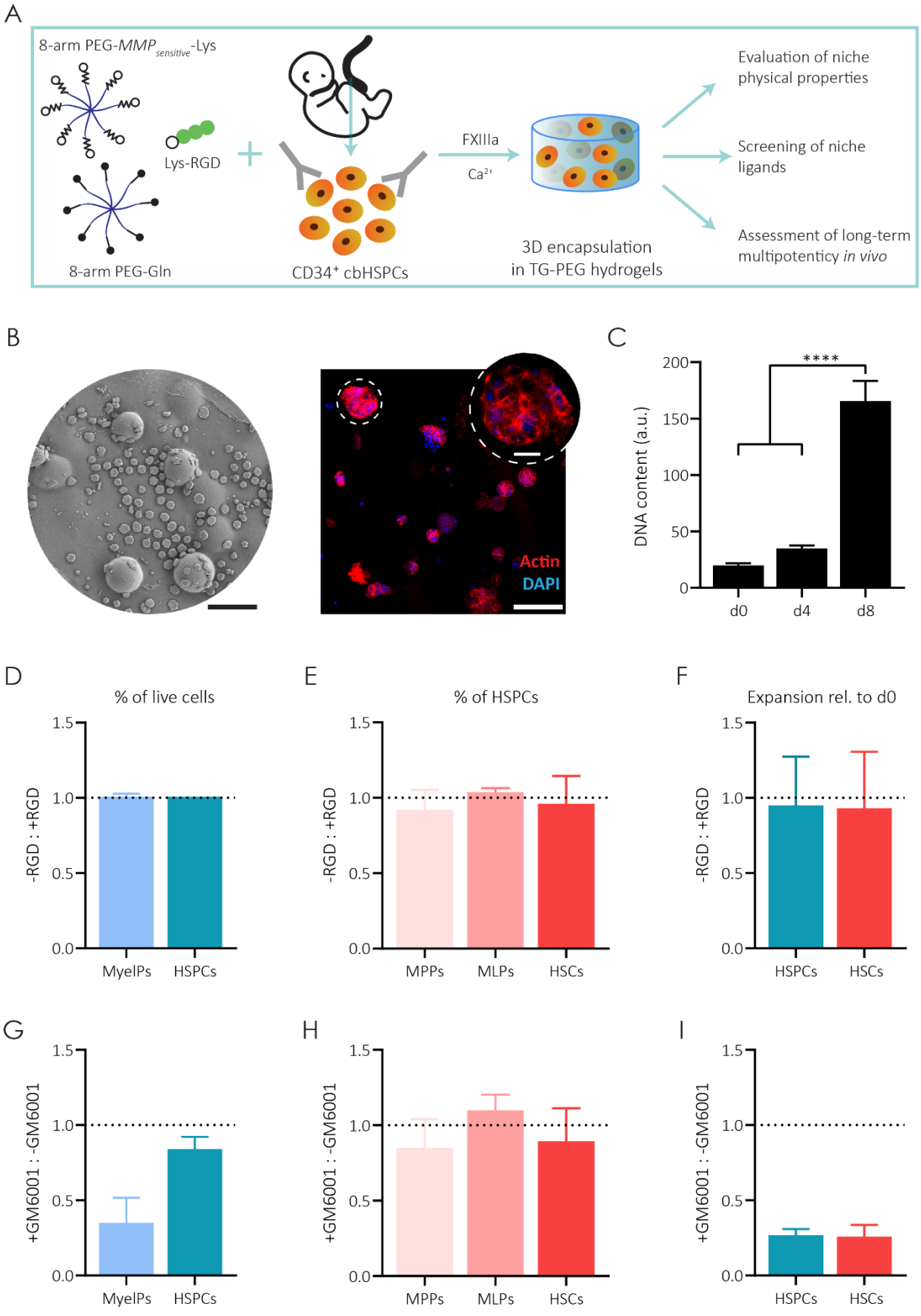

Figure 1. ECM-mimicking minimalistic matrices for cbHSPC culture

(**a**) Cord blood-derived CD34⁺ HSPCs ($1.5 \cdot 10^6$ cells per ml of hydrogel) were encapsulated in a PEG-based synthetic matrix. Inspired by natural extracellular matrices, RGD was added to the system and PEG precursors were modified with MMP-sensitive

degradable sites. Lastly, transglutaminase (TG) FXIII was added in the presence of calcium to initiate hydrogel crosslinking, hence the TG-PEG nomenclature. This system was used to systematically study the effect of physical and biological microenvironmental factors on culture of cbHSPCs. (**b**) cbHSPCs cultured in TG-PEG gels grew as individual sphere-shaped cell clusters as seen by scanning electron microscope (SEM) imaging (left, scale bar: 50 µm) and confocal laser scanning microscopy (CLSM) imaging of actin and DAPI (right, scale bar: 50 µm, inlet 10 µm). (**c**) Total encapsulated cells in TG-PEG proliferated exponentially during 8 days, as seen by an increase in the DNA content (n = 4). (**d-f**) The effect of the RGD cell-adhesion peptide was assessed by comparing cells encapsulated in TG-PEG hydrogels with or without the peptide. Data expressed as a ratio of found in –RGD : +RGD, (**d**) MyelP and HSPC percentages of total live cells, (**e**) MPP, MLP and HSC percentages within HSPCs, (**f**) expansion relative to day 0 of HSPCs and HSCs after 16 days culture (N = 3). (**g-h**) The effect of blocking cbHSPC MMPs by the addition of GM6001 MMP inhibitor was assessed by comparing cells encapsulated in TG-PEG hydrogels with or without the inhibitor. Data expressed as a ratio of found in +GM6001 : – GM6001, (**g**) MyelP and HSPC percentages of total live cells, (**h**) MPP, MLP and HSC percentages within HSPCs, (**i**) expansion relative to day 0 of HSPCs and HSCs after 16 days culture (N = 3). Dotted lines represent ratio 1, meaning no change between conditions. All data are reported as mean ± standard error. ANOVA with Tukey's *post hoc* test **** P < 0.0001.

When cells were analyzed after 16 days in culture, strikingly, both HSPCs and HSCs were significantly enriched in stiffer versus soft hydrogels reaching up to 24.83% of HSPCs of total live cells, from which a 34.11% were HSCs for 7.7 kPa TG-PEG hydrogels (Figure 2 b, c). These reported high percentages in stiff hydrogels were similar to those at day 0, indicating maintenance of HSPC and HSC populations in stiff conditions (Figure S4 a). In contrast, MyelP subpopulations, common myeloid progenitors/megakaryocyte-erythrocyte progenitors (CMP/MEP, Lin^- $CD34^+$ $CD38^+$ $CD45RA^-$) and B-/Natural Killer- cell progenitors/granulocyte -macrophage progenitors (B/NK/GMP, Lin^- $CD34^+$ $CD38^+$ $CD45RA^+$), were not significantly altered by increasing substrate stiffness (Figure 2 d).

Stiffer hydrogels, despite significantly increasing stem cell-like populations, resulted in overall lower HSPC and HSC expansion over time in culture, while softest hydrogels (0.04 kPa) accomplished up to 11.05 x and 5.82 x expansion of HSPCs and HSCs, respectively (Figure 2 e). It is also worth mentioning that a plateau in HSPC and HSC populations were observed at hydrogels above 6.3 kPa, where no expansion of stem cells was detected. Furthermore, encapsulated cells were compared to cbHSPCs cultured in 2D conditions. In 2D culture over 16 days, cbHSPCs rapidly lost phenotypically defined HSPC and HSC populations, resulting in lower percentages than in any other hydrogel condition. Additionally, achieved HSPC and HSC expansion were both reduced from soft hydrogels (Figure S4 b).

Conclusively, due to the fully defined TG-PEG approach employed, featuring the absence of any biochemical signals, we show that stiffness solely can control HSPC and HSC balance between maintaining a stem cell-like phenotype and cell expansion.

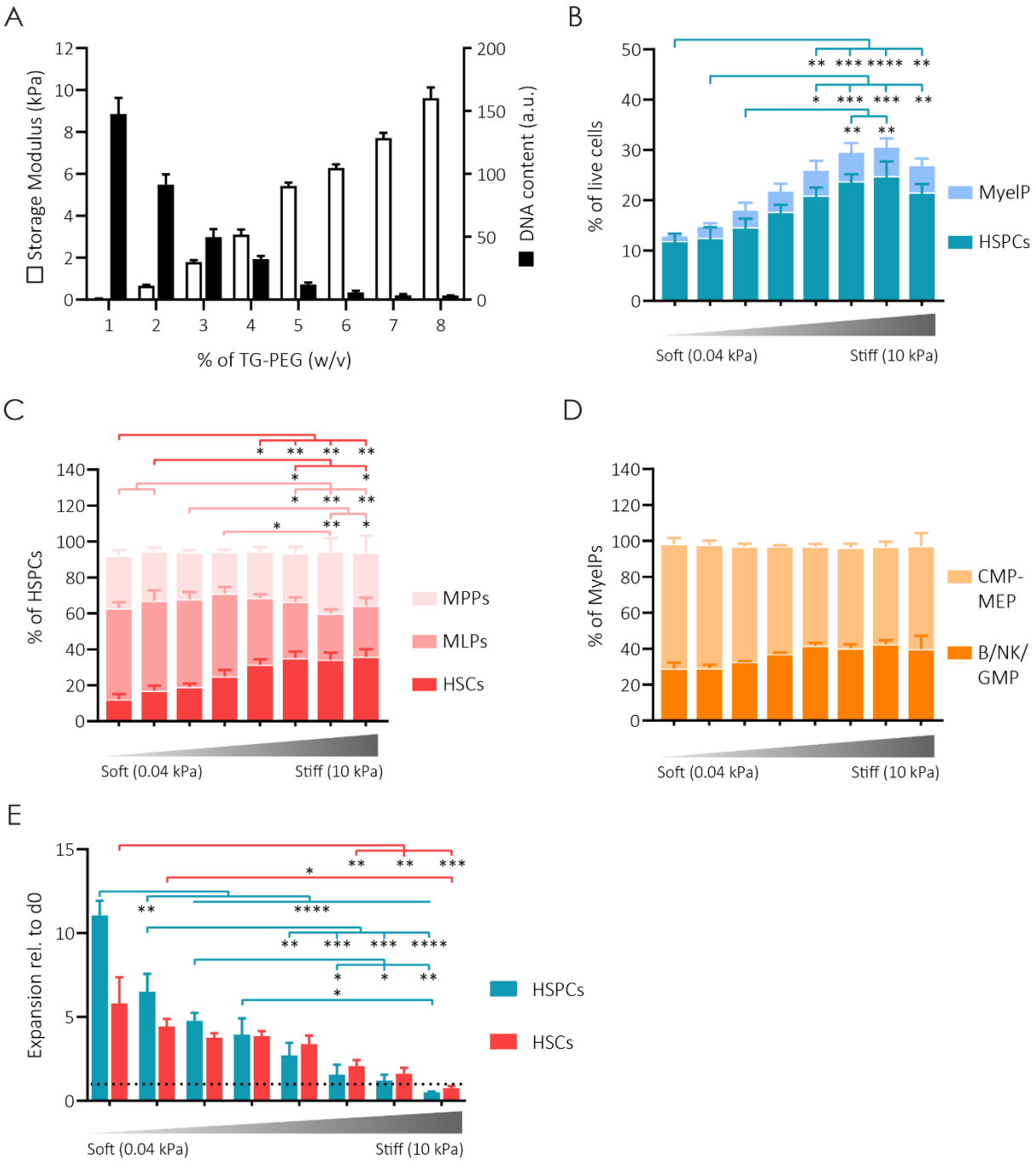

Figure 2. Microenvironmental stiffness regulates HSPC stemness and expansion

(**a**) Storage moduli of TG-PEG hydrogels (left axis, white bars) and DNA content at day 16 of total encapsulated cells (right axis, black bars) with increasing crosslinking density (n = 3). (**b-d**) Characterization of the specific populations found in cells cultured 16 days in the different hydrogel conditions. (**b**) MyelPs and HSPCs were determined as percentage of total live cells, (**c**) next MPPs, MLPs and HSCs were defined within HSPCs, and (**d**) last CMP/MEP and B/NK/GMP within MyelPs, (N = 3). (**e**) Expansion relative to day 0 of HSPCs and HSCs over 16 days cultured in hydrogels featuring different stiffness (N = 3). Dotted line indicates no expansion (i.e. one-fold). All data are reported as mean ± standard error. ANOVA with Tukey's *post hoc* test * $P < 0.05$, ** $P < 0.01$, *** $P < 0.001$, **** $P < 0.0001$.

Notch signaling ligand modified TG-PEG hydrogels promote selective expansion of HSCs

To further evaluate other parameters relevant to the hematopoietic stem cell niche, a soft (0.5 kPa) and a stiff (5 kPa) hydrogel were selected for the following evaluations. Fc-tagged niche-related ligands were immobilized within the TG-PEG backbone by incorporating a synthetic antibody-binding protein (a protein A analogue) into the hydrogel precursor mix (Figure 3 a). This included several cell-cell adhesion molecules: E-selectin, vascular cell adhesion molecule-1 (VCAM), E-cadherin and N-cadherin; cell surface proteins: Jagged1 and DLL4; and soluble factors: angiopoietin and stromal cell-derived factor-1α (SDF-1). Significantly higher percentages of HSPC and HSC-populations were detected for Jagged1 and DLL4-containing soft hydrogels as compared to no ligand or IgG controls (Figure 3 b, c). A similar pattern was also observed when ligands were incorporated in stiff hydrogels, even though the effects were dampened (Figure 3 e, f). In soft conditions, these increases in HSPC and HSC populations in Notch ligand-containing hydrogels stemmed from significantly higher cell expansion than without the ligand (Figure 3 d). Conversely, in stiff hydrogels containing Notch ligands, expansion remained similar to control conditions (Figure 3 g). This shows that cells are highly maintained as stem-like in stiff hydrogels, yet there is reduced expansion (< five-fold), likely due to the physical constraints that cells growing in these stiff matrices encounter. Taken all together, this demonstrates that soft hydrogels with Notch ligands did specifically expand the HSC and HSPC population, unlike stiff hydrogels that merely maintained the stem cell-like phenotype by reducing proliferation.

To have a first insight into the lineage potential of the cells encapsulated with Jagged1, they were subjected to colony forming units (CFU) assay. CFUs were counted based on their morphology into the subcolonies containing erythrocytes (CFU-E), granulocytes (CFU-G), macrophages (CFU-M), granulocytes and macrophages (CFU-GM) or granulocytes, erythrocytes, macrophages and megakaryocytes (CFU-GEMM). In line with the flow cytometry results, cells retrieved from Jagged1-soft hydrogels increased two-fold total CFU formation compared to control soft gels (Figure 3 h). More specifically CFU-GEMM colonies were up to four-fold more abundant in modified gels. The same held true in stiff hydrogels displaying higher CFU capacity on cells isolated from Jagged1-hydrogels, reflecting the higher percentage of stem cell-like cells in this condition (Figure 3 i). Yet, in stiff gels this increase was less pronounced than in soft analogues, as seen by the 2.5-fold more abundant CFU-GEMM in modified stiff gels, again in line with flow cytometry results.

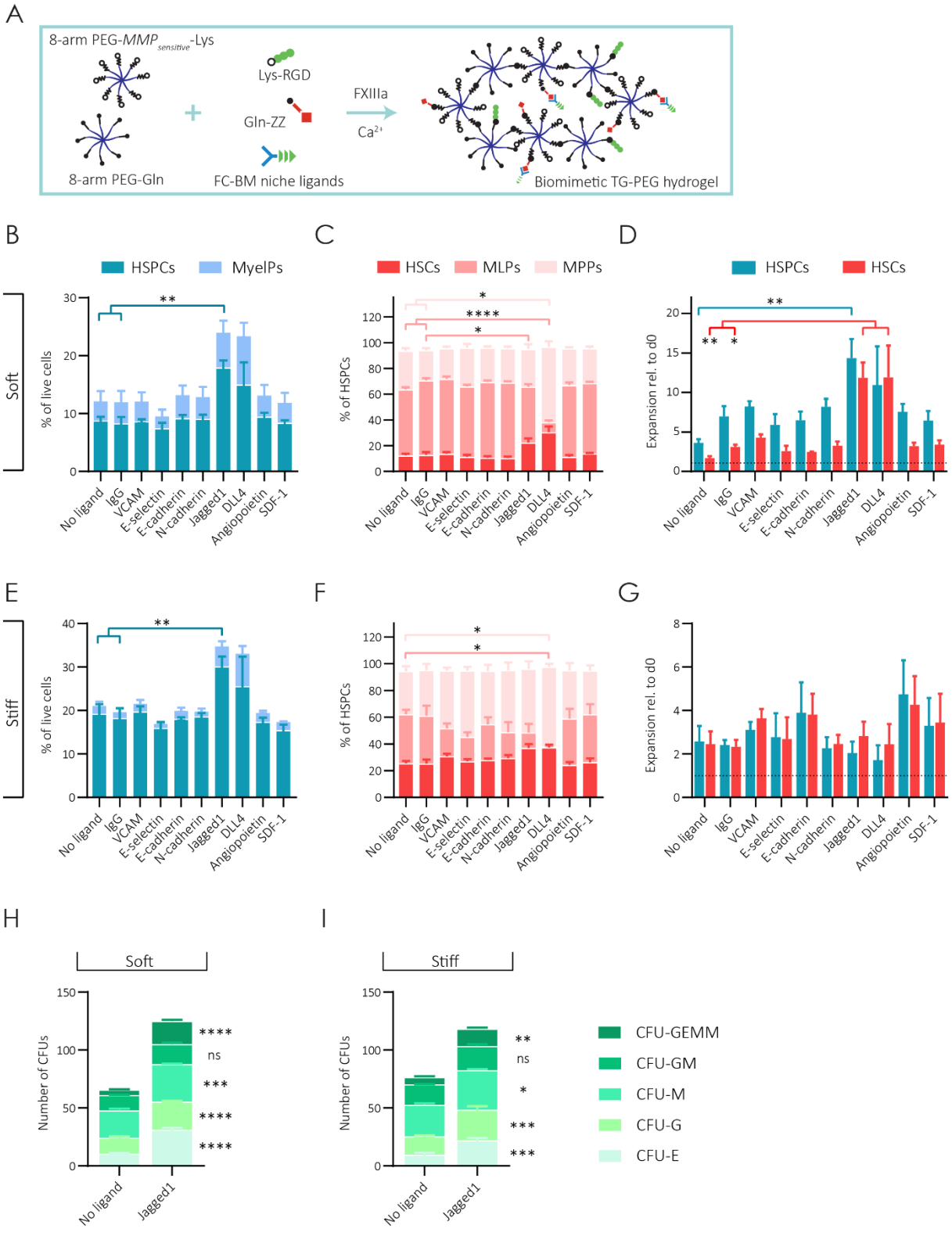

Figure 3. Screening bone marrow niche ligands impact on to cbHSPCs differentiation

(**a**) Overview of the immobilization strategy of niche-related ligands in the minimalistic microenvironment. Selected Fc-tagged ligands (vascular cell adhesion molecule-1 (VCAM), E-selectin, E-cadherin, N-cadherin, Jagged1, Delta-like-canonical Notch ligand 4 (DLL4), angiopoietin, stromal cell-derived factor-1α (SDF-1), and IgG control) were bound to an antibody binding protein (synthetic protein ZZ, a protein A analogue) that in turn was modified with the Gln-acceptor sequence in order to seamlessly be incorporated into the hydrogel backbone. (**b-d**) cbHSPCs were then cultured in soft matrices for 16 days when (**b**) HSPC and MyelP populations were determined as percentage of total live cells, and (**c**) furthermore, HSCs, MLPs and MPPs

were defined within HSPCs. (**d**) Expansion of HSPCs and HSCs relative to day 0 after 16 days cultured in soft matrices with different ligands (N = 4). (**e-g**) Next, cbHSPCs were cultured in stiff matrices for 16 days when (**e**) HSPC and MyelP populations were determined as percentage of total live cells, and (**f**) HSCs, MLPs and MPPs were defined within HSPCs. (**g**) Expansion relative to day 0 of HSPCs and HSCs over 16 days cultured in stiff matrices with different ligands (N = 4). (**h**) Distribution of different types of colonies based on their morphology formed by cells expanded in soft hydrogels containing or not Jagged1 (n = 3). (**i**) Idem for cells expanded in stiff hydrogels containing or not Jagged1 (n = 3). Dotted line indicates no expansion (i.e. one-fold). All data are reported as mean ± standard error. ANOVA with Tukey's *post hoc* test * P < 0.05, ** P < 0.01, *** P < 0.001, **** P < 0.0001.

HSPCs cultured in synthetic hydrogels maintain multipotency

Because HSCs can reconstitute the complete hematopoietic system for an entire lifetime, their stem potential must be proved by the capacity to regenerate and maintain the entire hematopoietic system[30]. To this aim, we transplanted equal numbers ($2.5 \cdot 10^5$ cells per animal) of sorted Lin^- $CD34^+$ cells, that had been cultured for 2 weeks in either soft TG-PEG hydrogels, soft hydrogels containing Jagged1, stiff hydrogels or in 2D culture, via intrafemoral injection into irradiated NOD/SCID gamma (NSG) mice (Figure 4 a). We then longitudinally evaluated the long-term repopulation capacity of these human cells by evaluating their participation in the reconstitution of the peripheral blood (PB) compartment (percentage of human $CD45^+$ over total mouse/human $CD45^+$ cells). Chimerism was already detected after 4 weeks of transplantation. Even though up to week 16 similar engraftment occurred for all conditions, cells derived from soft hydrogels containing Jagged1 ligand failed to long-term reconstitute the hematopoietic system (Figure 4 b). The same number of freshly isolated Lin^- $CD34^+$ cells that had not been in culture were used as control. These cells showed a higher repopulation capacity, as expected, reaching 50% of humanization in PB at week 20 (Figure S4 c). While same number of transplanted cells cultured in 2D conditions resulted in absence of chimerism for most cases (Figure S4 d). Interestingly, cells cultured in both soft and stiff hydrogels showed similar reconstitution potential and therefore contained multipotent HSCs. However, it is worth mentioning that over 16 days in culture, in soft hydrogels there were 2.4-fold more $CD34^+$ cells compared to stiff hydrogels. This, together with the *in vivo* results indicates that cbHSPCs cultured in soft TG-PEG hydrogels result in the highest number of functional HSCs.

Finally, detailed analysis of human cells showed that they underwent differentiation into diverse lineages (Figure 4 c). The specific human subpopulations in the PB revealed a prevalence of lymphoid B cells ($hCD19^+$, about 70% of total human cells), and almost absence of natural killer cells ($hCD335^+$) independently of the culture condition. Remarkably, cells from stiff hydrogels resulted in higher lymphoid T cells ($hCD3^+$), as well as significantly augmented myeloid ($hCD33^+$) and HSPCs in the PB compartment.

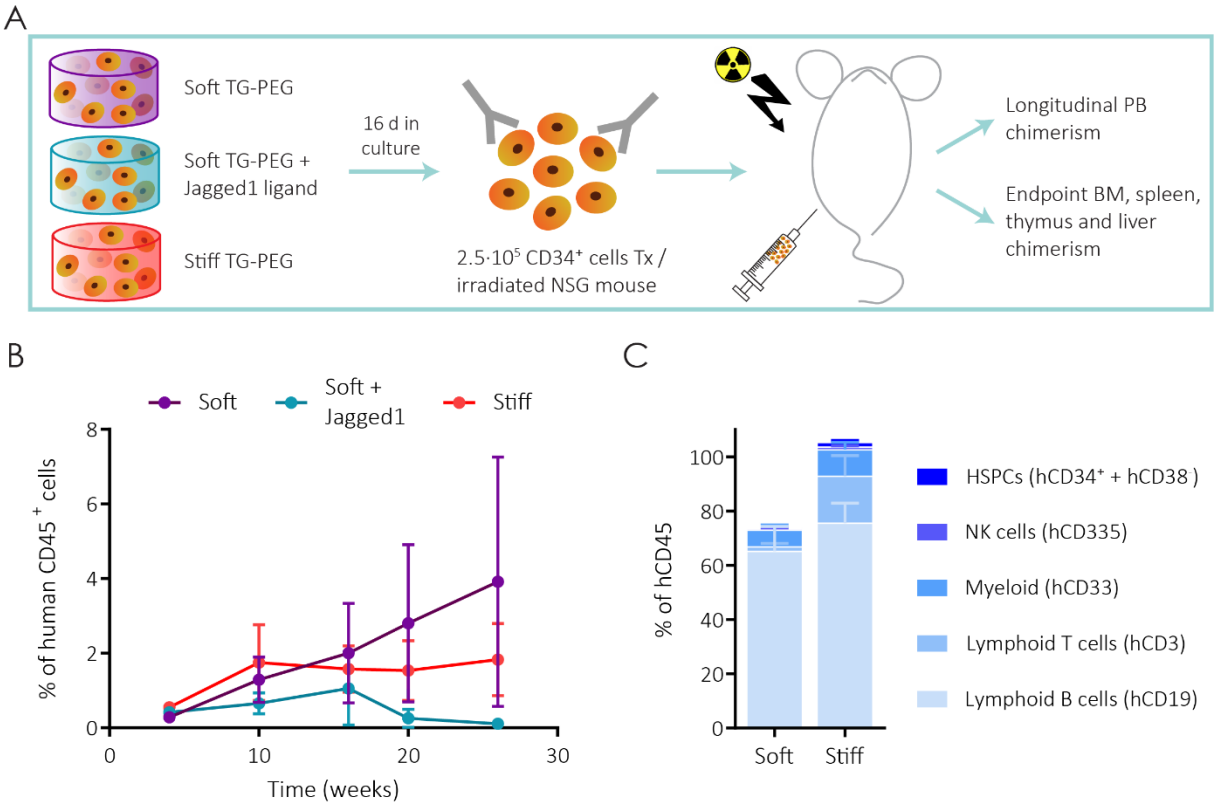

Figure 4. Transplantation of cultured HSPCs *in vivo*

(**a**) Overview of the workflow. cbHSPCs cultured for 16 days in different conditions (soft TG-PEG, soft TG-PEG with Jagged1 or stiff TG-PEG hydrogels) were FACS sorted by phenotypical characterization of live $CD45^+$ Lin^- $CD34^+$. Then, $2.5{\cdot}10^5$ cells were transplanted via intrafemoral injection in irradiated NSG mice. Human cell engraftment was monitored by longitudinal peripheral blood (PB) evaluation, and at endpoint bone marrow (BM), spleen, thymus and liver chimerism will be assessed. (**b**) Percentage of $hCD45^+$ cells of total $CD45^+$ (hCD45 + mCD45) found in PB of NSG mice up to 26 weeks post-transplantation. (**c**) Analysis of the human subpopulations found in PB at 26 weeks for soft and stiff conditions. All data are reported as mean ± standard error.

Discussion

In summary, we present a modular and versatile platform based on a biologically inspired hydrogel to systematically screen and dissociate the effect of different bone marrow niche parameters. To our knowledge, this is the first system that permits uncoupling of the biophysical and molecular stimuli permitting the contributions of each to be studied individually. Our data showed a key participation of stiffness in maintaining and expanding a phenotypically defined HSC population. This is in agreement with previous findings that showed HSPCs respond to biomechanical forces through extensional elasticity via actin-myosin cytoskeletal contractility[31,32]. Furthermore, the latter study highlighted that mouse HSPCs *in vitro* did not require integrin signaling[32], in line with what we have shown regarding RGD adhesion sites having no effect on proliferation nor differentiation of human HSCPs. On the other hand, we showed that MMPs were essential to expand HSPCs and HSCs in 3D hydrogels, as it is known for other stromal cell types[33] and in the *in vivo* microenvironments[34].

Other studies employing 3D biologically inspired materials had also reported morphological changes due to substrate stiffness[19,20]. This latter work elegantly showed that increased stiffness, and thus increased 3D confinement, resulted in lower proliferation yet higher frequency of phenotypically-defined HSPCs. However, in the used PEG-heparin system for the adaption of stiffness, it was required to increase along the heparin amount. In light of the growth factor binding properties of heparin, its variation could also result in stiffness-unrelated effects. Thus, the presented TG-PEG system offers a novel tool to fully uncouple mechanical and biochemical effects. Furthermore, this system is the first to validate the multipotency of HSCs cultured in fully synthetic hydrogels in an *in vivo* functional assay.

Blood chimerism was detected past 6 months post-transplantation for cells retrieved from soft or stiff gels, but not from Jagged1 gels or 2D conditions. This indicates that HSCs are preserved in pure synthetic hydrogels, and that both Jagged1 and 2D conditions exhausted the pool of stem cells likely due to high proliferation. Yet, it remains to be elucidated whether synthetic hydrogels successfully expanded HSCs, or whether the successful reconstitution capacity seen *in vivo* relies on cells that were maintained but did not proliferate in culture. Combining tools to track HSC divisions in culture, as previously established[22,35], could shed light on this. Remarkably, the rigorous set of markers used for flow cytometry analysis was yet not enough to predict these differences among culture conditions, thus, ultimately only *in vivo* reconstitution assays can determine the true HSC. Even more, complete HSC functionality would still need to be determined by serial transplantations to claim a successful expansion of HSCs.

Co-culturing HSPCs in 3D microenvironments together with other niche cell types has been extensively studied[15,17,18,36]. Uniquely, here we show that HSCs can be expanded in monoculture in the presence of niche-specific ligands to levels comparable to those seen during co-culture of HSCs with other niche cells (e.g. BMSCs). These results suggest that recapitulating some specific cell-cell or cell-ECM interactions may be sufficient for HSC maintenance, at least in a simplified *ex vivo* model. This is not to obviate the challenge of the complexity of the niche where multiple signalling pathways act in synergy and in competition to direct HSPC fate[4-6]. For this, our system is particularly well suited for screening parameters individually or in combination as was shown by investigating stiffness and ligand presentation.

Notch signaling has previously been described to deter HSC differentiation in the bone marrow niche *in vivo*[7,37]. In line with the results showed in here, other *in vitro* studies have shown that Jagged1 either presented by murine endothelial cells[38] or stromal cells[39] induced murine HSCs expansion. Therefore, our engineered hydrogels by simply presenting Notch ligands could closely recapitulate these previous findings, and effectively showcase Notch-mediated expansion for human HSCs. However HSC expansion under these conditions did only result in ST-HSCs and not LT-HSCs, as seen by limited *in vivo* multi-lineage reconstitution over time. This is likely due to the fact that excessive proliferation induces HSCs to exit quiescence, ultimately resulting in exhaustion of the HSC population[40].

It was surprising that some of the earlier described bone marrow-related ligands used did not elicit a clear response in the encapsulated cells compared to absence of ligand. While the linking of cell to cell adhesions, growth factors or cytokines into the hydrogel backbone could not induce HSPCs, employing cell surface proteins did show an effect. It may be logical to conclude that because they are either part of an adjacent cell or as soluble factors, being presented in the gel is not sufficient or does not mimic accurately enough the *in vivo* niche. Additionally, we cannot preclude that other concentrations or combinations of the used ligands could result in a different HSPC-specific effect. For instance, it has been reported that after lethal doses of irradiation in mice, a synergistic expression of P-selectin, E-selectin and VCAM-1 is required to recruit HSPCs into the bone marrow endothelium[41]. The caveat of oversimplification in this system might eventually be overcome in future work by reintroducing the complexity of synergistic biological interactions and combining several of the ligands described herein.

This project was devoted to study the proliferation versus differentiation or loss of stemness of the encapsulated cbHSPCs. It would also be of high importance to evaluate other stem cell states in the system such as quiescence or dormancy, key states that enable stem cells to escape from chemotherapy. These behaviors have been previously shown to be preferential in 3D systems compared to their 2D counterparts[36], which reinforces the use of such refined cultures to mimic the *in vivo* microenvironment and, thus, study stem cell fates upon perturbations.

Umbilical cord blood has been an interesting source of HSPCs in the clinics as it is easy to obtain, and HLA-mismatches can be tolerated[42]. However, because a single unit is usually insufficient to treat an adult, development of novel HSC-like cell sources from induced pluripotent stem cells has emerged in recent years as a promising approach to match the high cell demand in the clinics[43,44]. Our system has been validated by employing multiple cord blood donors showing robustness and reproducibility of the model. We are optimistic that due to the high versatility of the presented method to closely recapitulate the bone marrow niche, TG-PEG can be utilized with a wide gamut of cell types including genetically engineered cells or patient-derived cells, and thus serve as a tool to assess relevant pathological settings, which ultimately will enable the development of novel personalized treatments.

Outlook

Ongoing work is now focused on delving more deeply into the differential effects described in this chapter. Why did HSPCs cultured in Jagged1-containing hydrogels not elicit a long-term hematopoietic reconstitution? Could we predict such an outcome prior to transplantation? How do these cells molecularly differ from their counterparts without ligand? Which pathways are activated or deactivated in HSPCs cultured in stiff-conditions? Currently underway RNA sequencing analysis and proteomics could give us some of the answers to these intriguing questions. Moreover, thorough assessment of chimerism at the endpoint of the hematopoietic reconstitution

experiment (earlier data shown up to week 26) in other organs apart from PB, will offer a deeper insight in the reconstitution potential of the transplanted cells.

Acknowledgements

We would like to thank Dr. Christopher Millan (University of Zürich) for kindly reviewing and editing the manuscript; Esther Kleiner (University Hospital Zürich) for technical assistance including $CD34^+$ primary cell isolation; Eva Avilla-Royo (University Hospital Zürich) for proteomics discussions and future collaborations; Prof. Marcy Zenobi-Wong and Dr. Nicolas Broguiere (ETH Zürich) for support with rheological measurements; the Center for Microscopy and Image Analysis for SEM imaging (University of Zürich). This work has been supported by the Swiss National Science Foundation (CR33I3_153316/1), and the Center for Clinical Research, University Hospital Zürich and University of Zürich.

Experimental procedures

All chemicals and materials were purchased from Sigma Aldrich or Thermo Fisher Scientific unless otherwise specified.

Human CD34$^+$ HSPC isolation. Primary human CD34$^+$ cells were isolated from umbilical cord blood collected from healthy donors at the University Hospital Zürich after obtaining informed consent. The study was approved by the ethics board of the canton Zürich, Switzerland (approval date 21/03/2007; Ref Number 07/07). Blood (typically between 30-70 ml) was subsequently centrifuged to enrich for mononuclear cells, which were in turn further magnetically sorted based on their positive CD34 expression using positive immunomagnetic selection (CD34$^+$ MicroBead Kit, Miltenyi Biotec) according to the manufacturer's instructions. Cells were directly used or frozen down for future use.

cbHSPC encapsulation in 3D matrices. If frozen, cells were thawed in 50% IMDM 50% FBS, centrifuged 5 min at 300 g and subsequently encapsulated in hydrogels ($1.5 \cdot 10^6$ cells per ml of TG-PEG) as indicated. Cells were cultured in StemSpan SFEM (StemCell Technologies) complemented with penicillin (10 U ml^{-1}), streptomycin (10 μg ml^{-1}), human low density lipoprotein (hLDL, 10 μg ml^{-1}, StemCell Technologies), stem cell factor (hSCF, 100 ng ml^{-1}, PeproTech), thrombopoietin (hTPO, 100 ng ml^{-1}, Peprotech) and FMS-like tyrosine kinase 3 ligand (hFlt3L, 100 ng ml^{-1}, Peprotech). Cells were maintained in culture for up to 16 days at 37 °C in a humidified atmosphere at 5% CO_2. Medium was exchanged every 4 days. For **MMP inhibition experiments**, a broad spectrum MMP inhibitor (50 μM, GM6001, Calbiochem) was added in the cell medium and renewed every 4 days.

TG-PEG precursors synthesis and preparation. TG-PEG precursors were synthesized as previously described[23,24]. Briefly, 8-arm PEG-VS (PEG-vinylsulfone, 40 kDa MW; NOF) was functionalized with peptides (obtained with a purity of > 95% from Bachem AG) that contained an earlier described cysteine cassette (ERCG) optimized for its reaction with PEG-VS and either a factor XIII (FXIII) glutamine acceptor substrate sequence (Gln; H-NQEQVSPL-ERCG-NH_2) or a matrix metalloproteinase-degradable (*in italics*) lysine donor substrate ($MMP_{sensitive}$-Lys; Ac-FKGG-*GPQGIWGQ*-ERCG-NH_2). A 1.2 molar excess of peptides over PEG-VS was reacted in triethanolamine (TEA) at pH 8.0 for 2 h at 37 °C. Resulting 8-PEG-Gln and 8-PEG-$MMP_{sensitive}$-Lys precursors were excessively dialyzed against pure water, lyophilized and stored at -20 °C until further use. The crosslinking enzyme, transglutaminase FXIII (200 U ml^{-1}, Fibrogammin P, CSL Behring), was activated with thrombin (2 U ml^{-1}) for 30 min at 37 °C and stored in small aliquots at -80 °C until use.

3D TG-PEG hydrogel formation. Stoichiometrically balanced solutions of 8-arm PEG-Gln and 8-arm PEG-$MMP_{sensitive}$-Lys were prepared in Tris buffer (50 mM, pH 7.6) containing calcium chloride ($CaCl_2$, 50 mM). Additionally when stated, 50 μM Lys-RGD peptide (Ac-FKGG-

RGDSPG-NH_2) and indicated amounts of cells were added to the precursor solution. **In ligand-modified TG-PEG hydrogels**, to immobilize recombinant Fc-tagged ligands into TG-PEG hydrogels, these ligands (200 nM final concentration) were pre-incubated for 30 min with Gln-ZZ protein (2 μM final concentration, previously characterized[45]) to pre-form the Gln-ZZ/Fc-protein complex, which was then added to the gel precursor mix. The ligands were recombinant human vascular cell adhesion molecule-1 (VCAM1)-Fc protein (Sino Biological, 10113-H02H), E-selectin-Fc protein (Sino Biological, 10335-H03H), E-cadherin-Fc protein (Sino Biological, 10204-H02H), N-cadherin-Fc protein (Sino Biological, 11039-H03H), Jagged1-Fc protein (R&D Systems, 1277-JG-050), Delta-like-4 (DLL4)-Fc protein (Sino Biological, 10171-H02H), angiopoietin-2-Fc protein (Sino Biological, 10691-H02H), stromal cell-derived factor-1α (SDF-1)-Fc protein (Sino Biological, 10118-H01H) and IgG1-Fc control protein (R&D Systems, 110-HG-100). Subsequently, hydrogel crosslinking of final dry mass content of various w/v% was initiated by the addition of 10 U ml^{-1} of activated transglutaminase factor XIII, followed by vigorous mixing. Disc-shaped matrices were prepared between hydrophobic glass slides (treated with SigmaCote) and incubated for 30 min at 37 °C in a humidified atmosphere at 5% CO_2. After completed polymerization, hydrogels were released from glass slides and transferred to tissue-culture plates.

3D natural hydrogels. cbHSPCs (at final concentration of $1.5 \cdot 10^6$ cells per ml of hydrogel) were mixed in cold solutions of 3 mg ml^{-1} of collagen (PureCol EZ Gel solution, Sigma) or Matrigel (90%, Corning) following manufacturer's instructions. For fibrin gels as previously described[46], cbHSPCs were added to a solution of 5 mg ml^{-1} of fibrinogen containing 2.5 mM $CaCl_2$. Next, FXIII (2 U ml^{-1}) and thrombin (2 U ml^{-1}) were incorporated to begin hydrogel crosslinking. Cell-laden hydrogels were then incubated for 30 min at 37 °C to enable complete polymerization prior to transfer in tissue-culture plates for culture during 16 days.

Hydrogel stiffness characterization by *in situ* rheometry. Hydrogel gelation was analyzed on a rheometer (MCR 301, Anton Paar) equipped with 20 mm plate–plate geometry (PP20, Anton Paar) at 37 °C in a humidified atmosphere. Gel mixtures were precisely loaded onto the center of the bottom plate. The upper plate was lowered to a measuring gap size of 0.2 mm, ensuring proper loading of the space between the plates and gel precursors, the dynamic oscillating measurement was then started. The evolution of storage modulus (G') and loss modulus (G") at a constant angular frequency of 1 Hz and constant shear strain of 4% was recorded for 30 min when equilibrium was reached. Values recorded at 30 min were then compared for analysis.

Scanning electron microscopy. For scanning electron microscopy (SEM), cell-laden hydrogels were fixed in 50% osmium in phosphate buffered saline (PBS). After PBS washing, they were dehydrated by 30-minute incubation in 70% ethanol, followed by 80% and 100% ethanol and subsequently treated with hexamethyldisilazane (HMDS) for 1 hour, and then dried on air overnight. Lastly, samples were platinum sputter coated. Imaging was performed on a Zeiss Supra 50 VP at the UZH Center for Microscopy and Image Analysis (ZMB).

Immunocytochemistry of cells encapsulated in TG hydrogels. Cell-laden hydrogels were fixed in 4% paraformaldehyde for 30 min at room temperature (RT), followed by several washes of PBS and stored at 4 °C until staining. Cells were permeabilized in 0.1% Triton X-100 in 1% bovine serum albumin (BSA)/PBS at RT for 1 h. Next, samples were incubated with phalloidin-rhodamine (1:400) and 4',6-diamidino-2-phenylindole (DAPI, 1 μg ml^{-1}) in 1% BSA/PBS at RT for 3 h followed by overnight washing. Gels were imaged with Leica TCS SP5 confocal microscope. For brightfield imaging, Leica DMI 6000B inverted microscope was used. Image analysis and processing were performed using Fiji[47].

HSPC retrieval and preparation for flow cytometry analysis. To recover the encapsulated HSPCs, medium was removed, hydrogels were washed with PBS, and hydrogels were digested with collagenase A (100 μl, 2 mg ml^{-1}, Roche) at 37 °C for 30 min. In order to record adequate event numbers per sample during flow cytometry, the replicates (typically n = 3 unless differently stated) were pooled for each condition and pelleted by centrifugation. The resulting pellet was resuspended in pre-warmed trypsin- ethylenediaminetetraacetic acid (EDTA) (100 μl per pellet) and incubated for 2 min at 37 °C to dissociate cell aggregates before being washed with FACS buffer (1 mM EDTA and 2% FBS in PBS). From the resulting suspension cells were ready for DNA quantification, flow cytometry analysis and CFU assays.

Proliferation assessment of encapsulated cells. cbHSPCs retrieved from hydrogels were collected in Hank's balanced salt solution (HBSS) buffer, and DNA content was assessed by the CyQuant NF Cell Proliferation assay kit (Invitrogen, C35006) following the manufacturer's instructions. Finally, fluorescence was recorded with excitation at 485 nm and emission at 530 nm using a microplate reader.

Flow cytometry analysis. Cells were characterized by their surface expression of the following human markers: lineage (CD2, CD3, CD4, CD8, CD10, CD11b, CD14, CD19, CD20, CD56, CD235), CD45, CD34, CD38, CD90 and CD45-RA. Cells were stained for 30 min at 4 °C in the dark, washed, filtered through a 70 μm filter and analyzed by BD LSRFortessa. Dead cells were stained by Zombie Aqua AmCyan viability dye (1:1000, BioLegend) and were, alongside doublets, excluded from analysis. Data analysis was performed using FlowJo 10.0.8 software (TreeStar), and fluorescence minus one (FMO) control stainings were used for stringent gating. Immunophenotypic definitions of the hematopoietic populations of interest are specified in Table 1, and the gating strategy exemplified in Figure S2. Detailed information about the used antibodies is in Table 2.

Table 1 Phenotypes of hematopoietic cell populations

Population		Phenotype*
MyelP	Myeloid progenitor	$CD34^+$ $CD38^+$
CMP/MEP	Common Myeloid Progenitor/ Megakaryocyte-Erythrocyte Progenitor	$CD34^+$ $CD38^+$ $CD45RA^-$

B/NK/GMP	B- /Natural Killer- cell progenitor/ Granulocyte-Macrophage Progenitor	$CD34^+$ $CD38^+$ $CD45RA^+$
HSPC	Hematopoietic Stem Progenitor Cell	$CD34^+$ $CD38^-$
MLP	Multilymphoid Progenitor	$CD34^+$ $CD38^-$ $CD45RA^+$ $CD90^-$
MPP	Multipotent Progenitor	$CD34^+$ $CD38^-$ $CD45RA^-$ $CD90^-$
HSC	Hematopoietic Stem Cell	$CD34^+$ $CD38^-$ $CD45RA^-$ $CD90^+$

*All previously gated from single, live, $CD45^+$ Lin^- cells.

Colony forming units assay. To evaluate the functional potential of cells cultured in hydrogels, a colony forming unit (CFU) assay was performed. Briefly, 1000 cells from each sample were resuspended in 1 ml of methylcellulose media (MethoCult H4230, StemCell Technologies) with 200 µl of IMDM + GlutaMAX supplemented with penicillin (10 U ml^{-1}), streptomycin (10 µg ml^{-1}), human interleukin 3 (hIL-3, 100 ng ml^{-1}, PeproTech), interleukin 6 (hIL-6, 50 ng ml^{-1}, PeproTech), stem cell factor (hSCF, 50 ng ml^{-1}, PeproTech), granulocyte macrophage colony stimulating factor (hGM-CSF, 250 ng ml^{-1}, PeproTech), thrombopoietin (hTPO, 250 ng ml^{-1}, PeproTech), FMS-like tyrosine kinase 3 ligand (hFlt3L, 50 ng ml^{-1}, R&D Systems), interleukin 11 (hIL-11, 50 ng ml^{-1}, PeproTech) and erythropoietin (hEPO, 20 U ml^{-1}, EPREX). Cells were then cultured in 9 cm^2 for 10 to 14 days at 37 °C in a humidified atmosphere at 5% CO_2. At this time, CFUs were counted based on morphology into the subcolonies containing erythrocytes (CFU-E), granulocytes (CFU-G), macrophages (CFU-M), granulocytes and macrophages (CFU-GM) or granulocytes, erythrocytes, macrophages and megakaryocytes (CFU-GEMM).

Flow cytometry sorting. After 16-day culture, cells were retrieved from hydrogels or collected from 2D conditions as previously described. Single cell suspensions were then stained in the antibody mix and sorted for live single cells $CD45^+$ Lin^- $CD34^+$ using a 70 µm nozzle in a BD FACSAria cell sorter. Cells were pelleted and resuspended in PBS for injection into mice.

Animal care. All animal procedures were approved by the veterinary offices of the Swiss cantons Zürich under the ethical license (Application No. ZH169/2015). Experiments and handling of mice were conducted in accordance with the Swiss law of animal protection. 8-12-week-old immunodeficient NOD.Cg-*Prkdc*^{scid}*Il2rg*^{tm1Wjl}/SzJ (NSG) mice (purchased from The Jackson Laboratory) were used for the following experiments.

HSPC transplantation. Adult NSG mice were sublethally irradiated (X-ray irradiation with RS-2000 irradiator, Rad Source) with 1x 181 cGy then transplanted intra-femorally with $2.5 \cdot 10^5$ sorted HSPCs. Mice were analyzed 4 to > 26 weeks (undergoing) after transplantation.

Flow cytometry analysis of peripheral blood. To determine human engraftment, mice were sublingually bled and stained cells were analyzed on the BD LSRFortessa cell analyzer. Detailed information about the used antibodies is in Table 2.

Statistical analysis. All data are reported as mean ± standard error. All statistical analyses were performed using GraphPad Prism (version 8.0.0, GraphPad Software). Mean values were compared by one-way or two-way analysis of variance (ANOVA) followed by Tukey's *post hoc* test for multiple comparisons. Statistical significance was accepted for $P < 0.05$, and reported as follows * $P < 0.05$, ** $P < 0.01$, *** $P < 0.001$, **** $P < 0.0001$. For experiments involving different biological donors, a distinction between N (biological donors used) and n (technical replicates) was made. Further information is found in the particular figure legends.

Table 2. List of detailed antibodies used for flow cytometry and histological stainings

Antibody	Application & Dilution	Company	Catalog number
Mouse α hCD2 – PE-Cy5	FC 1:100	BioLegend	300209
Mouse α hCD3 – PE-Cy5	FC 1:100	BioLegend	300309
Mouse α hCD4 – PE-Cy5	FC 1:100	BioLegend	317411
Mouse α hCD8 – PE-Cy5	FC 1:100	BioLegend	300909
Mouse α hCD10 – PE-Cy5	FC 1:100	BioLegend	312206
Mouse α hCD11b – PE-Cy5	FC 1:100	BioLegend	301307
Mouse α hCD14 – PE-Cy5	FC 1:100	eBioscience	15-0149-41
Mouse α hCD19 – PE-Cy5	FC 1:100	BioLegend	302209
Mouse α hCD20 – PE-Cy5	FC 1:100	BioLegend	302307
Mouse α hCD56 – PE-Cy5	FC 1:100	BioLegend	304607
Mouse α hCD235a – PE-Cy5	FC 1:100	BD Biosciences	561776
Mouse α hCD45 – eFluor 450	FC 1:100	eBioscience	48-0459-42
Mouse α hCD34 – PE-Cy7	FC 1:50	BD Biosciences	561107
Mouse α hCD38 – FITC	FC 1:25	BD Biosciences	555459
Mouse α hCD45RA – APC-eFluor 780	FC 1:100	eBioscience	47-0458-42
Mouse α hCD90 – PE	FC 1:25	BD Biosciences	555596
Zombie Aqua Fixable Viability kit	FC 1:1000	BioLegend	423101
Mouse α hCD335 – BV786	FC 1:50	BD Bioscience	563329
Mouse α hCD33 – BV711	FC 1:100	BioLegend	303424
Rat α mCD45 – PE	FC 1:500	BioLegend	103105
Mouse α hCD14 – APC-Cy7	FC 1:100	BioLegend	301820
Mouse α hCD19 – APC	FC 1:50	BioLegend	302211
Mouse α hHLA-A2 – FITC	FC 1:100	BD Bioscience	561107

FC: flow cytometry

References

1 Velten, L. *et al.* Human haematopoietic stem cell lineage commitment is a continuous process. *Nature cell biology* **19**, 271 (2017).

2 Weissman, I. L. & Shizuru, J. A. The origins of the identification and isolation of hematopoietic stem cells, and their capability to induce donor-specific transplantation tolerance and treat autoimmune diseases. *Blood* **112**, 3543-3553 (2008).

3 Little, M.-T. & Storb, R. History of haematopoietic stem-cell transplantation. *Nature Reviews Cancer* **2**, 231 (2002).

4 Morrison, S. J. & Spradling, A. C. Stem cells and niches: mechanisms that promote stem cell maintenance throughout life. *Cell* **132**, 598-611 (2008).

5 Wilson, A. & Trumpp, A. Bone-marrow haematopoietic-stem-cell niches. *Nature Reviews Immunology* **6**, 93 (2006).

6 Morrison, S. J. & Scadden, D. T. The bone marrow niche for haematopoietic stem cells. *Nature* **505**, 327-334 (2014).

7 Calvi, L. *et al.* Osteoblastic cells regulate the haematopoietic stem cell niche. *Nature* **425**, 841 (2003).

8 Zhang, J. *et al.* Identification of the haematopoietic stem cell niche and control of the niche size. *Nature* **425**, 836-841 (2003).

9 Méndez-Ferrer, S. *et al.* Mesenchymal and haematopoietic stem cells form a unique bone marrow niche. *nature* **466**, 829-834 (2010).

10 Acar, M. *et al.* Deep imaging of bone marrow shows non-dividing stem cells are mainly perisinusoidal. *Nature* **526**, 126-130 (2015).

11 Kiel, M. J. *et al.* SLAM family receptors distinguish hematopoietic stem and progenitor cells and reveal endothelial niches for stem cells. *cell* **121**, 1109-1121 (2005).

12 Katayama, Y. *et al.* Signals from the sympathetic nervous system regulate hematopoietic stem cell egress from bone marrow. *Cell* **124**, 407-421 (2006).

13 Ogawa, M. Differentiation and proliferation of hematopoietic stem cells. *Blood* **81**, 2844-2853 (1993).

14 Rieger, M. A., Hoppe, P. S., Smejkal, B. M., Eitelhuber, A. C. & Schroeder, T. Hematopoietic cytokines can instruct lineage choice. *Science* **325**, 217-218 (2009).

15 Bourgine, P. E. *et al.* In vitro biomimetic engineering of a human hematopoietic niche with functional properties. *Proceedings of the National Academy of Sciences* **115**, E5688-E5695 (2018).

16 Raic, A., Rödling, L., Kalbacher, H. & Lee-Thedieck, C. Biomimetic macroporous PEG hydrogels as 3D scaffolds for the multiplication of human hematopoietic stem and progenitor cells. *Biomaterials* **35**, 929-940 (2014).

17 Leisten, I. *et al.* 3D co-culture of hematopoietic stem and progenitor cells and mesenchymal stem cells in collagen scaffolds as a model of the hematopoietic niche. *Biomaterials* **33**, 1736-1747 (2012).

18 Ferreira, M. S. V. *et al.* Cord blood-hematopoietic stem cell expansion in 3D fibrin scaffolds with stromal support. *Biomaterials* **33**, 6987-6997 (2012).

19 Cuchiara, M. L. *et al.* Bioactive poly (ethylene glycol) hydrogels to recapitulate the HSC niche and facilitate HSC expansion in culture. *Biotechnology and bioengineering* **113**, 870-881 (2016).

20 Gvaramia, D. *et al.* Combined influence of biophysical and biochemical cues on maintenance and proliferation of hematopoietic stem cells. *Biomaterials* **138**, 108-117 (2017).

21 Lutolf, M. P., Doyonnas, R., Havenstrite, K., Koleckar, K. & Blau, H. M. Perturbation of single hematopoietic stem cell fates in artificial niches. *Integrative biology* **1**, 59-69 (2008).

22 Roch, A. *et al.* Single-cell analyses identify bioengineered niches for enhanced maintenance of hematopoietic stem cells. *Nature communications* **8**, 221 (2017).

23 Ehrbar, M. *et al.* Biomolecular hydrogels formed and degraded via site-specific enzymatic reactions. *Biomacromolecules* **8**, 3000-3007 (2007).

24 Ehrbar, M. *et al.* Enzymatic formation of modular cell-instructive fibrin analogs for tissue engineering. *Biomaterials* **28**, 3856-3866 (2007).

25 Lutolf, M. P. *et al.* Repair of bone defects using synthetic mimetics of collagenous extracellular matrices. *Nature biotechnology* **21**, 513 (2003).

26 Gilbert, P. M. *et al.* Substrate elasticity regulates skeletal muscle stem cell self-renewal in culture. *Science* **329**, 1078-1081 (2010).

27 Kraehenbuehl, T. P. *et al.* Three-dimensional extracellular matrix-directed cardioprogenitor differentiation: systematic modulation of a synthetic cell-responsive PEG-hydrogel. *Biomaterials* **29**, 2757-2766 (2008).

28 Blache, U. *et al.* Notch-inducing hydrogels reveal a perivascular switch of mesenchymal stem cell fate. *EMBO reports* **19**, e45964 (2018).

29 Gjorevski, N. *et al.* Designer matrices for intestinal stem cell and organoid culture. *Nature* **539**, 560 (2016).

30 Kamel-Reid, S. & Dick, J. E. Engraftment of immune-deficient mice with human hematopoietic stem cells. *Science* **242**, 1706-1709 (1988).

31 Shin, J.-W. *et al.* Contractile forces sustain and polarize hematopoiesis from stem and progenitor cells. *Cell stem cell* **14**, 81-93 (2014).

32 Holst, J. *et al.* Substrate elasticity provides mechanical signals for the expansion of hemopoietic stem and progenitor cells. *Nature biotechnology* **28**, 1123 (2010).

33 Mannello, F., Tonti, G. A., Bagnara, G. P. & Papa, S. Role and function of matrix metalloproteinases in the differentiation and biological characterization of mesenchymal stem cells. *Stem Cells* **24**, 475-481 (2006).

34 Kessenbrock, K., Wang, C.-Y. & Werb, Z. Matrix metalloproteinases in stem cell regulation and cancer. *Matrix biology* **44**, 184-190 (2015).

35 Roch, A., Trachsel, V. & Lutolf, M. P. Brief report: Single-cell analysis reveals cell division-independent emergence of megakaryocytes from phenotypic hematopoietic stem cells. *Stem cells* **33**, 3152-3157 (2015).

36 Sharma, M. B., Limaye, L. S. & Kale, V. P. Mimicking the functional hematopoietic stem cell niche in vitro: recapitulation of marrow physiology by hydrogel-based three-dimensional cultures of mesenchymal stromal cells. *Haematologica* **97**, 651-660 (2012).

37 Duncan, A. W. *et al.* Integration of Notch and Wnt signaling in hematopoietic stem cell maintenance. *Nature immunology* **6**, 314 (2005).

38 Poulos, M. G. *et al.* Endothelial Jagged-1 is necessary for homeostatic and regenerative hematopoiesis. *Cell reports* **4**, 1022-1034 (2013).

39 Varnum-Finney, B. *et al.* The Notch ligand, Jagged-1, influences the development of primitive hematopoietic precursor cells. *Blood* **91**, 4084-4091 (1998).

40 Passegué, E., Wagers, A. J., Giuriato, S., Anderson, W. C. & Weissman, I. L. Global analysis of proliferation and cell cycle gene expression in the regulation of hematopoietic stem and progenitor cell fates. *Journal of Experimental Medicine* **202**, 1599-1611 (2005).

41 Frenette, P. S., Subbarao, S., Mazo, I. B., Von Andrian, U. H. & Wagner, D. D. Endothelial selectins and vascular cell adhesion molecule-1 promote hematopoietic progenitor homing to bone marrow. *Proceedings of the National Academy of Sciences* **95**, 14423-14428 (1998).

42 Schoemans, H. *et al.* Adult umbilical cord blood transplantation: a comprehensive review. *Bone marrow transplantation* **38**, 83 (2006).

43 Sugimura, R. *et al.* Haematopoietic stem and progenitor cells from human pluripotent stem cells. *Nature* **545**, 432 (2017).

44 Turner, M. *et al.* Toward the development of a global induced pluripotent stem cell library. *Cell stem cell* **13**, 382-384 (2013).

45 Lienemann, P. S. *et al.* A versatile approach to engineering biomolecule-presenting cellular microenvironments. *Advanced healthcare materials* **2**, 292-296 (2013).

46 Schense, J. C. & Hubbell, J. A. Cross-linking exogenous bifunctional peptides into fibrin gels with factor XIIIa. *Bioconjugate chemistry* **10**, 75-81 (1999).

47 Schindelin, J. *et al.* Fiji: an open-source platform for biological-image analysis. *Nature methods* **9**, 676 (2012).

Supplementary data

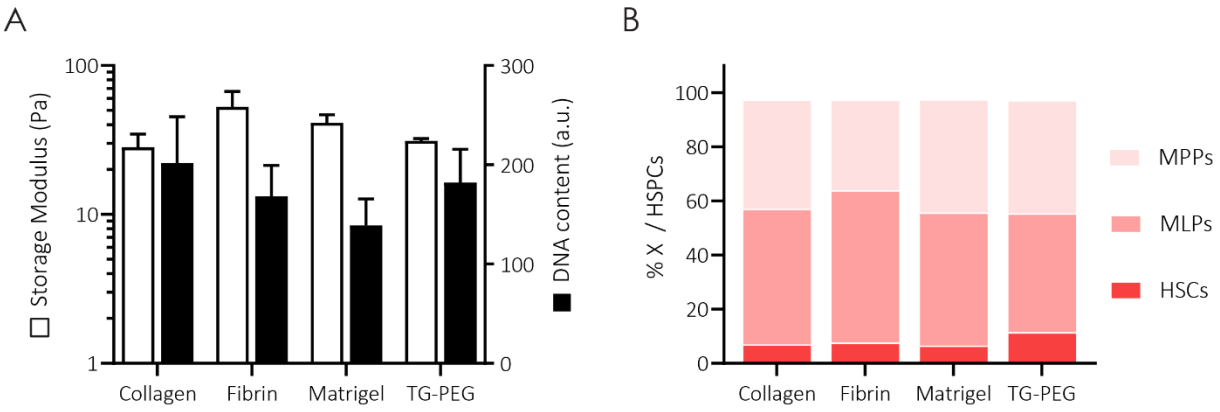

Figure S1. Synthetic TG-PEG matrices increase HSC phenotype compared to natural analogues

(**a**) Storage modulus of TG-PEG hydrogels, by solely adjusting crosslinking density, was matched to the storage moduli of natural matrices including collagen, fibrin and Matrigel (n = 2, left axis, white bars). Total DNA content of cbHSPCs cultured in these scaffolds for 16 days (n = 3, right axis, black bars). (**b**) Immunophenotypic characterization of hematopoietic subpopulations comprising MPPs, MLPs and HSCs were assessed after 16 days in culture (N = 1). All data are reported as mean ± standard error.

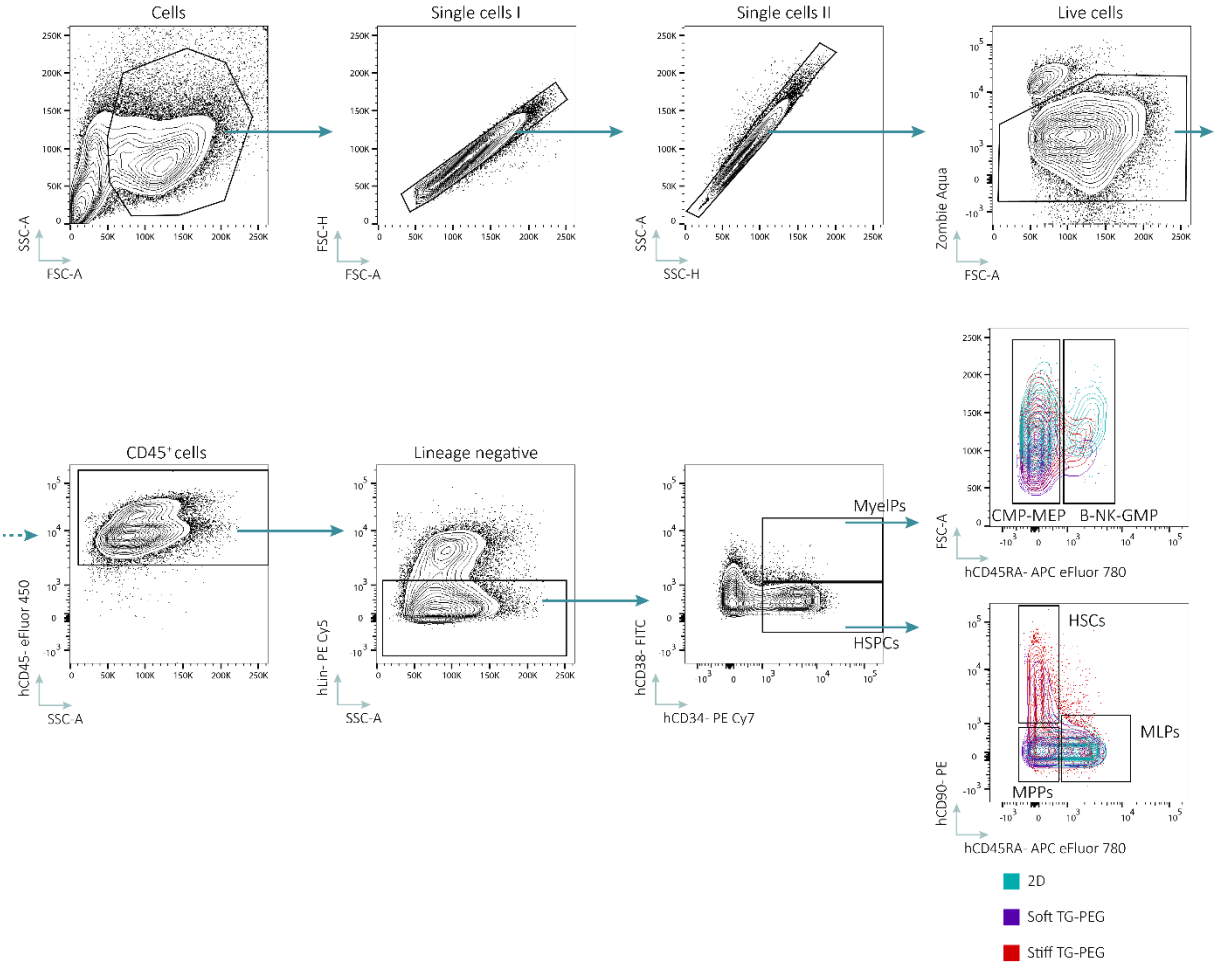

Figure S2. Flow cytometry gating strategy to characterize immunophenotypical hematopoietic subpopulations

Cells retrieved from hydrogels after 16 days in culture were analyzed by a set of 16 surface markers. Single and live cells were pre-selected and further classified into hematopoietic stem and progenitor cells (HSPCs, Lin^- $CD34^+$ $CD38^-$), myeloid progenitors (MyelP, Lin^- $CD34^+$ $CD38^+$), hematopoietic stem cells (HSCs, Lin^- $CD34^+$ $CD38^-$ $CD45RA^-$ $CD90^+$), multipotent progenitors (MPPs, Lin^- $CD34^+$ $CD38^-$ $CD45RA^-$ $CD90^-$), multilymphoid progenitors (MLPs, Lin^- $CD34^+$ $CD38^-$ $CD45RA^+$ CD90-), common myeloid progenitors/ megakaryocyte-erythrocyte progenitors (CMP/MEP, Lin^- $CD34^+$ $CD38^+$ $CD45RA^-$) or B-/Natural Killer- cell progenitors/granulocyte-macrophage progenitors (B/NK/GMP, Lin^- $CD34^+$ $CD38^+$ $CD45RA^+$). Fluorescence minus one (FMO) and isotype controls were used to design the gates. Color-coding of the HSPCs and MyelPs subpopulations representing cells retrieved from 2D condition, soft TG-PEG or stiff TG-PEG hydrogels.

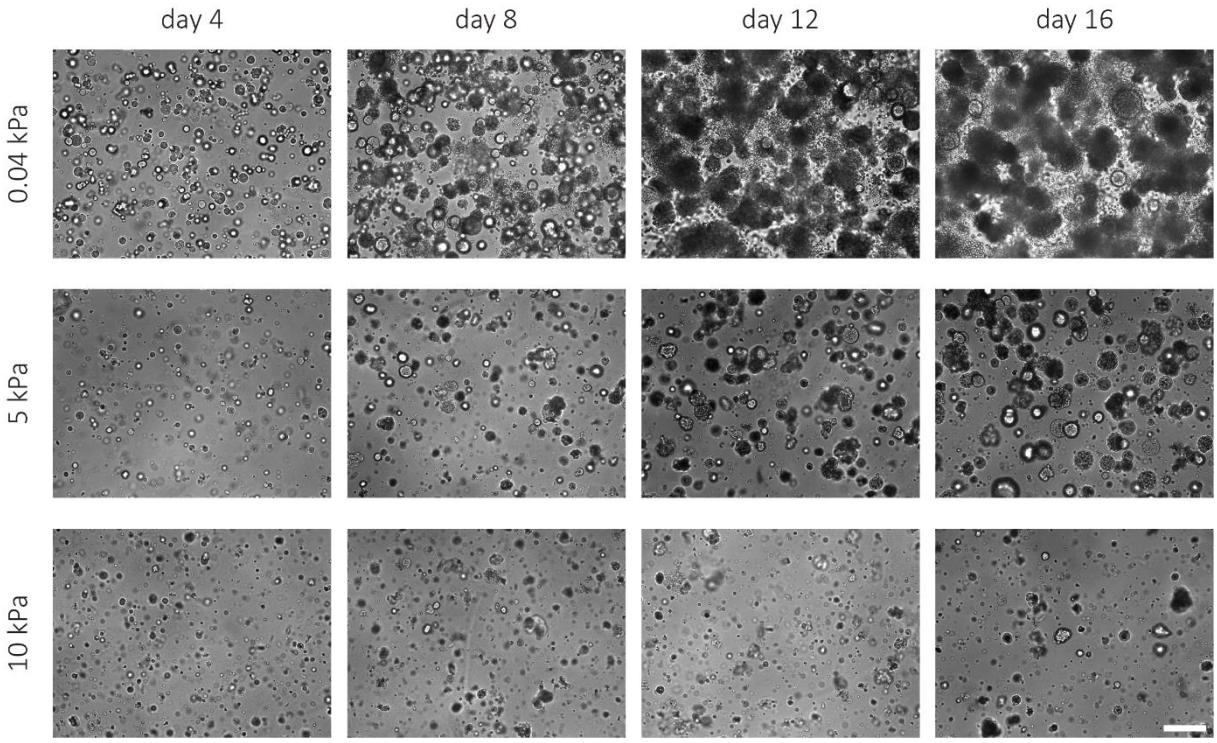

Figure S3. Encapsulated cbHSPCs acquired different morphologies based on stiffness

Longitudinal brightfield imaging representative of morphological differences of encapsulated cells in different hydrogels with stiffness of 0.04, 5 and 10 kPa at 4, 8, 12, and 16 days post-encapsulation (scale bar: 200 µm).

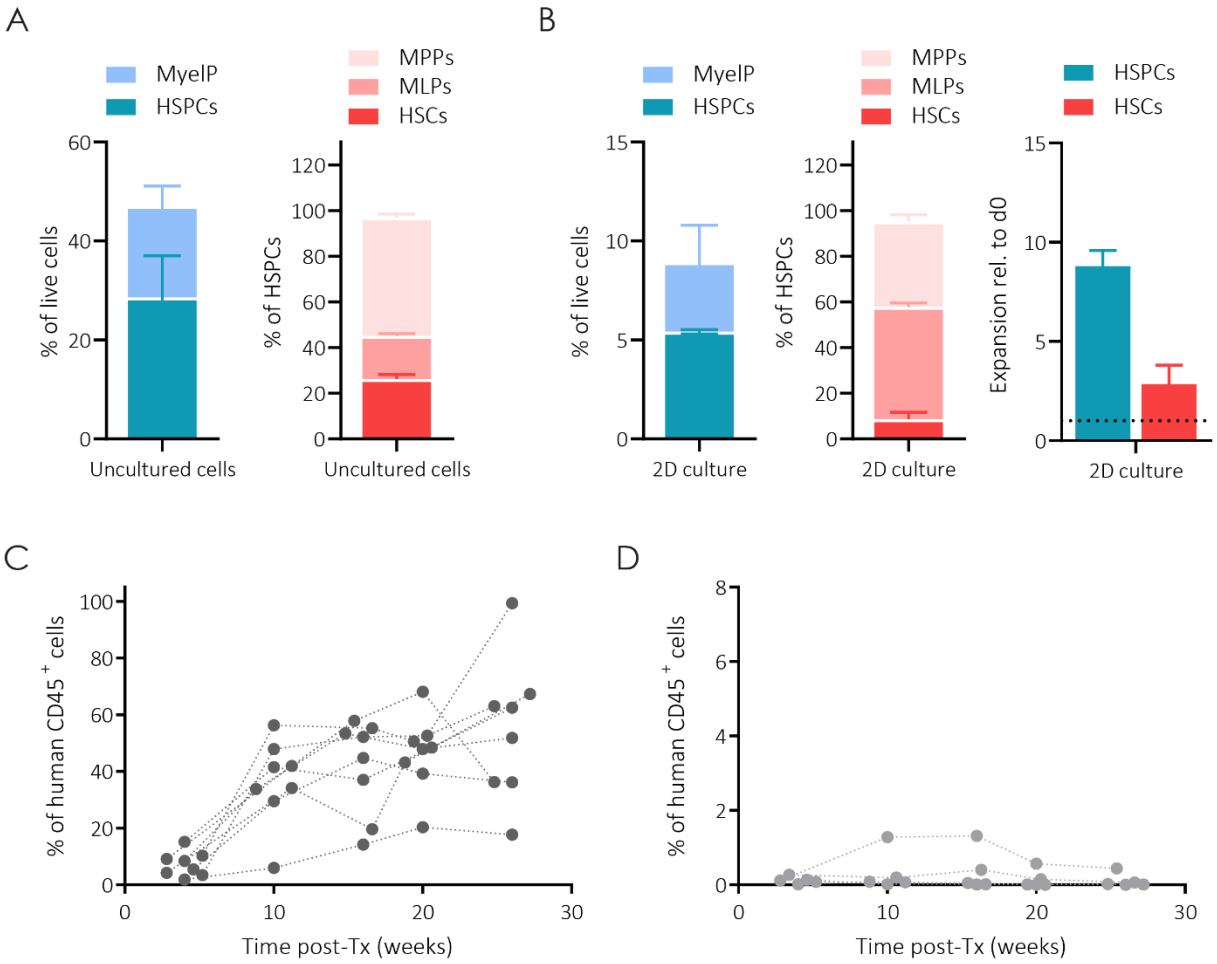

Figure S4. Transplantation of uncultured or cultured in 2D conditions HSPCs *in vivo*

(**a**) Analysis of uncultured cbHSPCs showing HSPC and MyeIP populations as percentage of total live cells, and HSC, MLP and MPP percentage within HSPCs (N = 4). (**b**) Analysis of cbHSPCs cultured 16 days in 2D conditions, showing HSPC and MyeIP populations as percentage of total live cells, and HSC, MLP and MPP percentage within HSPCs. And, expansion of HSPCs and HSCs relative to day 0 after 16 days in culture (N = 4). Dotted line indicates no expansion (i.e. one-fold). (**c-d**) $2.5 \cdot 10^5$ sorted cells (live $CD45^+$ Lin^- $CD34^+$ cells) were transplanted via intrafemoral injection in irradiated NSG mice to assess cell multipotency. Human cell engraftment was monitored by longitudinal peripheral blood (PB) evaluation. Percentage of $hCD45^+$ cells of total $CD45^+$ (hCD45 + mCD45) found in PB of NSG mice up to 26 weeks post-transplantation of (**c**) uncultured cells or (**d**) cells cultured for 16 days in 2D conditions. All data are reported as mean ± standard error.

I així pren tot el fruit que et pugui donar
el camí que, a poc a poc, escrius per a demà.
Què demà mancarà el fruit de cada pas;
per això, malgrat la boira, cal caminar. – Lluís Llach

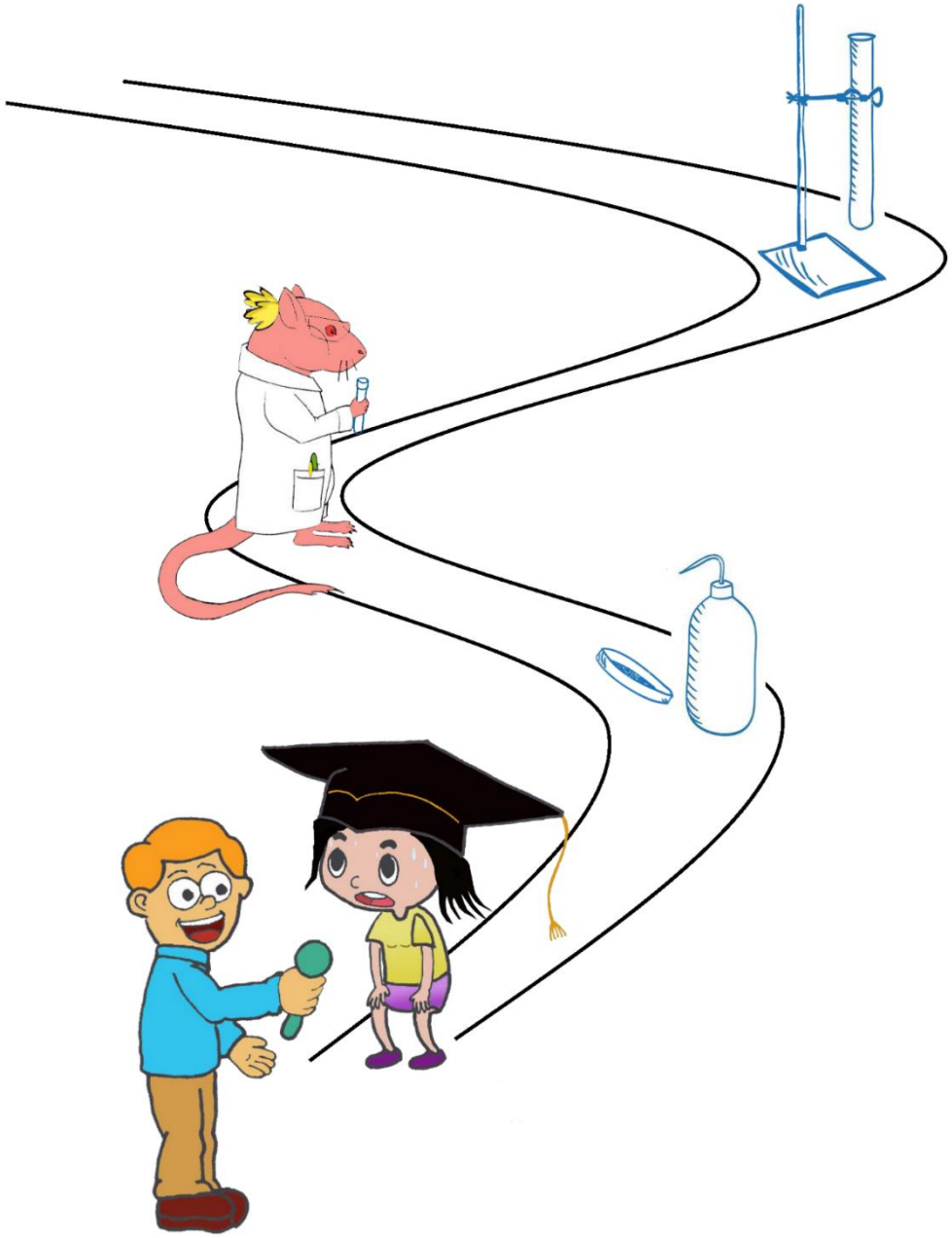

Artwork by Oriol Vallmajó Martín
Girona, Catalunya

CHAPTER 7

Closing remarks

In this thesis, engineered humanized 3D bone marrow models built on well-defined matrices are presented. They were employed to systematically assess bone marrow microenvironmental parameters, unravel cellular intrinsic functions, and study osteotropic metastasis of cancer cells.

More specifically, we determined that:

i) Chemically-defined synthetic poly(ethylene glycol) (PEG)-based hydrogels are optimal for a wide gamut of applications related to bone and bone marrow

ii) Skeletal stem cells (SSCs) elicit *de novo* bone formation in a critically-sized defect model

iii) Human bone marrow stromal cell (hBMSC) differentiation potential can be assessed in an *in vivo* minimalistic environment

iv) Humanized bone marrow organoids comprising human bone marrow stromal cells (hBMSCs) can serve as a model for osteotropic cancer

v) Addition of hyaluronic acid (HA) to the hydrogel backbone reduces immunogenicity and improves stem cell transplantation yield

vi) Soft minimal microenvironments support *in vitro* proliferation of multipotent hematopoietic stem cells (HSCs) while, in concert with Notch-signaling ligands, can only maintain their short-term reconstitution capacity

Multiple cell types and setups including *in vitro* cultures and *in vivo* xenografts or healing models were used to gain insight in bone marrow stem cell niche biology. The promising results presented here have engendered a series of follow-up studies on multiple research fronts.

Synthesis

As the choice of cell type for a given tissue engineering application is rigorously scrutinized, so too should be the case for deciding on the optimal biomaterial. Biomaterials should be rationally designed and tailored to meet the needs and properties of the aimed system to evaluate. To do so, well-defined synthetic hydrogels have emerged as promising tools, and are supplanting natural extracellular matrix (ECM)-based hydrogels for studying certain developmental and pathological settings[1,2]. These synthetic analogues permit systematic modifications of biophysical and biochemical properties while allowing encapsulated cells to deposit endogenous ECM and remodel the microenvironment, as highlighted in this and others' work[3-5].

In this thesis, we have shown over and again the importance of the material in **dictating cell behaviors**, and the necessity to methodically optimize each parameter affecting those behaviors. Remarkably, with TG-PEG alone we were able to screen intrinsic differences between hBMSC donors that were otherwise undetectable with current characterization methods. Additionally, TG-PEG allowed the formation of bone and bone marrow comprising ossicles with a minimal dose of osteogenic BMP-2 and without the need of cell pre-differentiation. Perhaps even more strikingly, TG-PEG also served to recapitulate a **humanized functional malignant niche** in a xenograft model overcoming some of the drawbacks met by alternative materials (i.e. via ease of material synthesis, reproducible properties, lack of confounding signals, and no need of cell pre-differentiation). Two key features of the employed TG-PEG make such studies possible: 1) its modularity afforded by the unique enzymatic crosslinking chemistry, and 2) the lack of inherent inductive or animal-derived factors.

The **modular nature** of TG-PEG hydrogels was exploited throughout this work to systematically evaluate the role of biophysical and biochemical parameters to suit diverse applications in order to gain further insight into stem cell biology. Stiffness, which is tuned in TG-PEG gels by simply altering the concentration (w/v) of PEG in the hydrogel precursor solution, was repeatedly optimized for each cell type and individual application explored. While natural materials frequently used for BM studies, such as fibrin and collagen, have maximum stiffness in the range of 50 Pa, TG-PEG gels could be formed with stiffness ranging from 20 Pa up to 5 kPa. For bone formation by BMSCs, an intermediate stiffness of 500 Pa was determined to be optimal and significantly improved total bone volume over softer TG-PEG gels or natural materials, that proved unstable over time. Alternatively, for HSPCs, stiff gels were found to preserve the differentiation capacity of encapsulated cells, while softer gels additionally promoted HSPC proliferation. TG-PEG alone allows determination of the ideal stiffness for these applications because its stiffness can be altered independently of any biochemical cues, which is not the case for natural materials or semi-synthetic analogues. Apart from mechanical cues presented by the microenvironment, cells are also profoundly influenced by interactions with proteins that bind ligands or receptors on the cell surface and trigger a particular reaction from the cell. The possibility to independently incorporate MMP-sensitive sites, the RGD cell-adhesion peptide or BM-specific ligands in the hydrogel

backbone, permitted elucidation here of their single or additive effects on different cell types and culture conditions (*in vitro* vs. *in vivo* xenograft models).

The **lack of inherent bioactivity** of TG-PEG hydrogels has also been key in this work. First and foremost, it has allowed the systematic screening of biochemical cues in a controlled-way. Additionally, the fixed composition and batch-to-batch reproducibility have considerably facilitated the repeatability of the described findings. And ultimately, the lack of animal-derived components will likely speed up their translation to clinical applications. Taken all together, the results of this work highlight the potential of building up controlled systems from a blank slate to identify key parameters affecting human health and pathology for a specific tissue type.

Conclusions and Outlook

Tuning the microenvironment

A number of the intriguing outcomes presented here should provoke further study and continuations of the work. Here, the focus was exclusively on 3D, but truly capturing the dynamic aspect of the native microenvironment necessitates consideration of a fourth dimension – time. Spatiotemporal release of growth factors or presentation of specific niche ligands can be pivotal in cell response[6,7]. Mimicking this could be accomplished by combining soluble factors directly encapsulated in TG-PEG hydrogels with additional growth factors tethered to the TG-PEG backbone. Several techniques have been established for growth factor binding to TG-PEG matrices, including the one described earlier via Fc and protein Z[8], or alternatively employing the high affinity streptavidin/biotin interaction[9]. Additionally, temporal changes in biophysical properties of the hydrogels have also been purported to control stem cell behavior and closely recapitulate morphological changes happening in native tissues upon development or diseases breakout[1,10,11].

One set of results presented here indicated that biophysical properties and biochemical moieties highly affect *in vitro* culture of cord blood-derived hematopoietic stem and progenitor cells (cbHSPCs). While encapsulation of cbHSPCs in stiff hydrogels successfully maintained HSC-like cells but restricted proliferation, soft hydrogels yielded significantly higher maintenance and expansion of those cells. Additionally, presentation of Jagged1 ligand resulted in high expansion and high maintenance of immunophenotypically-defined HSCs. However, these cells failed in long-term reconstitution of the hematopoietic system *in vivo*. Thus, we propose that by combining the promising features of both approaches, we can accomplish an improved HSC culture and potential expansion. cbHSPCs could first undergo an expansion step cultured in soft hydrogels, followed by substrate stiffening which should serve to maintain the expanded HSCs. Additionally, the Jagged1 ligand could be presented in this second step in stiff hydrogels to avoid complete HSC senescence for limited time, while avoiding to exhaust their multipotency.

Overall, the different applications presented of TG-PEG depict a wide gamut of possibilities that we are convinced will serve as stepping stones for future work towards customized design of biomaterials.

The mess of stem-ness

The parameters established for forming a bone marrow niche utilizing hBMSCs and TG-PEG in an *in vivo* setup circumvented the need for inducing differentiation with high doses of BMP-2, as had been the standard up until now. However, these early results prompted questions regarding

the specific role of the human cells during niche formation, and why stark variations were observed between cell types or between donors.

Though a clear functional assay was established long ago to determine the multipotency and self-renewal capabilities of HSCs via long-term reconstitution of the hematopoietic system in mice, no such assay was available in the field of SSCs. Through the work of Sacchetti et al.[12], it was made clear that true stemness of SSCs can ultimately only be assessed *in vivo*. A xenograft model in which interrogated stem cells are transplanted subcutaneously or underneath the renal capsule of immunodeficient mice are reported most often[12-14]. This system enables scrutinized cells to develop into a heterotopic ossicle containing bone, cartilage, or even bone marrow depending on their intrinsic capacity. However, in subsequent complimentary studies, each research group has worked with a different biomaterial – a fact that convolutes direct comparison of published findings. In this thesis, presented data reaffirms that the stem cell carrier is not a mere scaffold but instead contributes to cell behaviors. Stability of the material (or lack thereof) and inherent functions in their compositions trigger different stem cell behaviors, and thus, impact readouts. Thus, we propose the establishment of unified protocols for testing cell-intrinsic properties. We are convinced that employing well-defined matrices for such evaluations will drastically reduce the confounding results within the MSC/SSC field.

The setup

In vitro models can yield useful preliminary indications, but ultimately only *in vivo* experiments can provide a complete picture of the recapitulation capabilities for a given tissue model[15]. This thesis depicts that the setup in which we study stem or progenitor cells is of paramount importance. A comparison of osteogenic differentiation of different hBMSC donors (same cohort as in Chapter 3) in 2D or 3D conditions showed a markedly different pattern in terms of osteogenic capacity of these cells (Figure a). Whole transcriptome analysis of donors and control cells retrieved from 2D or 3D cultures corroborated these discrepancies. Results showed that for cells cultured in 3D, a clear and measurable separation between healthy and diseased cells was observed in principal component analysis (PCA) (Figure b). This was not the case in PCA from the same cells cultured in 2D. Still, despite the supposed improvement afforded by 3D cultures over 2D counterparts, their culture *in vitro* failed to illuminate clear interdonor distinctions in terms of ossicle formation capability. Only when taking this system *in vivo* did we observe that setup design is crucial. More specifically, since addition of BMP-2 also masked interdonor discrepancies during *in vivo* ossicle formation, it could finally be determined that an inducer-free *in vivo* setup sans BMP-2 would uniquely allow discernment between donors.

Though complete exclusion of BMP-2 from the system was necessary to compare intrinsic donor cell capacity, it was also essential to determine conditions under which cells from virtually any donor would yield robust ossicles. Determining optimal cell density and BMP-2 concentration for

this purpose yielded conditions for forming ossicles i*n vivo* in a robust manner enabling reproducibility for follow-on studies involving the bone marrow niche models. Encouragingly, these optimized conditions allowed for a substantially reduced dose of BMP-2 compared to current standards for induction of heterotopic ossicles[16-18]. We also observed that growth factors that induce proliferation and migration, namely FGF-2 and PDGF-BB, inhibited hBMSC intrinsic bone formation capacity.

Taken all together, this highlights that there is no ubiquitously applicable set of parameters, but that based on the necessity of every application, and given the available possibilities, customized models must be engineered.

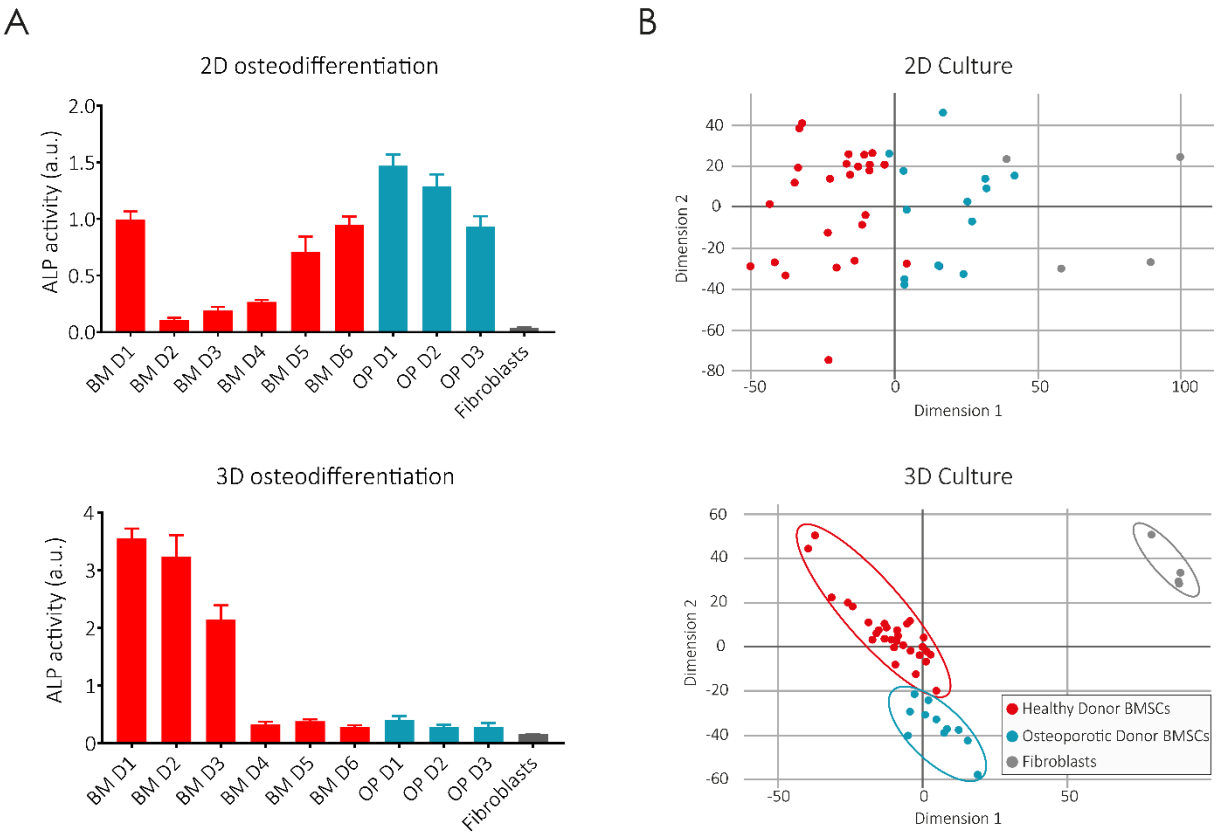

Figure 1. hBMSCs in 2D or 3D culture conditions

(**a**) ALP activity quantification normalized to DNA content, as a marker of osteogenic differentiation of hBMSCs from healthy and osteoporotic-derived patients, as well as fibroblasts used as control, in 2D (top) or 3D (bottom) conditions (n ≥ 4). (**b**) Principal component analysis (PCA) of bulk RNA sequencing of these cells cultured for 5 days in 2D (top) or 3D (bottom) revealed specific clusters separating healthy, osteoporotic and fibroblasts when cultured in 3D, while in 2D cultures samples could not be distinguished (n = 4).

Basic science vs. clinical translation: a classic tug-of-war

Despite the tremendous advance posed in developing stricter markers and assays to characterize SSCs and MSCs, the obvious yet not trivial clinical translation remains the biggest challenge in the field. Of course, during developing of stricter markers and assays to characterize SSCs and MSCs, it must not be forgotten that the final goal is to translate their use to the clinics. Deficiency in the number of cells available for transplantation remains a major challenge for cell-based therapies in the clinic. Thus, restricting the cell number often does not lead to a better clinical outcome. A dual effort is therefore needed to improve cell engraftment in clinical applications: 1) novel tools to preemptively evaluate outcomes of patient-derived cells, and 2) better identification of the cells that possess multipotency, self-renewal capabilities, and, ultimately, will actively participate in bone regeneration.

In the course of this thesis work, striking differences in performance were observed between different cell donors. Further investigations into the source of these interdonor discrepancies is required to better inform a potential clinical readout. Bulk transcriptomic analysis of these cells unfortunately did not expose potential targets attributed to the effect seen *in vivo*. This might be due to the following limitations: i) *in vitro* systems alone introduce more significant artefact than the cell differences themselves, or ii) differences between donors are averaged in bulk RNA-sequencing. The first limitation could be overcome by isolating transplanted cells of each donor from the established xenograft model, and then comparing their transcriptome. Interestingly, the second limitation could be solved by single cell transcriptome analysis. Single-cell RNA-sequencing is a powerful technique to discover low-abundant cells within heterogeneous populations[19], as well as to map distinct cell states[20]. In the past, the lack of phenotypical characterization to define certain cell populations has limited the elucidation of key cell types likely "masked" in larger cell populations. Additionally, genotyping hBMSCs from different donors is also a feasible approach that would prove highly valuable in case it yielded successful discrimination between features of donors with 'good' or 'bad' osteogenic potential.

Nonetheless, we are aware that the low number of donors used here would make such evaluations highly tedious, if not impossible. We therefore envision future collaborations with clinical partners to recruit a higher cohort of patient samples. In addition, it would be highly desirable to correlate the *in vivo* results with the long-term outcome of these cells in patients, which would be the ultimate validation of the presented system.

Successful transplantation of human cells and their role in niche formation

Since the onset of this project it has been paramount to continually assess the role and potential active participation of the transplanted human cells in the formation, and later maintenance, of xenograft BM niches. Both flow cytometry analysis and specific immunostainings have revealed

that the human cell population diminishes over time after subcutaneous implantation of hBMSCs in pure TG-PEG gels. Surprisingly, though longer persistence of hBMSCs of up to 8 weeks post-transplantation in HA-containing hydrogels was observed, it did not translate into higher bone volumes compared to pure TG-PEG gels, nor detectable differences in human matrix deposition. This may be due to the fact that the number of hBMSCs implanted is sufficiently high providing enough cells in all conditions to lead bone formation. Therefore, we postulate that human cells do play an active role in bone marrow formation and, based on our results, we can confirm that at least in the first weeks after transplantation their ECM deposition plays a critical role in the successful development of these niches. Further evaluation is needed, though, to better understand the role of the paracrine signaling induced by the delivered human cells. Again, strong differences in recruitment of murine host cells that populate the BM are observed when utilizing different hBMSC donors, but if this is directly mediated by soluble factors secreted by the transplanted cells, by particular ECM proteins they deposit, or by crosstalk with specific murine populations (e.g. cells of the immune system), remains to be investigated. It is worth noting that, despite being a humanized ossicle, it is ultimately still formed in a murine host. This limits the system and leaves room for interspecies effects that could confound some of these observations.

Another design parameter to keep in mind when evaluating these results is that these *in vivo* experiments were performed in immunocompromised mice as xenograft hosts. Animals with suppressed immune systems are selected to avoid graft-versus-host reaction to the xenograft implants. However, they poorly mimic the native human microenvironment. The immune system plays a pivotal role in a wide array of biological processes. More specifically, the immune system has been related to tissue regeneration[21], as well as tumor progression[22,23]. Thus, we need to be mindful of the limitations pertaining to lack of immunogenic capacity of the models employed here, and when possible corroborate the findings in other mouse strains or higher animal models. Additionally, when murine analogues are present (e.g. in the study of SSCs), mouse-mouse systems can be designed in immunocompetent mice to interrogate the immune system effect on specific setups, and combine these findings to overcome the limitation in the xenograft system counterpart.

Towards a higher degree of humanization

With the establishment of heterotopic bone models came the challenge of how much further we can humanize these structures and how close we can resemble the human niche. Several cell types are known to be part of the hematopoietic stem cell niche in the bone marrow. hBMSCs and hECs have been purported to play both independent and synergistic roles in the maintenance of the niche. Thus, it is an attractive idea to combine both cell types and study their potential co-operative effects in the BM niche.

We and others have devoted great efforts to establishing and optimizing co-cultures of hBMSCs and hECs in TG-PEG hydrogels[3,24]. We recently reported that 3D co-cultures of hBMSCs and

HUVECs in TG-PEG matrices *in vitro* can be directed towards vascularized bone-like tissue constructs[24]. This was possible by supplementing the culture with BMP-2, FGF-2 or a combination of both. Both BMP-2 and FGF-2 alone promoted the formation of vascular-like structures, while BMP-2 additionally induced osteogenic differentiation of the encapsulated hBMSCs. Thus, it is appealing to translate these findings to the *in vivo* setup described in this thesis to achieve human vasculature within the xenograft BM implants.

A pilot experiment was performed to evaluate the functionality of these *in vitro* pre-formed vascular-like structures upon *in vivo* implantation. Pre-vascularized co-cultures supplemented with FGF-2 for 2 weeks were subcutaneously implanted in nude mice. Already at 1 week post-implantation, the *in vitro* co-cultures contained erythrocyte-filled microvessels, indicating the inosculation with the host vasculature as well as their functionality (Figure 2 a). Immunostainings specific for human endothelial cells confirmed that the perfused microvessels were of human origin (Figure 2 a, b right panels). This first proof-of-concept experiment showed that *in vitro* pre-cultures fully integrated with the host tissue *in vivo*, that the structures formed by the human cells *in vitro* are also functional *in vivo*, and lastly, point to the fact that the implanted human cells are viable and participate with the host cells to remodel the construct. The next step would be to combine hBMSC bone formation with HUVEC vascularization *in vivo*. We have shown that successful pre-vascular network formation necessitates pre-culture *in vitro*. However, osteogenic pre-differentiation of hBMSCs prior to implantation impaired bone formation in this work. This is in keeping with another report that showed that for rat BMSCs, extended periods (> 4 days) of osteogenic differentiation reduced their *in vivo* bone forming potential in a calvarial defect model[25]. Therefore, future investigations will need to further explore whether we can omit the pre-vascularization process *in vitro*, perhaps by increasing the number of transplanted HUVECs, or whether supplementation of osteogenic growth factors in pre-differentiated constructs upon implantation can compensate for the loss of osteogenic potential.

The concepts described above for regarding vascularization of the engineered BM could be further built upon to generate large bone constructs. Often in the clinics successful regeneration of large bone constructs is limited by the lack of vascularization[26]. Thus, advanced bone models featuring a functional vascular tree that can enhance integration with the host vessels, and thus improve implant regeneration, are highly desirable.

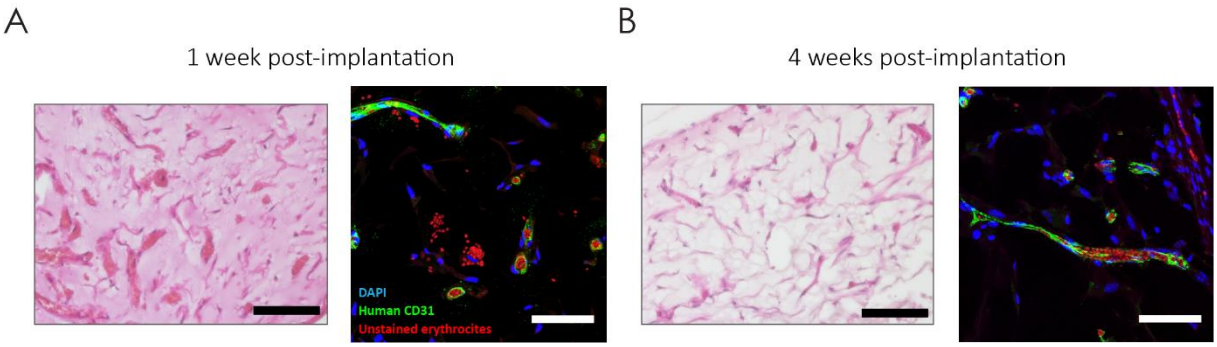

Figure 2. Functionality *in vivo* of the pre-vascularized co-cultures *in vitro*

Co-cultures of hBMSCs and HUVECs were encapsulated in TG-PEG scaffolds and cultured *in vitro* with FGF-2 for 2 weeks, followed by subcutaneous implantation in nude mice. (**a**) 1 week post-implantation H&E staining and immunohistochemistry for the human endothelial marker (CD31), and (**b**) idem for 4 weeks post-implantation, showed perfusion of host erythrocytes in the pre-formed human vascularized structures (H&E, scale bars: 50 µm; IF, scale bars: 60 µm). Nuclei were stained with DAPI, human $CD31^+$ cells in green, and in red autofluorescence of murine erythrocytes

Multiplexing approaches for heightened throughput *in vivo* screening

Recent discoveries are rapidly contributing to our knowledge regarding which cellular and molecular niche components participate in its homeostasis and the manner in which they do so. The same findings also help in unmasking the role that the niche plays in the onset and progression of several pathologies. Testing of individual contributions to these effects are becoming key to develop therapeutic approaches targeted to specific niche components. *In vitro* studies have repeatedly failed to recapitulate the full complexity of the niche, but working *in vivo* is costly and laborious, and often requires high cell numbers and amounts of molecular factors hampering the potential screening of multiple parameters in sufficiently high throughput. There is also the challenge of limited patient material that is highly valuable and difficult to harvest in large amounts. To efficiently keep up with the number of parameters involved in the niche that need to be screened, heightened throughput *in vivo* approaches must be developed[27]. Ideally, these approaches would miniaturize current xenograft models requiring reduced sampling amounts to accommodate low abundance clinical samples.

To accomplish this, an implantable device which can carry several miniaturized constructs simultaneously and which permits the formation of several niche conditions in parallel is envisioned (Figure 3 a). The design criteria of this implantable device are straightforward: it must compartmentalize several hydrogel-based constructs, isolate them from each other to prevent crosstalk, and do so in a limited space (max. 10 mm in length) that still allows for subcutaneous implantation. The material of the device must be inert and non-immunogenic, and flexible enough to adapt to the body and movements of the host. Polydimethylsiloxane (PDMS) is an attractive choice since it is inert, flexible, easy to mold, has low porosity that should prevent diffusion

between the conditions, and can be easily sterilized for *in vivo* implantation. Constructs should be in contact with muscle tissue, previously reported to enhance implants vascularization[18]. Conversely, interaction with the host skin, rich in adipocytes and related to compromised marrow formation[28], should be avoided by closing the PDMS device on one side. Encouraged by the results presented in this thesis, we envision that employing a well-defined hydrogel carrier that can systematically evaluate parameters is a rational starting point.

As a pilot experiment, a number of different rectangular molds were designed containing a range of well numbers and sizes ranging from 1 mm to 4 mm in diameter in which the hydrogels could be polymerized (Figure 3 b). Next, to determine the minimal size of construct that would allow the heightened screening of conditions and yet enable ossicle formation, TG-PEG hydrogels containing hBMSCs alone ($10 \cdot 10^6$ cells per ml, cell density that *per se* does not elicit bone formation) or hBMSCs and BMP-2 (100 ng μl^{-1}, high concentration) were polymerized in PDMS wells (Figure 3 c). Thus, bone was only expected in wells containing hydrogels supplemented with BMP-2. Devices were subcutaneously implanted and evaluated 8 weeks later for bone and bone marrow formation. MicroCT imaging revealed bone formation in wells bigger than 1 mm diameter and containing BMP-2. In some conditions, there were also low amounts of bone formation in some wells not supplemented with BMP-2, likely due to crosstalk among neighboring wells seeded with a high concentration of BMP-2. Histological analysis corroborated the formation of bone and bone marrow structures (Figure 3 d). Next steps will require further optimization of the presented screening device to avoid crosstalk (e.g. optimizing cell and growth factor concentrations or using growth factor immobilization techniques) while maximally exploring miniaturization. Finally, the production reproducibility of these devices will have to be carefully evaluated to ensure comparability between experiment sets.

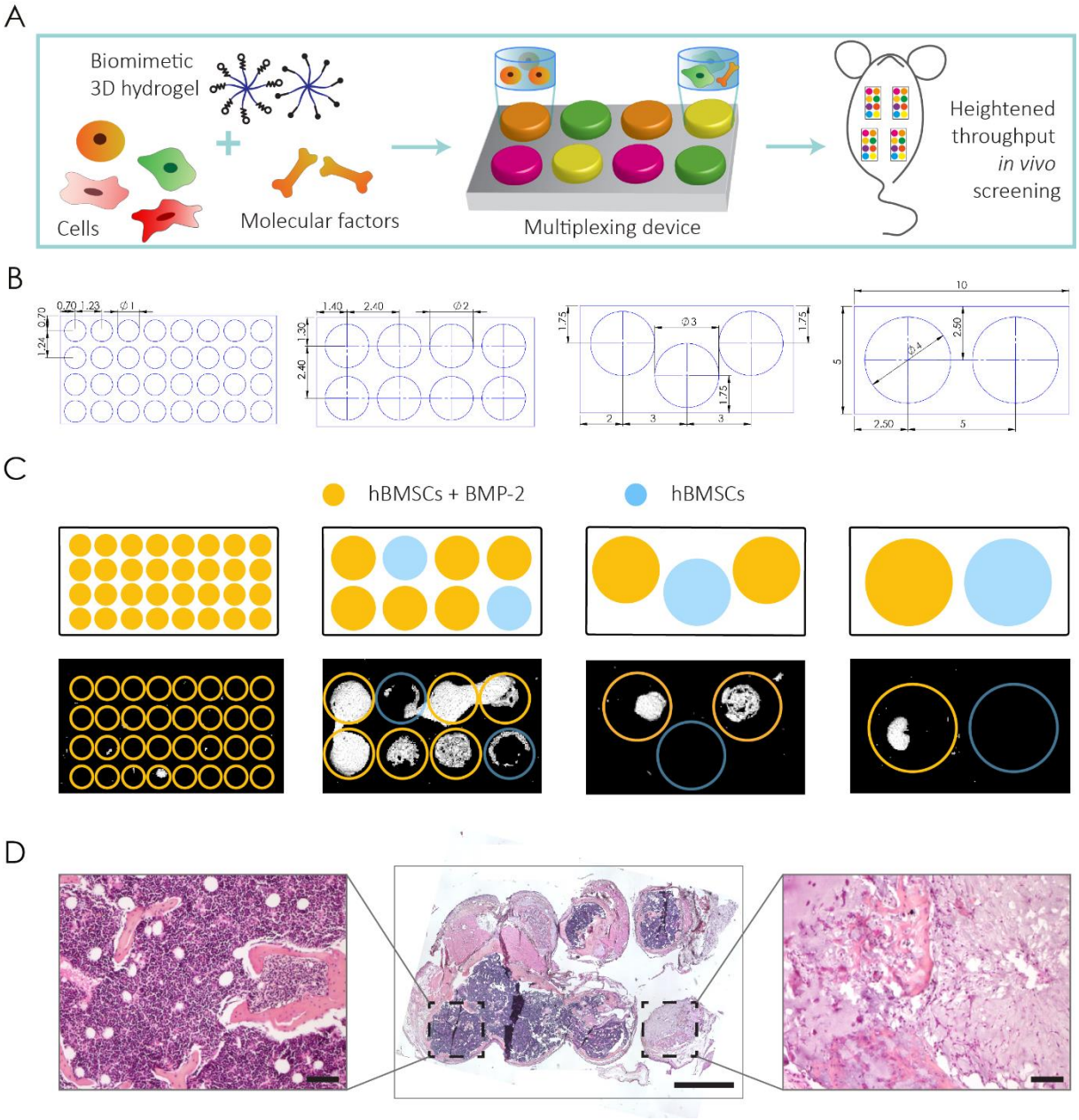

Figure 3. Multiplexing devices for heightened throughput screening *in vivo*

(**a**) Scheme of the workflow. Devices carrying up to 8 different conditions of TG-PEG hydrogels with different combinations of cells and molecular factors are subcutaneously implanted in mice. (**b**) Different geometries were designed including 32 wells of 1 mm diameter each, 8 wells of 2 mm, 3 wells of 3 mm and 2 wells of 4 mm. (**c**) Wells were filled with TG-PEG hydrogels containing hBMSCs and BMP-2 ($10 \cdot 10^6$ cells per ml, 100 ng μl^{-1}) (orange) or only hBMSCs (blue). Devices were implanted for 8 weeks subcutaneously, and bone formation was assessed by microCT. (**d**) Representative H&E staining of a whole device, and zoom-in wells indicating the formation of bone and bone marrow in wells containing hBMSCs and BMP-2 (center, scale bar: 2mm; higher mag., scale bars: 100 µm).

Applications of the multiplexing approach

Combining multiplexing devices with all the findings reported in this thesis opens the door to multiple exciting applications. The heightened throughput and miniaturization make these devices appealing to use in personalized medicine. For instance, in TG-PEG hydrogels without any inducing factors, we could detect differences in bone formation between hBMSCs derived from different donors. **Preemptively evaluating a patient's own hBMSCs to regenerate BM tissue** in a clinical setup would be of paramount importance towards determining parameters for personalized therapy. Depending on the intrinsic capability of patient-derived cells to form bone, the adequate dosing of growth factors or other stimulants could be determined on a patient-by-patient basis.

Furthermore, we envision the use of this *in vivo* platform as a **personalized osteotropic cancer model**. Using stromal and tumor cells derived from the same patient, the efficacy of potential therapeutic drugs could be screened for in patient-derived xenografts. This device is also a prominent tool for basic cancer biology. For instance, the effect of genetically modifying a panel of various targets in stromal cell genomes could be evaluated. Or, the presentation of diverse moieties within the hydrogel backbone could be evaluated in parallel for tumor progression *in vivo*.

Ultimately, with the development of single cell sequencing and other tools to rigorously purify and characterize cells, it is expected that rare cells with defined properties will be isolated. Thorough c**haracterization of these rare stem cells** will necessitate platforms, such as the one here envisioned, that can provide meaningful *in vivo* data on these cells' intrinsic properties.

Envisioning a bright future

We believe that the establishment of these models and the validation of their functionality is a stepping stone for future research. The stem cell research field is rapidly evolving and important considerations must be undertaken for future research in order to unify findings and be able to build on other's results. In this line, it is absolutely crucial to have well-defined stem cells and functional assays to assess their multipotency and self-renewal properties. So, in hand with stem cell biology, biomaterials to deliver these cells and enable these assays must be advanced towards robust and induction-free matrices. Additionally, the high speed discovery of niche factors is demanding higher throughput techniques to assess individual contributions to this niche. Complex animal models are limited in uncoupling single factors and present an interspecies challenge for translation into humans. However, *ex vivo* experiments likely highlight artefact effects of cells being taken out of their niche rather than true inherent cell behaviors. Xenograft *in vivo* models, when possible and available, offer a palatable compromise. However, interspecies-related complications, and the need to work preliminarily with immunocompromised systems still hampers their full potential. Despite the inherent limitations in each and every model, the development of novel tools

such as the ones reported in this thesis, with utility both *in vitro* and *in vivo,* are without doubt key to offering a deeper understanding of intriguing bone marrow biology, and ultimately aiding at clinically translating these findings. Faster and more meaningful developments from the bench, it follows, will naturally find timely and impactful applications at the bed-side. Thus, an interdisciplinary effort by biologists, engineers, and clinicians is clearly the path of the future and I am eager to participate and see where it leads.

References

1 Gjorevski, N. *et al.* Designer matrices for intestinal stem cell and organoid culture. *Nature* **539**, 560 (2016).

2 Cruz-Acuña, R. *et al.* Synthetic hydrogels for human intestinal organoid generation and colonic wound repair. *Nature cell biology* **19**, 1326 (2017).

3 Blache, U. *et al.* Notch-inducing hydrogels reveal a perivascular switch of mesenchymal stem cell fate. *EMBO reports* **19**, e45964 (2018).

4 Ferreira, S. A. *et al.* Bi-directional cell-pericellular matrix interactions direct stem cell fate. *Nature communications* **9**, 4049 (2018).

5 Loebel, C., Mauck, R. L. & Burdick, J. A. Local nascent protein deposition and remodelling guide mesenchymal stromal cell mechanosensing and fate in three-dimensional hydrogels. *Nature materials*, 1 (2019).

6 Kolambkar, Y. M. *et al.* Spatiotemporal delivery of bone morphogenetic protein enhances functional repair of segmental bone defects. *Bone* **49**, 485-492 (2011).

7 Silva, E. & Mooney, D. J. Spatiotemporal control of vascular endothelial growth factor delivery from injectable hydrogels enhances angiogenesis. *Journal of Thrombosis and Haemostasis* **5**, 590-598 (2007).

8 Lienemann, P. S. *et al.* A versatile approach to engineering biomolecule-presenting cellular microenvironments. *Advanced healthcare materials* **2**, 292-296 (2013).

9 Stüdle, C. *et al.* Spatially confined induction of endochondral ossification by functionalized hydrogels for ectopic engineering of osteochondral tissues. *Biomaterials* **171**, 219-229 (2018).

10 Stowers, R. S., Allen, S. C. & Suggs, L. J. Dynamic phototuning of 3D hydrogel stiffness. *Proceedings of the National Academy of Sciences* **112**, 1953-1958 (2015).

11 de Almeida, P. *et al.* Cytoskeletal stiffening in synthetic hydrogels. *Nature communications* **10**, 609 (2019).

12 Sacchetti, B. *et al.* Self-renewing osteoprogenitors in bone marrow sinusoids can organize a hematopoietic microenvironment. *Cell* **131**, 324-336 (2007).

13 Chan, C. K. *et al.* Identification of the human skeletal stem cell. *Cell* **175**, 43-56. e21 (2018).

14 Chan, C. K. *et al.* Identification and specification of the mouse skeletal stem cell. *Cell* **160**, 285-298 (2015).

15 Wang, X., Rivera-Bolanos, N., Jiang, B. & Ameer, G. A. Advanced Functional Biomaterials for Stem Cell Delivery in Regenerative Engineering and Medicine. *Advanced Functional Materials*, 1809009 (2019).

16 Abarrategi, A. *et al.* Versatile humanized niche model enables study of normal and malignant human hematopoiesis. *The Journal of clinical investigation* **127**, 543-548 (2017).

17 Seib, F. P., Berry, J. E., Shiozawa, Y., Taichman, R. S. & Kaplan, D. L. Tissue engineering a surrogate niche for metastatic cancer cells. *Biomaterials* **51**, 313-319 (2015).

18 Torisawa, Y.-s. *et al.* Bone marrow–on–a–chip replicates hematopoietic niche physiology in vitro. *Nature methods* **11**, 663-669 (2014).

19 Schwalie, P. C. *et al.* A stromal cell population that inhibits adipogenesis in mammalian fat depots. *Nature* **559**, 103 (2018).

20 Velten, L. *et al.* Human haematopoietic stem cell lineage commitment is a continuous process. *Nature cell biology* **19**, 271 (2017).

21 Sadtler, K. *et al.* Developing a pro-regenerative biomaterial scaffold microenvironment requires T helper 2 cells. *Science* **352**, 366-370 (2016).

22 Coussens, L. M. & Werb, Z. Inflammation and cancer. *Nature* **420**, 860 (2002).

23 Lin, E. Y., Nguyen, A. V., Russell, R. G. & Pollard, J. W. Colony-stimulating factor 1 promotes progression of mammary tumors to malignancy. *Journal of Experimental Medicine* **193**, 727-740 (2001).

24 Blache, U. *et al.* Dual Role of Mesenchymal Stem Cells Allows for Microvascularized Bone Tissue-Like Environments in PEG Hydrogels. *Advanced healthcare materials* **5**, 489-498 (2016).
25 Castano-Izquierdo, H. *et al.* Pre-culture period of mesenchymal stem cells in osteogenic media influences their in vivo bone forming potential. *Journal of biomedical materials research Part A* **82**, 129-138 (2007).
26 Mercado-Pagán, Á. E., Stahl, A. M., Shanjani, Y. & Yang, Y. Vascularization in bone tissue engineering constructs. *Annals of biomedical engineering* **43**, 718-729 (2015).
27 Bodhak, S. *et al.* Combinatorial cassettes to systematically evaluate tissue-engineered constructs in recipient mice. *Biomaterials* **186**, 31-43 (2018).
28 Naveiras, O. *et al.* Bone-marrow adipocytes as negative regulators of the haematopoietic microenvironment. *Nature* **460**, 259-263 (2009).

Imagination is more important than knowledge.

– Albert Einstein

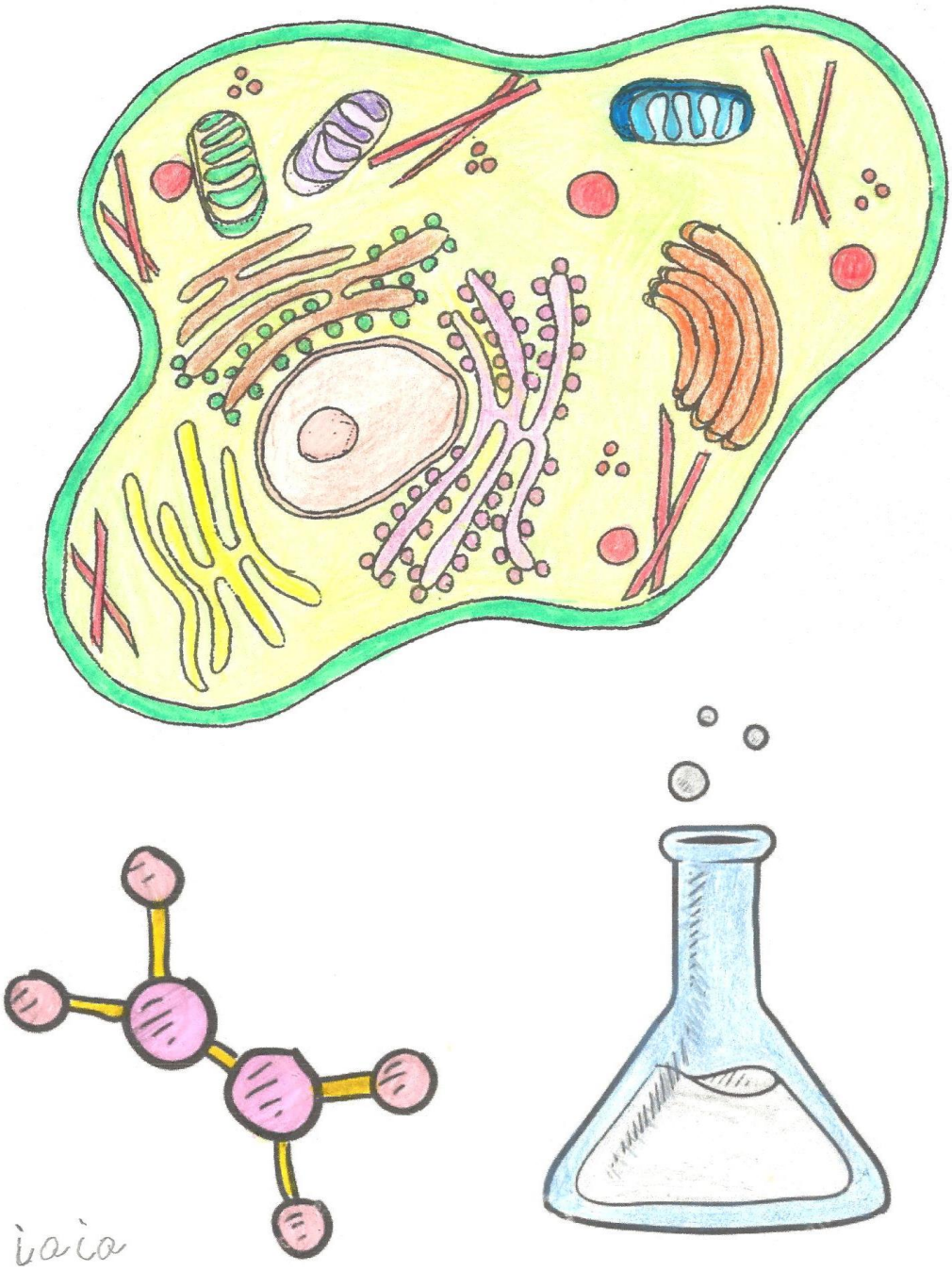

Artwork by María Dorado Prado

Girona, Catalunya

Queralt Vallmajó – Martín

University Hospital Zürich
Laboratory for Cell and Tissue Engineering
Schmelzbergstrasse 12
8091 Zürich, Switzerland

+41 78 684 0861 (mobile)
+41 44 255 3285 (office)

queralt.vallmajomartin@usz.ch

EDUCATION

10.2014 – current **PhD candidate in Biotechnology and Bioengineering**
Laboratory for Cell and Tissue Engineering
EPF Lausanne – UniversitätsSpital Zürich, Switzerland

09.2011 – 07.2014 **Master Degree in Biomedical Engineering, Molecular Bioengineering**
ETH Zürich, Switzerland; GPA: 5.34/6.00

09.2013 – 06.2014 **Master Thesis**
Harvard – MIT, USA

09.2007 – 06.2011 **Bachelor Degree in Biotechnology**
UA Barcelona, Spain; *Valedictorian*

09.2009 – 09.2010 **Exchange Program in Biomedical Engineering**
UC Santa Cruz, CA, USA; GPA: 3.92/4.00

RESEARCH EXPERIENCE

10.2014 – current PhD project, **EPF Lausanne – UniversitätsSpital Zürich**
Co-Directors: Prof. Matthias Lütolf; PD Dr. Martin Ehrbar

Bioengineering human bone marrow models to elucidate the triggers of the stem cell niche

- Studying the formation of ectopic humanized HSC niches *in vivo*
- Studying human and murine skeletal stem cell populations *in vivo*
- Designing an optimized device for high throughput screening *in vivo*
- Translating HSC niche to an *in vitro* model via novel biomaterials
- Optimizing 3D well-defined matrices

09.2013 – 06.2014 Master Thesis, **Harvard – MIT**
Advisor: Prof. Ali Khademhosseini | External ETHZ Advisor: Prof. Viola Vogel

Engineering elastin-like polypeptide (ELP) gels with highly elastic and tunable properties for soft tissue engineering applications

- Developed novel biologically inspired materials for tissue sealing
- Characterized material's physical, chemical and mechanical properties
- Defined cytocompatibility of the materials in 2D and 3D studies
- Planned and performed *in vivo* studies in rat models

04.2012 – 05.2013 Semester Project and Research Assistant, **ETH Zürich**
Advisor: Prof. Marcy Zenobi-Wong

Engineering chondrogenic microenvironments: modified PEG hydrogels and sulfated alginate hydrogels

- Modified biomaterials as 3D scaffolds for specific cell types
- Established embedding, sectioning and histology of cell-laden hydrogels

- Analyzed stem cell differentiation in 3D microenvironment

09.2010 – 05.2011 Senior Thesis Research, **Universitat Autònoma Barcelona**
Advisor: Prof. Francesc Gòdia | *Design of second-generation porcine vaccine against porcine circovirus type 2 for mass production in bioreactors*

01.2010 – 09.2010 Associated student researcher, **UC Santa Cruz**
Advisor: Prof. Nader Pourmand |*Calmodulin- modified nanopipette: a selective and reversible calcium biosensor*

RESEARCH AND TECHNICAL SKILLS

Laboratory experience	Wide-range of experience in biomaterial engineering, molecular biology, cellular biology and mouse experimental research
Biomaterial techniques	Material design, fabrication and engineering, rheology test, swelling tests
Molecular techniques	Quantitative RT-PCR, Western Blot, ELISA, ALP quantification, DNA quantification, NGS, LC-MS/MS, immunohistochemistry
	Courses: "Genome Engineering: CRISPR/Cas" (2018, EMBL Heidelberg)
Cellular techniques	Isolation and culture of primary cell lines (mouse & human), culture in 3D with different biomaterials, transient transfections (siRNA), generation of stable cell lines by lentivirus transduction, flow cytometry analysis and sorting, CFSE cell proliferation, colony formation, multilineage differentiation (osteo, adipo, chondrogenic)
	Courses: "Advanced Flow Cytometry" (2018, University of Zürich)
	Summer school: "Stem Cells & Regenerative Medicine" (2015, Hydra)
Animal experimentation	Mouse managing and maintenance (breeding), subcutaneous surgery, tail vein injection, necropsy, organ collection, processing for flow cytometry, fixation for microCT and histology
	Certificate and Training for Conducting Animal Experiments in Switzerland (2015, EPFL Lausanne)
Microscopy techniques	Confocal Microscopy and Scanning Electron Microscopy, X-ray microtomography
	Courses: "Practical Course in Advanced Microscopy" (2017, ETHZ Zürich)
Computing	ImageJ – Fiji, Imaris, FlowJo, DIVA, Adobe Photoshop, Illustrator/InDesign, Matlab, GraphPad-Prism, IBM SPSS Statistics, EndNote
Teaching/Supervision	Supervision of 3 Master Thesis students (6 month project, 2016-2018)
	Teaching assistant of the courses: "Biological Methods for Engineers" (2013 and 2014, ETHZ Zürich), "Cell Biology for Engineers" (2012 and 2013, ETHZ Zürich)
	Mentor of undergraduate students (2008-2009, UAB Barcelona)
Comm./Executive	Executive Member of the Swiss Society for Biomaterials & Regenerative Medicine
	Organizing committee of the Young Scientists of the Swiss Society for Biomaterials (Young Scientists Symposiums + Lab & Networking events)
Languages	Catalan (native), Spanish (native), English (full professional proficiency), German (conversational), French (basic)

REFERENCES

PD Dr. Martin Ehrbar, University Hospital Zürich (martin.ehrbar@usz.ch, +41 44 255 8513)

Prof. Matthias Lütolf, EPFL Lausanne (matthias.lutolf@epfl.ch, +41 21 693 7213)

Prof. Ali Khademhosseini, UCLA (khademh@ucla.edu, +1 310 794 7179)

Prof. Marcy Zenobi–Wong, ETHZ Zürich (marcy.zenobi@hest.ethz.ch, +41 44 632 5089)

APPENDIX

Publications

PS Lienemann, Q Vallmajo-Martin, P Papageorgiou, U Blache, S Metzger, AS Kiveliö, V Milleret, A Sala, S Hoehnel, R Reuten, M Koch, O Naveiras, FR Weber, W Weber, MP Lutolf, M Erhbar. Smart hydrogels for the augmentation of bone regeneration by endogenous skeletal stem cell recruitment. *(Manuscript under revision)*.

BJ Klotz, LA Oosterhoff, L Utomo, KS Lim, Q Vallmajo-Martin, H Clevers, TBF Woodfield, AJWP Rosenberg, J Malda, M Ehrbar, B Spee, D Gawlitta. A versatile semi-synthetic hydrogel platform for the engineering of tissue analogues. *(Manuscript under revision)*.

P Papageorgiou*, Q Vallmajo-Martin*, M Kisielow, A Sancho-Puchades, E Kleiner, M Ehrbar. Expanded skeletal stem and progenitor cells promote and participate in induced bone regeneration at subcritical BMP-2 dose. **Biomaterials**, 2019. **Indicates equal contribution as 1st author*

F Mushtaq, H Torlakcik, Q Vallmajo-Martin, EC Siringil, J Zhang, C Röhrig, Y Shen, Y Yu, XZ Chen, R Müller, BJ Nelson, S Pané. Magnetoelectric inverse opal scaffolds for bone tissue engineering. **Applied Materials Today**, 2019.

P Occhetta, A Mainardi, E Votta, Q Vallmajo-Martin, M Ehrbar, I Martin, A Barbero, M Rasponi. Hyperphysiological compression of articular cartilage induces an osteoarthritic phenotype in a cartilage-on-a-chip model. **Nature Biomedical Engineering**, 2019.

HD Sparks, F Anjum, Q Vallmajo-Martin, M Ehrbar, S Abbasi, MS Kallos, J Biernaskie. Flowable polyethylene glycol hydrogels support the *in vitro* survival and proliferation of dermal progenitor cells in a mechanically dependent manner. **ACS Biomaterials Science & Engineering**, 2019.

U Blache, Q Vallmajo-Martin, E Horton, J Guerrero, Djonov, A Scherberich, I Martin, J Snedeker, V Milleret, M Ehrbar. Notch-inducing PEG-hydrogels mimic perivascular niche controlled commitment of human MSCs. **EMBO Reports**, 2018.

C Stüdle, Q Vallmajo-Martin, A Haumer, J Guerrero, M Centola, A Mehrkens, M Ehrbar, A Barbero, I Martin. Functionalized hydrogels to engineer in vivo osteochondral composites by spatially controlled induction of endochondral ossification. **Biomaterials**, 2018.

J Zimoch, J Simo-Padial, AS Klar, Q Vallmajo-Martin, M Meuli, T Biedermann, CJ Wilson, A Rowan, E Reichman. Polyisocyanopeptide hydrogels: a novel thermo-responsive hydrogel supporting pre-vascularization and the development of organotypic structures. **Acta Biomaterialia**, 2018.

PS Lienemann, T Rossow, AS Mao, Q Vallmajo-Martin, M Ehrbar, DJ Mooney. Single cell-laden protease-sensitive microniches for long-term culture in 3D. **Lab-on-a-chip**, 2017.

L Zhang, LH Cai, PS Lienemann, T Rossow, I Polenz, Q Vallmajo-Martin, M Ehrbar, H Na, DJ Mooney, DA Weitz. One-step microfluidic fabrication of polyelectrolyte microcapsules in aqueous conditions for protein release. **Angewandte Chemie**, 2016.

U Blache, S Metzger, Q Vallmajo-Martin, I Martin, V Djonov, M Ehrbar. Dual role of mesenchymal stem cells allows for microvascularized bone tissue-like environments in PEG hydrogels. **Advanced Healthcare Materials**, 2016.

Y Zhang*, R K Avery*, Q Vallmajo-Martin*, A Assmann, A Vegh, A Memic, B D Olsen, N Annabi, A Khademhosseini. A highly elastic and rapidly crosslinkable elastin-like polypeptide-based hydrogel for biomedical applications. **Advanced Functional Materials,** 2015. **Indicates equal contribution as 1st author*

R Mhana, A Kashyap, G Palazzolo, Q Vallmajo-Martin, J Becher, S Möller, M Schnabelrauch, M Zenobi-Wong. Chondrocyte Culture in 3D Alginate Sulfate Hydrogels Promotes Proliferation While Maintaining Expression of Chondrogenic Markers. **Tissue Engineering Part A**, 2014.

R Mhana, E Öztürk, Q Vallmajo-Martin, C Millan, M Müller, M Zenobi-Wong. GFOGER Modified MMP-Sensitive Polyethylene Glycol Hydrogels Induce Chondrogenic Differentiation of Human Mesenchymal Stem Cells. **Tissue Engineering Part A**, 2014.

B Vilozny, P Actis, A Seger, Q Vallmajo-Martin, N Pourmand. Reversible cation response with a Protein-modified nanopipette. **Analytical Chemistry**, 2011.

Conference presentations (as presenting author)

- TERMIS European Congress, May 2019, Rhodes, Greece **(oral presentation)**
- 25th Annual Meeting SSB+RM, May 2019, Muttenz, Switzerland **(oral presentation)**
- Brupbacher Symposium: Breakthroughs in cancer research and therapy, January 2019, Zürich, Switzerland **(poster presentation)**
- TERMIS World Congress, September 2018, Kyoto, Japan **(oral presentation)**
- Biointerfaces International, August 2018, Zürich, Switzerland **(rapid fire + awarded oral presentation)**
- Keystone Conference: Novel aspects of bone biology, June 2018, Snowbird, USA **(poster presentation)**
- 24th Annual Meeting SSB+RM, June 2018, Fribourg, Switzerland **(rapid fire presentation)**
- 17th Clinical Research day USZ, April 2018, Zürich, Switzerland **(poster presentation)**
- IBI-EDBB symposium, March 2018, Lausanne, Switzerland **(oral presentation)**
- 13th SSCN meeting, September 2017, Lausanne, Switzerland **(poster presentation)**
- TERMIS European Congress, June 2017, Davos, Switzerland **(poster presentation)**
- EMBO Conference: Advances in stem cells and regenerative medicine, May 2017, Heidelberg, Germany **(poster presentation)**
- 23rd Annual Meeting SSB+RM, May 2017, Saint Gallen, Switzerland **(oral presentation)**
- 16th Clinical Research day USZ, February 2017, Zürich, Switzerland **(oral presentation)**
- Biointerfaces International, August 2016, Zürich, Switzerland **(poster presentation)**
- EPFL Bioengineering Day, September 2016, Lausanne, Switzerland **(poster presentation)**
- TERMIS European Congress, July 2016, Uppsala, Sweden **(oral presentation)**
- 22nd Annual Meeting SSB+RM, June 2016, Zürich, Switzerland **(oral presentation)**
- Young Scientists SSB+RM, February 2016, Zürich, Switzerland **(oral presentation)**

Distinctions and career support

- Winner of the Best Poster Award at Biointerfaces International (2018)
- Traveling award for TERMIS World by the Swiss Society for Biomaterials (2018)
- Best Student Oral Presentation at 22nd SSB+RM (2016)
- Best Podium Presentation at YSBM Graduate Research Symposium (2016)
- Excellence scholarship from “La Caixa” to support the Master Studies at ETHZ (2011 – 2013)
- Valedictorian of class in Bachelor studies in Biotechnology at UAB, Barcelona (2011)

- MEC Collaboration fellowship at the “ADV vaccines”, Prof. Gòdia in UAB, Barcelona (2010 – 2011)
- CSIC grant for a lab stay in “Development of new peptides”, Dra.Reig, Barcelona (Summer 2008)
- Prize for senior thesis and participation to *Jóvenes Investigadores* congress, Málaga (Summer 2007)

**Ce document a été imprimé au Centre d'impression EPFL,
imprimerie climatiquement neutre, certifiée myClimate.**